

**Hydrological and biogeochemical cycling along the Greenland ice sheet margin**

by

Maya Pilar Bhatia

B.S., Queen's University (Kingston, Canada), 2001  
M.S., University of Alberta (Edmonton, Canada), 2004

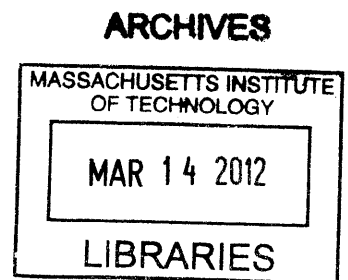
Submitted in partial fulfillment of the requirements for the degree of

Doctor of Philosophy

at the  
MASSACHUSETTS INSTITUTE OF TECHNOLOGY  
and the  
WOODS HOLE OCEANOGRAPHIC INSTITUTION


February 2012


© 2012 Maya Pilar Bhatia.  
All rights reserved.




The author hereby grants MIT and WHOI permission to reproduce and to distribute publicly paper and electronic copies of this thesis document in whole or in part in any medium now known or hereafter created.

Author.....  
Joint Program in Oceanography/Applied Ocean Science and Engineering  
Massachusetts Institute of Technology and Woods Hole Oceanographic Institution

Certified by.....  
  
Sarah B. Das  
Thesis Co-Supervisor

Certified by.....  
  
Elizabeth B. Kujawinski  
Thesis Co-Supervisor

Accepted by.....  
  
Rob L. Evans  
Senior Scientist, Department of Geology and Geophysics, WHOI  
Chairman, Joint Committee for Geology and Geophysics



# Hydrological and biogeochemical cycling along the Greenland ice sheet margin

by

Maya Pilar Bhatia

Submitted to the Department of Marine Geology and Geophysics,  
MIT/WHOI Joint Program in Oceanography/Applied Ocean Science and  
Engineering on December 30, 2011 in partial fulfillment of the requirements  
for the degree of Doctor of Philosophy

## **Abstract**

Global warming has led to a significant increase in Greenland ice sheet (GrIS) melt and runoff since 1990, resulting in escalated export of fresh water and associated sediment to the surrounding North Atlantic and Arctic Oceans. Similar to alpine glacial systems, surface meltwater on ice sheet surface drains to the base (subglacial) where it joins a drainage system and can become chemically enriched from its origin as dilute snow- and ice-melt. In this thesis, I examine the interdependence of glacial hydrology and biogeochemical cycling in terms of export of carbon and iron from the Greenland ice sheet. I develop a new isotope mixing-model to quantify water source contributions to the bulk meltwater discharge draining a GrIS outlet glacier. Results illustrate (a) the new application of a naturally occurring radioisotope (radon-222) as a quantitative tracer for waters stored at the glacier bed, and (b) the seasonal evolution of the subglacial drainage network from a delayed-flow to a quick-flow system. Model results also provide the necessary hydrological context to interpret and quantify glacially-derived organic carbon and iron fluxes. I combine bulk- and molecular-level studies of subglacial organic carbon to show that GrIS discharge exports old (radiocarbon depleted), labile organic matter. Similar investigations of dissolved and particulate iron reveal that GrIS discharge may be a significant flux of labile iron to the North Atlantic Ocean during the summer meltseason. Both carbon and iron are subject to proglacial processing prior to export to the marine environment, and exhibit strong seasonal variability in correlation with the subglacial drainage evolution. Low, chemically concentrated fluxes characterize the spring discharge, whereas higher, chemically dilute fluxes typify the summer discharge. Collectively, this thesis provides some of the first descriptions and flux estimates of carbon and iron, key elements in ocean biogeochemical cycles, in GrIS meltwater runoff.

## Acknowledgments

This thesis represents over half a decade of work for which there is a village of people to thank. First and foremost, my co-advisors, Elizabeth Kujawinski and Sarah Das: I feel so fortunate to have had the chance to work with such amazing scientists. I indebted to them for taking me on when we only had unfunded ideas, for tirelessly writing grants until we were funded, for always encouraging scientific discourse, and for their unfailing support, empathy, and encouragement. I feel that the mark of a great advisor is one who ultimately cares as much, if not more, for the student's development as for the research, and I am thankful to have had this in Sarah and Liz. They will be role models and friends throughout my scientific career. Matt Charette was in many ways a third advisor to me – a deal I'm not sure he bargained for! He graciously (and patiently) offered me his time, expertise, and free reign in his lab. My thesis is much richer as a result of his heavy involvement. I am also grateful to my committee members, Bernhard Peucker-Ehrenbrink, Taylor Perron, Jemma Wadham, and my thesis defense chair, Fiamma Straneo, who all generously donated their time, and always gave me free access to their incredible range of expertise.

One of the best things about WHOI is the access to the amazingly talented scientific and technical staff. I am deeply (deeply) indebted to Krista Longnecker, Crystal Brier, Valier Galy, Melissa Soule, Mark Behn, the NOSAMS prep staff, Phoebe Lam, Meagan Gonnee, Ann McNichol, Sean Sylva, and Scot Birdwhistell. They all generously donated their time and expertise to assist me with analyses, and answer my easy and difficult questions alike. I'm honestly not sure what I would have done without each of them. A special BIG thank you goes out to Paul Henderson, my partner-in-crime in the field and lab. Thank you also to Julia Westwater, Christine Charette, and all the other kind souls in academic programs.

This work would not have been possible without the contributions of my two excellent Greenland field teams. Paul Henderson, Ben Gready, Sarah Das, Elizabeth Kujawinski, Matt Charette, Matt Evans, and Ali Criscitiello all graciously donated their time, filtering abilities, and sheer muscle power to make the foundation of my thesis a success. Additionally, throughout the years, Mark Behn, Ian Joughin, and Kristen Ponair have graciously collected samples for me, despite their inherent geophysist's fear of chemicals.

My MSc advisors at the University of Alberta, Martin Sharp and Julia Foght, have continued to offer their encouragement and support. Indeed, the ideas motivating this thesis first germinated in my MSc, and for that I have Martin and Julia to thank. Martin particularly has generously continued to offer me access to his encyclopedic glaciological mind, office-space in Edmonton, and introduced me to a special field assistant.

I have had the great fortune to have wonderful officemates at WHOI, who became some of my closest friends here. Dave Griffith in the trailer, my marine chemistry p-set partner and research-sounding board. Krista Longnecker in Fye introduced me to MATLAB, and always offered her editing-skills to curtail my tendencies towards verbiage. Without her, this thesis would be 3x longer! I was in Laura Hmelo's office so frequently she may as well have been my officemate. My running and climbing partner, Laura's humour brightened my day in Fye for 4 years. And finally, Evy Mervine, Helen Feng, Andrea Burke, and Emily Roland in Clark, with whom I have been able to finish this wonderful time of my life with. Runs with Andrea, Emily and Erin Bertrand were precious outlets that propelled me to the end. In addition, my JP class cohorts, Carter Esche and Rachel Horwitz, have been wonderful neighbors, and Liz & Mark, have fed me supper many times, including every Thanksgiving! Finally, Sarah Johnson, a dear friend and one of the most generous souls I know – her friendship and advice were instrumental throughout my degree.

My family and Ben are the rocks that I constantly lean on. This thesis is dedicated to my wonderful, inspirational, loving parents, for their amazing support and encouragement to always chase my interests, to my brother, Amar, and sister-in-law, Meghan, who have unfailingly supported me in everything and tirelessly offered me advice, to Benny, who's humour and perspective have kept me centered and very happy, and to Dr. Hopper, who recently left us, but who's tutelage and faith in me I'll never forget.



This research was supported the *WHOI Arctic Research Initiative* (EBK, SBD, MAC), the *National Science Foundation* (EBK, SBD), *NASA* (SBD), a *National Science and Engineering Research Council of Canada* Postgraduate Doctoral Fellowship (MPB), an *American Geophysical Union Horton Hydrology Award* (MPB), *the Ocean Ventures Fund* (MPB), and the *WHOI Climate Change Institute* (MPB).

# Table of Contents

Abstract.....	3
Acknowledgments .....	4
Chapter 1. Introduction .....	7
Chapter 2. Seasonal evolution water contributions to discharge from a Greenland outlet glacier: insight from a new isotope-mixing model .....	16
Chapter 3. Molecular-level characterization of dissolved organic matter associated with the Greenland ice sheet .....	30
Chapter 4. Organic carbon export from the Greenland ice sheet.....	48
Chapter 5. Iron export from the Greenland ice sheet.....	86
Appendix A1. Data Tables .....	111
Appendix A2. Supplementary Material for Chapter 3 .....	139

# Chapter 1

## Introduction

Glaciation is one of the most transformative processes on the Earth's surface, with cycles of glaciation and deglaciation capable of contributing significant quantities of meltwater and associated material to the oceans repeatedly throughout much of Earth's history. Yet, until recently, biogeochemical contributions from glaciers and ice sheets to the oceans were unstudied. Today, the Greenland and Antarctic ice sheets serve as the best analogue for the large Pleistocene ice sheets that covered the continents in the past. Furthermore, global warming has led to a significant increase in Greenland ice sheet (GrIS) melt and runoff since 1990, enhancing export of biogeochemically significant species (e.g. carbon, iron) to the surrounding North Atlantic and Arctic Oceans.

The total GrIS freshwater flux is comprised of surface melt, basal melting, and iceberg calving, and is estimated to be close to 800 km<sup>3</sup>/y (Mernild et al., 2009), with more than half of this contribution coming from surface melting. In 2007, the Greenland ice sheet meltwater runoff contributed an estimated 523 km<sup>3</sup>/y, equivalent to the mean annual discharge from the largest river contributors (e.g. Yenisey, Lena, Ob) to the Arctic Ocean (Dittmar and Kattner, 2003). Similar to processes observed on many alpine glaciers, recent evidence indicates that surface meltwater runoff does not take a direct path from the ice sheet surface (supraglacial) to the sea. Instead, a significant quantity drains to the base of the ice sheet (subglacial), via hydrofractures and moulins (vertical englacial channels through a glacier cross-section) (Das et al., 2008). At glacier beds, surface meltwater joins a subglacial system drainage system, where there is potential for substantial interaction with the underlying bedrock and sediments along seasonally-evolving flowpaths (Brown, 2002). Previous work in alpine systems has shown that interaction of glacial meltwaters with subglacial till and bedrock produces discharge with significant chemical enrichment relative to its origin as dilute snow- and ice-melt

(Brown, 2002; Tranter et al., 2002). Meltwater at the bed also fuels subglacial microbial activities, which facilitate the release of additional nutrients and metals, amplify chemical weathering reactions, and/or utilize the organic carbon present in overridden soils and vegetation (Sharp et al., 1999; Tranter et al., 2005). Recent studies from the Gulf of Alaska have suggested that glacial systems may be capable of supplying old, labile organic matter to coastal marine ecosystems (Hood et al., 2009). Glacier meltwater may also be an important source of limiting nutrients such as nitrogen, phosphorous and trace metals to downstream environments (Hodson et al., 2005; Hood and Scott, 2008; Lafreniere and Sharp, 2005). For example, studies have hinted that glacially-sourced bioavailable iron (Fe) may be a significant input to coastal oceans surrounding Greenland and Antarctica during the height of summer when primary productivity can be Fe-limited (Raiswell et al., 2008; Raiswell et al., 2006; Statham et al., 2008). Thus, the geochemical cycles of elements in the coastal waters surrounding the GrIS may be strongly influenced by the dynamics of meltwater discharge from the ice sheet.

The overarching goal of my PhD research is to characterize the dynamics of carbon and iron export from the margin of the GrIS to the surrounding North Atlantic Ocean. This region has been subject to an increasing amount of surface melting in the past decade. In this thesis, I use a multi-disciplinary approach to examine the interdependence of glacier hydrology and biogeochemical export from the GrIS. Through a targeted study on a land-terminating outlet glacier system on the southwestern margin of the ice sheet, the questions I explore in Chapters 2-5 are relevant to other outlet glacial systems draining both the Greenland and Antarctic ice sheets. Specifically, I address three questions:

- (1) What are the different water sources comprising the meltwater discharge and how do these contributions change throughout a meltseason?

- (2) What is the concentration, age, and composition of the organic carbon stores beneath the GrIS and how does the exported carbon in glacial runoff change throughout a meltseason?
- (3) Does meltwater runoff from the Greenland ice sheet contribute a significant flux of labile Fe to the surrounding North Atlantic and Arctic Oceans?

In glacial systems, biogeochemical cycles are intrinsically linked to the structure of the subglacial hydrological system, which dictates the extent of water:rock interaction. In alpine glaciers, subglacial flowpaths seasonally evolve from a delayed-flow (channelized system) to a quick-flow (distributed system) drainage (Paterson, 1994; Richards et al., 1996). However, the seasonal evolution of subglacial drainage is poorly constrained for the GrIS. To address this gap in our knowledge, I developed an isotope-mixing model in Chapter 2 to quantify water source contributions to bulk meltwater discharge from a GrIS outlet glacier. Previously, chemical mixing-models in glacial systems were based on bulk parameters, such as electrical conductivity (EC) (Collins, 1979; Gurnell and Fenn, 1984), or individual dissolved ions (e.g. chloride, sulfate) (Brown et al., 1994; Tranter and Raiswell, 1991). However, both of these approaches are hindered by the non-conservative chemical nature of these chemical species under different subglacial conditions. My isotope-mixing model improves upon these past methods by using a combination of conservative stable (oxygen-18, deuterium) and radioactive isotopes (radon-222), illustrating the new application of radon-222 as a quantitative tracer for waters stored at the glacier bed. Results from this work revealed the presence of relatively constant, chemically-enriched delayed flow that becomes progressively diluted with ice-melt throughout the meltseason. This finding is consistent with seasonal subglacial drainage evolution found in alpine systems. Moreover, my model results provide the fundamental hydrological context necessary to interpret and quantify the fluxes of carbon and iron that I focus on for the remainder of my thesis.

In Chapters 3 and 4, I combine molecular- and bulk-level techniques to comprehensively describe for the first time the organic carbon exported in meltwater runoff from the Greenland ice sheet. Specifically I use: (a) ultra-high resolution mass spectrometry to investigate organic carbon composition and infer potential sources, (b) radiocarbon to infer the age, and (c) dissolved C/N ratios to infer the lability. I focus particularly on subglacial organic carbon dynamics and export since our conception of these processes underwent a paradigm shift just over a decade ago, with the revelation that large, active microbial communities are present beneath glaciers (Sharp et al., 1999). This discovery introduced the hypothesis that biological communities are oxidizing the organic carbon stores beneath glaciers, and by extension beneath ice caps and ice sheets. Such a hypothesis has ramifications for global carbon budgets on glacial-interglacial (Sharp et al., 1999) and shorter-term timescales. Approximately  $400 \times 10^{15}$  grams of carbon (equivalent to ~25% of the world's soil organic carbon pool) are presently stored in soils located in regions that were covered by ice during the last glacial maximum (Schlesinger, 1997). Assuming a similar carbon pool was present in these soils during the last interglacial period, then at least some of this carbon was overridden by glaciers and ice sheets during the last glaciation. Microbial utilization (e.g. oxidation/fermentation) of this carbon beneath warm-based sectors of continental ice sheets may have converted some of it to carbon dioxide or methane during the glacial phase of a glacial-interglacial cycle, with considerable impact on carbon budgets for mid-latitude regions (Skidmore et al., 2000). On shorter-term timescales, a couple scenarios exist for the fate of glacially overridden relict organic carbon: (1) the carbon is not utilized, either because it is not bioavailable or there is insufficient subglacial microbial activity, and is simply stored beneath the ice; (2) The carbon is not bioavailable, but is being exported by meltwaters to the marine environment where it is stored (Ohkouchi and Eglinton, 2006); (3) Subglacial microbiota are able to utilize the fossil carbon as a substrate, thus returning to the active global carbon cycle very old organic carbon (Petsch et al., 2001); (4) The relict carbon is bioavailable, but is not entirely consumed by subglacial microbiota and is exported to and utilized in surrounding marine ecosystems. Discernment of which of these scenarios

is occurring presently provides insight as to whether organic carbon respiration, storage, or export is most likely to have occurred beneath the continental glaciers during the glacial phase of a glacial-interglacial cycle, and will increasingly occur as the subglacial hydrological system beneath the GrIS expands. Results from this thesis hint that scenario (4) is most likely, and reveal that the Greenland ice sheet exports a unique type of old, labile organic carbon, distinct from riverine export. The organic carbon exported throughout the meltseason is variable and closely linked to the seasonal evolution of subglacial drainage system, which accesses different carbon stores at the ice sheet bed.

Finally, in Chapter 5, I further explore the potential downstream impact of GrIS discharge on oceanic biogeochemical cycles by quantifying the release of iron from Greenland outlet glaciers to surrounding fjords. Iron is an essential micronutrient for phytoplankton growth, thus its availability ultimately has ramifications for regional and global carbon cycling. This chapter provides new insight into dissolved and particulate Fe concentrations from the GrIS, revealing a potentially significant flux of bioavailable Fe to the North Atlantic ocean in the summer. The labile Fe flux I calculate is on the same order of magnitude as the annual soluble dust flux to the North Atlantic Ocean, a primary source of bioavailable Fe to this ocean (Jickells et al., 2005).

Each chapter in this thesis builds upon the last, to collectively provide a comprehensive view of seasonal biogeochemical cycling and export from ice sheet glacial systems. The hydrology in Chapter 2 is the foundation from which I can determine the annual flux of carbon and iron, and ultimately explain their seasonal variability in glacial runoff rivers. Chapters 3, 4, and 5 then provide more detailed analysis of carbon and iron, key elements in ocean biogeochemical cycles. Glacial biogeochemistry is a new and exploding field of study. This thesis provides some of the first descriptions and estimates of fluxes of biogeochemically significant species (carbon, iron) in ice sheet discharge to surrounding oceans. While the potential contribution of accelerated melt of glaciers, ice caps, and ice sheets to global sea-level rise has been documented (e.g. Box et al., 2006) and is an area of continuing scientific interest (e.g. Joughin et al., 2008; Rignot and Kanagaratnam, 2006) this work reveals that glacier

discharge also carries a unique biogeochemical signature distinct from other (river, hydrothermal) inputs to the oceans. Ultimately by establishing baseline values of the type and amount of organic carbon and iron present beneath the GrIS, this thesis hopefully serves as a foundation for broader investigations into the impact of glacial meltwater runoff to downstream marine environments in the future and the past.



## References

- Box, J.E., Bromwich, D.H., Veenhuis, B.A., Bai, L.S., Stroeve, J.C., Rogers, J.C., Steffen, K., Haran, T., Wang, S.H., 2006. Greenland ice sheet surface mass balance variability (1988-2004) from calibrated polar MM5 output. *Journal of Climate* 19, 2783-2800.
- Brown, G.H., 2002. Glacier meltwater hydrochemistry. *Appl. Geochem.* 17, 855-883.
- Brown, G.H., Sharp, M.J., Tranter, M., Gurnell, A.M., Nienow, P.W., 1994. Impact of post-mixing chemical reactions on the major ion chemistry of bulk meltwaters draining the Haut Glacier D'Arolla, Valais, Switzerland. *Hydrol. Processes* 8, 465-480.
- Collins, D., 1979. Quantitative determination of the subglacial hydrology of two Alpine glaciers. *J. Glaciol.* 23, 347-362.
- Das, S.B., Joughin, I., Behn, M.D., Howat, I.M., King, M.A., Lizarralde, D., Bhatia, M.P., 2008. Fracture propagation to the base of the Greenland Ice Sheet during supraglacial lake drainage. *Science* 320, 778-781.
- Dittmar, T., Kattner, G., 2003. The biogeochemistry of the river and shelf ecosystem of the Arctic Ocean: a review. *Mar. Chem.* 83, 103-120.
- Gurnell, A., Fenn, C., 1984. Flow separation, sediment source areas and suspended sediment transport in a proglacial stream *Catena Supplement* 5, 109-119.
- Hodson, A.J., Mumford, P.N., Kohler, J., Wynn, P.M., 2005. The High Arctic glacial ecosystem: new insights from nutrient budgets. *Biogeochemistry* 72, 233-256.
- Hood, E., Fellman, J., Spencer, R.G.M., Hernes, P.J., Edwards, R., D'Amore, D., Scott, D., 2009. Glaciers as a source of ancient and labile organic matter to the marine environment. *Nature* 462, 1044-U1100.
- Hood, E., Scott, D., 2008. Riverine organic matter and nutrients in southeast Alaska affected by glacial coverage. *Nat. Geosci.* 1, 583-587.
- Jickells, T.D., An, Z.S., Andersen, K.K., Baker, A.R., Bergametti, G., Brooks, N., Cao, J.J., Boyd, P.W., Duce, R.A., Hunter, K.A., Kawahata, H., Kubilay, N., laRoche, J., Liss, P.S., Mahowald, N., Prospero, J.M., Ridgwell, A.J., Tegen, I., Torres, R., 2005. Global iron connections between desert dust, ocean biogeochemistry, and climate. *Science* 308, 67-71.

- Joughin, I., Das, S.B., King, M.A., Smith, B.E., Howat, I.M., Moon, T., 2008. Seasonal speedup along the western flank of the Greenland Ice Sheet. *Science* 320, 781-783.
- Lafreniere, M.J., Sharp, M.J., 2005. A comparison of solute fluxes and sources from glacial and non-glacial catchments over contrasting melt seasons. *Hydrol. Processes* 19, 2991-3012.
- Mernild, S.H., Liston, G.E., Hiemstra, C.A., Steffen, K., Hanna, E., Christensen, J.H., 2009. Greenland Ice Sheet surface mass-balance modelling and freshwater flux for 2007, and in a 1995-2007 perspective. *Hydrol. Processes* 23, 2470-2484.
- Ohkouchi, N., Eglinton, T.I., 2006. Radiocarbon constraint on relict organic carbon contributions to Ross Sea sediments. *Geochem. Geophys. Geosyst.* 7.
- Paterson, W., 1994. *The Physics of Glaciers*, 3rd ed. Butterworth-Heinemann, Oxford, UK.
- Petsch, S.T., Eglinton, T.I., Edwards, K.J., 2001. C-14-dead living biomass: Evidence for microbial assimilation of ancient organic carbon during shale weathering. *Science* 292, 1127-1131.
- Raiswell, R., Benning, L.G., Tranter, M., Tulaczyk, S., 2008. Bioavailable iron in the Southern Ocean: the significance of the iceberg conveyor belt. *Geochem. Trans.* 9.
- Raiswell, R., Tranter, M., Benning, L.G., Siegert, M., De'ath, R., Huybrechts, P., Payne, T., 2006. Contributions from glacially derived sediment to the global iron (oxyhydr)oxide cycle: Implications for iron delivery to the oceans. *Geochim. Cosmochim. Acta* 70, 2765-2780.
- Richards, K., Sharp, M., Arnold, N., Gurnell, A., Clark, M., Tranter, M., Nienow, P., Brown, G., Willis, I., Lawson, W., 1996. An integrated approach to modelling hydrology and water quality in glacierized catchments. *Hydrol. Processes* 10, 479-508.
- Rignot, E., Kanagaratnam, P., 2006. Changes in the Velocity Structure of the Greenland Ice Sheet. *Science* 311, 986-990.
- Schlesinger, W., 1997. *Biogeochemistry: An analysis of global change*, 2nd ed. Academic Press, Boston, MA.

- Sharp, M., Parkes, J., Cragg, B., Fairchild, I.J., Lamb, H., Tranter, M., 1999. Widespread bacterial populations at glacier beds and their relationship to rock weathering and carbon cycling. *Geology* 27, 107-110.
- Skidmore, M.L., Foght, J.M., Sharp, M.J., 2000. Microbial life beneath a high Arctic glacier. *Appl. Environ. Microbiol.* 66, 3214-3220.
- Statham, P.J., Skidmore, M., Tranter, M., 2008. Inputs of glacially derived dissolved and colloidal iron to the coastal ocean and implications for primary productivity. *Global Biogeochem. Cycles* 22.
- Tranter, M., Raiswell, R., 1991. The composition of the englacial and subglacial component in bulk meltwaters draining the Gornergletscher, Switzerland. *J. Glaciol.* 37, 59-66.
- Tranter, M., Sharp, M.J., Lamb, H.R., Brown, G.H., Hubbard, B.P., Willis, I.C., 2002. Geochemical weathering at the bed of Haut Glacier d'Arolla, Switzerland - a new model. *Hydrol. Processes* 16, 959-993.
- Tranter, M., Skidmore, M., Wadham, J., 2005. Hydrological controls on microbial communities in subglacial environments. *Hydrol. Processes* 19, 995-998.

## Chapter 2

### Seasonal evolution water contributions to discharge from a Greenland outlet glacier: insight from a new isotope-mixing model \*

#### Abstract

The Greenland ice sheet (GrIS) subglacial hydrological system may undergo a seasonal evolution, with significant geophysical and biogeochemical implications. We present results from a new isotope mixing model to quantify the relative contributions of surface snow, glacial ice, and delayed flow to the bulk meltwater discharge from a small (~5-km<sup>2</sup>) land-terminating GrIS outlet glacier during melt onset (May) and at peak melt (July). We use radioactive (radon-222) and stable isotopes (oxygen-18, deuterium) to differentiate the source-water contributions. Atmospherically-derived beryllium-7 further constrains meltwater transit time from the glacier surface to the ice margin. We show that (i) radon-222 is a promising tracer for glacial waters stored at the bed and (ii) a quantitative chemical mixing model can be constructed by combining radon-222 and the stable water isotopes. Applying this model to the bulk subglacial outflow from our study area, we find a constant delayed flow (stored) component from melt onset through peak melt. This component is diluted first by snow-melt and then by increasing glacial ice-melt as the season progresses. Results from this pilot study are consistent with the hypothesis that subglacial drainage beneath land-terminating sections of the GrIS undergoes a seasonal evolution from a distributed system to a channelized one.

---

\* Published as: Bhatia, M., S.B. Das, E.B. Kujawinski, P. Henderson, A. Burke, and M.A. Charette (2011). Seasonal evolution water contributions to discharge from a Greenland outlet glacier: insight from a new isotope-mixing model, *Journal of Glaciology*, 57(205): 929-940.

## Seasonal evolution of water contributions to discharge from a Greenland outlet glacier: insight from a new isotope-mixing model

Maya P. BHATIA,<sup>1</sup> Sarah B. DAS,<sup>2</sup> Elizabeth B. KUJAWINSKI,<sup>3</sup> Paul HENDERSON,<sup>3</sup>  
Andrea BURKE,<sup>1</sup> Matthew A. CHARETTE<sup>3</sup>

<sup>1</sup>MIT/WHOI Joint Program in Oceanography/Applied Ocean Sciences and Engineering, Department of Geology and Geophysics, Woods Hole Oceanographic Institution, Woods Hole, Massachusetts 02543, USA  
E-mail: mayab@mit.edu

<sup>2</sup>Department of Geology and Geophysics, Woods Hole Oceanographic Institution, Woods Hole, Massachusetts 02543, USA

<sup>3</sup>Department of Marine Chemistry and Geochemistry, Woods Hole Oceanographic Institution, Woods Hole, Massachusetts 02543, USA

**ABSTRACT.** The Greenland ice sheet (GrIS) subglacial hydrological system may undergo a seasonal evolution, with significant geophysical and biogeochemical implications. We present results from a new isotope-mixing model to quantify the relative contributions of surface snow, glacial ice and delayed flow to the bulk meltwater discharge from a small ( $\sim 5 \text{ km}^2$ ) land-terminating GrIS outlet glacier during melt onset (May) and at peak melt (July). We use radioactive ( $^{222}\text{Rn}$ ) and stable isotopes ( $^{18}\text{O}$ , deuterium) to differentiate the water source contributions. Atmospherically derived  $^7\text{Be}$  further constrains meltwater transit time from the glacier surface to the ice margin. We show that (1)  $^{222}\text{Rn}$  is a promising tracer for glacial waters stored at the bed and (2) a quantitative chemical mixing model can be constructed by combining  $^{222}\text{Rn}$  and the stable water isotopes. Applying this model to the bulk subglacial outflow from our study area, we find a constant delayed-flow (stored) component from melt onset through peak melt. This component is diluted first by snowmelt and then by increasing glacial ice melt as the season progresses. Results from this pilot study are consistent with the hypothesis that subglacial drainage beneath land-terminating sections of the GrIS undergoes a seasonal evolution from a distributed to a channelized system.

### 1. INTRODUCTION

The Greenland ice sheet (GrIS) contributes significant quantities of meltwater to the surrounding North Atlantic and Arctic Oceans (Solomon and others, 2007). During the high-melt year of 2007, for example, the GrIS contributed an estimated  $523 \text{ km}^3 \text{ a}^{-1}$  surface runoff (Mernild and others, 2009), equivalent to the combined mean annual discharge from the four large North American pan-Arctic rivers, Yukon, Mackenzie, Peel and Beck (Shiklomanov, 2009). Recent evidence that a large fraction of annual surface meltwater likely drains to the bed of the GrIS (McMillan and others, 2007; Das and others, 2008; Krawczynski and others, 2009) suggests that significant portions of the GrIS subglacial hydrological system may undergo a seasonal evolution, akin to those observed beneath alpine glaciers (Shepherd and others, 2009; Bartholomew and others, 2010). This routing suggests there is potential for substantial meltwater interaction with underlying subglacial till and bedrock along seasonally evolving flow paths. Despite recent interest in the GrIS subglacial hydrological system (Box and Ski, 2007; Joughin and others, 2008; Shepherd and others, 2009; Bartholomew and others, 2010; Tsai and Rice, 2010), understanding of the subglacial drainage seasonal evolution remains limited and poorly constrained.

In alpine glacial systems, subglacial flow paths can vary seasonally between two end-member systems: channelized drainage (quick flow) and distributed drainage (delayed flow) (Paterson, 1994). Channelized drainage systems are a series of large tunnels incised into the bedrock, the overlying ice or the till, which facilitate localized and rapid water flow ( $\sim 1 \text{ m s}^{-1}$ ) to the glacier front. They are prevalent at the peak

of the summer melt season (Paterson, 1994; Benn and Evans, 1998) and transport the bulk of surface ice melt that has drained to the bed (Richards and others, 1996; Nienow and others, 1998). In comparison, distributed drainage systems, envisioned as a series of linked cavities, lie along the ice/bed interface, and may include a constant source of water from basal ice melt and groundwater in contact with glacial till (Paterson, 1994). Such systems have characteristically slower water transit times ( $\sim 0.01 \text{ m s}^{-1}$ ), higher water pressures and are water-full for most of the year (Richards and others, 1996; Benn and Evans, 1998). Additionally, they may transport a significant proportion of early-season snowmelt to the glacier front (Nienow and others, 1998).

The seasonal evolution of subglacial drainage conditions has important geophysical and biogeochemical implications. From a geophysical perspective, the partitioning of meltwater between these two different drainage systems strongly influences basal water pressures and thus sliding velocities (Paterson, 1994). From a biogeochemical perspective, the degree of water/rock contact dictates the chemical enrichment of discharge waters exported to surrounding marine ecosystems, and may fuel subglacial microbial processes (Sharp and others, 1999; Skidmore and others, 2000). Microbial communities could in turn facilitate the release of additional nutrients and metals, amplify chemical weathering reactions and/or utilize previously overridden organic carbon (Tranter and others, 2002; Wadhwa and others, 2008; Bhatia and others, 2010). Thus, the geochemical cycles of major and minor elements in the coastal waters surrounding the GrIS may be strongly influenced by the temporal dynamics of subglacial discharge (as observed

in other regions: Raiswell and others, 2006; Hood and Scott, 2008; Hood and others, 2009), and in particular by the release of water that has been stored at the bed.

The development of a chemical mixing model that can successfully differentiate water source contributions and subglacial flow paths will complement existing geophysical and active-tracer methods used to study seasonally evolving subglacial hydrological systems (Nienow and others, 1998; Bartholomew and others, 2010). The interaction of surface meltwater with the glacier bed alters its chemical composition from dilute snow- and ice melt to chemically enriched subglacial discharge waters. Thus, in theory, variations in solute concentrations could be used to infer the evolution of the subglacial drainage network by differentiating water source contributions. This approach is promising because distributed drainage systems produce discharge waters with significantly enriched chemical signatures due to the longer residence time at the bed compared to channelized drainage systems. Initial mixing-model efforts based the separation of discharge components on bulk properties such as electrical conductivity (EC) (Collins, 1979; Gurnell and Fenn, 1984). However, a model with EC as its defining chemical parameter is poorly constrained because EC is not conservative in glacial systems, and is subject to temporal variations in chemical signature and to post-mixing solute acquisition (Sharp and others, 1995). Consequently, individual dissolved species (e.g. sulfate, chloride) whose provenance is exclusive to specific discharge components have been increasingly used instead of EC (Tranter and Raiswell, 1991; Brown and others, 1994; Tranter and others, 1997; Mitchell and others, 2001). Despite this progress, discharge component separations remain challenging because individual solutes may not retain unique signatures over time and may be involved in subglacial biological reactions across glacial catchments (Sharp and others, 1995; Brown, 2002). Thus, the potential of hydrochemical separation methods in glacier systems has yet to be fully realized (Sharp and others, 1995; Brown, 2002).

Here we introduce a new multi-component isotope-mixing model combining the radioactive isotope radon-222 ( $^{222}\text{Rn}$ ) with the stable water isotopes oxygen-18 ( $^{18}\text{O}$ ) and deuterium (D) as passive flow tracers. These natural isotopic tracers have unique end-member signatures for different reservoirs ultimately contributing to the total glacial outflow, and are not subject to additional post-mixing enrichment or alteration. We then apply this model to quantify the relative contributions of different water reservoirs to the bulk meltwater discharge at a small land-terminating outlet glacier along the western margin of the GrIS in three stages: (1) identified conceptual end-member water reservoirs (surface snow, glacial ice and delayed flow), (2) identified unique passive flow isotopic tracers for each water reservoir ( $\delta^{18}\text{O}$ , D and  $^{222}\text{Rn}$ ), and (3) applied end-member mixing analysis to estimate relative contributions of each conceptual water reservoir. We limit our separation to these three conceptual reservoirs because hydrographic separation of all potential drainage components is not possible without additional isotopes or end-member analyses. Finally, we investigate the potential for using beryllium-7 ( $^7\text{Be}$ ), a naturally occurring radioisotope produced in the atmosphere, as a tracer for the transit of snowmelt through the subglacial drainage system. To our knowledge, this is the first time that beryllium has been used in a glacial system as a tracer of hydrological flow.

Through the application of radioisotopes, this pilot study represents a new direction in the use of chemical mixing models to delineate subglacial drainage structure, even though full hydrograph separation of all potential drainage components remains elusive.

## 2. MODEL THEORY

The basic tenets of radon radiochemistry suggest that it has the potential to be an effective tracer of delayed-flow basal waters characteristic of distributed subglacial drainage systems. Radon, an inert noble gas, is a daughter product of radium-226 within the uranium-238 decay series that is naturally present in soil, sediment and rocks. Since the uranium content of solids and the degree of water/rock interaction will determine the amount of radon enrichment in a given water parcel, groundwater will be highly enriched in radon, as should any surface meltwater or basal ice melt that has been stored subglacially. In contrast, surface snowmelt and glacial ice melt that is quickly routed through the subglacial environment has minimal lithogenic sediment contact, and so should be relatively devoid of radon. Radon has been successfully applied as a tracer of submarine groundwater discharge (Cable and others, 1996; Corbett and others, 1997; Burnett and Dulaiova, 2003) but has only recently been applied in a glacial setting (Kies and others, 2010). Moreover, the high uranium content of the Greenland fractured silicate bedrock suggests that waters in contact with the GrIS subglacial environment will be particularly enriched in radon (Kraemer and Geneux, 1998).

Our new model is also based on the hypothesis that the surface snow and glacial ice at a GrIS outlet glacier have unique  $\delta^{18}\text{O}$  and  $\delta\text{D}$  signatures. Stable water isotopes have been used extensively in glacial settings for a variety of applications from ice-core paleotemperature reconstructions (e.g. Jouzel and others, 1997) to delineation of drainage basins on the GrIS (Reeh and Thomsen, 1993). The GrIS margin, in contrast to alpine catchments (Theakstone, 2003), possesses large isotopic differences between snow and ice components (e.g. Reeh and Thomsen, 1993). This is because seasonal surface snow carries the enriched signature of present-day precipitation at relatively high temperatures and low elevation across the ablation zone, whereas underlying marginal glacial ice will have comparatively more depleted values, reflecting its depositional and flow history from higher elevations and/or colder times (Dansgaard and others, 1971).

## 3. FIELD SITE AND SAMPLING OVERVIEW

Sampling for this study was conducted at two primary field locations along the GrIS southwestern margin. Samples were collected in 2008 in the vicinity of a small ( $\sim 5\text{ km}^2$ ; see Section 3.3 for more details) land-terminating outlet glacier 125 km south of Jakobshavn Isbræ ('N' glacier;  $68^\circ 02' 34''\text{ N}$ ,  $50^\circ 16' 08''\text{ W}$ ), with a surface elevation range from  $\sim 100$  to  $\sim 500\text{ m}$  (Fig. 1a and b). Supraglacial samples were collected from surface snow and a meltwater pond on the surface of 'N' glacier (Fig. 1c), and glacial ice samples at the margin of the glacier; subglacial samples were collected from the outflow stream (Fig. 1d) exiting the base of the glacier at two locations: the mouth where the outflow first emerged, and a downstream site  $\sim 0.15\text{ km}$  from the outflow mouth.

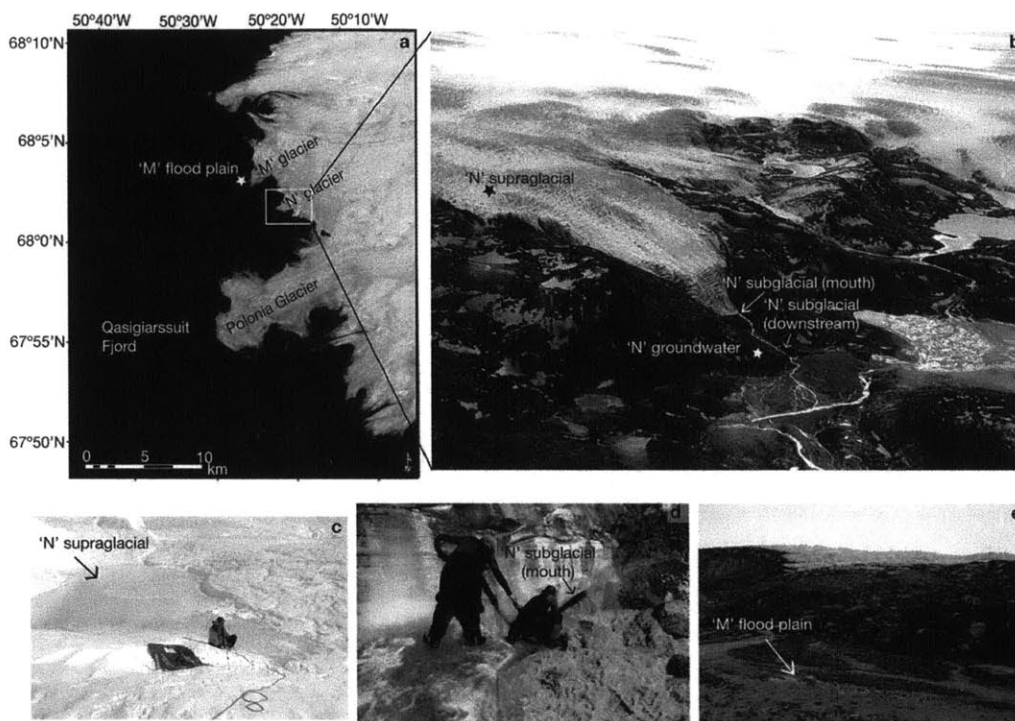


**Fig. 1.** (a) Landsat image of the 2008 ice-margin field site. Sampling was concentrated at 'N' glacier and on the 'M' flood plain. (b) Air photo of the land-terminating outlet glacier ('N' glacier) focused upon in this study, with specific sample sites labeled. (c) Photo of the supraglacial pond sampled on the surface of 'N' glacier. (d) Photo of the mouth of the 'N' glacier outflow stream. (e) Photo of the 'M' flood-plain sample site.

Groundwater samples were taken from the bank of the 'N' glacier proglacial stream and the flood plain of an adjacent larger glacier ('M' glacier) (Fig. 1e). Most samples were acquired while field personnel were on-site in late spring (16 May–1 June) and at the height of the summer melt season (10–17 July); automated instrumentation was used to measure and/or sample selected parameters between 2 June and 15 July. Constraints on end-member values were supplemented with supraglacial snow, ice and meltwater samples collected in July 2007 and 2008 within the ablation zone (980 m elevation) 70 km north of the primary study site (68°34'16" N, 49°21'29" W).

### 3.1. Meteorological measurements

Local meteorological conditions were obtained using a HOBO U30-NRC weather station equipped with a tipping-bucket rain gauge and data logger installed at 100 m elevation and ~1.5 m above the ground in the proglacial area in the vicinity of 'N' glacier. Shielded air temperatures and precipitation (0.2 mm resolution) were recorded every 5 min for the duration of the 2008 field season (16 May–17 July) with some gaps (73 min on day 138, 7 min on day 146, and 72.45 hours from day 151 to day 154). Hourly and daily moving averages were calculated for temperature, and daily total values were summed for precipitation. All times are reported in Greenland local time (GMT–3 h).

### 3.2. Discharge measurements

Stream discharge was measured at the 'N' glacier outflow stream using the velocity–area method and pressure transducers (HOBO U20 Water Level Logger and InSitu Level TROLL 300 Logger) at a location ~0.15 km downstream of the glacier mouth. Stream velocities were measured using a manual flowmeter (General Oceanics Mechanical Flow-meter, model 2030R). A horizontal transect was established across the stream, and triplicate velocity measurements were taken at evenly spaced subsections (verticals) along the stream transect. The triplicate measurements were averaged to produce a single velocity at each vertical. Discharges for each stream subsection were calculated as the product of the subsection velocity and area (Dingman, 2002) and summed to obtain a total stream discharge ( $\text{m}^3 \text{s}^{-1}$ ). Pressure transducers were used to continuously measure stream stage (depth). Water pressure was sensed in 10 min intervals from 31 May (19:00) to 16 July, and was converted to stream stage after correction for atmospheric pressure using a record sensed by an InSitu BaroTROLL Logger. A stage–discharge rating curve ( $r^2=0.76$ ,  $p<0.01$ ) was developed using 12 discharge measurements. The rating curve was used to produce a continuous discharge record for the period with continuous stage measurements with point discharges only available from 19 to 27 May. Total meltwater discharge measured

from 'N' glacier between 31 May and 16 July is  $6.4 \times 10^6 \text{ m}^3$ . The error associated with the discharge is estimated to be  $\pm 7\%$  (following Dingman, 2002).

### 3.3. Catchment delineation

Lacking adequately resolved ice thickness and surface and basal topography for this region, we rely on interferometric synthetic aperture radar (InSAR)-derived ice velocity (personal communication from I. Joughin, 2011) to delineate the 'N' glacier surface area. We defined the catchment area at the downstream end to be bounded by the margins of the outlet glacier at the ice-sheet edge. We delimited the top of the catchment area where the background ice-sheet flow diverged from 'N' glacier. We were further limited in this approach by the coarse resolution (500m) of the InSAR, so we defined divergence as separation of streamlines by one or more grid spacings. Using this method, we estimate the glacier length to be 5 km and the surface area to be  $5 \text{ km}^2$ , which we defined as the catchment area for the purposes of evaluating surface meltwater input. To evaluate the reasonableness of this estimate, we calculated the total surface melt over this area required to match the cumulative discharge measured at the front of 'N' glacier. This calculation yielded a mean melt rate of  $\sim 0.03 \text{ m d}^{-1}$  (i.e. 1.28 m/46 days), a value well within the range of summer melt rates previously reported for the western margin of the GrIS (Box and others, 2006), thus providing an independent assessment of our catchment area.

## 4. END-MEMBER WATER RESERVOIRS AND ISOTOPE MEASUREMENTS

Three conceptual end-member water reservoirs contributing to the bulk subglacial discharge from 'N' glacier were defined: (1) surface snow, (2) glacier ice and (3) delayed flow, where surface snow and glacier ice represent water sources, and delayed flow is a hydrological flow path. Samples were collected from the bulk discharge as well as each end-member (where possible) across the catchment. Samples were then analyzed for  $\delta^{18}\text{O}$ ,  $\delta\text{D}$ ,  $^{222}\text{Rn}$  and  $^7\text{Be}$ . In this study, delayed flow is operationally defined as water stored at the base on a timescale of days to weeks. These waters could consist of supraglacial waters stored at the base, basal-ice melt and groundwater. The timescale is dictated by the time required for radon ( $\tau^{1/2} = 3.8$  days) to approach secular equilibrium activity with its parent radium-226. At this activity, the production rate of radon is equal to its decay rate, and the radon content of waters stored at the bed is constant.

### 4.1. Stable water isotopes

Both seasonal-snow and glacial-ice  $\delta^{18}\text{O}$  and  $\delta\text{D}$  values vary with surface elevation, so samples were collected from this study to constrain these values. Samples include measurements from surface snow ( $\sim 300 \text{ m}$  elevation), glacial ice ( $\sim 100$ ,  $\sim 300$  and  $\sim 1000 \text{ m}$  elevation), groundwater ( $\sim 100 \text{ m}$  elevation) and basal ice ( $\sim 100 \text{ m}$  elevation). We then estimated the range of expected  $\delta^{18}\text{O}$  values over the 'N' glacier catchment (100–500 m surface elevation). Snow  $\delta^{18}\text{O}$  values were estimated using a 0.5‰ depletion per 100 m rise in elevation to account for the effect of altitude on  $\delta^{18}\text{O}$  (Clark and Fritz, 1997). Glacial ice  $\delta^{18}\text{O}$  values were estimated using an empirical relationship defined by Reeh

and Thomsen (1993) at a nearby GrIS location. The average difference (+2.5%) between the measured ice  $\delta^{18}\text{O}$  at both 100 and 300 m and that calculated using the relationship defined by Reeh and Thomsen (1993) was used to correct the calculated  $\delta^{18}\text{O}$  ice value at 500 m. Bulk discharge samples for  $\delta^{18}\text{O}$  and  $\delta\text{D}$  measurements from the 'N' glacier outflow stream mouth and downstream sites were also collected. The discharge samples were collected at least daily from 18 May to 1 June and 10 to 16 July. Between 2 June and 9 July an ISCO 3700 autosampler (Teledyne Isco Inc.) was used to collect samples in intervals ranging from 1.5 to 4.5 days.

All samples were collected in acid-cleaned and sample-rinsed 250 or 1000 mL polypropylene bottles from which two 10 mL aliquots were taken for  $\delta^{18}\text{O}$  and  $\delta\text{D}$  analysis. Samples were frozen upon return to the laboratory until analysis. Thawed water samples were analyzed for  $\delta^{18}\text{O}$  and  $\delta\text{D}$  at the University of California Davis Stable Isotope Facility on a Laser Water Isotope Analyzer V2 (Los Gatos Research, Inc., Mountain View, CA, USA) with precisions of  $\leq 0.3\%$  for  $\delta^{18}\text{O}$  and  $\leq 0.8\%$  for  $\delta\text{D}$ .

### 4.2. Radon-222

Water samples were collected for end-member  $^{222}\text{Rn}$  activity from a supraglacial meltwater pond near the edge of 'N' glacier (22 and 31 May), from groundwater along the stream bank 0.15 km from the mouth of 'N' glacier (25 May) and from groundwater in the flood plain of 'M' glacier (28 May). Groundwater samples were taken at  $\sim 0.4 \text{ m}$  depth, using a stainless-steel drive point piezometer. Daily 'N' glacier outflow samples were collected on 18, 21–23, 27 and 29–31 May and 10–16 July from the mouth of 'N' glacier. Higher-resolution time-series samples (6 hour intervals) were taken on 31 May and 12 July. EC was also measured on-site using a Russell RF060C meter (Thermo Electron). Radon-222 samples were collected without headspace in glass 250 mL bottles, and were quantified using a RAD-7 continuous radon monitor (DurrIDGE Inc.) (Burnett and Dulaiova, 2003). Typical RAD-7 uncertainties were 14%, with a range of 8–37% for the lowest measured  $^{222}\text{Rn}$  activities in this study. All samples were analyzed within 24 hours of collection. Results were corrected for radioactive decay between the time of collection and analysis and reported as an activity in disintegrations per minute per liter ( $\text{dpm L}^{-1}$ ). A model II (geometric mean) regression was used to compare the radon and EC data since both are measured (dependent) parameters with different units (Ricker, 1973; Sofal and Rohlf, 1995).

In order to determine the maximum potential radon activities in saturated subglacial sediments, laboratory equilibration experiments were conducted using sediment collected from the proglacial area at the mouth of the 'N' glacier outflow ( $n=1$ ) and downstream ( $n=2$ ). Approximately 100 g of wet sediment were incubated with  $\sim 0.5 \text{ L}$  radium-free water in sealed 1 L high-density polyethylene bottles, following methods described by Dulaiova and others (2008). The sediment was incubated for at least 3 weeks and the radon was subsequently quantified via an alpha scintillation technique. Each sediment equilibration sample was analyzed twice. The measured radon activities ( $\text{dpm g}^{-1}$ ) in the wet sediment were converted to pore-water radon activities ( $\text{dpm L}^{-1}$ ) using a wet bulk density of  $2.3 \text{ g cm}^{-3}$  and a porosity of 0.2 (Dulaiova and others, 2008).



**Table 1.** Isotope tracer values used to initially solve the end-member mixing model equations (Equations (1–4)). For the delayed-flow waters a basal ice sample collected at 100 m elevation was used for the  $\delta^{18}\text{O}$  and  $\delta\text{D}$  ratios, while the maximum ‘N’ glacier outflow radon activity was used as the  $^{222}\text{Rn}$  end-member. The radon activity of the surface snow and glacial ice reservoirs was set to zero

Water source	Elevation m	$\delta^{18}\text{O}$ ‰	$\delta\text{D}$ ‰	$^{222}\text{Rn}$ dpm L <sup>-1</sup>
Surface snow	300	-12.3	-89.9	0
Glacial ice	300	-28.2	-216.1	0
Delayed-flow waters	100	-29.6	-227.2	209.5

### 4.3. Beryllium-7

Water samples (~190L) for measuring  $^7\text{Be}$  activity were collected from a supraglacial meltwater pond near the edge of ‘N’ glacier (22 May) and from a supraglacial meltwater stream at the inland ice-sheet site (20 July). Two ‘N’ glacier discharge samples were collected for  $^7\text{Be}$  (21 May and 11 July). Water was collected in a large plastic container and processed on-site. The supraglacial samples were not filtered prior to collection due to the lack of particles in these waters; however, the ‘N’ glacier outflow stream sample was filtered through a 10  $\mu\text{m}$  Hytrec II cartridge prior to collection. A 1 mL aliquot of stable  $^9\text{Be}$  (10 000 ppm) was added as a yield monitor, and iron oxide ( $\text{Fe}(\text{OH})_3$ ) fibers were used to pre-concentrate both the  $^7\text{Be}$  and  $^9\text{Be}$  from the water sample (Andrews and others, 2008). Periodic aliquots (20 mL) of the fiber column filtrate were taken and subsequently analyzed on an inductively coupled plasma mass spectrometer (ICP-MS) at the Woods Hole Oceanographic Institution (WHOI) to determine the collection efficiencies for  $^7\text{Be}$  (Andrews and others, 2008). The fibers were combusted at 820°C for 16 hours and the ash was analyzed for  $^7\text{Be}$  via gamma spectroscopy (Andrews and others, 2008). Samples were counted for 2 days, and corrected for decay since the time of collection. Beryllium recovery on the fibers averaged 75%. Results are presented as activities in units of dpm L<sup>-1</sup>.

## 5. MODEL DESCRIPTIONS

### 5.1. Isotope-mixing model

A multi-component isotope-mixing model using the stable water isotope values and radon measurements described above was constructed to quantify the relative fraction of flow contributed by each end-member water source to the total discharge exiting ‘N’ glacier using

$$\text{Mass conservation: } f_1 + f_2 + f_3 + f_4 = 1 \quad (1)$$

$$\delta^{18}\text{O: } f_1\delta^{18}\text{O}_1 + f_2\delta^{18}\text{O}_2 + f_3\delta^{18}\text{O}_3 = \delta^{18}\text{O}_4 \quad (2)$$

$$\delta\text{D: } f_1\delta\text{D}_1 + f_2\delta\text{D}_2 + f_3\delta\text{D}_3 = \delta\text{D}_4 \quad (3)$$

$$^{222}\text{Rn: } f_1^{222}\text{Rn}_1 + f_2^{222}\text{Rn}_2 + f_3^{222}\text{Rn}_3 = ^{222}\text{Rn}_4, \quad (4)$$

where  $f$  is the fraction of flow and subscripts indicate the following: 1 is the snow end-member, 2 is the glacial ice end-member, 3 is the delayed-flow end-member and 4 is the ‘N’ glacier outflow. The end-member water source and ‘N’

**Table 2.** Range of isotope tracer values used in end-member mixing model sensitivity analysis

Water source	$\delta^{18}\text{O}$ ‰	$\delta\text{D}$ ‰	$^{222}\text{Rn}$ dpm L <sup>-1</sup>
Surface snow	-11 to -16	-78 to -118	0
Glacial ice	-25 to -30	-190 to -230	0
Delayed-flow waters	-27 to -30	-206 to -230	200–1600

glacier outflow stream isotope values (Table 1) were used to solve the system of equations using singular value decomposition. The radon content in the snow and glacial ice end-members ( $^{222}\text{Rn}_1$  and  $^{222}\text{Rn}_2$ ) was set to zero (negligible in situ source of  $^{222}\text{Rn}$ ). To initially solve the model, the highest radon activity measured in the ‘N’ outflow stream (210 dpm L<sup>-1</sup>) was operationally defined as  $^{222}\text{Rn}_3$ , effectively normalizing the entire dataset to this maximum concentration. In this study the sediment radon flux to the delayed-flow reservoir is assumed to be a continuous, steady-state process, so a loss term due to radioactive decay is not included in the radon end-member mixing equation.

### 5.2. Mixing-model sensitivity analysis

A sensitivity analysis employing a range of end-member values (Table 2) was conducted to put envelopes of uncertainty on the model fraction results ( $f_1$ ,  $f_2$ ,  $f_3$ ) by simultaneously varying each of the end-member water reservoir values across a range of reasonably determined limits. The range of surface snow  $\delta^{18}\text{O}$  values utilized was chosen to incorporate a maximum isotopic depletion from the original snow during metamorphism and melting (Taylor and others, 2001). Though the mean snowmelt will become progressively enriched throughout the summer melt season due to the early removal of isotopically light water (Cooper, 1998; Taylor and others, 2001), this isotopic enrichment is difficult to predict without additional samples of the total snowpack oxygen isotope signature. However, the model results will be most affected by the potential for depleted snow end-member values, which encroach on the glacial ice  $\delta^{18}\text{O}$  values. The glacial ice  $\delta^{18}\text{O}$  values were chosen to reflect the range of ice isotopic values across the elevation range of the ‘N’ glacier catchment that could potentially contribute to the outflow waters. The range of delayed-flow  $\delta^{18}\text{O}$  values employed in the sensitivity analysis encapsulated the  $\delta^{18}\text{O}$  content of the groundwater and basal ice at ‘N’ glacier. Corresponding  $\delta\text{D}$  ranges for each end-member water source were calculated directly from these  $\delta^{18}\text{O}$  values using the global meteoric waterline ( $\delta\text{D} = 8\delta^{18}\text{O} + 10$ ). The range of potential  $^{222}\text{Rn}$  activities in the delayed-flow end-member was defined using the maximum activity measured in the ‘N’ outflow stream as the lower bound and the lowest groundwater radon activity measured in this study as an upper bound. A better estimate of the  $^{222}\text{Rn}$  activity in the delayed-flow waters could be attained by sampling outflow waters during the early season before they are diluted by any surface input. This could be achieved with standard automated continuous radon monitors that measure the  $^{222}\text{Rn}$  activity of the outflow stream (e.g. Dulaiova and others, 2005; Schmidt and others, 2008).

### 5.3. Transit time model

The surface snow and glacial ice fraction results ( $f_1$  and  $f_2$ ) from the isotope model were used to estimate a transit time for snowmelt from the surface to its exit at the glacier front using  $^7\text{Be}$ .  $^7\text{Be}$  is continuously produced in the atmosphere and is deposited to the surface environment (e.g. the ice-sheet surface) via wet (precipitation events) and dry (aerosol) deposition (Nimz, 1998). Its unique atmospheric source in combination with its short half-life ( $\tau_{1/2} = 53.3$  days) suggests that  $^7\text{Be}$  should be present in the surface snow end-member, while occurring below detection levels in glacial ice and delayed-flow waters that are older than  $\sim 300$  days. Thus, assuming constant production on the surface and no  $^7\text{Be}$  in the delayed-flow reservoir ( $f_3$ ), the  $^7\text{Be}$  activity in the outflow stream can be described using a steady-state model:

$$^7\text{Be}: \left( f_1 ^7\text{Be}_{1,t0} + f_2 ^7\text{Be}_2 \right)_{t0} e^{-\lambda t} = ^7\text{Be}_{4\text{eff},t} \quad (5)$$

where  $t$  is time (days),  $\lambda$  is the decay constant for  $^7\text{Be}$  ( $0.013 \text{ d}^{-1}$ ),  $^7\text{Be}_{1,t0}$  is the  $^7\text{Be}$  activity of the surface snow end-member water source,  $^7\text{Be}_2$  is the  $^7\text{Be}$  activity of the glacial ice, and  $^7\text{Be}_{4\text{eff},t}$  is the effective  $^7\text{Be}$  activity in the 'N' glacier outflow stream.  $^7\text{Be}_{4\text{eff},t}$  accounts for any scavenging of  $^7\text{Be}$  onto subglacial particles and is calculated as the sum of the  $^7\text{Be}$  in the 'N' glacier outflow stream ( $^7\text{Be}_{\text{dissolved}}$ ) and the  $^7\text{Be}$  scavenged by particles in the subglacial environment ( $^7\text{Be}_{\text{particulate}}$ ). The former was measured in the 'N' outflow stream on 21 May, and the latter was estimated using

$$^7\text{Be}_{\text{particulate}} = K_d C_p ^7\text{Be}_{\text{dissolved}}, \quad (6)$$

where  $K_d$  is particle-water coefficient ( $(^7\text{Be}/\text{mass of particles})/(^7\text{Be}/\text{mass of water})$ ) and  $C_p$  is suspended sediment concentration ( $\text{mg mL}^{-1}$ ) measured in May. A  $K_d$  value of 5000 was assumed, which is within the range of previously published  $^7\text{Be}$   $K_d$  values ( $10^3$ – $10^4$ ) (Olsen and others, 1986). Rearranging Equation (5) to solve for time yields

$$t = -1/\lambda \ln \left( \frac{^7\text{Be}_{4\text{eff},t}}{f_1 ^7\text{Be}_{1,t0} + f_2 ^7\text{Be}_{2,t0}} \right). \quad (7)$$

Here time is defined as the transit time from the glacier surface to the front since  $^7\text{Be}$  is only produced on the surface, and we have accounted for any sinks (scavenging) in the subglacial environment.

## 6. RESULTS AND DISCUSSION

### 6.1. Climatology and discharge

'N' glacier discharge was highly sensitive to air-temperature fluctuations, with the two clearly co-varying throughout the melt season (Fig. 2a and b). We did not capture the melt onset, as there was already meltwater discharge on our arrival at the field site on 19 May. Nonetheless, a cold period towards the beginning of our record (days 142–144), characterized by subfreezing air temperatures, reduced discharge almost to zero. Following this cold period, air temperature and discharge increased from mid-May to early June as the melt season progressed. Daily-average temperatures at the ice edge then generally remained above  $6^\circ\text{C}$  for the remainder of the study period. Daily-average discharge also stabilized around  $1.6$ – $1.8 \text{ m}^3 \text{ s}^{-1}$  until late July, when a cold period precipitated a drop in discharge back towards early-season values. We also observed a strong diurnal cycle

in subglacial stream discharge that was highly responsive to, although offset from, the insolation-driven diurnal temperature cycle. Peak discharge lagged peak air temperature by an average of 2.4 hours (range 1–5.6 hours), while the average lag in minimum discharge was 2.7 hours (range 0.35–4.7 hours) from the minimum temperature. The mean diurnal amplitude in the temperature and discharge records was  $7.3^\circ\text{C}$  and  $0.39 \text{ m}^3 \text{ s}^{-1}$ , with maximum and minimum daily discharges occurring between 15:00 and 21:00 and 4:00 and 8:00, respectively.

### 6.2. Radon as a tracer for delayed-flow waters

We did not detect any radon in a sample from a supraglacial meltwater pond on the surface of 'N' glacier, thus confirming our assumption that surface snow and glacial ice would be devoid of radon due to negligible sediment inventories on the ice-sheet surface. Conversely, as expected, radon activities in the groundwater samples were very high ( $1626 \pm 48.8$  and  $2750 \pm 63.3 \text{ dpm L}^{-1}$ ). These activities were consistent with the laboratory-derived pore-water radon activities (range  $1285 \pm 43.3$  to  $3045 \pm 132 \text{ dpm L}^{-1}$ ), thus indicating that the groundwater samples collected in this study represent saturated flow. We observed seasonal differences in the amount of radon detected in the 'N' glacier outflow stream waters. The mean activity of the May samples was much higher ( $75.6 \text{ dpm L}^{-1}$ ) than that of the July samples ( $25.4 \text{ dpm L}^{-1}$ ). Furthermore, we observed a greater range in the radon activities of the outflow stream in May ( $16.9$ – $210 \text{ dpm L}^{-1}$ ) compared to July ( $10.4$ – $35.7 \text{ dpm L}^{-1}$ ) (Fig. 2c). Thus, during at least some periods in the late spring, the 'N' stream outflow waters had high radon activities, whereas at the height of the summer melt season the outflow waters had universally low radon activities. For comparison, the open ocean has an average radon activity of  $\sim 0.01 \text{ dpm L}^{-1}$  (Broecker and Peng, 1982). In groundwater, radon activities can vary greatly, but, in general, activities range from hundreds to thousands of  $\text{dpm L}^{-1}$  (Charette and others, 2008 and references therein). We were not able to resolve a diurnal cycle in the 'N' outflow radon activity during the 12 July high-resolution time series due to the low activities measured throughout this day ( $27.3$ – $31.8 \text{ dpm L}^{-1}$ ). Earlier in the season, however, we found that the maximum daily radon activity on 31 May ( $75.5 \text{ dpm L}^{-1}$  at 06:45) occurs within the period when daily discharge was at a minimum (although we lack continuous discharge measurements during that time). Moreover, we observed the lowest radon activity ( $47.5 \text{ dpm L}^{-1}$ ) at 18:25, when daily discharge was at a maximum. These preliminary data indicate that radon may be useful in resolving the diurnal contribution of delayed-flow waters to total outflow in the early season, but this application requires more frequent sampling. Thus, we limit further discussion of radon to seasonal trends.

Radon in water that is physically decoupled from its sediment or rock source is subject to decay on a timescale determined by its half-life (Kraemer and Genereux, 1998). Thus, subglacial outflow radon activities in line with published groundwater values require substantial steady-state sediment–water interaction. To quantify the potential for suspended sediment to explain the observed radon values, we collected replicate unfiltered samples from the mouth of the 'N' outflow; one sample was analyzed immediately, while the other was measured after one radon half-life. The decay-corrected activities of the samples were

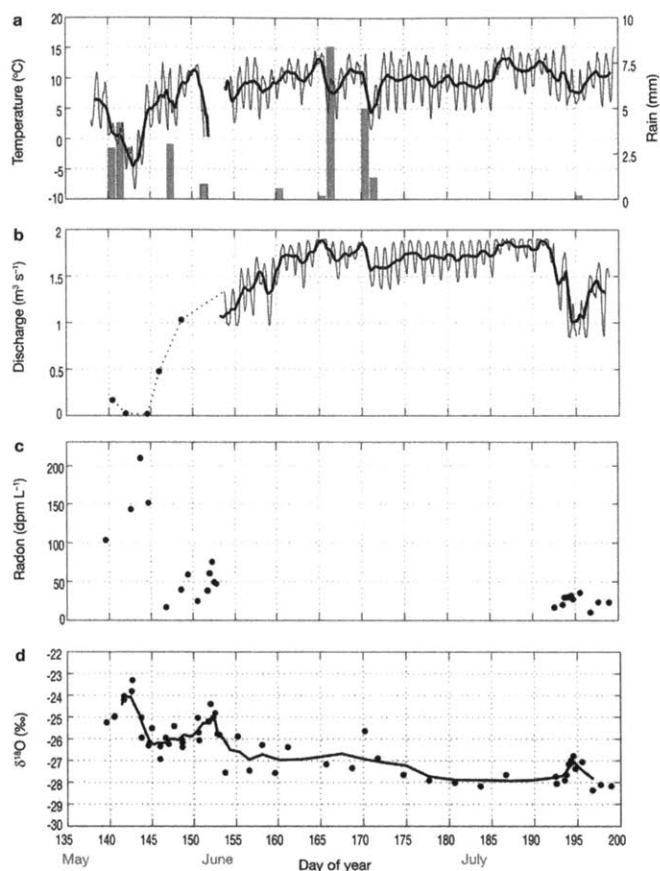


**Fig. 2.** (a) Plot of 3 hour (thin black line) and daily (thick black line) average air temperatures, with total daily rainfall in the gray bars. (b) Three-hour (thin black line) and daily (thick black line) average discharge at 'N' glacier. (c) Radon activities. (d)  $\delta^{18}\text{O}$  content (black dots) and five-point moving average (black line) in the 'N' glacier outflow stream. The discharge record is confined to point measurements from 19 to 31 May. Discontinuous lines in the temperature and discharge records reflect gaps in the data.

the same, indicating that  $^{226}\text{Ra}$  in the stored sample sediment was not a significant source of radon. We therefore conclude that the presence of radon in bulk outflow waters necessitates some delayed-flow component that has had substantial interaction with the bed. As further evidence of this idea, the regression (model II, geometric mean) of radon and EC was significant ( $r^2 = 0.87$ ,  $p < 0.01$ ) (Fig. 3). However, unlike EC, radon is not subject to the dissolution chemistries of a wide range of solutes and thus can potentially be utilized for quantitative hydrograph separation.

### 6.3. Radon evasion in subglacial channels

Although radon is water-soluble, the radon will partition into the air phase in an air-water system (Kraemer and Geneux, 1998). Loss due to evasion is a function of temperature and the amount of radon present in the air, so evasion could be problematic late in the melt season when subglacial channels may not be entirely water-full. Moreover, water flow in the subglacial channels is often faster

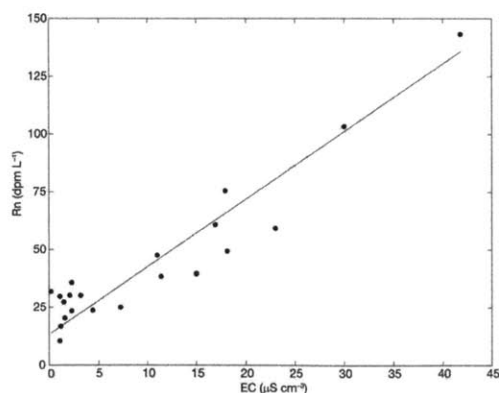


**Fig. 3.** Model II regression (geometric mean) of EC and radon activity in the 'N' glacier outflow stream waters.

**Table 3.**  $^{222}\text{Rn}$  activities in the 'N' glacier outflow stream on falling and rising discharge limbs from 10 to 16 July 2008

Julian day	Discharge observations	Mean daily discharge	$^{222}\text{Rn}$
		$\text{m}^3 \text{s}^{-1}$	$\text{dpm L}^{-1}$
192	Start of falling limb	1.7	16.7
193	Falling limb	1.5	20.3
194	Falling limb	1.2	31.8
195	Bottom of falling limb	1.0	35.7
196	Rising limb	1.2	10.4
197	Top of rising limb	1.4	23.7
198	Falling limb	1.3	23.4

and more turbulent at the peak of the summer melt season, which may enhance gas exchange loss (Kraemer and Geneux, 1998). Thus, if evasion were the dominant process influencing radon in the 'N' glacier outflow stream we would expect to find lower radon activities toward the end of a falling discharge limb. Instead we observed increases in radon during times when discharge was decreasing and subglacial channels were less full (e.g. days 192–195), and the largest radon activities occurred at the discharge minimum (Table 3). Thus, dilution of the delayed-flow waters with radon-free surface input appears to have had the greatest effect on radon values in the 'N' outflow stream.

#### 6.4. Water isotopes as a tracer in a GRIS outlet glacier

We found distinct  $\delta^{18}\text{O}$  values for the surface-snow (–11 to –13‰) and glacial-ice (–26 to –30‰) end-members measured across our study region (Table 4). This difference means that the snow and glacial ice reservoir  $\delta^{18}\text{O}$  values do not overlap and thus are useful as passive flow tracers. Conversely, our 'basal-ice' (ice collected at 100 m elevation at the glacier margin) sample values (–29.6‰) were not sufficiently isotopically distinct from glacial ice values estimated across the surface of the catchment (–25.5 to –28.2‰) to separate the delayed-flow water source from the glacier ice reservoir. Thus it was necessary to delineate these reservoirs from each other with the radon end-member mixing equation. An additional groundwater sample near the front of 'N' glacier also possessed a depleted  $\delta^{18}\text{O}$  signature (–27.8‰), suggesting that groundwater in this region is derived primarily from glacial ice melt. Although we limit our discussion to the  $\delta^{18}\text{O}$  values, the trends observed in the oxygen isotope values are also applicable to the deuterium data, since  $\delta^{18}\text{O}$  and  $\delta\text{D}$  covary on a global scale (Craig, 1961).

#### 6.5. Isotope-mixing model

The end-member mixing equations used in this study assume a simplified drainage system limited to three conceptual end-member water sources: (1) surface snow, (2) glacial ice and (3) delayed-flow waters. This was necessary to determine the applicability of radon as a hydrological tracer in a glacial setting, and to produce an initial chemical mixing model, although we recognize that we have oversimplified the subglacial drainage system by categorizing glacial flow components into three broad water source reservoirs (Sharp and others, 1995).

Model results showed that the snowmelt and delayed-flow waters comprised a greater fraction of the total outflow

**Table 4.** Measured and estimated(\*)  $\delta^{18}\text{O}$  ratios of surface-snow, glacial-ice and groundwater samples

Water source	$\delta^{18}\text{O}$			
	100 m elev.	300 m elev.	500 m elev.	1000 m elev.
Surface snow	–11‰*	–12.3‰ ( $n=1$ )	–13‰*	
Glacial ice	–29.6‰ ( $n=2$ )	–28.2‰ ( $n=3$ )	–25.5‰*	–23.9‰ ( $n=9$ )
Groundwater	–27.8‰ ( $n=1$ )			

in May (Fig. 4a) than in July (Fig. 4b). In May, delayed flow dominated the discharge (mean 41%), followed by nearly equal contributions from surface snowmelt (mean 23%) and glacial ice melt (mean 26%). In July, however, the mean fractional contributions from the surface snowmelt and delayed-flow reservoirs decreased to 6% and 12%, respectively, while the mean glacial ice contribution rose to 82%. This finding was likely due to the removal of seasonal snow from the glacier surface by this time, and dilution of delayed-flow reservoirs with increased glacial ice melt. Scaling the model results with the measured discharge allowed us to compare the discharge contribution of surface snow, glacial ice and delayed flow to the total 'N' stream discharge from 18 May to 1 June (Fig. 4c) and 11 to 17 July (Fig. 4d). The average snow component ( $n=11$ ) of total discharge decreased by more than half from May (mean  $0.17 \pm 0.04 \text{ m}^3 \text{ s}^{-1}$ ; 1 standard error) to July (mean  $0.07 \pm 0.01 \text{ m}^3 \text{ s}^{-1}$ ), whereas the average glacial ice component ( $n=11$ ) more than doubled from May (mean  $0.43 \pm 0.10 \text{ m}^3 \text{ s}^{-1}$ ) to July (mean  $1.1 \pm 0.09 \text{ m}^3 \text{ s}^{-1}$ ). By comparison, the average delayed-flow component ( $n=11$ ) remained a relatively constant contribution between May ( $0.19 \pm 0.05 \text{ m}^3 \text{ s}^{-1}$ ) and July ( $0.16 \pm 0.01 \text{ m}^3 \text{ s}^{-1}$ ).

The results of our isotope-mixing model were a direct consequence of the shifts we observed in the  $^{222}\text{Rn}$  activities and  $\delta^{18}\text{O}$  and  $\delta\text{D}$  ratios of the 'N' outflow stream composition from May to July. The highest radon activities were found during times of lowest discharge (Fig. 5a). During the 3 day subfreezing period in May when discharge dropped to near zero, radon activities in the 'N' outflow stream peaked at  $>100 \text{ dpm L}^{-1}$  (Fig. 5a). In July, even though the radon activities were overall much lower than in May, elevated radon ( $35.7 \text{ dpm L}^{-1}$ ) coincides with a prominent drop in discharge on day 195 (Fig. 5b). This behavior can best be explained by varying levels of dilution of the delayed-flow waters with a supraglacial water source devoid of radon. This reasoning is consistent with a seasonal evolution of the subglacial drainage structure from a distributed system characterized by chemically enriched outflow waters to a channelized system that facilitates rapid transit of dilute glacial ice melt.

The difference between the stable-isotope signatures of the snow and ice reservoirs at 'N' glacier is sufficiently large that a change in  $\delta^{18}\text{O}$  runoff composition can likely be attributed to a water source change. In late spring when discharges are low, and snowmelt feeds a predominantly distributed subglacial drainage system, we measured enriched  $\delta^{18}\text{O}$  values in the 'N' outflow stream, compared to

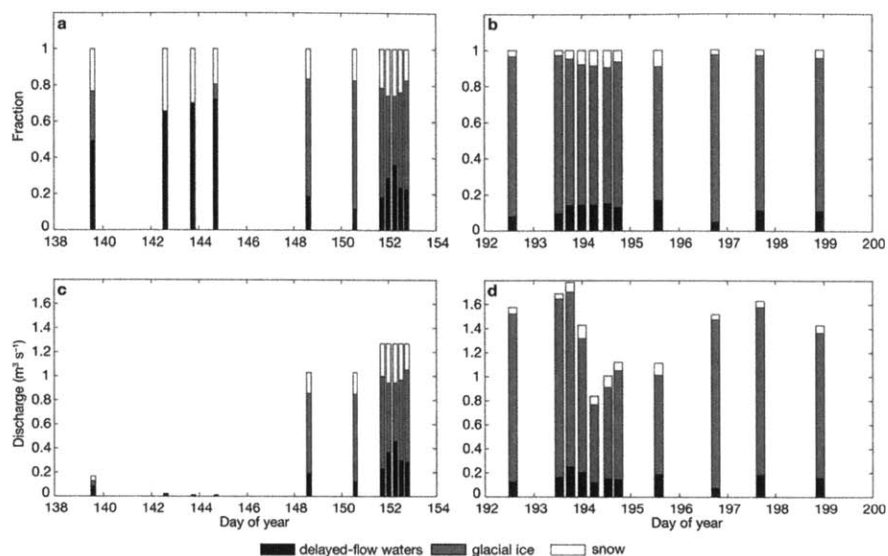


Fig. 4. Stacked bar plots of isotope-mixing model solutions for the fractions of surface snow, glacial ice and delayed-flow waters comprising the 'N' glacier outflow stream waters from (a) 18 May to 1 June and (b) 11 to 17 July, and scaled contributions from each reservoir in (c) May and (d) July.

later in the season (Fig. 2d). Indeed, the most enriched values occurred over the 3 day span that discharge dropped to near zero. Subsequently there is a decrease in the stable-isotope signature of the 'N' glacier discharge as the melt season progresses from late spring to the summer. This trend is consistent with a seasonal shift in water source reservoirs from a snow and ice contribution in late spring to a purely glacial ice contribution at the height of the summer melt season.

In addition to the overall seasonal decline, our  $\delta^{18}\text{O}$  record exhibited higher-frequency variability, suggesting that changes in meltwater source contributions and/or drainage system evolution may also have occurred during synoptic-scale events. Although we lacked the temporal resolution required to explore this variability in full, one such event late in the melt season is reasonably well resolved. On day 195 there was a notable spike in the 'N' glacier subglacial stream  $\delta^{18}\text{O}$  values above the late-season mean coincident with a prominent drop in air temperature and discharge, and an increase in radon activity (Fig. 2). One possible explanation for this event is cooling air temperatures across the glacier surface leading to a decrease in  $\delta^{18}\text{O}$ -depleted glacier ice melt. This decrease in total surface meltwater input to the subglacial resulted in a relatively higher base flow contribution (characterized by residual stored  $\delta^{18}\text{O}$ -enriched snowmelt) to the bulk runoff during this event. Another possible explanation for this isotopic excursion is a rainfall event (0.2 mm) recorded that day (Fig. 2a) which would also yield an enriched  $\delta^{18}\text{O}$  signature. Larger rainfall events in our record (e.g. 8.4 mm on day 166), however, did not correspond to enriched  $\delta^{18}\text{O}$  runoff values. Furthermore, rainfall events should increase stream discharge, whereas we observed a decrease in stream discharge during this event.

## 6.6. Mixing-model sensitivity analysis

The sensitivity analysis revealed that for the entire dataset (May and July) the contribution from the surface snow reservoir to the total outflow varied from a mean maximum of 26% to a mean minimum of 0.9%. Similarly, the delayed-flow fraction varied from a mean maximum of 26% to a slightly higher mean minimum of 3.4%. Not surprisingly, the glacial ice fraction exhibited the highest mean maximum and minimum values, varying from 97% to 49%. Results of the sensitivity analysis are also displayed as the maximum and minimum flow contributions ( $\text{m}^3 \text{s}^{-1}$ ) from the surface snow, glacial ice and delayed-flow reservoirs from May (Fig. 6a) and July (Fig. 6b). In order to identify meaningful estimates, we constrained the sensitivity analysis so that no flow contribution was permitted to fluctuate below zero. When discharge was very low, we were not able to differentiate the flow contribution ( $\text{m}^3 \text{s}^{-1}$ ) from the different component reservoirs accurately (Fig. 6a). Additionally, though we were able to drive the snow contribution to zero, there was always a delayed-flow component that is diluted by an increasing ice component throughout the season. This analysis illustrates that we are currently able to determine the flow contribution from each of the defined water source reservoirs within an absolute maximum and minimum value. Further improvements to the flow estimates would benefit most from better characterization of the delayed-flow radon end-member.

## 7. TRANSIT TIME ESTIMATES

We observed detectable  $^7\text{Be}$  activity ( $7.7 \text{ dpm L}^{-1}$ ) in the 'N' supraglacial pond in May, which we use as an analogue for the potential  $^7\text{Be}$  activity of surface snow in this study. This

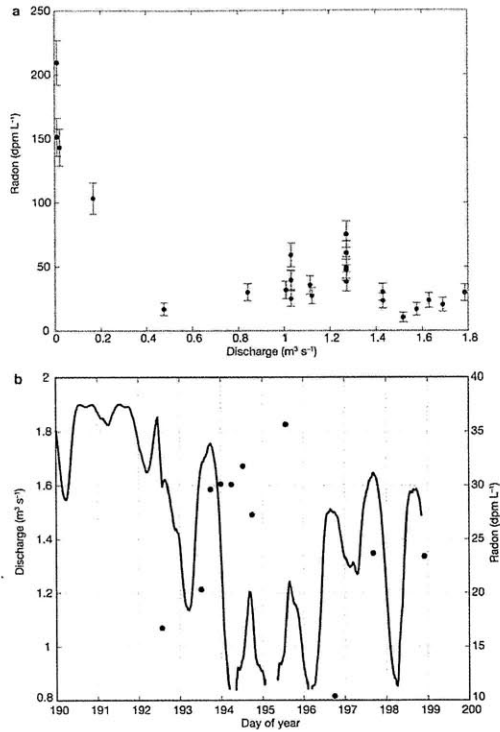


**Fig. 5.** (a) Radon activities ( $\pm$  one standard error) in the 'N' glacier outflow stream plotted against daily average discharge, and (b) 3 hour average discharge and measured radon activities in the 'N' glacier outflow stream from 11 to 17 July. Discontinuous lines in the discharge record reflect gaps in the data.

activity is within the range of previously reported  $^7\text{Be}$  activities in fresh snow at Summit, Greenland (2.67–76.5 dpm L<sup>-1</sup>), but below the reported median (15.3 dpm L<sup>-1</sup>) (Dibb, 1990). The wide variability in reported fresh-snow  $^7\text{Be}$  activities likely reflects atmospheric inventory depletion and wet deposition-related dilution effects of precipitation-event frequency and duration (Nimz, 1998). For example, high  $^7\text{Be}$  activities may result from a short snowfall event following a period of minimal precipitation. Conversely, lower snow activities may be explained by a relatively large snowfall event following a series of recent precipitation events. Our sample may have had lower  $^7\text{Be}$  activity compared to the fresh snow collected at Summit because it represents a composite of fresh and older snow on the surface of 'N' glacier. Comparatively, meltwater derived from recent glacial ice melt measured at the inland site in July had an extremely low  $^7\text{Be}$  activity (0.04 dpm L<sup>-1</sup>), an indication that its original  $^7\text{Be}$  inventory had been lost via decay. Thus,  $^7\text{Be}$  in outflow water can only be derived from a young supraglacial source that has originated at the surface <1 year before. On 21 May the  $^7\text{Be}$  activity of the 'N' glacier outflow stream was 1.05 dpm L<sup>-1</sup>, and on 11 July the  $^7\text{Be}$  activity was 0.03 dpm L<sup>-1</sup>. The low July  $^7\text{Be}$  signal was similar to the recent glacial ice-melt  $^7\text{Be}$  signal, and most likely represented a switch in end-member contribution from snowmelt to ice melt. The May value, however, was consistent with a hydrological connection between surface melt and subsurface discharge at this point in the season. However, we cannot rule out the possibility that the May  $^7\text{Be}$  signal in the 'N' glacier outflow stream resulted from the release of supraglacial waters that had been stored at the bed for <300 days or in basal crevasses (Harper and others, 2010).

We used the fractions from the isotope-mixing model for the surface snow and glacial ice contributions on 21 May to solve for a transit time (Equation (7)). Since  $^7\text{Be}$  is particle-reactive (Hawley and others, 1986; Olsen and others, 1986)

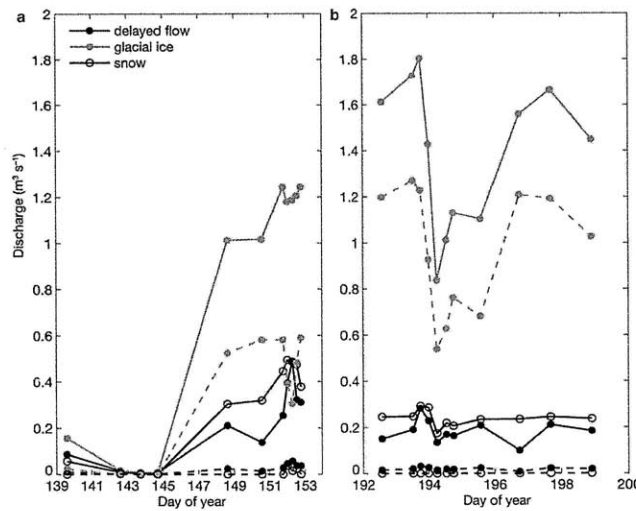


**Fig. 6.** Sensitivity analysis illustrating maximum (solid lines) and minimum (dashed lines) flow contributions from the surface snow, glacial ice and delayed-flow water sources from (a) 18 May to 1 June and (b) 11 to 17 July.

and thus could have adsorbed to solids during travel through the subglacial environment, we also included a correction that describes scavenging of  $^7\text{Be}$  onto particles in the subglacial environment (Equation (6)). Given these assumptions, we estimated that supraglacial waters took  $\sim 7.5$  days to travel from the surface to the glacier mouth. For comparison, distributed drainage-system transit times (estimated using velocities from dye-tracing experiments in Nienow and others, 1998) at Haut Glacier d'Arolla, Switzerland, which has a similar catchment size to 'N' glacier, range from  $\sim 6$  to  $<1$  day(s) for a 5 km flow path. However, we should note that our calculated time estimate depends on the accuracy of our assumed partition coefficient,  $K_d$ , and the surface  $^7\text{Be}$  activity. Nonetheless,  $^7\text{Be}$  may hold promise as a tracer for snowmelt in early-season distributed drainage systems with similar or longer transit times.

## 8. SYNTHESIS

Results from our multi-component isotope-mixing model provide broad separation of water reservoir contributions, thus providing a potential new direction in the application of chemical mixing models to study glacier hydrology. Based on the results from this study, we furthermore suggest that these methods could be successfully scaled up to investigate the subglacial hydrology of the much larger outlet glaciers that drain the bulk of the GrIS. Some practical and technological challenges remain to be solved in regularly sampling discharge and radon at large land-terminating glaciers (e.g. in flood plains, large channels or braided river environments) and in large marine-terminating glaciers (tidewater environments). This effort would also require comprehensive sampling of the glacial ice end-member water isotope values across each of these larger catchments.

Focusing our study on a small land-terminating glacier on the southwestern margin of the GrIS, we show that there is a relatively constant and chemically enriched delayed (basal) flow component present throughout the melt season. These delayed-flow waters comprise a greater fraction of the total discharge in May compared to July, and are diluted first by snowmelt and then by increasing amounts of rapidly flowing ice melt as the season progresses. In alpine glaciers, chemically enriched delayed-flow waters (e.g. snowmelt, basal melt, groundwater) are characteristic of distributed drainage systems, which transmit meltwater slowly through the glacier via a hydraulically inefficient network. As the snowline retreats and surface meltwater input to the bed increases, the subglacial drainage system structure evolves to a channelized drainage system, which can more efficiently export the surface glacial ice melt. Though such seasonal subglacial drainage evolution is well documented in alpine systems (Hubbard and Nienow, 1997; Nienow and others, 1998; Cuffey and Paterson, 2010), its existence under land-terminating sectors of the GrIS has only recently been hypothesized (Shepherd and others, 2009; Bartholomew and others, 2010) and has not been directly observed. The findings from this study offer a hydrochemical line of evidence for this hypothesis, albeit at a comparatively much smaller outlet glacier, and bolster the need to incorporate these dynamically significant subglacial processes into GrIS modeling efforts.

From a biogeochemical perspective, knowledge of the seasonal controls on end-member water-source contributors to bulk discharge provides greater understanding of the

potential for high temporal variability of carbon, nutrient and metal export from subglacial environments to downstream marine ecosystems. Previous studies have suggested that water draining a distributed drainage system contains much greater concentrations of these biogeochemically important species, compared to the waters draining a channelized system (Tranter and others, 2005). Thus, total annual flux calculations of carbon, nutrient and metal export require knowledge of the base flow ( $\text{m}^3 \text{a}^{-1}$ ) exiting a glacier. Our isotope-mixing model shows promise at being able to provide reasonable quantitative estimates of snow, ice and delayed-flow components comprising bulk meltwater discharge from a land-terminating GrIS glacier. These flow estimates can be used as a first-order approximation of base flow emanating from similar catchments around the GrIS throughout the year.

## ACKNOWLEDGEMENTS

This research was supported by the WHOI Clark Arctic Research Initiative (E.B.K., S.B.D., M.A.C.), the WHOI Ocean Ventures Fund (M.P.B.), the US National Science Foundation ARC-05200077 (S.B.D.), NASA (S.B.D.), the Natural Sciences and Engineering Research Council of Canada (M.P.B.) and the WHOI Climate Change Institute (M.P.B.). We acknowledge I. Joughin for kindly providing InSAR velocity data. We are very grateful to M. Behn and D. Glover for assistance with data analysis, to M. Sharp and K. Longnecker for comments and advice that improved the manuscript, and to B. Gready, M. Behn, I. Joughin, M. Evans, A. Criscitello and R. Harris for assistance in the field.

## REFERENCES

- Andrews, J.E., C. Hartin and K.O. Buesseler. 2008.  $^7\text{Be}$  analyses in seawater by low background gamma-spectroscopy. *J. Radioanal. Nucl. Chem.*, **277**(1), 253–259.
- Bartholomew, I., P. Nienow, D. Mair, A. Hubbard, M.A. King and A. Sole. 2010. Seasonal evolution of subglacial drainage and acceleration in a Greenland outlet glacier. *Nature Geosci.*, **3**(6), 408–411.
- Benn, D.I. and D.J.A. Evans. 1998. *Glaciers and glaciation*. London, Arnold.
- Bhatia, M.P., S.B. Das, K. Longnecker, M.A. Charette and E.B. Kujawinski. 2010. Molecular characterization of dissolved organic matter associated with the Greenland ice sheet. *Geochim. Cosmochim. Acta*, **74**(13), 3768–3784.
- Box, J.E. and K. Ski. 2007. Remote sounding of Greenland supraglacial melt lakes: implications for subglacial hydraulics. *J. Glaciol.*, **53**(181), 257–265.
- Box, J.E. and 8 others. 2006. Greenland ice sheet surface mass balance variability (1988–2004) from calibrated Polar MM5 output. *J. Climate*, **19**(12), 2783–2800.
- Broecker, W.S. and T.H. Peng. 1982. *Tracers in the sea*. New York, Eldigio Press.
- Brown, G.H. 2002. Glacier meltwater hydrochemistry. *Appl. Geochem.*, **17**(7), 855–883.
- Brown, G.H., M.J. Sharp, M. Tranter, A.M. Gurnell and P.W. Nienow. 1994. Impact of post-mixing chemical reactions on the major ion chemistry of bulk meltwaters draining the Haut Glacier d'Arolla, Valais, Switzerland. *Hydrol. Process.*, **8**(5), 465–480.
- Burnett, W.C. and H. Dulaiova. 2003. Estimating the dynamics of groundwater input into the coastal zone via continuous radon-222 measurements. *J. Environ. Radioactiv.*, **69**(1–2), 21–35.

- Cable, J.E., W.C. Burnett, J.P. Chanton and G.L. Weatherly. 1996. Estimating groundwater discharge into the northeastern Gulf of Mexico using radon-222. *Earth Planet. Sci. Lett.*, **144**(3–4), 591–604.
- Charette, M.A., W.S. Moore and W.C. Burnett. 2008. Uranium- and thorium-series nuclides as tracers of submarine groundwater discharge. In Krishnaswami, S. and J. Kirk Cochran, eds. *U-Th series nuclides in aquatic systems*. Amsterdam, Elsevier, 155–191. (Radioactivity in the Environment 13.)
- Clark, I.D. and P. Fritz. 1997. *Environmental isotopes in hydrogeology*. Boca Raton, FL, CRC Lewis.
- Collins, D.N. 1979. Quantitative determination of the subglacial hydrology of two Alpine glaciers. *J. Glaciol.*, **23**(89), 347–362.
- Cooper, L.W. 1998. Isotopic fractionation in snow cover. In Kendall, C. and J.J. McDonnell, eds. *Isotope tracers in catchment hydrology*. New York, Elsevier, 119–136.
- Corbett, D.R., W.C. Burnett, P.H. Cable and S.B. Clark. 1997. Radon tracing of groundwater input into Par Pond, Savannah River Site. *J. Hydrol.*, **203**(1–4), 209–227.
- Craig, H. 1961. Isotopic variations in meteoric waters. *Science*, **133**(3465), 1702–1703.
- Cuffey, K.M. and W.S.B. Paterson. 2010. *The physics of glaciers. Fourth edition*. Oxford, Butterworth-Heinemann.
- Dansgaard, W., S.J. Johnsen, H.B. Clausen and N. Gundestrup. 1973. Stable isotope glaciology. *Medd. Grøn.*, **197**(2), 1–53.
- Das, S.B. and 6 others. 2008. Fracture propagation to the base of the Greenland Ice Sheet during supraglacial lake drainage. *Science*, **320**(5877), 778–781.
- Dibb, J.E. 1990. Beryllium-7 and lead-210 in the atmosphere and surface snow over the Greenland ice sheet in the summer of 1989. *J. Geophys. Res.*, **95**(D13), 22,407–22,415.
- Dingman, S.L. 2002. *Physical hydrology. Second edition*. Long Grove, IL, Waveland Press.
- Dulaiova, H., R. Peterson, W.C. Burnett and D. Lane-Smith. 2005. A multi-detector continuous monitor for assessment of  $^{222}\text{Rn}$  in the coastal ocean. *J. Radioanal. Nucl. Chem.*, **263**(2), 361–363.
- Dulaiova, H., M.E. Gonnera, P.B. Henderson and M.A. Charette. 2008. Geochemical and physical sources of radon variation in a subtropical estuary – implications for groundwater radon activities in submarine groundwater discharge studies. *Mar. Chem.*, **110**(1–2), 120–127.
- Gurnell, A.M. and C.R. Fenn. 1984. Flow separation, sediment source areas and suspended sediment transport in a pro-glacial stream. *Catena*, Suppl. 5, 109–119.
- Harper, J.T., J.H. Bradford, N.F. Humphrey and T.W. Meierbachotl. 2010. Vertical extension of the subglacial drainage system into basal crevasses. *Nature*, **467**(7315), 579–582.
- Hawley, N., J.A. Robbins and B.J. Eadie. 1986. The partitioning of  $^7\text{beryllium}$  in fresh water. *Geochim. Cosmochim. Acta*, **50**(6), 1127–1131.
- Hood, E. and D. Scott. 2008. Riverine organic matter and nutrients in southeast Alaska affected by glacial coverage. *Nature Geosci.*, **1**(9), 583–587.
- Hood, E. and 6 others. 2009. Glaciers as a source of ancient and labile organic matter to the marine environment. *Nature*, **462**(7276), 1044–1047.
- Hubbard, B. and P. Nienow. 1997. Alpine subglacial hydrology. *Quat. Sci. Rev.*, **16**(9), 939–955.
- Joughin, I., S.B. Das, M.A. King, B.E. Smith, I.M. Howat and T. Moon. 2008. Seasonal speedup along the western flank of the Greenland Ice Sheet. *Science*, **320**(5877), 781–783.
- Jouzel, J. and 12 others. 1997. Validity of the temperature reconstruction from water isotopes in ice cores. *J. Geophys. Res.*, **102**(C12), 26,471–26,487.
- Kies, A., O. Hengesch, Z. Tosheva, J. Jania and A. Nawrot. 2010. Natural radioactive isotopes in glacier studies. In Barnett, I. and P. Pacheroová, eds. *Proceedings of the 10th International Workshop on the Geological Aspects of Radon Risk Mapping, 22–25 September 2010, Prague, Czech Republic*. Prague, Czech Geological Survey, 162–172.
- Kraemer, T.F. and D.P. Genereux. 1998. Applications of uranium- and thorium-series radionuclides in catchment hydrology studies. In Kendall, C. and J.J. McDonnell, eds. *Isotope tracers in catchment hydrology*. New York, Elsevier, 679–722.
- Krawczynski, M.J., M.D. Behn, S.B. Das and I. Joughin. 2009. Constraints on the lake volume required for hydro-fracture through ice sheets. *Geophys. Res. Lett.*, **36**(10), L10501. (10.1029/2008GL036765.)
- McMillan, M., P. Nienow, A. Shepherd, T. Benham and A. Sole. 2007. Seasonal evolution of supra-glacial lakes on the Greenland Ice Sheet. *Earth Planet. Sci. Lett.*, **262**(3–4), 484–492.
- Mernild, S.H., G.E. Liston, C.A. Hiemstra, K. Steffen, E. Hanna and J.H. Christensen. 2009. Greenland ice sheet surface mass-balance modelling and freshwater flux for 2007, and in a 1995–2007 perspective. *Hydrol. Process.*, **23**(17), 2470–2484.
- Mitchell, A., G.H. Brown and R. Fuge. 2001. Minor and trace element export from glacierized Alpine headwater catchment (Haut Glacier d'Arolla, Switzerland). *Hydrol. Process.*, **15**(18), 3499–3524.
- Nienow, P., M. Sharp and I. Willis. 1998. Seasonal changes in the morphology of the subglacial drainage system, Haut Glacier d'Arolla, Switzerland. *Earth Surf. Process. Landf.*, **23**(9), 825–843.
- Nimz, G.J. 1998. Lithogenic and cosmogenic tracers in catchment hydrology. In Kendall, C. and J.J. McDonnell, eds. *Isotope tracers in catchment hydrology*. New York, Elsevier, 247–289.
- Olsen, C.R., I.L. Larsen, P.D. Lowry, N.H. Cutshall and M.M. Nichols. 1986. Geochemistry and deposition of  $^7\text{Be}$  in river-estuarine and coastal waters. *J. Geophys. Res.*, **91**(C1), 896–908.
- Paterson, W.S.B. 1994. *The physics of glaciers. Third edition*. Oxford, etc., Elsevier.
- Raiswell, R. and 6 others. 2006. Contributions from glacially derived sediment to the global iron (oxyhydr)oxide cycle: implications for iron delivery to the oceans. *Geochim. Cosmochim. Acta*, **70**(11), 2765–2780.
- Reeh, N. and H.H. Thomsen. 1993. Using stable isotopes as natural tracers to delineate hydrological drainage basins on the Greenland ice-sheet margin. *Chemical Geol.*, **109**(1–4), 281–291.
- Richards, K.S. and 9 others. 1996. An integrated approach to modelling hydrology and water quality in glacierized catchments. *Hydrol. Process.*, **10**(4), 479–508.
- Richter-Menge, J., ed. 2009. The Arctic. *Bull. Am. Meteorol. Soc.*, **90**, Special issue, S1–S196.
- Ricker, W.E. 1973. Linear regressions in fishery research. *J. Fish. Res. Board Can.*, **30**(3), 409–434.
- Schmidt, A., M. Schlueter, M. Melles and M. Schubert. 2008. Continuous and discrete on-site detection of radon-222 in ground- and surface waters by means of an extraction module. *Appl. Radiat. Isotop.*, **66**(12), 1939–1944.
- Sharp, M., G.H. Brown, M. Tranter, I.C. Willis and B. Hubbard. 1995. Comments on the use of chemically based mixing models in glacier hydrology. *J. Glaciol.*, **41**(138), 241–246.
- Sharp, M., J. Parkes, B. Cragg, I.J. Fairchild, H. Lamb and M. Tranter. 1999. Widespread bacterial populations at glacier beds and their relationship to rock weathering and carbon cycling. *Geology*, **27**(2), 107–110.
- Shepherd, A., A. Hubbard, P. Nienow, M. McMillan and I. Joughin. 2009. Greenland ice sheet motion coupled with daily melting in late summer. *Geophys. Res. Lett.*, **36**(1), L01501. (10.1029/2008GL035758.)
- Skidmore, M.L., J.M. Foght and M.J. Sharp. 2000. Microbial life beneath a High Arctic glacier. *Appl. Environ. Microbiol.*, **66**(8), 3214–3220.
- Sokal, R.R. and F.J. Rohlf. 1995. *Biometry: the principles and practice of statistics in biological research. Third edition*. New York, W.H. Freeman.
- Solomon, S. and 7 others, eds. 2007. *Climate change 2007: the physical science basis. Contribution of Working Group I to the*



- Fourth Assessment Report of the Intergovernmental Panel on Climate Change*. Cambridge, etc., Cambridge University Press.
- Taylor, S., X. Feng, J.W. Kirchner, R. Osterhuber, B. Klauke and C.C. Renshaw. 2001. Isotopic evolution of a seasonal snowpack and its melt. *Water Resour. Res.*, **37**(3), 759–769.
- Theakstone, W.H. 2003. Oxygen isotopes in glacier-river water, Austre Okstindbreen, Okstindan, Norway. *J. Glaciol.*, **49**(165), 282–298.
- Tranter, M. and R. Raiswell. 1991. The composition of the englacial and subglacial component in bulk meltwaters draining the Gornergletscher, Switzerland. *J. Glaciol.*, **37**(125), 59–66.
- Tranter, M. and 9 others. 1997. Variability in the chemical composition of *in situ* subglacial meltwaters. *Hydrol. Process.*, **11**(1), 59–78.
- Tranter, M., M.J. Sharp, H.R. Lamb, G.H. Brown, B.P. Hubbard and I.C. Willis. 2002. Geochemical weathering at the bed of Haut Glacier d'Arolla, Switzerland – a new model. *Hydrol. Process.*, **16**(5), 959–993.
- Tranter, M., M. Skidmore and J. Wadham. 2005. Hydrological controls on microbial communities in subglacial environments. *Hydrol. Process.*, **19**(4), 995–998.
- Tsai, V.C. and J.R. Rice. 2010. A model for turbulent hydraulic fracture and application to crack propagation at glacier beds. *J. Geophys. Res.*, **115**(F3), F03007. (10.1029/2009JF001474.)
- Wadham, J.L., M. Tranter, S. Tulaczyk and M. Sharp. 2008. Subglacial methanogenesis: a potential climatic amplifier? *Global Biogeochem. Cycles*, **22**(2), GB2021. (10.1029/2007GB002951.)

MS received 30 November 2010 and accepted in revised form 23 July 2011

## Chapter 3

### Molecular-level characterization of dissolved organic matter associated with the Greenland ice sheet \*

#### Abstract

Subsurface microbial oxidation of overridden soils and vegetation beneath glaciers and ice sheets may affect global carbon budgets on glacial-interglacial timescales. The likelihood and magnitude of this process depends on the chemical nature and reactivity of the subglacial organic carbon stores. We examined the composition of carbon pools associated with different regions of the Greenland ice sheet (subglacial, supraglacial, proglacial) in order to elucidate the type of dissolved organic matter (DOM) present in the subglacial discharge over a melt season. Electrospray ionization (ESI) Fourier transform ion cyclotron resonance (FT-ICR) mass spectrometry coupled to multivariate statistics permitted unprecedented molecular level characterization of this material and revealed that carbon pools associated with discrete glacial regions are comprised of different compound classes. Specifically, a larger proportion of protein-like compounds were observed in the supraglacial samples and in the early melt season (spring) subglacial discharge. In contrast, the late melt season (summer) subglacial discharge contained a greater fraction of lignin-like and other material presumably derived from underlying vegetation and soil. These results suggest (1) that the majority of supraglacial DOM originates from autochthonous microbial processes on the ice sheet surface, (2) that the subglacial DOM contains allochthonous carbon derived from overridden soils and vegetation as well as autochthonous carbon derived from *in situ* microbial metabolism, and (3) that the relative contribution of allochthonous and autochthonous material in subglacial discharge varies during the melt season. These conclusions are consistent with the hypothesis that, given sufficient time (e.g., overwinter storage), resident subglacial microbial communities may oxidize terrestrial material beneath the Greenland ice sheet.

---

\* Published as: Bhatia, M., S.B. Das, K.L. Longnecker, M.A. Charette, and E.B. Kujawinski (2010). Molecular-level characterization of dissolved organic matter associated with the Greenland ice sheet, *Geochimica et Cosmochimica Acta*, 74(2010): 3468-3784.



## Molecular characterization of dissolved organic matter associated with the Greenland ice sheet

Maya P. Bhatia<sup>a</sup>, Sarah B. Das<sup>b</sup>, Krista Longnecker<sup>c</sup>, Matthew A. Charette<sup>c</sup>, Elizabeth B. Kujawinski<sup>c,\*</sup>

<sup>a</sup> MIT/WHOI Joint Program in Oceanography/Applied Ocean Sciences and Engineering, Department of Geology and Geophysics, Woods Hole Oceanographic Institution, Woods Hole, MA 02543, USA

<sup>b</sup> Department of Geology and Geophysics, Woods Hole Oceanographic Institution, Woods Hole, MA 02543, USA

<sup>c</sup> Department of Marine Chemistry and Geochemistry, Woods Hole Oceanographic Institution, Woods Hole, MA 02543, USA

Received 3 November 2009; accepted in revised form 9 March 2010; available online 7 April 2010

### Abstract

Subsurface microbial oxidation of overridden soils and vegetation beneath glaciers and ice sheets may affect global carbon budgets on glacial–interglacial timescales. The likelihood and magnitude of this process depends on the chemical nature and reactivity of the subglacial organic carbon stores. We examined the composition of carbon pools associated with different regions of the Greenland ice sheet (subglacial, supraglacial, proglacial) in order to elucidate the type of dissolved organic matter (DOM) present in the subglacial discharge over a melt season. Electrospray ionization (ESI) Fourier transform ion cyclotron resonance (FT-ICR) mass spectrometry coupled to multivariate statistics permitted unprecedented molecular level characterization of this material and revealed that carbon pools associated with discrete glacial regions are comprised of different compound classes. Specifically, a larger proportion of protein-like compounds were observed in the supraglacial samples and in the early melt season (spring) subglacial discharge. In contrast, the late melt season (summer) subglacial discharge contained a greater fraction of lignin-like and other material presumably derived from underlying vegetation and soil. These results suggest (1) that the majority of supraglacial DOM originates from autochthonous microbial processes on the ice sheet surface, (2) that the subglacial DOM contains allochthonous carbon derived from overridden soils and vegetation as well as autochthonous carbon derived from *in situ* microbial metabolism, and (3) that the relative contribution of allochthonous and autochthonous material in subglacial discharge varies during the melt season. These conclusions are consistent with the hypothesis that, given sufficient time (e.g., overwinter storage), resident subglacial microbial communities may oxidize terrestrial material beneath the Greenland ice sheet.

© 2010 Elsevier Ltd. All rights reserved.

### 1. INTRODUCTION

Anticipating how carbon flux patterns might respond to climate change is a principal motivation for understanding the different sources and reservoirs contributing to the global carbon cycle. In aquatic systems, carbon flux patterns

result from complex metabolic interactions of diverse biota with a pool of organic matter (Azam, 1998). Previously it was believed that glacial environments were devoid of life and thus, that carbon dynamics in these systems should be dominated by abiotic processes (Raiswell, 1984; Chillrud et al., 1994). However, the recent discovery of large, active microbial communities beneath glaciers and ice sheets has enlightened our understanding of biogeochemical reactions and organic carbon cycling in glaciated regions, namely that subglacial microbial communities may play an active role in the carbon cycle through oxidation of organic carbon stores beneath ice masses (Sharp et al., 1999; Tranter

\* Corresponding author. Address: Department of Marine Chemistry and Geochemistry, Woods Hole Oceanographic Institution, 360 Woods Hole Rd. MS#4, Woods Hole, MA 02543, USA. Tel.: +1 508 289 3493.

E-mail address: [ekujawinski@whoi.edu](mailto:ekujawinski@whoi.edu) (E.B. Kujawinski).

et al., 2002; Lanoil et al., 2009). On glacial–interglacial timescales, microbial activity might provide an important source of acidity to fuel chemical weathering of silicate rocks, a long-term control on atmospheric CO<sub>2</sub> levels (Berner et al., 1983; Brown, 2002). In addition, microbes may respire or ferment soil organic carbon (to CO<sub>2</sub> or to CH<sub>4</sub>, respectively), previously considered inert until deglaciation (Sharp et al., 1999). Wadham et al. (2008) estimated that between 418 and 610 Pg of organic carbon was present beneath ice sheets during the last glacial period, of which 63 Pg C was available for conversion to methane over a glacial cycle. Additionally, Skidmore et al. (2000) calculated that aerobic respiration of subglacial organic carbon could convert 8.1 Pg C to carbon dioxide over a glacial cycle. These calculations, however, are constrained by a lack of knowledge concerning the availability of the subglacial organic carbon stores to microbial degradation. This is a potentially large limitation, given the range in biological reactivity within all other organic carbon stores (Hedges et al., 2000; Eglinton and Repeta, 2003). In order to examine the impact of microbial oxidation on subglacial organic carbon stores, it is critical to assess the composition and reactivity of this material.

Carbon is derived from two distinct regions of the glacial environment: (1) on the glacier surface (i.e., the supraglacial environment) from inorganic and organic carbon in snow and ice; and (2) at the glacier base (i.e., the subglacial environment) where carbon is derived from the underlying bedrock, sediments, and ice. These two regions are linked by a hydrological network that becomes activated during the summer melt season when accumulated surface meltwaters drain through crevasses, moulins, and englacial channels to the bed (e.g. Nienow et al., 1998; Das et al., 2008). Once at the bed, the supraglacial meltwaters become connected to a broad subglacial hydrological drainage network, in contact with the underlying till and bedrock (Nienow et al., 1998). Generally, dissolved organic carbon (DOC) concentrations in supraglacial snow and meltwater are very low (~10–40 μM) (Lafreniere and Sharp, 2004; Lyons et al., 2007). In contrast, available organic carbon sources in subglacial environments have variable DOC concentrations ranging from 60 to 700 μM as reflected in subglacial outflow waters (Lafreniere and Sharp, 2004; Skidmore et al., 2005) and concentrations up to ~4 mM (Dry Valleys, Antarctica) and ~20 mM (Ellesmere Island, Canada) in basal ice samples (Barker et al., 2006; Bhatia et al., 2006). Although measurements are limited, this variability observed among subglacial DOC concentrations is likely a function of sampling time and/or of different physical characteristics (e.g. lithologies, sediment content, proximity to land) between and within specific field sites.

While bulk DOC abundance studies are useful as first-order investigations, they offer little information regarding the provenance, reactivity and bioavailability of the glacial organic carbon pools. In an effort to address these issues, Lafreniere and Sharp (2004) and Barker et al. (2006) used spectrofluorometric techniques to distinguish subglacial fulvic acids (the portion of humic material which is water-soluble at any pH) derived from terrestrial precursor material from those of microbial origin. Terrestrially derived dis-

solved organic matter (DOM) would contain fulvic acids from plant and soil organic matter, which are typically more aromatic, due to the presence of compounds such as lignins (McKnight et al., 2001). Alternatively, microbially-derived DOM would contain fulvic acids from microbial cell components and metabolism, and are typically less aromatic (McKnight et al., 1994; McKnight et al., 2001). Both Lafreniere and Sharp (2004) and Barker et al. (2006) found that supraglacial samples contained microbially-derived fulvic acids, which they attributed to primary productivity of algae and bacteria in the snow, ice, and meltwater on the glacial surface. However, results from the subglacial runoff were more variable, with both studies finding sources of fulvic acids with both microbial and terrestrial provenance. These findings were attributed to changing subglacial flow-routing regimes throughout the melt season that access different carbon pools as well as to *in situ* subglacial microbial metabolisms that alter the subglacial carbon pools.

Though an important first step in compositional assessment of glacial organic carbon pools, fluorescence spectroscopy studies are limited because (1) they can only assess one fraction of DOM (fulvic acids), and (2) they do not directly identify the presence of specific compounds within the DOM pool, thus permitting only broad distinctions between ‘microbial’ and ‘terrestrial’ components. In contrast, electrospray ionization (ESI) coupled to Fourier transform ion cyclotron resonance mass spectrometers (FT-ICR MS) provides an opportunity to study a larger portion of the DOC pool (intact polar molecules), and to characterize the reactivity of specific molecules in biogeochemical processes. ESI is a ‘soft’ (low-fragmentation) ionization technique that detects polar molecules with acidic and basic functional groups. When coupled to a mass spectrometer, such as FT-ICR MS which is capable of ultrahigh mass resolution (>100,000) and mass accuracy (<1 ppm), tens of molecules can be accurately resolved at each nominal mass (Kujawinski, 2002; Marshall and Rodgers, 2008). The mass accuracy achievable is the key to this technique as it enables the assignment of elemental formulae solely from the mass measurement (Kim et al., 2006; Kujawinski and Behn, 2006). Therefore, ESI FT-ICR MS can be used to identify compositional differences among pools of DOM, as well as to determine the elemental compositions of specific molecules within DOM. Recently, ESI FT-ICR MS has been utilized to characterize DOM in a range of diverse environments, including freshwater systems (Sleighter and Hatcher, 2008), marine systems (Koch et al., 2005), and ice cores (Grannas et al., 2006).

The goal of this study was to investigate the compositional nature of carbon pools associated with different regions of the Greenland ice sheet in order to elucidate the type of dissolved organic matter present in the subglacial discharge over a melt season. The carbon pools explored were (1) the supraglacial environment: snow and meltwater on the ice surface, (2) the subglacial environment: water exiting the base of a land-terminating outlet glacier, and (3) the proglacial tundra environment: non-glacially derived pond water. From a hydrological perspective, these environments are serially connected to each other as the

majority of the supraglacial meltwater on a glacier surface penetrates to the subglacial environment and eventually exits into the proglacial environment. Thus, the compositional characteristics of the contributing carbon pools as well as physical and microbial processes en route ultimately dictate the composition of the DOM in the subglacial discharge. We employed ESI FT-ICR MS to detect compositional differences among the different carbon pools sampled, and to gain insight into the molecular-level impact of microbial metabolism on subglacial organic carbon. By establishing baseline values of the type of organic carbon present beneath glaciated areas, this study serves as the foundation for broader investigations into the impact of increased meltwater runoff from the Greenland ice sheet to surrounding marine environments, and into the extent of subglacial microbial oxidation of overridden soils and vegetation.

## 2. METHODS

### 2.1. Field sites

This study was conducted at two locations along the western margin of the Greenland ice sheet in 2007 and 2008. In July 2007 two snow samples and one supraglacial meltwater sample were collected from the ablation zone on the ice sheet surface, at 980-m elevation approximately 40 km inland from the edge of the ice sheet (Fig. 1). By July most of the seasonal snow deposited the previous winter had already melted, thus our samples were collected from isolated pockets of heavily metamorphosed and colored snow from drifts along the banks of relict stream channels. Of the two snow samples analyzed for this study, one exhibited a yellow and green hue (Yellow Snow) and the other a red and black hue (Red Snow). The supraglacial meltwater sample (Supraglacial Inland) was collected from the edge of a large meltwater lake (~1 km in diameter). Given the scarcity of seasonal snow on the ice sheet surface during our sampling period, and the high annual ablation rates we measured at this site (~2-m ice melt  $\text{yr}^{-1}$ ), this meltwater sample is assumed to be derived almost entirely from glacial ice melt rather than from seasonal snow melt or rainfall.

In May and July 2008, samples were collected in the vicinity of a small land-terminating outlet glacier (named glacier 'N' here), approximately 70 km south of the 2007 site (Fig. 1). In May, one sample was collected from a small supraglacial meltwater pond (~20 m in diameter) within 1 km of the ice sheet margin (Supraglacial Margin). The water here consisted primarily of snow and ice melt. A second sample was collected from the subglacial stream exiting at the base of glacier 'N' (Subglacial May). A third sample was collected at a proglacial pond (Tarn). In July, two additional samples were collected from the subglacial stream exiting the base of glacier 'N' (Subglacial July-1 and Subglacial July-2, referred to collectively as Subglacial July). A synopsis of the samples collected in this study and the filtration and extraction procedures (details below) is presented in Table 1. Electrical conductivity (EC) measurements were made on-site using a Russell RL060C meter (Thermo Electron) for the Subglacial May and July and

Supraglacial Margin samples, and are also presented in Table 1.

### 2.2. Sample collection and filtration

The snow samples were collected aseptically using sterile plastic bags (WhirlPak; Nasco Products), and melted onsite in a warm water bath; conditions in the field precluded melting the samples at a controlled 4 °C. The water samples were collected in either combusted glass or acid-cleaned Teflon bottles. All samples were filtered on-site through 0.2- $\mu\text{m}$  filters prior to extraction, except for the Red Snow sample, which was processed back in the laboratory. Most samples (Yellow Snow, Supraglacial Inland, Supraglacial Margin, Subglacial May, Tarn) were filtered using 0.2- $\mu\text{m}$  Sterivex cartridges (Millipore), that had been pre-cleaned by soaking in a 10% HCl bath for at least one day, followed by rinsing with 20 L of Milli-Q water. The background DOC concentration of the pre-cleaned units was approximately 9  $\mu\text{M}$ . Due to limited availability of pre-cleaned Sterivex units in the field, the remaining samples (Red Snow, Subglacial July-1, Subglacial July-2) were filtered through a combusted GFF (Whatman) pre-filter and a combusted 0.2- $\mu\text{m}$  Anodisc membrane (Whatman). All solvents were purchased from Thermo Fisher Scientific (Waltham, MA) and were Optima grade or better. Concentrated HCl was Trace-Metal grade. The final volumes of 0.2- $\mu\text{m}$  filtrate (Table 1) differed to accommodate a range of anticipated DOC contents as well as the difficulties encountered with filtering some samples (for example, Subglacial May contained a significant amount of rock flour that quickly clogged the filters). An aliquot of the 0.2- $\mu\text{m}$  filtrate was acidified and stored in a combusted vial for DOC analysis.

### 2.3. Solvent extraction

Immediately following 0.2- $\mu\text{m}$  filtration, all samples were acidified to pH 3 with 12 M HCl and dissolved organic matter (DOM) was extracted with either  $\text{C}_{18}$  cartridges (Mega Bond Elut, UTC) or  $\text{C}_{18}$  extraction discs (3 M) (Table 1). All of the solvent extractions except for the Subglacial July and Red Snow samples were done on-site. The Subglacial July and Red Snow samples were kept as cold as possible, and extracted approximately two months later. The solvent extraction protocol employed was modified from Kim et al. (2003b). Briefly, the cartridges or discs were pre-cleaned according to manufacturer's instructions. The acidified sample was then passed through the cleaned cartridge/disc and the cartridge/disc was left to dry for 15 min prior to solvent extraction with methanol (MeOH) (Table 1). Extracts were evaporated to dryness under vacuum at 30 °C. For Red Snow, the 70% and 100% MeOH aliquots were combined prior to vacuum evaporation. A procedural blank (MeOH) was also evaporated to dryness under vacuum. The samples and solvent blank were stored dry at -20 °C until further analysis. We estimated our DOM extraction efficiency by drying an aliquot of the solvent extract on a pre-weighed combusted GFF, and measuring the carbon by dynamic flash combustion on a ThermoQuest EA1112 Carbon/Nitrogen Analyzer. The

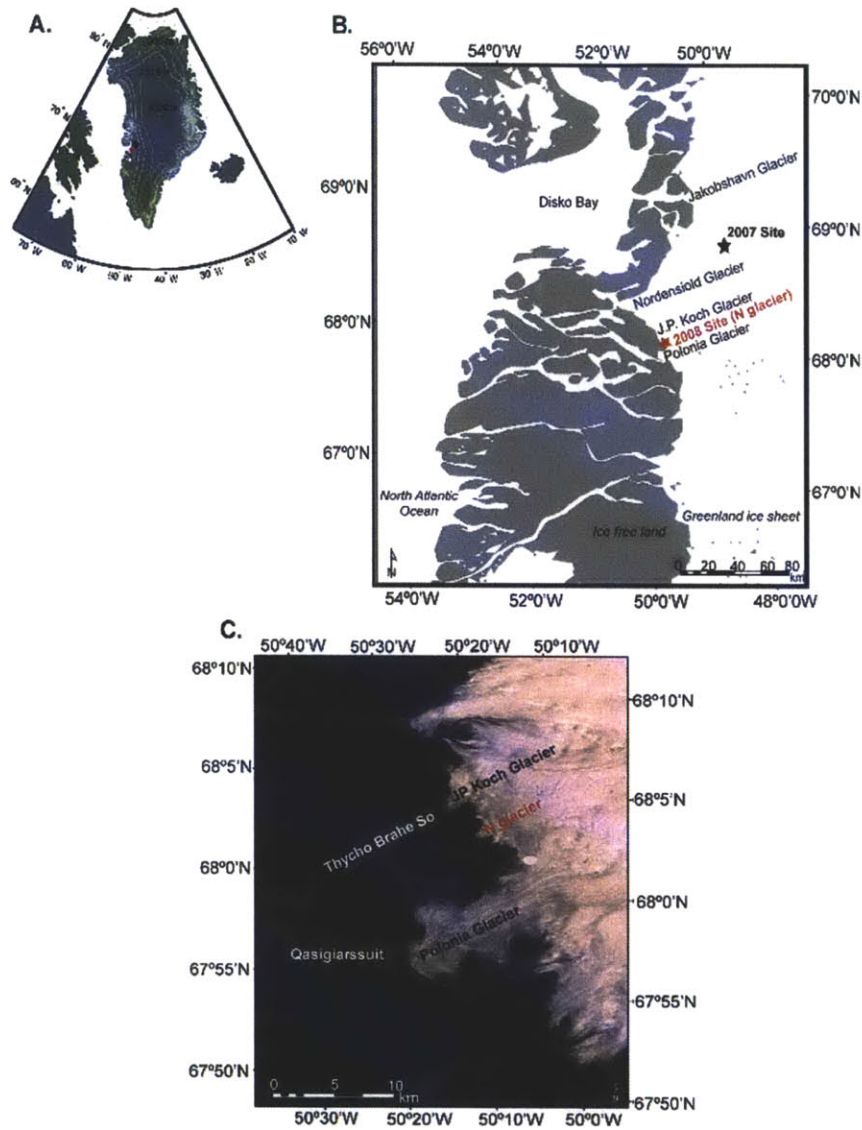


Fig. 1. Locations of the 2007 and 2008 sample sites. (A) A map of Greenland, with the black circle representing the 2007 field site and the red circle representing the 2008 field site. The green contour lines represent the surface elevation (5-km DEM from Bamber et al., 2001; Layberry and Bamber, 2001). (B) An expanded image of the two field sites. The 2007 ice surface field site is ~40 km inland from the ice sheet edge, and approximately 70 km north of the 2008 field site, located at the glacier margin. (C) A Landsat image of the 2008 ice marginal sample location (named 'N' glacier in this study). (For interpretation of the references to colour in this figure legend, the reader is referred to the web version of this article.)

extraction efficiency for each sample was calculated as the percent of carbon recovered from the solvent extract relative to the total amount of carbon in the sample (as determined by TOC analysis). The extraction efficiencies (Table 1) ranged from 10% to 94%, with a mean of 44% and a median of 28%. Although we obtained a low extrac-

tion efficiency (10%) for the Subglacial July-2 sample, we do not anticipate being limited in our conclusions since this sample is duplicated by Subglacial July-1 and the mass spectral characteristics of the two samples are nearly identical (see Section 3.2 and Fig. 3). The Tarn sample was the one most similar to previously described freshwater

Table 1

Synopsis of the samples collected in this study in preparation for DOM extraction and mass spectrometry analysis. (\*) – The [DOC] reported for Subglacial July-1 is from a sample collected 6 h prior to the sample analyzed for DOM composition in this study. N/A = data not available.

Region	Sample	Collection date	Location	Volume filtered	C <sub>18</sub> DOM extraction	Solvent extract	DOC concentration(μM)	Electrical conductivity (μS/cm <sup>3</sup> )	Extraction efficiencies (%)
Snow	Yellow Snow	July 17 2007	68°33'N49°23'W	2 L	Cartridge	40 mL 100% MeOH	N/A	N/A	N/A
Snow	Red Snow	July 17 2007	68°34'N49°22'W	87 mL	Discs	5 mL 70%, 5 mL 100% MeOH	N/A	N/A	N/A
Supraglacial	Supraglacial Inland	July 14 2007	68°34'N49°21'W	15 L	Cartridge	40 mL 100% MeOH	N/A	N/A	N/A
Supraglacial	Supraglacial Margin	May 31 2008	68°02'N50°15'W	4 L	Cartridge	15 mL 100% MeOH	16 ± 0.7	0.2	28
Subglacial	Subglacial May	May 31 2008	68°02'N50°16'W	500 mL	Cartridge	15 mL 100% MeOH	28 ± 0.2	17	94
Proglacial	Tarn	May 29 2008	68°02'N50°17'W	1 L	Cartridge	15 mL 100% MeOH	406 ± 3	N/A	57
Subglacial	Subglacial July-1	July 12 2008	68°02'N50°16'W	4.5 L	Cartridge	15 mL 100% MeOH	*15 ± 0.4	3.2	28
Subglacial	Subglacial July-2	July 16 2008	68°02'N50°16'W	3.45 L	Cartridge	15 mL 100% MeOH	51 ± 0.3	2.3	10

samples and the extraction efficiency of this sample (60%) is well within the range documented to other freshwater studies (Kim et al., 2003b; Dittmar et al., 2008).

#### 2.4. DOC concentrations

Total and dissolved organic carbon (TOC, DOC) concentrations were quantified as non-purgeable organic carbon (NPOC) by high temperature combustion (680 °C) with a Shimadzu TOC-V<sub>CSH</sub> analyzer equipped with a high sensitivity platinum catalyst (Shimadzu Scientific Instruments). Samples were quantified using a 5-point standard curve made with potassium hydrogen phthalate (KHP). Blanks and reference standards were analyzed routinely within each sample run. Reference standards for low carbon water and deep-sea water were obtained from the Consensus Reference Materials Project, Hansell Laboratory, University of Miami. DOC was not quantified for the 2007 samples due to post-acquisition contamination in Greenland.

#### 2.5. FT-MS data acquisition

All samples and the solvent blank were analyzed on a 7-T ESI FT-ICR mass spectrometer (LTQ-FT-MS, Thermo Fisher Scientific, Waltham, MA). For positive ion mode analyses, sample aliquots were reconstituted in 80% MeOH

with 0.1% acetic acid (final concentration). Acetic acid promoted positive ion formation. For negative ion mode analyses, reconstituted sample aliquots were reconstituted in 70% MeOH. The solvents used to dilute the samples were also analyzed as instrument blanks (100% MeOH in positive ion mode and 70% MeOH in negative ion mode).

For both positive and negative ion modes, samples were infused into the ESI interface at 4 μL min<sup>-1</sup>, and instrument parameters were optimized for each sample. Samples were diluted to optimize spray conditions; dilutions ranged from 1:5 to 1:40. The capillary temperature was set at 250 °C, and the spray voltage varied between 4.40 and 4.60 kV. About 200 scans were collected for each sample, a sufficient number of scans for peak reproducibility in our samples. The mass ranges for full-scan collection were 200 < *m/z* < 1200 and 200 < *m/z* < 1000 in positive and negative ion modes, respectively. Weekly mass calibrations were performed with an external standard (Thermo Calibration Mix), and resulted in mass accuracy errors <1 ppm. The target average resolving power was 400,000 at *m/z* 400 (where resolving power is defined as  $m/\Delta m_{50\%}$  where  $\Delta m_{50\%}$  is the width at half-height of peak *m*). Good quality data could not be collected for the Subglacial July-2 sample in positive ion mode, nor for the Red Snow sample in negative ion mode. This was due to unacceptable spray stabilities in the former and fluctuating ion currents in the latter.

## 2.6. FT-MS data analysis

### 2.6.1. Peak detection and blank correction

We collected individual transients as well as a combined raw file using *xCalibur 2.0*. Transients were co-added and processed with custom-written MATLAB code provided by Southam et al. (2007). This code was used as provided with the following parameters. Within each sample, only those transients whose total ion current (TIC) was greater than 20% of the maximal TIC were co-added and then processed with Hanning apodisation, and zero-filled once prior to fast Fourier transformation. We retained all *m/z* values with a signal-to-noise ratio above 5 (as calculated in Southam et al. (2007)). The individual sample and solvent blank peak lists were then aligned using MATLAB code provided by Mantini et al. (2007). Positive and negative ion mode data were aligned separately in MATLAB with an error tolerance of 1 ppm. Following alignment, all peaks found in each mode's solvent blanks were removed from the appropriate master list. These blank-corrected master peak lists in each sample were used in all downstream statistical analyses and elemental formula assignments.

### 2.6.2. Calibration

Positive and negative ion mode spectra were internally re-calibrated using a short list of *m/z* values present in a majority of samples. This list of calibrants was chosen according to the following criteria: (1) presence in the majority of samples; (2) elemental formulae could be assigned with C, H, O and N; (3) similar mass errors for all; and (4) distribution along the *m/z* range of each spectrum. The resulting calibrants and their elemental formulae are provided in EA Table 1a and b. After internal re-calibration, the root mean square (RMS) errors for the calibrants ranged from 0.09 to 0.12 in positive ion mode and 0.04 to 0.69 in negative ion mode.

### 2.6.3. Elemental formula assignments

Elemental formulae were assigned to the aligned blank-corrected peaks (*m/z* values) using the Compound Identification Algorithm (CIA), described by Kujawinski and Behn (2006) and modified in Kujawinski et al. (2009). In the CIA, we set the following parameters: (a) formula error was 1 ppm, (b) the relationship error was 20 ppm, and (c) the mass limit above which elemental formulae were only assigned by functional group relationships was 500 Da. For this study, elemental formulae were determined for *m/z* values below 500 Da by comparison to an in-house database of mathematically and chemically legitimate formulae within the 1 ppm error window. Elemental formula assignments were constrained to  $^{12}\text{C}$ ,  $^{13}\text{C}$ ,  $^1\text{H}$ ,  $^{16}\text{O}$ ,  $^{14}\text{N}$ ,  $^{34}\text{S}$ , and  $^{31}\text{P}$ . Error testing for formula assignments containing these elements was done using synthetic datasets and is documented in Kujawinski and Behn (2006). Accuracy of formula assignments ranges from 78% to 100%, depending on included elements (Kujawinski and Behn, 2006). These elemental formulae were extended to *m/z* values above 500 Da through identification of functional group relationships. The functional group relationships used by CIA are common to refractory dissolved organic matter (e.g. humic

acids); CIA does not presently include many functional group relationships resulting from metabolic (biological) reactions (Kujawinski and Behn, 2006). Isotopomers with a  $^{13}\text{C}$  atom are identified in the last step of CIA and elemental formulae are corrected to reflect  $^{13}\text{C}$  content. In order to identify terrestrially-derived components of our samples, we compared the elemental formulae for our Greenland samples with those assigned to Suwannee River Fulvic Acid Standard I (Suwannee River – International Humic Substances Society, Stock #1S101F), previously analyzed in our laboratory with negative ion mode ESI FT-ICR MS. Magnitude-averaged elemental ratios and double bond equivalencies were calculated (Sleighter and Hatcher, 2008).

### 2.6.4. Assessment of potential contamination

Analysis of the negative and positive ion mode mass spectra revealed potential contamination likely originating from plasticizers or the  $\text{C}_{18}$  extraction cartridges/discs. In negative ion mode, potential contamination was most prevalent in the Yellow Snow sample. We assigned elemental formulae to the contaminated *m/z* values (18 peaks) and identified peaks belonging to this series in other negative ion mode spectra. Contaminated peaks did not occupy any particular region of the van Krevelen diagram (EA Fig. 1). We realize that any contamination may skew the overall composition of the DOM through ion suppression; nonetheless, we believe we attained an adequate representation of DOM composition within our samples because the maximum percentage of peaks represented by the suspected plasticizer contamination was less than 0.6% in any one sample. In addition, to further minimize the potential impact of this contamination, we based our statistical analyses and subsequent conclusions on the diversity of resolved peaks (presence/absence) rather than on their relative peak heights. In positive ion mode, the potential contamination was more pervasive. Inspection of the raw mass spectra revealed likely contamination in the Yellow Snow, Subglacial May, and Tarn samples. Given this observation, we focused our statistical analyses and interpretations on the negative ion mode dataset.

### 2.6.5. Multivariate statistics

We assessed differences in our samples in negative ion mode with cluster analysis as described in Kujawinski et al. (2009). In our analysis, we transformed all relative peak heights to presence (peak height = 1) or absence (peak height = 0). We recognize that ESI is not quantitative and that differences in ionization efficiencies among compounds can lead to misrepresentations of ion peak height, relative to the abundance of the parent molecule in neutral solution (Stenson et al., 2003). To circumvent this known problem, we have used presence/absence comparisons rather than those that rely on relative peak height.

The presence/absence transformation allows assessment of how samples differ based solely on peak diversity. A distance matrix was calculated between all the samples in each mode using the Bray–Curtis distance measure (MATLAB code written by David Jones, University of Miami, as part of the Fathom toolbox); a distance measure of 0 indicates samples are identical with regards to peak diversity,



whereas a distance measure of 1 indicates that samples share none of their peaks. Ward's linkage method was used to group the samples followed by presentation of the results as a dendrogram.

#### 2.6.6. Indicator species analysis

We identified specific  $m/z$  values characteristic of the observed negative ion mode cluster groupings with indicator species analysis (ISA – as implemented in Kujawinski et al., 2009). ISA combines the relative abundance and relative frequency of a peak within a pre-defined group of samples to assign an indicator value (IV) to each peak (McCune and Grace, 2002). A perfect IV (equal to 100) of a particular group would constitute an  $m/z$  value that was present exclusively in the samples comprising that group (McCune and Grace, 2002). Statistical significance of IVs is calculated by comparison with Monte-Carlo simulations of randomized data. ISA requires a priori assignment of samples to groups; this was achieved using the protocol and criteria described in McCune and Grace (2002). The best number of groups occurred when we used four groups of samples: Group 1 = Yellow Snow; Group 2 = Supraglacial Inland; Group 3 = 'N' glacier May samples (Subglacial May and Supraglacial Margin); and Group 4 = 'N' glacier July and Tarn samples (Subglacial July-1, 2 and Tarn). This group assignment was used to find indicator  $m/z$  values for Groups 3 and 4; use of ISA is restricted to those groups with more than one sample, thus no 'indicator peaks' were identified for Groups 1 and 2. The final list of indicator  $m/z$  values for each group was manually curated using the criteria outlined in Kujawinski et al. (2009).

### 3. RESULTS AND DISCUSSION

#### 3.1. Sample overview

The eight samples analyzed in this study represent carbon pools associated with different regions of a glacier sys-

tem. The supraglacial pools are represented by snow (Yellow Snow, Red Snow) and meltwater (Supraglacial Inland) samples from the inland ice surface as well as the meltwater sample collected on the surface of 'N' glacier (Supraglacial Margin). The subglacial pool at the glacier base is represented by samples collected from the subglacial stream exiting at the base of 'N' glacier (Subglacial May, Subglacial July-1, 2). Since surface ice melting is minimal in May, the Subglacial May water sample most likely represents early/spring discharge waters that have been stored at the bed overwinter. These waters likely drain a more distributed subglacial hydrological system with relatively slower flow rates, but they may access a greater areal extent of the subglacial bed (Nienow et al., 1998; Sharp et al., 1999). Conversely, the July subglacial water samples represent late/summer discharge waters fed primarily by supraglacial inflow. These waters likely drain through a channelized hydrological system characterized by relatively much higher flow rates, but they may access a more limited part of the bed (Bingham et al., 2005; Nienow et al., 1998). The electrical conductivity (EC) measurements (Table 1) support this interpretation. The Subglacial May sample has a greater content of dissolved solutes compared to the Subglacial July samples. Finally, a proglacial tarn (Tarn) represents a terrestrial carbon end-member, comprised of non-glacial water, situated in the deglaciated arctic tundra and likely containing a large terrestrial contribution from the surrounding vegetation.

#### 3.2. Comparison of ultra-high resolution mass spectra

All of the samples contained highly complex DOM with numerous peaks per nominal mass in both positive and negative ion modes. The total numbers of peaks resolved in each sample in negative ion mode following blank correction are presented in Table 2. Qualitative differences among the raw mass spectra illustrate that samples representing different regions of the Greenland ice sheet have distinct

Table 2

Synopsis of general parameters regarding negative ion mode formula assignments. Elemental ratios were calculated as magnitude-averaged values (Sleighter and Hatcher, 2008) for  $m/z$  values with assigned elemental formulae.

Sample	Total number of peaks	Number of formulae assigned	% Formulae assigned	H:C <sub>w</sub>	O:C <sub>w</sub>	N:C <sub>w</sub>	S:C <sub>w</sub>	P:C <sub>w</sub>	DBE <sub>w</sub>	% Formulae with CHO	% Formulae with CHON	% Formulae with CHONP, CHONS, CHONSP
Yellow Snow	5113	4380	85.7	1.22	0.41	0.30	0.04	0.05	9.79	17.4	23.4	42.5
Supraglacial Inland	1865	1169	62.7	1.16	0.40	0.33	0.03	0.05	12.15	1.7	32.0	50.1
Supraglacial Margin	2331	1980	84.9	1.68	0.27	0.27	0.01	0.03	6.21	23.3	34.7	25.0
Subglacial May	1737	1662	95.7	1.56	0.38	0.17	0.00	0.01	6.66	55.6	26.1	11.3
Subglacial July-1	3330	3249	97.6	1.26	0.38	0.16	0.00	0.02	9.62	69.2	8.1	18.9
Subglacial July-2	3048	2800	91.9	1.24	0.38	0.21	0.00	0.02	10.08	58.9	10.8	26.2
Tarn	5958	5826	97.8	1.27	0.43	0.12	0.00	0.01	10.28	65.7	12.3	17.5
Suwannee River	2092	2079	99.4	1.05	0.55	0.03	0.00	0.01	10.85	91.3	2.0	4.5

DOM compositions (Fig. 2). Although ultra-high resolution mass spectrometry has not been used to date to compare DOM from different glacial sub-environments, this result is not surprising since both bulk DOC concentrations and *in situ* microbial communities can differ vastly among glacial sub-environments (Bhatia et al., 2006).

Cluster analysis based on the presence/absence of resolved peaks in negative ion mode (Fig. 3) revealed that the samples collected on the inland ice sheet (Yellow Snow, Supraglacial Inland) were distinct from each other as well as from those collected at the ice sheet margin (Subglacial May, Supraglacial Margin, Tarn, Subglacial July-1, 2). Indeed, the Yellow Snow and Supraglacial Inland samples share very few peaks (<20%) with any of the samples col-

lected at the ice margin (Table 3). The cluster analysis for positive ion mode data (not shown) confirmed that the three samples from the inland ice sheet (Yellow Snow, Red Snow, and Supraglacial Inland) were distinct from the ice margin samples (Subglacial May, Supraglacial Margin, Tarn, Subglacial July-1). Differentiation between these sample groups is expected since the Yellow Snow and Red Snow should represent very different, localized regions on the ice sheet surface with unique algal and microbial communities. The lack of similarity between the supraglacial meltwater samples (Supraglacial Inland and Supraglacial Margin, only sharing 13% and 10% of their peaks respectively, Table 3) could be attributed to geographical, seasonal and water source differences. For

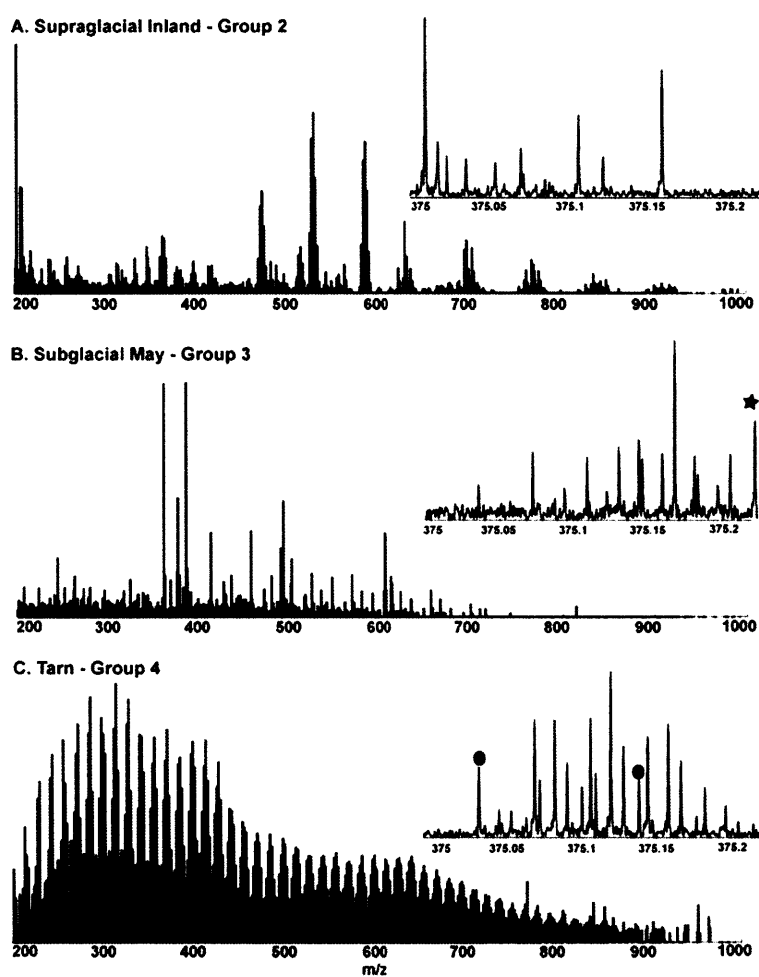


Fig. 2. Negative ion mode blank-corrected, calibrated mass spectra from the groups identified in indicator species and cluster analysis. Group 1: Yellow Snow (not shown); Group 2: Supraglacial Inland; Group 3: N glacier May (Subglacial May and Supraglacial Margin); and Group 4: terrestrial/N glacier July (Tarn and Subglacial July-1, 2). The inset shows the region  $375.0 \leq m/z \leq 375.2$  and the indicator  $m/z$  values for Group 3 (black stars) and Group 4 (black ovals).

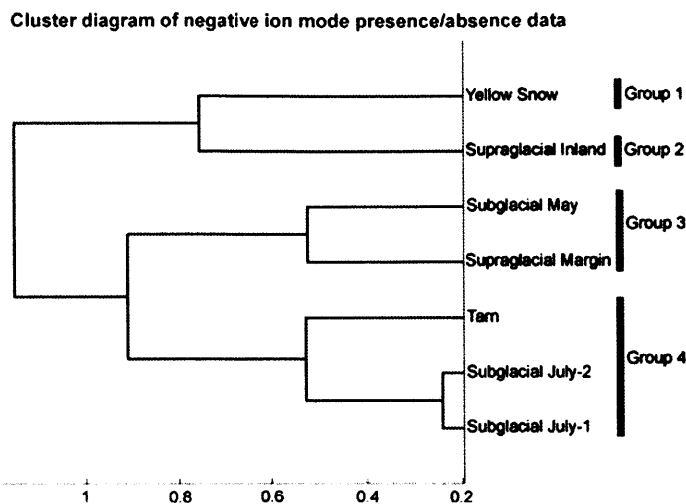


Fig. 3. Cluster diagram of the seven negative ion mode samples, based on Bray–Curtis distance measure and Ward's linkage method.

Table 3

Percentage of negative ion mode peaks shared between the different samples analyzed in this study and Suwannee River.

Sample	Yellow Snow	Supraglacial Inland	Supraglacial Margin	Subglacial May	Subglacial July-1	Subglacial July-2	Tarn	Suwannee River
% Yellow Snow shared with	100	17	16	13	15	15	18	9
% Supraglacial Inland shared with	46	100	13	7	11	14	9	4
% Supraglacial Margin shared with	35	11	100	42	39	35	35	11
% Subglacial May shared with	39	7	56	100	61	56	60	36
% Subglacial July-1 shared with	23	6	27	32	100	73	79	39
% Subglacial July-2 shared with	24	9	27	32	79	100	73	39
% Tarn shared with	16	3	14	18	44	37	100	25
% Suwannee River shared with	22	4	12	29	62	57	70	100

example, the Supraglacial Inland sample was collected from a large supraglacial lake composed almost entirely of inland ice melt. In contrast, the Supraglacial Margin sample was collected from a small meltwater pool closer to the ice edge and much earlier in the melt season, and thus is comprised of a mixture of marginal snow and ice melt.

Among the margin-site samples, results from the cluster analyses for positive and negative ion modes indicate that the DOM composition in the subglacial runoff changes during the melt season. Specifically, the negative ion mode cluster analysis illustrates that the 'N' glacier May samples (Supraglacial Margin and Subglacial May) were grouped (sharing 42% and 56% of their peaks respectively, Table 3) as were the Subglacial July-1, 2 and Tarn samples (Subglacial July samples sharing 73–79% of their peaks with the Tarn sample, Table 3). Interestingly, the Subglacial July samples are quite distinct from the Subglacial May sample

even though the two samples were collected from the same location. In addition, there is significant peak overlap between Suwannee River and the Tarn sample (70%) and between the Subglacial July samples (57–62%), but much less between Suwannee River and the Subglacial May sample (30%). Thus, although our samples are temporally limited (May and July), we infer that the type of DOM in subglacial discharge changed during the 2008 melt season.

### 3.3. Elemental formula assignments and indicator species analysis

We were able to assign formulae to over 90% of the resolved peaks in the Suwannee River and the Tarn, Subglacial July-1, 2, and Subglacial May samples. We achieved slightly lower percentages of formulae assigned to the Yellow Snow (86%) and Supraglacial Margin (85%) samples, with the

lowest percentage of formulae found for the Supraglacial Inland sample (63%). In an effort to increase the percentage of formula assignments in this sample, we made two temporary modifications to CIA. First, we included halogens (F, Cl, Br, and I) in our formula assignments; and second, we attempted to account for multiply-charged molecules. Inclusion of halogens did not increase our formula assignment rate appreciably. In contrast, corrections for doubly- and triply-charged molecules produced a marked increase in the Supraglacial Inland formula assignment percentage (up to 98%), suggesting that a good portion of our  $m/z$  values represented multiply-charged molecules with multiple de-protonation sites. We discarded these improvements, however, because the modified CIA lowered the formula assignment accuracy when tested with Suwannee River formulae and because multiply-charged isotopomers were rarely available for reliable charge-state determination. Thus, we were forced to retain the original lower formula assignment percentages made to the Supraglacial Inland sample.

Elemental formulae containing only C, H, and O dominated the formula assignments for the Tarn and subglacial samples (Subglacial May and Subglacial July-1, 2) (Table 2). Conversely, the supraglacial samples were dominated by formulae containing C, H, O, and N (Supraglacial Margin), or C, H, O, N, and S/P (Yellow Snow, Supraglacial Inland) (Table 2). We should note that this result differs from analysis of other supraglacial organic material in ice cores collected from Russia where formulae containing C, H, and O were the most abundant (Grannas et al., 2006). However, the snow and meltwater samples analyzed in this study (i.e., collected from marginal areas where there is snow melt and water in the residual snowpack) are quite different from bulk ice core material (i.e., collected from inland areas where ice is formed in the dry snow zone), so it is not surprising that we resolved different compounds.

For comparison with other DOM compositional studies, we calculated the magnitude-averaged bulk elemental ratios and double-bond equivalency (DBE) for all samples (Table 2) (Koch et al., 2008; Sleighter and Hatcher, 2008). Molecular H:C and O:C ratios have been reported previously to range broadly from 0.3 to 1.8 and 0 to 0.8, respectively (Koch et al., 2008; Sleighter and Hatcher, 2008; Stenson et al., 2003). The elemental ratios of all of our samples fall within this range (Table 2), with Suwannee River being the most aromatic (H:C = 1.05), and the Subglacial May and Supraglacial Margin samples being the most aliphatic (H:C = 1.68 and 1.56, respectively). The low DBE of the Supraglacial Margin and Subglacial May samples also imply that DOM in these samples is relatively aliphatic. The DBE was the highest in the Supraglacial Inland sample. This fact, combined with the relatively lower H:C ratio (1.16) and relatively higher N:C ratio (0.33) of this sample (Table 2), suggest that molecules within this sample may contain condensed nitrogen functionalities (i.e., aromatic nitrogen or nitro groups). Finally, the supraglacial samples (Yellow Snow, Supraglacial Inland, Supraglacial Margin) generally had relatively high N:C ratios (0.30, 0.33, 0.27, respectively, Table 2), suggesting that nitrogen-containing molecules could be major contributors to DOM in these samples (Reemtsma et al., 2008).

Van Krevelen diagrams were generated for all Greenland samples and Suwannee River in order to compare DOM composition across our samples (representative sample plots in Fig. 4). Van Krevelen diagrams illustrate the O:C molar ratio and the H:C molar ratio of each elemental formula on the  $x$ - and  $y$ -axes, respectively. Generally, major biogeochemical compound classes (such as condensed hydrocarbons, lipids, proteins, lignins, and carbohydrates) have characteristic H:C and/or O:C molar ratios, and thus should occupy specific regions of the plot (Kim et al., 2003a; Wu et al., 2004; Kujawinski and Behn, 2006). The percentages of negative ion mode formula assignments located in the different regions of the van Krevelen diagram are presented in Table 4. However, we should note that van Krevelen diagrams should be interpreted with caution as inconsistent definitions of particular compound classes across the literature (e.g., lipid), and variable O:C or H:C ratios within particular compound classes (e.g., proteins) may lead to exclusion of elemental formulae from the prescribed compound class regions (Kujawinski and Behn, 2006). Nonetheless, at present, they remain the best way to graphically depict elemental formula assignments for mass spectra comprised of thousands of peaks.

The van Krevelen plot of the negative ion mode Suwannee River sample (not shown) is consistent with previous work (Stenson et al., 2003). Over 99% of formulae were assigned and most occur in the region associated with lignin-derived materials (Stenson et al., 2003). Very few formulae are present in the regions associated with proteins and lipids (Table 4). Because of these results and the fact that Suwannee River is well-cited as a terrestrial DOM end-member (e.g. McKnight et al., 2001; Stenson et al., 2003), we label the region encompassing the majority of its elemental formula assignments as "terrestrial" (shown in Figs. 4 and 5), and use this information to aid our analyses of our negative ion mode spectra.

The van Krevelen diagrams may explain the observed cluster groupings in Fig. 3. In negative ion mode, the separation between the samples collected on the ice sheet surface and those collected at the margin may be the result of the Yellow Snow and Supraglacial Inland samples having a greater representation in the condensed hydrocarbon region and a lower proportion in the lignin region (Table 4). The grouping of the Subglacial May and Supraglacial Margin samples may be due to greater proportions of protein-like and lipid-like material in these samples compared to the remainder of the dataset (Table 4). The grouping of the Tarn and Subglacial July samples results from a commonality in every region of the van Krevelen plot, particularly in the terrestrial Suwannee River and lignin regions (Table 4).

Apart from these general trends, each sample also has some noteworthy features on the van Krevelen diagram. In addition to a large protein-like component, the Supraglacial Margin sample also contains more formulae in the lipid and the condensed hydrocarbon regions than the Subglacial May sample (Table 4). Even though both the Supraglacial Margin and Subglacial May samples contain lignin-like molecules, the Subglacial May sample has a larger proportion of formulae in the "terrestrial" Suwannee

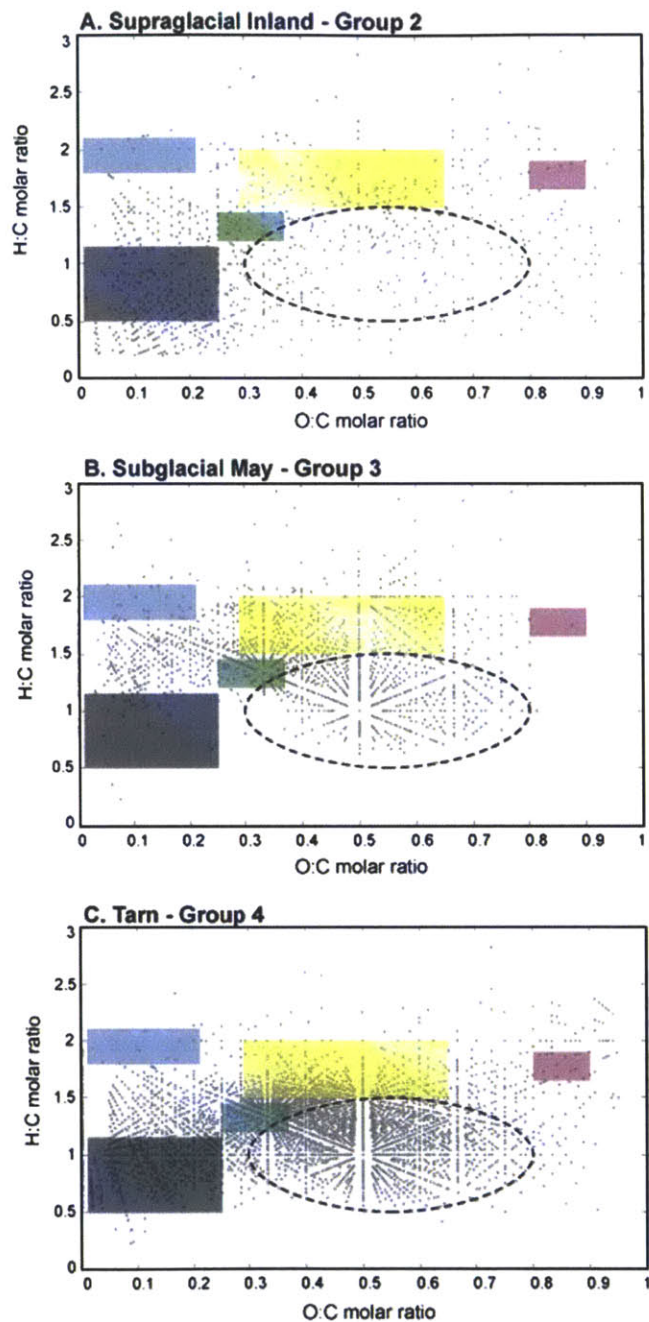


Fig. 4. Van Krevelen diagrams of all formulae assigned (grey dots) to negative ion mode peaks detected within the Supraglacial Inland (A), Subglacial May (B), and Tarn (C) samples. The colored boxes represent elemental compositions for some major compound classes, as approximated from Kim et al. (2003) and Hedges (1990). The grey box represents condensed hydrocarbons, the blue box represents lipids, the green box represents lignin, the yellow box represents proteins, and the pink box represents carbohydrates. The black oval represents elemental formula assignments made for a sample of Suwannee River Fulvic Acid. (For interpretation of the references to colour in this figure legend, the reader is referred to the web version of this article.)

Table 4

Percentage of negative ion mode formula assignments located in different regions of the van Krevelen diagram. Group numbers refer to groups determined by indicator species analysis (see text for details).

Sample	Condensed hydrocarbons	Lipids	Lignin	Protein	Carbohydrate	Terrestrial
Yellow Snow (Group 1)	12.6	1.1	3.0	12.7	0.6	29.2
Supraglacial Inland (Group 2)	16.0	0.5	2.4	9.2	0.6	23.5
Supraglacial Margin (Group 3)	6.8	4.7	3.6	27.0	0.3	14.3
Subglacial May (Group 3)	1.1	1.5	5.5	25.5	0.1	39.2
Subglacial July-1 (Group 4)	6.9	0.9	10.2	10.4	0.1	55.6
Subglacial July-2 (Group 4)	7.8	1.1	8.5	8.4	0.0	55.8
Tarn (Group 4)	9.8	0.1	7.5	13.3	0.3	59.3
Suwannee River	2.0	0.0	4.5	1.9	0.0	85.6

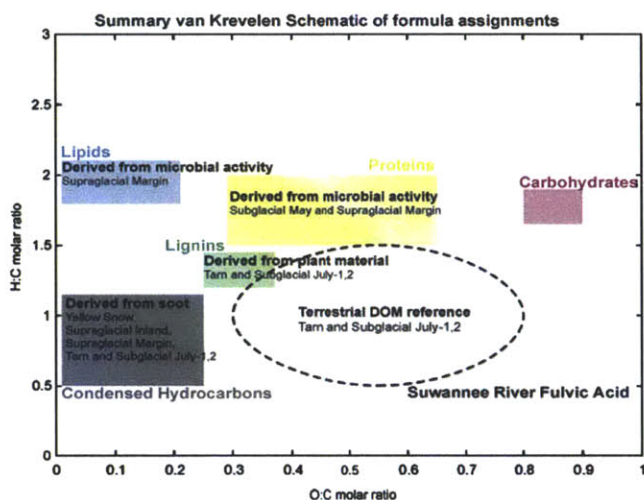


Fig. 5. Van Krevelen diagram summarizing the formula assignments for the negative ion mode samples. The samples/groups containing a high proportion of peaks in the different compound classes are named.

River region (Table 4). The Tarn and Subglacial July samples all contain a larger proportion of formulae in the condensed hydrocarbon and protein regions than the Suwannee River sample (Table 4). The results of our analyses of the van Krevelen plots for each of the samples are summarized in Fig. 5.

Indicator species analysis revealed that a higher content of biologically-derived elemental formulae is responsible for the differentiation of the Subglacial May and Supraglacial Margin samples (Group 3) from the Tarn and Subglacial July samples (Group 4). Indicator  $m/z$  values for the Group 3 samples are dominated by high H:C compounds occupying the protein region of the van Krevelen diagram (Fig. 6A). Conversely, the indicator  $m/z$  values for the Group 4 samples are dominated by low H:C compounds found in the terrestrial Suwannee River region. There is a significant terrestrial component within all the ice margin samples, as evidenced by the presence of indicator  $m/z$  values common to Groups 3 and 4 (yellow dots, Fig. 6B) in this region. This component is absent in the samples collected on the inland ice sheet surface (Yellow Snow and Supraglacial Inland, Groups 1 and 2).

### 3.4. Potential sources of observed peaks

#### 3.4.1. Microbially-derived material (lipid-like and protein-like signatures)

Similar to previous fluorescence studies (Lafreniere and Sharp, 2004; Barker et al., 2006), the distinct microbial character of the Supraglacial Margin sample (reflected by its high proportion of protein-like formulae) is likely derived from photosynthetic algae and bacteria communities widely observed to be present in supraglacial environments (Carpenter et al., 2000; Grannas et al., 2004; Foreman et al., 2007). The presence of lipid-like material in the Supraglacial Margin sample also correlates well with previous work identifying biologically-derived lipids in organic matter from snow collected at Summit atop the Greenland ice sheet (Grannas et al., 2004; Grannas et al., 2006).

Early season (spring) subglacial waters have also been observed to have a microbial fluorescence signature (Lafreniere and Sharp, 2004; Barker et al., 2006), despite the fact that terrestrial carbon from overridden soils and vegetation is also present at the glacier base (Sharp et al., 1999). The larger proportion of protein-like formulae in



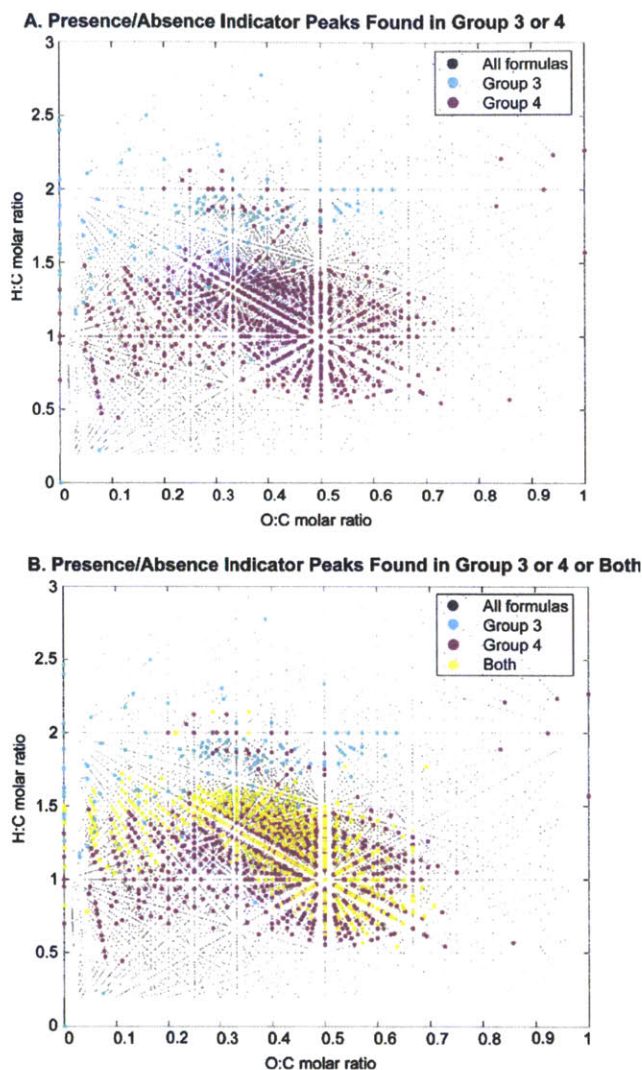


Fig. 6. Van Krevelen negative ion mode diagrams with indicator peaks determined by Indicator Species Analysis. In (A), indicator peaks exclusive to either Group 3 (N glacier May (Subglacial May and Supraglacial Margin)) or Group 4 (terrestrial/N glacier July (Tarn and Subglacial July-1, 2)) are shown; in (B), peaks from (A) are shown as well as indicator peaks found in both Groups 3 and 4.

the early season subglacial waters (Subglacial May) may reflect *in situ* subglacial microbial metabolism of some component of the subglacial organic carbon stores during over winter storage (Tranter et al., 2005). The May subglacial water likely drains a broad distributed hydrological network along the ice-bed interface, and consequently experiences prolonged storage at the bed where active subglacial microbial communities are thought to be present (Tranter et al., 2005). Although no study has documented the presence of subglacial communities beneath the Greenland ice sheet specifically, a mounting body of literature

indicates that large, active microbial communities are present beneath glaciers in diverse regions on varying lithologies (the Swiss Alps, southern New Zealand Alps, Alaska, Svalbard, Antarctica, and the Canadian high Arctic) (Sharp et al., 1999; Skidmore et al., 2000; Lanoil et al., 2009; Mikucki et al., 2009). Furthermore, studies show that the abundances of subglacial communities (as high as  $1.8 \times 10^9$  cells  $g^{-1}$ ) are similar to the highest microbial abundances in permafrost ( $10^7$ – $10^9$  cells  $g^{-1}$ ) (Sharp et al., 1999). Documented subglacial communities include heterotrophic bacteria (e.g., aerobic respirers, nitrate- and sulfate-

reducers) as well as autotrophic bacteria (e.g., methanogens) (Skidmore et al., 2000; Foght et al., 2004; Cheng and Foght, 2007). The existence of numerically-abundant, enduring biological communities implies that any microbially-mediated biogeochemical activities occur on a continuous temporal basis. The diverse DOM composition in the Subglacial May sample is consistent with the idea of high subglacial microbial activity due in particular to its significant protein and terrestrial components (Table 4).

#### 3.4.2. Terrestrial-derived material (lignins and Suwannee River-like components)

Lignins and formulae located in the “terrestrial” region of our van Krevelen plots are likely derived from previously overridden soils and vegetation (subglacial samples) or surrounding terrestrial soils and vegetation (Tarn). The large component of terrestrially-derived DOM in the Tarn sample (overlap between Suwannee River and the Tarn sample is 70%), is likely derived from its location in the developed soils and vegetation at our study site. In contrast, the subglacial samples contain terrestrially-derived DOM, present in both May and July, that is most likely derived from previously overridden soils and vegetation during glacial advance. The lack of lignin material in the samples collected on the inland ice sheet surface (Yellow Snow, Supraglacial Inland) suggests that organic matter from these environments is not influenced significantly by non-charred terrestrial inputs. This is in contrast to Grannas et al. (2004) who noted the presence of vascular plant tissue (i.e., lignin) in snow collected from Summit, Greenland.

#### 3.4.3. Condensed hydrocarbons

Condensed hydrocarbons are generally compounds with a deficiency in both oxygen and hydrogen and often contain aromatic ring structures. Previous studies have illustrated that these compounds originate from black carbon-like molecules (Kim et al., 2004), and could be derived from atmospheric deposition of soot particles (Slater et al., 2002). Evidence of these compound types is present in all ice sheet surface samples (Yellow Snow, Supraglacial Inland, Supraglacial Margin) and the late/summer discharge samples (Subglacial July-1, 2). On the ice sheet surface, this material likely originates from atmospheric deposition of combustion products. We do not anticipate a novel source of condensed hydrocarbons in the subglacial environment. Rather, the presence of condensed hydrocarbons in late season subglacial waters (Subglacial July-1, 2) may reflect either (1) the increased contribution of supraglacial meltwater to the subglacial outflow at the peak of the summer melt season, or (2) an increased flux of condensed hydrocarbons from the ice sheet surface after the snow cover has melted. Support for this second hypothesis may be provided by Clarke and Noone (1985), who found that soot may be enriched in Arctic snowmelt compared to the snowpack.

### 3.5. Implications for understanding subglacial flow regimes

The fact that the late season subglacial waters still possess an overwhelming terrestrial signature may reflect the ability of the summer hydrological flow regime to mobilize

subglacial organic carbon stores. As the melt season progresses on the Greenland ice sheet, meltwater from seasonal snow and ice collects in streams and lakes on the ice sheet surface. The majority of this surface meltwater is thought to descend to the bed via crevasses and moulins at the peak of the summer melt season (Das et al., 2008; Krawczynski et al., 2009). Thus, the late season subglacial waters are primarily comprised of supraglacial inflow passing rapidly through the subglacial environment. Over the course of a melt season, the ice sheet subglacial drainage system is predicted to evolve from a distributed to a more channelized network facilitating rapid water flow to the glacier front, similar to what has been observed in alpine glacier systems (Nienow et al., 1998). The faster flow rates characteristic of this channelized system do not permit extensive water-sediment interaction, thus minimizing the impact of *in situ* microbial metabolism (Tranter et al., 2005). Additionally, the larger volumes of water passing through the subglacial system may facilitate turbulent incidental contact that allows the meltwaters to mobilize terrestrial sources of DOC at the glacier base (i.e., previously overridden soil and vegetation). Previous work in alpine catchments has illustrated that suspended sediment concentrations increase throughout a melt season as sediment sources are accessed by an extending and integrating subglacial drainage network (Clifford et al., 1995; Richards et al., 1996). This reasoning is also consistent with previous fluorescence spectroscopy work by Barker et al. (2006) at a polythermal Canadian high Arctic glacier, which showed that the late season subglacial meltwaters bear a terrestrially-derived signature. The change in subglacial flow rate may explain why condensed hydrocarbons are not present in the early season subglacial waters. Increased residence times of these waters at the glacier bed throughout the preceding winter would permit non-polar hydrocarbon-like, soot-derived compounds to adsorb quantitatively to organic particles in the subglacial environment (Kramer et al., 2004) and thus to be removed from discharge waters. At the peak of the summer melt season, the higher meltwater flow rates and potentially elevated hydrocarbon concentrations would preclude quantitative removal by adsorption, allowing the subglacial waters to retain these compounds in the late season subglacial runoff.

### 3.6. Implications for understanding glacial organic matter cycling

The microbial signatures of the subglacial discharge samples analyzed in our study support the suggestion that glacial systems supply labile material to downstream marine and terrestrial environments (Lafreniere and Sharp, 2004; Barker et al., 2006; Hood et al., 2009) extending these results to an ice sheet environment for the first time. This hypothesis follows earlier discoveries of abundant, active microbial communities associated with supraglacial, subglacial, and proglacial environments (Sharp et al., 1999; Anesio et al., 2009; Bhatia et al., 2006). It has been substantiated by direct investigations of glacially-derived DOM, including fluorescence spectrometry (Lafreniere and Sharp, 2004; Barker et al., 2006), compound specific analyses (i.e.



lignin phenols) (Hood et al., 2009), and bulk organic carbon characterizations (C:N ratios,  $\delta^{13}\text{C}$  values) (Hood and Scott, 2008; Hood et al., 2009). Most recently, Hood et al. (2009) demonstrated that the bioavailability of glacial organic carbon is indirectly correlated with age, so that DOM from glaciated catchments is labile despite having ancient  $\Delta^{14}\text{C}$  ages. Thus, meltwater streams and rivers draining glaciated areas may potentially provide a significant, previously overlooked source of labile reduced carbon to downstream ecosystems (Barker et al., 2006; Hood et al., 2009). Our study corroborates these findings through a comprehensive molecular-level description of glacially-derived DOM in meltwater runoff from the Greenland ice sheet and offers a novel line of evidence that glacial DOM has a microbial source.

#### 4. CONCLUSIONS

Previous studies illustrate that the majority of supraglacial DOM likely originates from autochthonous microbial processes, whereas subglacial DOM contains both allochthonous carbon derived from previously overridden soils and vegetation, and autochthonous carbon derived from *in situ* microbial metabolism. Our findings support these provenances. Generally the supraglacial and early season subglacial discharge had a higher proportion of protein-like and lipid-like elemental formulae, whereas the tarn and late season subglacial water DOM had a higher proportion of lignin and terrestrial Suwannee River-like materials. However, evolving subglacial flow regimes also likely exert a heavy influence on the type of DOM present in the subglacial outflow at different times of the year. In this study, this influence is reflected in a smaller terrestrial component in the early season subglacial waters, and the detection of condensed hydrocarbon-like material in late season subglacial waters. Based on the samples analyzed, the DOM composition of subglacial outflow shifts from a terrestrial to microbial signature over winter storage and then back to a terrestrial signature through a melt season. We propose that this shift is dependent on the degree of subglacial microbial metabolism that has occurred. However, additional samples and measurements constraining the subglacial flow regime and resident microbial communities are required to fully test the validity of this conjecture.

This study represents the first molecular-level analyses of subglacial organic carbon stores, and as such, has illustrated that ultra-high resolution mass spectrometry can provide unprecedented compositional information regarding the interplay among different glacial carbon pools. In addition to these qualitative results, further work with both bulk and compound-specific measurements will be required to confirm that specific compound classes (e.g., proteins, lipids) are present and to constrain the temporal provenances of these pools. Nevertheless, our results suggest that a much more complex and reactive carbon system is associated with glacial environments than previously thought and merit further investigation, given the extent and frequency of glaciation events through Earth's history.

#### ACKNOWLEDGEMENTS

This research was supported by: the National Science Foundation (CAREER-OCE-0529101 (E.B.K.), ARC-0520077 (S.B.D.)), National Atmospheric and Space Administration (S.B.D.), the WHOI Clark Arctic Research Initiative (E.B.K., S.B.D., M.-A.C.), the WHOI Ocean Ventures Fund (M.P.B.), and the National and Science Engineering Research Council of Canada (M.P.B.). We acknowledge M. Kido Soule for assistance with data collection and the funding sources of the WHOI FT-MS Users' facility (National Science Foundation OCE-0619608 and the Gordon and Betty Moore Foundation). We are grateful to I. Joughin, M. Behn, R. Harris, B. Gready, P. Henderson, A. Criscitiello, and M. Evans for their assistance in the field, to P. Henderson for conducting the carbon/nitrogen analyses, and to G. Wolken for his assistance in constructing maps of our field site. We also thank three anonymous reviewers whose comments improved the manuscript.

#### APPENDIX A. SUPPLEMENTARY DATA

Supplementary data associated with this article can be found, in the online version, at doi:10.1016/j.gca.2010.03.035.

#### REFERENCES

- Anesio A. M., Hodson A. J., Fritz A., Psenner R. and Sattler B. (2009) High microbial activity on glaciers: importance to the global carbon cycle. *Global Change Biol.* **15**, 955–960.
- Azam F. (1998) Microbial control of oceanic carbon flux: the plot thickens. *Science* **280**, 694–696.
- Bamber J. L., Layberry R. L. and Gogineni S. (2001) A new ice thickness and bed data set for the Greenland ice sheet 1. Measurement, data reduction, and errors. *J. Geophys. Res. D: Atmos.* **106**, 33773–33780.
- Barker J. D., Sharp M. J., Fitzsimons S. J. and Turner R. J. (2006) Abundance and dynamics of dissolved organic carbon in glacier systems. *Arct. Antarct. Alp. Res.* **38**, 163–172.
- Berner R. A., Lasaga A. C. and Garrels R. M. (1983) The carbonate-silicate geochemical cycle and its effect on atmospheric carbon-dioxide over the past 100 million years. *Am. J. Sci.* **283**, 641–683.
- Bhatia M., Sharp M. and Foght J. (2006) Distinct bacterial communities exist beneath a high arctic polythermal glacier. *Appl. Environ. Microbiol.* **72**, 5838–5845.
- Bingham R. G., Nienow P. W., Sharp M. J. and Boon S. (2005) Subglacial drainage processes at a high Arctic polythermal valley glacier. *J. Glaciol.* **51**, 15–24.
- Brown G. H. (2002) Glacier meltwater hydrochemistry. *Appl. Geochem.* **17**, 855–883.
- Carpenter E., Lin S. and Capone D. (2000) Bacterial activity in South Pole snow. *Appl. Environ. Microbiol.* **66**, 4514–4517.
- Cheng S. M. and Foght J. M. (2007) Cultivation-independent and -dependent characterization of bacteria resident beneath John Evans Glacier. *FEMS Microbiol. Ecol.* **59**, 318–330.
- Chillrud S. N., Pedrozo F. L., Temporetti P. F., Planas H. F. and Froelich P. N. (1994) Chemical weathering of phosphate and germanium in glacial meltwaters: effects of subglacial pyrite oxidation. *Limnol. Oceanogr.* **39**, 1130–1140.
- Clarke A. D. and Noone K. J. (1985) Soot in the Arctic snowpack: a cause for perturbations in radiative transfer. *Atmos. Environ.* **19**, 2045–2053.

- Clifford N. J., Richards K. S., Brown R. A. and Lane S. N. (1995) Scales of variation of suspended sediment concentration and turbidity in a glacial meltwater stream. *Geogr. Ann. Ser. A – Phys. Geogr.* **77A**, 45–65.
- Das S. B., Joughin I., Behn M. D., Howat I. M., King M. A., Lizarralde D. and Bhatia M. P. (2008) Fracture propagation to the base of the Greenland Ice Sheet during supraglacial lake drainage. *Science* **320**, 778–781.
- Dittmar T., Koch B., Hertkorn N. and Kattner G. (2008) A simple and efficient method for the solid-phase extraction of dissolved organic matter (SPE-DOM) from seawater. *Limnol. Oceanogr. Methods* **6**, 230–235.
- Eglinton T. I. and Repeta D. J. (2003) Organic matter in the contemporary ocean. In *Treatise on Geochemistry: Marine Organic Geochemistry*, vol. 6 (ed. H. Elderfield). Elsevier, pp. 145–180.
- Foght J., Aislabie J., Turner S., Brown C. E., Ryburn J., Saul D. J. and Lawson W. (2004) Culturable bacteria in subglacial sediments and ice from two Southern Hemisphere glaciers. *Microbiol. Ecol.* **47**, 329–340.
- Foreman C. M., Sattler B., Mikucki J. A., Porazinska D. L. and Priscu J. C. (2007) Metabolic activity and diversity of cryocoinites in the Taylor Valley, Antarctica. *J. Geophys. Res. Biogeosci.* **112**, 11.
- Grannas A. M., Hockaday W. C., Hatcher P. G., Thompson L. G. and Mosley-Thompson E. (2006) New revelations on the nature of organic matter in ice cores. *J. Geophys. Res. D: Atmos.* **111**, D04304.
- Grannas A. M., Shepson P. B. and Filley T. R. (2004) Photochemistry and nature of organic matter in Arctic and Antarctic snow. *Global Biogeochem. Cycles* **18**, GB1006.
- Hedges J. I. (1990) Compositional indicators of organic acid sources and reactions in natural environments. In *Organic Acids in Aquatic Ecosystems* (eds. E. M. Perdue and E. T. Gjessing). John Wiley & Sons, Ltd.
- Hedges J. I., Eglinton G., Hatcher P. G., Kirchman D. L., Arnosti C., Derenne S., Evershed R. P., Kogel-Knabner I., de Leeuw J. W., Littke R., Michaelis W. and Rullkotter J. (2000) The molecularly-uncharacterized component of non-living organic matter in natural environments. *Org. Geochem.* **31**, 945–958.
- Hood E., Fellman J., Spencer R. G. M., Hernes P. J., Edwards R., D'Amore D. and Scott D. (2009) Glaciers as a source of ancient and labile organic matter to the marine environment. *Nature* **462**, 1044–1047.
- Hood E. and Scott D. (2008) Riverine organic matter and nutrients in southeast Alaska affected by glacial coverage. *Nat. Geosci.* **1**, 583–587.
- Kim S., Kaplan L. A., Benner R. and Hatcher P. G. (2004) Hydrogen-deficient molecules in natural riverine water samples – evidence for the existence of black carbon in DOM. *Mar. Chem.* **92**, 225–234.
- Kim S., Kramer R. W. and Hatcher P. G. (2003a) Graphical method for analysis of ultrahigh-resolution broadband mass spectra of natural organic matter, the Van Krevelen diagram. *Anal. Chem.* **75**, 5336–5344.
- Kim S., Rodgers R. P. and Marshall A. G. (2006) Truly “exact” mass: elemental composition can be determined uniquely from molecular mass measurement at similar to 0.1 mDa accuracy for molecules up to similar to 500 Da. *Int. J. Mass Spectrom.* **251**, 260–265.
- Kim S., Simpson A. J., Kujawinski E. B., Freitas M. A. and Hatcher P. G. (2003b) High resolution electrospray ionization mass spectrometry and 2D solution NMR for the analysis of DOM extracted by C-18 solid phase disk. *Org. Geochem.* **34**, 1325–1335.
- Koch B. P., Ludwiczowski K. U., Kattner G., Dittmar T. and Witt M. (2008) Advanced characterization of marine dissolved organic matter by combining reversed-phase liquid chromatography and FT-ICR-MS. *Mar. Chem.* **111**, 233–241.
- Koch B. P., Witt M. R., Engbrodt R., Dittmar T. and Kattner G. (2005) Molecular formulae of marine and terrigenous dissolved organic matter detected by electrospray ionization Fourier transform ion cyclotron resonance mass spectrometry. *Geochim. Cosmochim. Acta* **69**, 3299–3308.
- Kramer R. W., Kujawinski E. B. and Hatcher P. G. (2004) Identification of black carbon derived structures in a volcanic ash soil humic acid by Fourier transform ion cyclotron resonance mass spectrometry. *Environ. Sci. Technol.* **38**, 3387–3395.
- Krawczynski M. J., Behn M. D., Das S. B. and Joughin I. (2009) Constraints on the lake volume required for hydro-fracture through ice sheets. *Geophys. Res. Lett.* **36**, L10501.
- Kujawinski E. B. (2002) Electrospray ionization Fourier transform ion cyclotron resonance mass spectrometry (ESI FT-ICR MS): characterization of complex environmental mixtures. *Environ. Forensics* **3**, 207–216.
- Kujawinski E. B. and Behn M. D. (2006) Automated analysis of electrospray ionization Fourier transform ion cyclotron resonance mass spectra of natural organic matter. *Anal. Chem.* **78**, 4363–4373.
- Kujawinski E. B., Longnecker K., Blough N. V., Vecchio R. D., Finlay L., Kitner J. B. and Giovannoni S. J. (2009) Identification of possible source markers in marine dissolved organic matter using ultrahigh resolution mass spectrometry. *Geochim. Cosmochim. Acta* **73**, 4384–4399.
- Lafreniere M. J. and Sharp M. J. (2004) The concentration and fluorescence of dissolved organic carbon (DOC) in glacial and nonglacial catchments: interpreting hydrological flow routing and DOC sources. *Arct. Antarct. Alp. Res.* **36**, 156–165.
- Lanoil B., Skidmore M., Priscu J. C., Han S., Foo W., Vogel S. W., Tulaczky S. and Engelhardt H. (2009) Bacteria beneath the West Antarctic Ice Sheet. *Environ. Microbiol.* **11**, 609–615.
- Layberry R. L. and Bamber J. L. (2001) A new ice thickness and bed data set for the Greenland ice sheet 2. Relationship between dynamics and basal topography. *J. Geophys. Res. D: Atmos.* **106**, 33781–33788.
- Lyons W. B., Welch K. A. and Doggett J. K. (2007) Organic carbon in Antarctic snow. *Geophys. Res. Lett.* **34**.
- Mantini D., Petrucci F., Pieragostino D., Del Boccio P., Di Nicola M., Di Ilio C., Federici G., Sacchetta P., Comani S. and Urbani A. (2007) LIMPIC: a computational method for the separation of protein MALDI-TOF-MS signals from noise. *BMC Bioinf.* **8**.
- Marshall A. G. and Rodgers R. P. (2008) Petroleomics: chemistry of the underworld. *Proc. Nat. Acad. Sci. USA* **105**, 18090–18095.
- McCune B. and Grace J. 2002. *Analysis of Ecological Communities*. MjM Software Design, Gleneden Beach, Oregon.
- McKnight D. M., Andrews E. D., Spaulding S. A. and Aiken G. R. (1994) Aquatic fulvic acids in algal rich antarctic ponds. *Limnol. Oceanogr.* **39**, 1972–1979.
- McKnight D. M., Boyer E. W., Westerhoff P. K., Doran P. T., Kulbe T. and Andersen D. T. (2001) Spectrofluorometric characterization of dissolved organic matter for indication of precursor organic material and aromaticity. *Limnol. Oceanogr.* **46**, 38–48.
- Mikucki J. A., Pearson A., Johnston D. T., Turchyn A. V., Farquhar J., Schrag D. P., Anbar A. D., Priscu J. C. and Lee P. A. (2009) A contemporary microbially maintained subglacial ferrous “ocean”. *Science* **324**, 397–400.

- Nienow P., Sharp M. and Willis I. C. (1998) Seasonal changes in the morphology of the subglacial drainage system, Haut Glacier d'Arolla, Switzerland. *Earth Surf. Process. Landf.* **23**, 825–843.
- Raiswell R. (1984) Chemical models of solute acquisition in glacial meltwaters. *J. Glaciol.* **30**, 49–57.
- Reemtsma T., These A., Linscheid M., Leenheer J. and Spitz A. (2008) Molecular and structural characterization of dissolved organic matter from the deep ocean by FTICR-MS, including hydrophilic nitrogenous organic molecules. *Environ. Sci. Technol.* **42**, 1430–1437.
- Richards K., Sharp M., Arnold N., Gurnell A., Clark M., Tranter M., Nienow P., Brown G., Willis I. and Lawson W. (1996) An integrated approach to modelling hydrology and water quality in glacierized catchments. *Hydrol. Processes* **10**, 479–508.
- Sharp M., Parkes J., Cragg B., Fairchild I. J., Lamb H. and Tranter M. (1999) Widespread bacterial populations at glacier beds and their relationship to rock weathering and carbon cycling. *Geology* **27**, 107–110.
- Skidmore M., Anderson S. P., Sharp M., Foght J. and Lanoil B. D. (2005) Comparison of microbial community compositions of two subglacial environments reveals a possible role for microbes in chemical weathering processes. *Appl. Environ. Microbiol.* **71**, 6986–6997.
- Skidmore M. L., Foght J. M. and Sharp M. J. (2000) Microbial life beneath a high Arctic glacier. *Appl. Environ. Microbiol.* **66**, 3214–3220.
- Slater J. F., Currie L. A., Dibb J. E. and Benner B. A. (2002) Distinguishing the relative contribution of fossil fuel and biomass combustion aerosols deposited at Summit, Greenland through isotopic and molecular characterization of insoluble carbon. *Atmos. Environ.* **36**, 4463–4477.
- Sleighter R. L. and Hatcher P. G. (2008) Molecular characterization of dissolved organic matter (DOM) along a river to ocean transect of the lower Chesapeake Bay by ultrahigh resolution electrospray ionization Fourier transform ion cyclotron resonance mass spectrometry. *Mar. Chem.* **110**, 140–152.
- Southam A. D., Payne T. G., Cooper H. J., Arvanitis T. N. and Viant M. R. (2007) Dynamic range and mass accuracy of wide-scan direct infusion nanoelectrospray Fourier transform ion cyclotron resonance mass spectrometry-based metabolomics increased by the spectral stitching method. *Anal. Chem.* **79**, 4595–4602.
- Stenson A. C., Marshall A. G. and Cooper W. T. (2003) Exact masses and chemical formulas of individual Suwannee River fulvic acids from ultrahigh resolution electrospray ionization Fourier transform ion cyclotron resonance mass spectra. *Anal. Chem.* **75**, 1275–1284.
- Tranter M., Sharp M. J., Lamb H. R., Brown G. H., Hubbard B. P. and Willis I. C. (2002) Geochemical weathering at the bed of Haut Glacier d'Arolla, Switzerland – a new model. *Hydrol. Processes* **16**, 959–993.
- Tranter M., Skidmore M. and Wadham J. (2005) Hydrological controls on microbial communities in subglacial environments. *Hydrol. Processes* **19**, 995–998.
- Wadham J. L., Tranter M., Tulaczyk S. and Sharp M. (2008) Subglacial methanogenesis: a potential climatic amplifier? *Global Biogeochem. Cycles* **22**, GB2021.
- Wu Z., Rodgers R. P. and Marshall A. G. (2004) Two- and three-dimensional van krevelen diagrams: a graphical analysis complementary to the kendrick mass plot for sorting elemental compositions of complex organic mixtures based on ultrahigh-resolution broadband fourier transform ion cyclotron resonance mass measurements. *Anal. Chem.* **76**, 2511–2516.

Associate editor: Carol Arnosti

## Chapter 4

### Organic carbon export from the Greenland ice sheet

#### Abstract

Rivers fed primarily by glacial meltwater potentially export a unique type of organic carbon to marine systems, distinct from non-glacially derived riverine export. Here we build on our earlier results that identified a high degree of temporal and spatial variability in the molecular-level composition of dissolved organic matter associated with the Greenland ice sheet (GrIS). We describe for the first time the bulk-level carbon composition of glacial meltwater from the GrIS. We investigate the dissolved (DOC) and particulate organic carbon (POC) concentration, age, and lability in the subglacial discharge throughout the melt season. By then scaling our measurements up across the ice sheet we suggest that the annual DOC flux (0.16 Tg/y) from the GrIS may be equivalent to that from a small Arctic river (e.g. Yana), and that the annual POC flux (1.9 Tg/y) may be comparable to that of a large Arctic river (e.g. Mackenzie). The DOC flux is derived primarily from the glacier base (>75%) in the early season, and from ice-melt (up to 100%) at the peak of the meltseason. The POC flux is primarily derived from the subglacial environment throughout the meltseason. The early season glacier discharge contains higher dissolved organic carbon concentrations (0.5 – 4.1 mg/L), and exports younger carbon ( $\text{DO}\Delta^{14}\text{C} \sim -250\text{‰}$ ) compared to the peak season discharge, when the concentrations are lower (0.1 – 0.6 mg/L) and the  $\Delta^{14}\text{C}$  is more depleted ( $\text{DO}\Delta^{14}\text{C} \sim -400\text{‰}$ ). Conversely, the POC export (1.4 – 13.2 mg/L,  $\text{PO}\Delta^{14}\text{C} \sim -250\text{‰}$ ) shows no temporal variation in either concentration or radiocarbon content throughout the meltseason. The dissolved carbon:nitrogen (C/N) ratios are also invariant with time, but are low (~4-25), indicative of labile carbon, despite the antiquity of the DOC. The particulate C/N ratios are more variable, but are similarly low (~8-21) during peak discharge. We use the dissolved ion loads in the glacial outflow to test the hypothesis that the type of DOC exported shifts with the seasonal evolution of the subglacial drainage system. These results illustrate that (1) different mechanisms control the DOC and POC flux from glacial systems; (2) chemically-distinct DOC pools are accessed by seasonally-evolving hydrological flow-paths; and (3) the GrIS can deliver labile, old carbon to downstream proglacial and marine environments.

## 1        **1. Introduction**

2  
3            Glacial environments possess a dynamic and reactive carbon system (Hood et al.,  
4 2009; Hood and Scott, 2008; Pautler et al., 2011). From a glacial-interglacial perspective,  
5 *in situ* microbial metabolism of subglacial organic carbon beneath the Laurentide ice  
6 sheet could produce CO<sub>2</sub> and CH<sub>4</sub> (Skidmore et al., 2000; Wadham et al., 2008) that may  
7 have been released following deglaciation. From a present-day perspective, Hood et al.  
8 (2010) has recently shown that glacier runoff along the Gulf of Alaska (GOA) is capable  
9 of exporting ancient, labile dissolved organic carbon to surrounding coastal ecosystems.  
10 This hypothesis has important implications for the coastal waters surrounding Greenland,  
11 where glacier runoff contributes ~500 km<sup>3</sup> per year (Mernild et al., 2009), comparable to  
12 the average annual discharge from the Lena River (Siberia) (524-533 km<sup>3</sup>/y), the second  
13 largest river contributor to the Arctic Ocean (Dittmar and Kattner, 2003). Yet, there are  
14 very few studies of organic carbon export from these large ice sheets.

15            Extant studies have focused primarily on end-member carbon pools found on the  
16 ice sheet surface and the bed, rather than on bulk meltwater runoff. These studies reveal  
17 that in comparison to riverine, marine, and estuarine environments, organic carbon from  
18 the ice sheet surface (i.e. supraglacial snow, ice, and meltwater) and base (basal ice) is  
19 nitrogen-rich, containing proteinaceous and other biologically-derived compounds  
20 (Bhatia et al., 2010; Dubnick et al., 2010; Pautler et al., 2011). The source of these  
21 compounds is presumed to be *in situ* microbial communities on the glacier surface and at  
22 the ice-bed interface (Bhatia et al., 2006; Carpenter et al., 2000; Hodson et al., 2008;  
23 Skidmore et al., 2000).

24            Recent studies have shown that the majority of the meltwater draining the  
25 Greenland ice sheet drains first to the bed, and is then discharged via a seasonally-  
26 evolving subglacial (beneath the ice) drainage system (Bartholomew et al., 2010; Bhatia  
27 et al., 2011; Das et al., 2008). Thus, an understanding of the meltwater outflow  
28 (hydrology and volume) is essential to determine the ice sheet carbon contribution to  
29 surrounding coastal oceans. Previous work in glacial systems indicates that transit

30 through the subglacial environment alters the original character of ice-derived organic  
31 carbon by adding a radiocarbon- ( $^{14}\text{C}$ ) depleted, terrestrial-like component to the runoff  
32 organic carbon (Barker et al., 2006; Bhatia et al., 2010; Dubnick et al., 2010; Hood et al.,  
33 2009). However, the presence of abundant, uniquely-adapted subglacial microbes hints  
34 that additional *in situ* microbial metabolism occurs at the glacier bed (Cheng and Foght,  
35 2007; Sharp et al., 1999; Skidmore et al., 2005). Such subglacial microbial activity may  
36 be able to utilize old organic carbon sources (Petsch et al., 2001), and add its own unique  
37 brand of  $^{14}\text{C}$ -depleted, proteinaceous material to the organic carbon exported in glacial  
38 runoff.

39         Previously, we investigated glacially-derived organic carbon using molecular-  
40 level analyses (i.e. ultra-high resolution mass spectrometry) (Bhatia et al., 2010). Here,  
41 we combine these observations with bulk-level analyses of abundance, age, and lability  
42 of organic carbon in glacial meltwater draining a land-terminating GrIS outlet glacier. A  
43 general consideration in the combination of bulk- and molecular-level analyses is that  
44 each of these approaches has intrinsic advantages and disadvantages. Bulk measurements  
45 such as C/N ratios, stable isotopic compositions, and radiocarbon content provide  
46 information on the major components comprising the organic carbon pool. However,  
47 they are limited because they are not particularly sensitive to subsidiary constituents, and  
48 can only differentiate broad source perspectives (Hedges et al., 1997). Conversely,  
49 though molecular-level analyses are highly sensitive to specific components of the  
50 organic carbon pool, they necessarily offer perspective on only select constituents or can  
51 be biased by trace component contributions. By combining bulk- and molecular-level  
52 approaches we aim to establish a comprehensive description of cycling and export of  
53 organic carbon from the Greenland ice sheet.

54         In this study we investigate whether meltwater draining a land-terminating GrIS  
55 outlet glacier exports chemically distinct organic carbon driven by seasonally-evolving  
56 flow-paths, and whether processing in the proglacial environment alters the organic  
57 carbon prior to export to a surrounding fjord. We utilize the major ion chemistry to gain  
58 insight into the evolution of the subglacial drainage system, and the dominant subglacial

59 chemical weathering regimes. We hypothesize that different temporal and spatial controls  
60 act on glacially-derived organic carbon, with temporal controls dictating the type  
61 (concentration, age, source, lability) of organic matter initially released from glacial  
62 systems, and spatial controls influencing the organic matter alteration prior to export to  
63 downstream environments. We investigate both the dissolved and particulate organic  
64 carbon (DOC, POC) pools, since they are likely influenced by different dynamics in the  
65 subglacial system, and have different fates in the marine environment. By definition,  
66 POC sinks through the water column, transferring carbon from the surface to the deep  
67 ocean, whereas DOC is concomitant with a water parcel, and is among the largest  
68 exchangeable carbon pools on Earth (Hansell, 2002). Results from this study provide the  
69 first radiocarbon measurements of organic carbon exported from the Greenland ice sheet,  
70 and reveal new insight about carbon export from glacial environments.

71

## 72 **2. Field Site Description and Sampling Overview**

73

74 Our study site is located on the southwestern margin of the Greenland ice sheet  
75 (Figure 1), approximately 125-km south of Jaokobshavn Isbrae and 120-km north of  
76 Sondre Stromfjord. Our field area consists of three land-terminating outlet glaciers  
77 (identified here as glaciers ‘M’, ‘N’, and ‘O’) that drain into a large (~10-km in length)  
78 proglacial lake (Thycho Brahe So / Qasigiatsigit), which discharges into Arfersiorfik  
79 Fjord. The bedrock geology of this area consists primarily of quartz diorite rocks of the  
80 Nagssugtqidian Orogenic Complex (K/Ar age 1790-1650 m.y.), most likely from an  
81 intrusive sheet metamorphosed in its outer parts (Escher, 1971).

82 Daily stream samples were collected from the ‘N’ glacier outflow during the late  
83 spring (May 16 to June 1) and at the height of the summer melt season (July 10 to July  
84 17) in 2008. Samples were generally collected in the afternoon (between 1 and 5 pm,  
85 local Greenland time), but the precise collection times vary throughout the sampling  
86 periods. Additional proglacial point samples were collected from the ‘M’ and ‘O’ glacier  
87 floodplains; from a small closed basin in front of ‘N’ glacier (rain-water fed tarn,

88 abbreviated 'Proglacial Tarn'); from the eastern shore of Qasigiatsigit Lake (abbreviated  
89 'Proglacial Lake'); and from the lake outflow channel (abbreviated 'Lake Outflow').  
90 Additional supraglacial point samples were collected from pooled meltwater on the  
91 surface of 'N' glacier (300-m a.s.l., abbreviated 'N' Supraglacial) as well as from an  
92 inland site (980-m, abbreviated 'Inland Supraglacial', 980-m) 70-km north-east of our  
93 primary field site.

94 'N' glacier (68°02'34"N, 50°16'08"W) is a small (~5 km<sup>2</sup> catchment) outlet  
95 glacier, whose physical characteristics, local meteorology, and hydrology have been  
96 described in detail elsewhere (Bhatia et al., 2011). In brief, we proposed that the  
97 subglacial drainage at 'N' glacier seasonally evolves from a distributed to channelized  
98 flow system, in which the 'Early May' runoff drains a delayed flow dominated,  
99 hydraulically inefficient network and the 'Late May' and 'July' runoff drains an  
100 increasingly glacial ice-melt dominated, hydraulically efficient network [Bhatia et al.,  
101 2011]. Based on results from this model, we identified three time periods throughout the  
102 melt season, named 'Early May' (May 18-24; JD 138-144), 'Late May' (May 25-June 1;  
103 JD 145-152), and 'July' (July 10-16; JD 191-198), with distinct hydrological regimes.  
104 The Early May waters were comprised of ≥ 49% contribution from delayed flow waters,  
105 whereas the Late May and July waters had between 12-36% and 5-17% respective  
106 contributions from delayed flow (Bhatia et al., 2011). These time periods have distinct  
107 ion and carbon signatures as well, and so we retain usage of these terms throughout this  
108 study.

109

### 110 **3. Methods**

111

112 All glassware was combusted at 450°C for at least 4 hours and all Teflon- and plastic-  
113 ware was soaked overnight in 10% hydrochloric (HCl) acid and rinsed extensively with  
114 Milli-Q water. All samples were collected in bottles that were rinsed three times with  
115 sample (or filtrate, as appropriate) prior to collection. All chemicals were obtained from  
116 Thermo Fisher Scientific. Organic solvents were Optima grade or better. Concentrated



117 acids were trace-metal grade or better. Samples for major ions, dissolved organic carbon  
118 (DOC), total dissolved nitrogen (TDN), particulate organic carbon (POC), particulate  
119 organic nitrogen (PON), and bulk organic radiocarbon were collected at approximately  
120 the same time.

121

### 122 3.1. Major Ion, Alkalinity, and Nutrient Analyses

123 Water samples for ion ( $\text{Cl}^-$ ,  $\text{NO}_3^-$ ,  $\text{NO}_2^-$ ,  $\text{SO}_4^{2-}$ ,  $\text{Na}^+$ ,  $\text{K}^+$ ,  $\text{Mg}^+$ ,  $\text{Ca}^+$ ,  $\text{NH}_4^+$ ) and  
124 nutrient ( $\text{PO}_4^{2-}$  and silicate) analyses were collected in 500-mL high-density polyethylene  
125 (HDPE) wide-mouth bottles (Nalgene). All samples were filtered on-site immediately  
126 through 0.22  $\mu\text{m}$  cellulose acetate membranes (GE) with a polypropylene vacuum  
127 filtration apparatus (Nalgene). Filtrate was collected, with minimal headspace, in 20-mL  
128 HDPE scintillation vials (Nalgene). Samples were kept as cold as possible in the field,  
129 and frozen upon return to the laboratory. pH ( $\pm 0.2$  units) was measured on-site  
130 immediately following filtration with an YSI 556MPS hand-held meter. Dissolved  
131 inorganic and organic anions and cations were measured by ion chromatography at  
132 Queen's University's Facility for Biogeochemical Research on Environmental Change  
133 and the Cryosphere (Fa.B.R.E.C.C.) (Kingston, ON, Canada). Anions and cations were  
134 determined simultaneously on separate systems using a Dionex ICS 3000, following the  
135 methods in Lafreniere and Lamoureux (2008). Analytical error for most analyses was less  
136 than 10%, based on replicate analyses of samples. Alkalinity (as  $\text{HCO}_3^-$ ) was calculated  
137 from the ionic charge deficit using the ion chromatography data. All cations (excluding  
138  $\text{NH}_4^+$ ) and sulfate concentrations were corrected for their sea-salt derived components  
139 using standard ratios to  $\text{Cl}^-$  reported for these ions in seawater (Holland, 1978). The  
140 residual crustal-derived component is denoted with an asterisk (\*). Dissolved inorganic  
141 nitrogen (DIN) is reported as the sum of  $\text{NO}_3^-$ -N,  $\text{NO}_2^-$ -N, and  $\text{NH}_4^+$ -N. Phosphate ( $\text{PO}_4^{3-}$   
142 ) and silicate were measured on a Lachat QuickChem 8000 flow injection analyzer at the  
143 Woods Hole Oceanographic Institution Nutrient Facility (Woods Hole, MA). Blanks  
144 (Milli-Q water) and standards were analyzed routinely within each sample run. Standards  
145 were made fresh daily using ACS certified chemicals (potassium phosphate and sodium

146 fluorosilicate), and were compared daily to inter-calibration performance standards  
147 (Quasiaeme and GEOTRACES). The coefficient of variability between replicate  
148 standards was <1% for both phosphate and silicate.

149

### 150 3.2. Dissolved Organic Carbon (DOC) and Total Dissolved Nitrogen (TDN) 151 Analyses

152 Samples for DOC and TDN analyses were collected in 250-mL glass bottles. All  
153 samples were filtered on-site, within 24-h of collection, using a combusted glass filtration  
154 apparatus, through a combusted pre-weighed glass-fiber pre-filter (GF/F; Whatman;  
155 nominal pore-size 0.7- $\mu\text{m}$ ) and a combusted 0.2- $\mu\text{m}$  Anodisc membrane (Whatman). The  
156 GFF pre-filter was stored for particulate organic carbon (POC) analyses. The 0.2- $\mu\text{m}$   
157 filtrate was acidified to pH 2 with concentrated HCl, and stored in a 40-mL glass vial.  
158 Samples were kept as cold as possible in the field and stored at 4°C upon return the  
159 laboratory. DOC and TDN concentrations were quantified simultaneously as non-  
160 purgeable organic carbon (NPOC) and total nitrogen by high temperature combustion  
161 (680°C) with NDIR and chemiluminescent detection on a Shimadzu TOC-V<sub>CSH</sub>/TNM  
162 system equipped with a high sensitivity platinum catalyst (Shimadzu Scientific  
163 Instruments). Samples were quantified using 5-point standard curves made with  
164 potassium hydrogen phthalate and potassium nitrate. Blanks (Milli-Q water) and deep-sea  
165 reference standards (provided by Prof. D. Hansell, University of Miami) were analyzed  
166 routinely within each sample run, and reported concentrations are corrected for the mean  
167 Milli-Q blank concentration. The limit of detection (based on instrument blanks) was  
168 ~0.02 mg/L. Analytical error was less than 2% ( $\pm$  0.01 mg/L) for DOC, and typically less  
169 than 5% ( $\pm$  0.004 mg/L) for TDN based on replicate injections. Dissolved organic  
170 nitrogen (DON) was calculated as the difference between TDN and DIN ( $\text{NO}_3^-$ -N,  $\text{NO}_2^-$ -  
171 N, and  $\text{NH}_4^+$ -N) (propagated error in DON was  $\pm$  0.006 mg/L). DON concentrations less  
172 than twice the propagated DON error were excluded from further analysis. This criterion  
173 excluded four of the 'N' glacier outflow samples. DOC to DON ratios were then  
174 calculated from division between these two parameters.

175

### 176 3.3. Particulate Organic Carbon (POC) and Nitrogen (PON) Analyses

177 POC and PON was determined on the GF/F pre-filter by dynamic flash  
178 combustion with thermal conductive detection on a Flash EA1112 Carbon/Nitrogen  
179 Analyzer (ThermoQuest) at the Woods Hole Oceanographic Institution Nutrient Facility  
180 (Woods Hole, MA). An acetanilide certified standard (Microanalysis Limited) was used  
181 to make 9-point standard curve, and blanks (empty high purity tin discs) and standards  
182 were analyzed routinely within each sample run. Analytical error is less than .01%, based  
183 on replicate standards. The limit of detection for carbon was  $\leq 0.7 \mu\text{mols}$ , and  $\leq 0.1 \mu\text{mols}$   
184 for nitrogen.

185 The average discharge-weighted POC and DOC concentrations were calculated  
186 using the measured discharge at the time closest to the sample collection. The flux ( $\text{kg}$   
187  $\text{km}^{-2} \text{d}^{-1}$ ) of POC and DOC from 'N' glacier was calculated as the product of the  
188 measured concentrations and the 24-h moving average discharge at the time closest to the  
189 collection time (from (Bhatia et al., 2011)).

190

### 191 3.4. Bulk Organic Radiocarbon Analyses

192 Samples for dissolved and particulate organic radiocarbon ( $\text{DO}^{14}\text{C}$  and  $\text{PO}^{14}\text{C}$ ,  
193 respectively) analyses were collected in two 2-L Teflon bottles. One of the 2-L aliquots  
194 was used for  $\text{DO}^{14}\text{C}$ , and the second was used for  $\text{PO}^{14}\text{C}$ . The majority of the  $\text{DO}^{14}\text{C}$   
195 samples were filtered on-site immediately after collection, using the DOC protocol  
196 described above. The 0.2- $\mu\text{m}$  filtrate was stored in 1.25-L Teflon bottles. Aqueous  
197 samples were acidified to pH 2-3 with concentrated phosphoric acid ( $\text{H}_3\text{PO}_4$ ), kept as  
198 cold as possible in the field, and frozen upon return to the laboratory until analysis. The  
199 aliquot collected for  $\text{PO}^{14}\text{C}$  was not filtered in the field, but was acidified, and frozen  
200 upon return to the laboratory.

201 Prior to radiocarbon analysis,  $\text{DO}^{14}\text{C}$  and  $\text{PO}^{14}\text{C}$  samples were thawed at  $4^\circ\text{C}$ , and  
202 analyzed at the National Ocean Sciences Accelerator Mass Spectrometry (NOSAMS)  
203 Facility (Woods Hole, MA). DOC was converted into carbon dioxide ( $\text{CO}_2$ ) for  $\Delta^{14}\text{C}$

204 analysis using an ultraviolet (UV) oxidation and vacuum line system similar to that  
205 described by Beaupre et al., (2007). Analytical blanks (UV-oxidized acidified milli-Q  
206 water) and reference standards (oxalic acid II (modern  $^{14}\text{C}$ ) and glycine hydrochloride  
207 ( $^{14}\text{C}$  dead)) were analyzed routinely between samples. The analytical blank was  $<0.3 \mu\text{M}$ .  
208 The  $\text{PO}^{14}\text{C}$  aliquots were thawed at room temperature, and filtered in the laboratory  
209 through a combusted GFF pre-filter. The POC on the GFF pre-filter was converted into  
210  $\text{CO}_2$  for  $^{14}\text{C}$  analysis using high temperature combustion at NOSAMS. For both  $\text{DO}^{14}\text{C}$   
211 and  $\text{PO}^{14}\text{C}$ , a split of  $\text{CO}_2$  gas was taken for analysis of  $\delta^{13}\text{C}$  on a VG Prism-II Stable  
212 Isotope Ratio Mass Spectrometer. The remaining  $\text{CO}_2$  gas was converted to graphite by  
213 heating it in the presence of  $\text{H}_2$  gas and an iron catalyst. The graphite was pressed into  
214 target cartridges and its  $^{14}\text{C}/^{12}\text{C}$  was measured on the accelerator mass spectrometer at  
215 NOSAMS. Radiocarbon results are normalized to a  $\delta^{13}\text{C} = -25\text{‰}$  and are reported as  
216 Fraction modern ( $F_m$ ), where ‘modern’ is defined as 95% of the 1950 AD radiocarbon  
217 concentration of NBS Oxalic Acid I (NIST-SRM-4990) normalized to a  $\delta^{13}\text{C} = -19\text{‰}$   
218 (see NOSAMS data reporting protocol for more details). The activity ( $\Delta^{14}\text{C}$ ) is a measure  
219 of the relative difference between the NBS Oxalic Acid I international standard and a  
220 sample’s radiocarbon activity after correction for both  $\delta^{13}\text{C}$  and radioactive decay  
221 between 1950 and the year of measurement. On average, an enriched  $\Delta^{14}\text{C}$  signature  
222 represents newly formed (younger) organic carbon, whereas a depleted  $\Delta^{14}\text{C}$  signature  
223 represents relatively older organic carbon.

224

## 225 **4. Results**

226

### 227 4.1. Major Ion Hydrochemistry

228 The concentrations of the major dissolved anions ( $\text{Cl}^-$ ,  $\text{NO}_3^-$ ,  $\text{NO}_2^-$ ,  $\text{SO}_4^{2-}$ ) and  
229 cations ( $\text{Na}^+$ ,  $\text{K}^+$ ,  $\text{Mg}^+$ ,  $\text{Ca}^+$ ) in the ‘N’ glacier outflow stream are distinct in the three  
230 periods of our isotope-mixing model (Figure 2), with the Early May samples being  
231 markedly higher (408 – 746  $\mu\text{eq/L}$ ), compared to Late May (125 – 329  $\mu\text{eq/L}$ ) and July  
232 (39.3 - 79.2  $\mu\text{eq/L}$ ). Over the entire meltseason, the sum of crustal cation equivalents

233 ( $\Sigma^+_{\text{avg}}$ ) averaged to 121  $\mu\text{eq/L}$ . However, the Early May samples are distinctly more  
234 concentrated ( $\Sigma^+_{\text{avg}} = 282 \mu\text{eq/L}$ ) compared to Late May ( $\Sigma^+_{\text{avg}} = 112 \mu\text{eq/L}$ ) and July  
235 ( $\Sigma^+_{\text{avg}} = 29 \mu\text{eq/L}$ ). The silicate concentrations in the 'N' glacier outflow stream mirrored  
236 the trends seen in the major ion data in that the Early May waters had generally higher  
237 concentrations ( $23.1 \pm 7.9 \mu\text{M}$ ), whereas the July waters were more dilute ( $5.1 \pm 0.1 \mu\text{M}$ ).  
238 However, the Late May silicate concentrations were more variable ( $15.4 \pm 8.7 \mu\text{M}$ ), and  
239 did not fit the temporal evolution pattern established by major ion data. An outlier sample  
240 (excluded from Figure 2 for scaling purposes) that drained the lowest discharge waters on  
241 May 21<sup>st</sup>, and had the greatest delayed flow contribution according to our isotope mixing-  
242 model, had an especially high dissolved ion ( $2354 \mu\text{eq/L}$ ), crustal cation sum ( $\Sigma^+ = 1161$   
243  $\mu\text{eq/L}$ ), and silicate ( $45.4 \mu\text{M}$ ) load.

244 Generally, sulfate ( $\text{SO}_4^{2-*}$ ) and bicarbonate ( $\text{HCO}_3^{-*}$ ) were the major (5 – 45%)  
245 anionic contributors in all of the 'N' stream waters, with nitrate ( $\text{NO}_3^-$ ) and chloride ( $\text{Cl}^-$ )  
246 being minor ( $\leq 2\%$ ) contributors (Table 1). Notably, the Early May waters had a greater  
247 percentage contribution of  $\text{SO}_4^{2-*}$  (21%) compared to the Late May (10%) and July  
248 waters (5%). Among the cations, calcium ( $\text{Ca}^{2+*}$ ) was the major (16 – 21%) contributor  
249 across the different time periods, followed by magnesium ( $\text{Mg}^{2+*}$ ), sodium ( $\text{Na}^{+*}$ ), and  
250 potassium ( $\text{K}^{+*}$ ).  $\text{Mg}^{2+*}$  and  $\text{Na}^{+*}$  had generally consistent contributions in all the 'N'  
251 glacier waters, between 13 – 14% and 8 – 10% respectively. However,  $\text{K}^{+*}$  was a  
252 notably smaller contributor to the Early May waters (6%), than to the Late May (10%),  
253 and July (11%) waters.

254 We used associations between different ions to gain insight into the nature of the  
255 subglacial chemical weathering regime, following Wadham et al., (2010b). The specific  
256 ionic indices used were (i) the ratio of monovalent to divalent crustal cations in order to  
257 assess the relative contributions of carbonate and silicate weathering (Figure 3a), (ii)  
258 associations between  $^*\text{SO}_4^{2-}$  vs  $\text{HCO}_3^-$  (Figure 3b) to examine whether microbial  
259 oxidation of organic matter is occurring, and (iii) linear regressions between ( $^*\text{Mg}^{2+} +$   
260  $^*\text{Ca}^{2+}$ ) vs  $^*\text{SO}_4^{2-}$  and  $\text{HCO}_3^-$  (Figure 3c,d) to estimate the extent to which sulfide  
261 oxidation is coupled to carbonate dissolution.

262

#### 263 4.2. DOC and POC concentrations

264 The DOC concentrations at 'N' glacier are generally dilute throughout the melt  
265 season (Figure 4a,b), with the exception of the May 21 outlier sample, which had a DOC  
266 concentration of 4.1 mg/L (not shown in Figure 4a). Excluding this outlier, on average,  
267 the DOC concentrations were slightly higher in Early May ( $0.61 \pm 0.09$  mg/L), compared  
268 to Late May ( $0.39 \pm 0.08$  mg/L) and July ( $0.27 \pm 0.15$  mg/L). However an elevated pulse  
269 of DOC (0.62 mg/L), similar to concentrations found in Early May, was measured on  
270 July 16. There was no evident temporal trend in the POC concentrations of the 'N'  
271 outflow waters (average concentration =  $3.5 \pm 1.1$  mg/L, or  $1.0 \pm 0.5\%$  organic carbon).  
272 This average value excludes the May 21 outlier (excluded from Figure 4), which also had  
273 a high POC concentration (13.2 mg/L, which equates to 9.9% organic carbon).

274 The DOC concentrations of the point samples collected from the proglacial area  
275 in May and July, along with average 'N' and 'M' glacier outflow and 'N' supraglacial  
276 samples are shown in Table 2. The 'N' supraglacial samples exhibited the lowest  
277 concentration, whereas the proglacial samples (i.e. 'O' Glacier Floodplain, Proglacial  
278 Lake, and Lake Outflow) were more concentrated. The Proglacial Lake sample had a  
279 particularly high DOC concentration in the Early May point sample, though this  
280 decreased substantially on June 1 and even further on July 13<sup>th</sup>. The POC concentrations  
281 in the proglacial samples collected were generally lower than that in the glacier runoff  
282 (Table 2).

283

#### 284 4.3. Bulk Organic Radiocarbon

285 The  $\delta^{13}\text{C}$  and  $\Delta^{14}\text{C}$  signatures of a subset of supraglacial, subglacial, and  
286 proglacial DOC and POC samples are shown in Figure 5. Excluding the proglacial tarn  
287 end-member sample, which was enriched in both  $\delta^{13}\text{C}$  and  $\Delta^{14}\text{C}$ , the  $\text{DO}\delta^{13}\text{C}$  values  
288 range from -21.08 to -28.49‰, whereas the  $\text{PO}\delta^{13}\text{C}$  values only range over  $\sim 2\%$  (-24.82  
289 to -26.96‰). The  $\text{DO}\Delta^{14}\text{C}$  range is  $^{14}\text{C}$  depleted and similar (-210.7 to -400.9‰) to the  
290  $\text{PO}\Delta^{14}\text{C}$  range (-109.4 to -351.7‰) with the exception of an enriched  $\text{DO}\Delta^{14}\text{C}$  sample

291 (0.4‰) from the ‘O’ glacier floodplain. Focusing on the subset of samples collected from  
 292 ‘N’ glacier and its end-members (Figure 6), we noted that the ‘N’ supraglacial, ‘N’  
 293 subglacial May, and proglacial tarn samples all fall on the 1:1 line between dissolved and  
 294 particulate radiocarbon, indicating that the dissolved and particle carbon dynamics are  
 295 coupled for these samples. Conversely, the ‘N’ subglacial July samples have depleted  
 296  $DO\Delta^{14}C$  values relative to their  $PO\Delta^{14}C$  values, suggesting de-coupled dynamics. De-  
 297 coupling is also evident in the proglacial lake outflow (depleted  $DO\Delta^{14}C$ ) and ‘O’ glacier  
 298 floodplain (enriched  $DO\Delta^{14}C$ ) samples (Figure 5).

299 In order to determine the DOC contribution and  $DO\Delta^{14}C$  signature of the basal  
 300 material exported in the ‘N’ glacier outflow, we employ our previous estimates of the  
 301 snow, ice, and delayed flow (basal) mass contributions to the ‘N’ glacier outflow (Bhatia  
 302 et al., 2011). Combining this information with the DOC concentrations, we can solve for  
 303 the fractional DOC contribution of the snow, ice, and basal components using:

$$f_c = q_c \times [DOC]_c / [DOC]_o$$

304 where  $f_c$  is the fractional DOC for a component (snow, ice, basal),  $q_c$  is the proportional  
 305 flow contribution of a component (from the isotope mixing model), and  $[DOC]$  are the  
 306 respective DOC concentrations in a component ( $[DOC]_c$ ) and the outflow ( $[DOC]_o$ ). For  
 307 the ice and snow fractions, we did not have a complete dataset of coupled DOC and  
 308 radiocarbon values. Consequently, we solved for the ice fraction an average ice DOC  
 309 concentration from the surface of ‘N’ glacier ( $0.19 \pm 0.01$  mg/L) and the average  $DO\Delta^{14}C$   
 310 of ice-melt from the ‘Inland Supraglacial’ site ( $-233.9 \pm 32.7\%$ ). To calculate the snow  
 311 fraction, we assumed that the snow DOC concentration was similar to that of the average  
 312 glacial ice, and used the  $DO\Delta^{14}C$  of pooled early-season (frozen) meltwater on the  
 313 surface of ‘N’ glacier ( $-340.1\%$ ). Using the calculated fractional DOC contributions  
 314 (Figure 7a), the basal  $DO\Delta^{14}C$  was estimated for the days when we had a bulk  
 315 radiocarbon value of the ‘N’ outflow stream (May 19, July 12, and July 16). We defined  
 316 the mass-balance equation as follows:

$$317 \quad DO\Delta^{14}C_o = f_s \times DO\Delta^{14}C_s + f_i \times DO\Delta^{14}C_i + f_b \times DO\Delta^{14}C_b$$

318 where the subscripts ‘o’, ‘s’, ‘i’, and ‘b’ refer to the outflow, snow, ice, and basal  
319 components respectively. We re-arranged this equation to solve for the  $\text{DO}\Delta^{14}\text{C}_b$  term.  
320 This yielded  $\Delta^{14}\text{C}$ -depleted basal DOC signatures on May 19 (-238.0‰) and July 16 (-  
321 714.8‰), and a radiocarbon dead signature ( $\leq -1000\text{‰}$ ) on July 12. Performing an  
322 analogous calculation for the POC, we used  $[\text{POC}]_i = 0.43 \pm 0.19 \text{ mg/L}$ ,  $\text{PO}\Delta^{14}\text{C}_i = -111.4$   
323  $\pm 2.8\text{‰}$ , and  $\text{PO}\Delta^{14}\text{C}_s = -351.7\text{‰}$  to solve for the fractional contributions from the snow,  
324 ice, and basal reservoirs to the runoff POC (Figure 7b). Solving for the basal  $\text{PO}\Delta^{14}\text{C}$ ,  
325 we find depleted basal POC signatures on May 19 (-258.6‰), July 12 (-288.6‰), and  
326 July 14 (-281.1‰).

327

#### 328 4.4. Carbon:Nitrogen Ratios

329 The DOC:DON ratios among the ‘N’ glacier outflow samples range widely from  
330 4.3 to 24.5, and there is no evident temporal trend between the early May, late May, and  
331 July samples (data not shown). The supraglacial and proglacial data is primarily limited  
332 to only a few samples, but based on these few values, we observe a general increase in  
333 the DOC:DON ratios from the ice edge to the lake outflow (Figure 8). However, we  
334 should note that where we have multiple measurements across temporal periods, the  
335 range of values is large (e.g. 4.5 to 16.2 for the ‘N’ Supraglacial, 6.0 to 30.7 for the ‘M’  
336 glacier outflow, 4.3 to 24.5 for the ‘N’ glacier outflow, and 9.5 to 50.0 for the proglacial  
337 lake). The POC:PON ratios of the ‘N’ glacier outflow show a clearer temporal trend, in  
338 that the May samples are variable (range: 7.9 to 66.4), whereas the July samples are more  
339 consistently lower (range: 8.4 to 21.1; Figure 8). The PON of the ‘N’ supraglacial ice and  
340 ‘O’ glacier floodplain samples were below the limit of detection. The ‘M’ glacier outflow  
341 POC:PON values ranged from 8.9 to 15.5.

342

### 343 5. Discussion

344

#### 345 5.1. Temporal Dynamics at ‘N’ glacier

##### 346 5.1.1. Subglacial chemical weathering regimes over a meltseason



347 The major ion hydrochemistry of the 'N' glacier runoff is broadly similar in  
348 composition to that previously reported from other glacial systems, but is much more  
349 dilute ( $\Sigma^+_{\text{avg}} = 121 \mu\text{eq/L}$ ) than typical glacier runoff ( $\Sigma^+_{\text{avg}} \sim 700 \mu\text{eq/L}$ ) (Skidmore et al.,  
350 2010), suggesting a comparatively unreactive bedrock on shorter subglacial residence  
351 times. For comparison, the  $\Sigma^+_{\text{avg}}$  of river waters in the Mackenzie River basin is 2900  
352  $\mu\text{eq/L}$  (Milot et al., 2003). Generally, glacial runoff is a dilute  $\text{Ca}^{2+}$ - $\text{HCO}_3^-$ - $\text{SO}_4^{2-}$   
353 dominated mixture, with varying contributions from  $\text{Na}^+$  and  $\text{Cl}^-$  ( $\Sigma^+$  ranging from 10 to  
354 3500  $\mu\text{eq/L}$ ) (Tranter, 2003). This composition reflects the fact that subglacial chemical  
355 weathering is typically dominated by carbonate (calcite) hydrolysis followed by sulfide  
356 oxidation coupled to carbonate dissolution (Tranter, 2003). Previous studies in alpine  
357 catchments have shown that even when a bedrock is dominated by silicates, trace  
358 carbonates are still preferentially weathered, generating a high ratio of carbonate to  
359 silicate dissolution ( $\sim 5:1$  in glacial catchments (Tranter, 2003)). We calculated the ratio  
360 of divalent ( $*\text{Ca}^{2+} + *\text{Mg}^{2+}$ ) to monovalent ( $*\text{Na}^+ + *\text{K}^+$ ) crustal cations (Figure 3a) because  
361  $\text{Na}^+$  and  $\text{K}^+$  are pre-dominantly derived from silicate dissolution (Wadham et al., 2010b)  
362 and thus ratio values  $< 1$  indicate preferential silicate dissolution. Although 'N' glacier  
363 drains a silicate-dominated bedrock, the average divalent:monovalent ratio is 1.8,  
364 suggesting that trace carbonates are being weathered preferentially over the silicate  
365 bedrock. This is consistent with previous work (Wadham et al., 2010b), although 'N'  
366 glacier has a greater silicate weathering index (lower divalent:monovalent ion ratio)  
367 compared to other glacial catchments (Wadham et al., 2010b), particularly in late May  
368 and July ( $((*\text{Ca}^{2+} + *\text{Mg}^{2+})/(*\text{Na}^+ + *\text{K}^+))_{\text{avg}} = 1.5$ ). The higher divalent:monovalent ion ratio  
369 in the Early May runoff ( $((*\text{Ca}^{2+} + *\text{Mg}^{2+})/(*\text{Na}^+ + *\text{K}^+))_{\text{avg}} = 2.6$ ) hints that these waters may  
370 drain a different subglacial environment, in which proportionally greater carbonate  
371 dissolution occurs. This hypothesis is reinforced by the strong relationship between  
372  $*\text{SO}_4^{2-}$  and  $(*\text{Mg}^{2+} + *\text{Ca}^{2+})$  for the Early May waters (Figure 3c) which are indicative of  
373 sulfate derived from saturated porewaters along the ice/land margin (Wadham et al.,  
374 2010a). Furthermore, poor relationships in plots of  $*\text{SO}_4^{2-}$  vs.  $\text{HCO}_3^-$  (Figure 3b) and  
375  $\text{HCO}_3^-$  vs.  $(*\text{Mg}^{2+} + *\text{Ca}^{2+})$  (Figure 3d) in Early May waters compared to the stronger

376 relationships in the late May and July waters indicate that later discharge waters are not  
377 draining saturated marginal porewaters (Wadham et al., 2010a) but instead may be  
378 accessing unsaturated headward regions.

379

#### 380 5.1.2. Carbon export over a meltseason

381 The organic carbon concentrations measured in the 'N' glacier runoff (Figure 4)  
382 are dilute, but within the range ( $< 1 \text{ mg C L}^{-1}$ ) previously reported for runoff from other  
383 glacial systems (Barker et al., 2006; Hood et al., 2009; Lafreniere and Sharp, 2004). The  
384 organic carbon in the 'N' glacier runoff is an amalgamation of supraglacial, englacial,  
385 and subglacial sources. Using our model results (Bhatia et al., 2011) in combination with  
386 the organic carbon concentrations (section 4.3), we can estimate the mass contributions  
387 from the snow, ice, and basal pools to the runoff DOC and POC (Figure 7). Since the  
388 supraglacial (snow, ice) and englacial environments share ice-melt as their primary  
389 carbon source, we can roughly assume a similar mass contribution from the englacial  
390 source as found in the supraglacial samples. Doing this we find that approximately  $>75\%$   
391 of the DOC, on average, in the early May samples is likely derived from the subglacial  
392 environment. In contrast in late May this contribution decreases to  $\sim 30\%$ , with the  
393 remaining majority from supraglacial and englacial sources. The July runoff, on average,  
394 could be entirely derived from the supraglacial and englacial sources. However,  
395 individual July samples with DOC concentrations above  $0.2 \text{ mg/L}$  are an exception, and  
396 likely have some subglacial contribution (between  $\sim 10\text{-}30\%$ ). We should also note that  
397 the May 21 outlier sample ( $[\text{DOC}] = 4.1 \text{ mg/L}$ ) is a clear exception, as the carbon mass  
398 observed on that day almost certainly has a large subglacial component. From a POC  
399 mass balance perspective, since the supraglacial and englacial sources contribute, on  
400 average, only  $\sim 10\%$  of the mean 'N' glacial runoff POC concentration, we conclude that  
401 the majority ( $\sim 90\%$ ) of the runoff POC originates in the subglacial environment  
402 throughout the meltseason. As with DOC, the May 21<sup>st</sup> outlier sample ( $[\text{POC}] = 13.2$   
403  $\text{mg/L}$ ) likely represents an end-member and its carbon mass is likely almost entirely  
404 subglacial in origin.

405           The seasonal flux of DOC and POC generally mimics the discharge curve (Figure  
406 4 c,d), illustrating that discharge, rather than concentrations, drives the mass flux of DOC  
407 and POC from 'N' glacier. Thus, the majority of glacially-derived organic carbon is  
408 annually released in a relatively small period of time (i.e. a few months), during the peak  
409 of the summer melt-season. Generally, the POC fraction is the quantitatively important  
410 pool as it comprises, on average, between 84 and 93% of the total organic carbon mass  
411 flux. The proportional average contribution from the DOC pool diminishes from Early  
412 May (16%) to Late May (11%) and July (7%), as discharge increases. This is the opposite  
413 of major riverine systems (e.g. the Amazon), where the DOC is exported in excess of the  
414 POC (e.g. DOC/POC ~1.8) (Hedges et al., 1997). However, since a portion of the POC  
415 pool likely quickly settles out upon exit from the glacier terminus, the DOC pool, as the  
416 mobile phase, may still have important downstream effects depending on its lability.

417

#### 418           5.1.3. Mobilization of subglacial organic carbon pools over a meltseason

419           From a bulk compositional perspective, the DOC and POC of the 'N' glacier  
420 outflow samples analyzed in this study were all depleted in radiocarbon in both May and  
421 July (Figure 5), suggesting relict carbon sources or new microbial production based on  
422 depleted in/organic carbon stores. Few studies exist for robust comparison with these data  
423 but we can derive some insights from previous work on river systems and glacial runoff  
424 into the Gulf of Alaska. The radiocarbon values for DOC exported in the 'N' glacier  
425 runoff were more depleted in  $\Delta^{14}\text{C}$  than those from large Arctic rivers, but within the  
426 range of  $\text{DO}\Delta^{14}\text{C}$  signatures previously reported from runoff draining glaciers along the  
427 Gulf of Alaska (Figure 5). Comparatively, the 'N' glacier runoff  $\text{PO}\Delta^{14}\text{C}$  signatures were  
428 within the range of previously reported POC from small mountainous rivers (Figure 5). In  
429 riverine systems, DOC is derived from recently fixed plant organic matter or is generated  
430 during chemical weathering of near surface soil horizons (Benner et al., 2004; Raymond  
431 and Bauer, 2001b). Conversely, POC generally enters through mechanical weathering of  
432 underlying soil and rock material (Raymond and Bauer, 2001b). Since chemical  
433 weathering is a process generally associated with new production, DOC is often younger

434 than POC in river systems, being enriched in radiocarbon or only mildly depleted  
435 (Raymond and Bauer, 2001b). In contrast, POC is often considerably depleted in  
436 radiocarbon due to contribution from antiquated carbon sources such as old soil horizons,  
437 sedimentary fossil carbon, and sorbed petroleum (Raymond and Bauer, 2001b). Our data  
438 contrast with river systems in that the  $\text{DO}\Delta^{14}\text{C}$  is more depleted than  $\text{PO}\Delta^{14}\text{C}$  and grows  
439 increasingly so over the meltseason. Thus we must invoke a different mechanism to  
440 explain the glacial runoff  $\text{DO}\Delta^{14}\text{C}$  values.

441 We hypothesize that the different  $\text{DO}\Delta^{14}\text{C}$  signatures in the May and July runoff  
442 is a function of seasonally-evolving subglacial hydrological conditions, whereas the  
443 constant  $\text{PO}\Delta^{14}\text{C}$  signature is that of the bulk material overridden by the ice mass. For the  
444 DOC pool, this hypothesis is consistent with our previous work at 'N' glacier speculating  
445 that the seasonal head-ward evolution of the subglacial drainage system resulted in  
446 quickly transiting meltwaters accessing relict subglacial organic carbon stores in July  
447 (Bhatia et al., 2010). A mass-balance calculation of the July basal  $\text{DO}\Delta^{14}\text{C}$  (see section  
448 4.3) further supports this hypothesis, revealing that the late-season waters are accessing  
449 antiquated, radiocarbon-dead basal material and/or contain radiocarbon-dead surface-  
450 derived hydrocarbons. Since July runoff waters are characterized by very low DOC  
451 concentrations, even a small mass contribution of  $\Delta^{14}\text{C}$ -dead material would yield a more  
452 depleted bulk  $\text{DO}\Delta^{14}\text{C}$  signature. Conversely, in May, when the subglacial drainage  
453 system contains a large delayed flow component, and is potentially draining saturated  
454 porewaters, the basal  $\text{DO}\Delta^{14}\text{C}$  (-243.6‰) is similar to that of the outflow signature (-  
455 245.9‰), indicating that the  $\text{DO}\Delta^{14}\text{C}$  exported in the May outflow is derived primarily  
456 from marginal porewaters. Thus, the DOC pool is sensitive to shifts between the  
457 distributed and channelized drainage systems because its contents are mobile, and its  
458 concentrations are very low.

459 The majority of the 'N' runoff  $\text{PO}\Delta^{14}\text{C}$  signatures are within the range of  
460 previously reported  $\Delta^{14}\text{C}$ -POC from small mountainous rivers. Thus, we propose that,  
461 akin to small mountainous rivers, a relict soil/rock contribution from the subglacial  
462 environment, in this case, yields the depleted glacial runoff  $\text{PO}\Delta^{14}\text{C}$  signature (Raymond

463 and Bauer, 2001b). A mass balance calculation of the basal  $\text{PO}\Delta^{14}\text{C}$  pool (-262 to -  
464 299‰) confirms that the bulk runoff  $\text{PO}\Delta^{14}\text{C}$  signature (-257 to -263‰) is primarily  
465 driven by the subglacial contribution. In comparison to the DOC pool, the runoff POC  
466 pool is much larger (in mass), and thus is less susceptible to variable mass contributions  
467 resulting from changes in the subglacial drainage system. As a result, its radiocarbon  
468 content is invariant with hydrology and the POC in general is affected more by regional-  
469 scale glacier advance and/or retreat than by hydrology.

470

#### 471 5.1.4. Organic carbon source and lability

472 The bulk-level  $\Delta^{14}\text{C}$  differences between the May and July ‘N’ outflow samples  
473 are consistent with our previous work at ‘N’ glacier showing that the DOC composition  
474 exported in late May and July differs on a molecular level (Bhatia et al., 2010). Using  
475 ultra-high resolution mass spectrometry we showed that the July (12 and 16) samples had  
476 a higher proportion of lignin and terrestrial-like material, consistent with the flushing of  
477 relict organic carbon from overridden soil and vegetation, as discharge increases  
478 throughout the summer meltseason. Comparatively, the organic carbon in a May 31  
479 outflow, though still possessing terrestrial-like compounds, had a distinct protein-like and  
480 lipid-like signature. We previously ascribed these signatures to microbial metabolic  
481 influence on DOC composition (Bhatia et al., 2010). However, this differentiation  
482 between the May and July runoff was not evident from the bulk  $\delta^{13}\text{C}$  signature, which  
483 can also be used to glean source information. The  $\text{DO}\delta^{13}\text{C}$  signatures of ‘N’ glacier  
484 runoff sampled on May 19, July 12, and July 14 (-23.7‰ to -25.8‰, Figure 3) all fell  
485 within the range of a terrestrial (C3 plant) derivation (Hedges et al., 1997).

486 Regardless of source, the dissolved and particulate C:N ratios can be used to  
487 give a broad perspective on the lability of organic carbon. Generally, proteins,  
488 carbohydrates/sugars, and plant tissues have C:N ratios of ~4, ~15-20, and ~20-500,  
489 respectively (Hedges et al., 1986). Since material such as proteins and carbohydrates is  
490 generally more reactive to microbial metabolism, lower ratios typically correlate with  
491 more labile material (Hunt et al., 2000). Although there is no temporal trend among the

492 'N' glacier outflow samples with respect to the DOC:DON ratios, the overall range is  
493 relatively low (~4-25). The DOC:DON ratios reported here from 'N' glacier are  
494 consistent with previous results from runoff draining glaciers along the GOA (DOC:DON  
495 < 20), suggesting that glaciers generally may be a source of nitrogen-rich DOC (Hood  
496 and Berner, 2009). Although it is difficult to assess lability at the bulk-level based solely  
497 on DOC:DON ratios, this hypothesis is bolstered by our previous work using ultra-high  
498 resolution mass spectrometry, showing that (i) protein-like and lipid-like compounds are  
499 present in both the May and July 'N' glacier outflow samples, and (ii) that nitrogen-  
500 containing molecules may be major contributors to glacial DOM, compared to riverine  
501 and open ocean DOM (Bhatia et al., 2010; Kujawinski et al., 2009). Finally, though we  
502 have lack complementary mass spectrometry analysis of the POC fraction, similar  
503 POC:PON ratios in the July runoff (range: 8.3 to 21.1) hints that the bulk material from  
504 which the dissolved load is derived may be nitrogen-rich (Figure 8). However, the  
505 variability within the May runoff POC:PON ratios (range: 7.9 to 66.4) is perplexing, and  
506 requires additional class-specific analyses (e.g. lipid biomarkers) of the POC pool to  
507 more fully determine its composition.

508

#### 509 5.1.5. Evidence for microbially-mediated subglacial chemical weathering?

510 Previous studies have suggested that nitrogen-rich DOM in glacial systems  
511 originates from proteinaceous material associated with subglacial microbial communities  
512 (Barker et al., 2006; Hood and Scott, 2008; Lafreniere and Sharp, 2004). To investigate  
513 this hypothesis in our system we examined the bulk runoff hydrochemistry for evidence  
514 of widespread microbial activity facilitating subglacial chemical weathering beneath 'N'  
515 glacier. This approach relies heavily on the supposition that subglacial weathering at 'N'  
516 glacier is similar to that of other glacial systems, and can be challenging due to  
517 differential impact of competing subglacial chemical weathering reactions on the bulk  
518 runoff ion chemistry. Nonetheless, previous studies in glacial environments have shown  
519 that a runoff signature significantly perturbed from that expected from a purely abiotic  
520 system can be indicative of active microbial communities. Two reactions which have

521 been previously documented to be microbially-mediated in subglacial environments are  
522 (i) oxidation of organic matter, and (ii) sulfide oxidation (Wadham et al., 2010b).

523 Carbonate hydrolysis is generally the first reaction to occur when dilute  
524 supraglacial meltwater interacts with the glacier bed, and results in the rapid generation  
525 of  $\text{HCO}_3^-$  and  $\text{Ca}^{2+}$  independently of sulfate (Wadham et al., 2010b). Thus, a plot of  
526  $\text{SO}_4^{2-}$  vs  $\text{HCO}_3^-$  would ideally have a y-intercept of  $\sim 220 \mu\text{eq/L}$  (Wadham et al., 2010b),  
527 the theoretical solubility of calcite in pure water at  $0^\circ\text{C}$  (Tranter et al., 2002). A y-  
528 intercept above  $220 \mu\text{eq/L}$  suggests an additional source of  $\text{CO}_2$  to the subglacial  
529 meltwaters, most likely from microbial oxidation of organic matter (Wadham et al.,  
530 2010b). Among the ‘N’ outflow samples, only the Late May and July samples have  
531 significant linear relationships between  $\text{SO}_4^{2-}$  and  $\text{HCO}_3^-$  and both have y-intercepts  
532 well below  $220 \mu\text{eq/L}$  (Figure 3a). These low y-intercepts indicate little (or no)  
533 microbially-generated  $\text{CO}_2$  and suggest that the silicate bedrock underneath ‘N’ glacier is  
534 not favorable to microbial colonization. This result is not unexpected considering that  
535 hard bed-rock (e.g. silicate) systems are less amenable to large-scale microbial  
536 colonization than systems with softer bedrocks (e.g. carbonate) (Wadham et al., 2010b).  
537 However, the higher DOC concentrations in early May, and in the May 21 outlier sample  
538 particularly, hint that an available organic carbon source for microbial oxidation is  
539 present in the ‘N’ subglacial environment, particularly in the early season.

540 High sulfate concentrations in glacial runoff have previously been found to be a  
541 consequence of microbially-mediated anoxic sulfide oxidation. In oxic sulfide oxidation  
542 the typical rate-limiting step is the oxidation of  $\text{Fe}^{2+}$  to  $\text{Fe}^{3+}$  but since this step can be  
543 microbially mediated, the rate of sulfide oxidation can thereby be exponentially increased  
544 above that of abiotic systems (Sharp et al., 1999). Sulfide oxidation consumes oxygen,  
545 and microbial mediation hastens this process, thus driving regions of the subglacial  
546 system anoxic. The maximum sulfate concentration that can be generated from sulfide  
547 oxidation using oxygen-saturated waters at  $0^\circ\text{C}$  is  $\sim 400 \mu\text{eq/L}$  (Tranter et al., 2002).  
548 Thus, runoff  $\text{SO}_4^{2-}$  concentrations well above this value suggest alternative oxidizing  
549 agents (e.g.  $\text{Fe}^{3+}$ ) are present at the glacier bed, and additional sulfate contributions may

550 be generated via microbially-mediated anoxic sulfide oxidation (Tranter et al., 2002).  
551 The 'N' glacier outflow waters exhibit sulfate concentrations (1.5 – 162  $\mu\text{eq/L}$ ) well  
552 below 400  $\mu\text{eq/L}$ , thereby providing no evidence for microbially-mediated anoxic sulfide  
553 oxidation. However, Tranter (2003) noted that it is difficult to ascertain the subglacial  
554 biogeochemical environment solely from bulk runoff waters. For example, at Haut  
555 Glacier d'Arolla, a similarly-sized Swiss Alps glacier with a schist-gneiss-amphibolite  
556 bedrock, sulfate concentrations in the bulk runoff are typically less than 200  $\mu\text{eq/L}$ , but  
557 borehole waters sampled at the bed could have a sulfate concentrations up to 1200  $\mu\text{eq/L}$   
558 (Tranter et al., 2002). An exception to dilute sulfate concentrations in the 'N' glacier  
559 runoff was the May 21<sup>st</sup> sample which drained the lowest measured discharge waters with  
560 the largest modeled delayed (basal) flow component (Bhatia et al., 2011). The sulfate  
561 concentration in this sample was 929  $\mu\text{eq/L}$ , thus hinting that some component of the 'N'  
562 subglacial hydrological system may drain regions that support microbially-mediated  
563 anoxic sulfide oxidation.

564 In summary, if a microbially community is present, there does not appear to be  
565 sufficient activity to impact the bulk signature of the major ion chemistry in a similar  
566 fashion to that previously observed in some glacial systems. Thus, any subglacial  
567 microbial community at 'N' glacier is likely not large enough to mediate large-scale  
568 subglacial weathering processes. Yet, the lack of such a hydrochemical signal, does not  
569 negate the possibility that a microbial community exists beneath 'N' glacier. The  
570 hydrochemistry and DOC concentrations observed in the base flow (May 21<sup>st</sup>) sample is  
571 compelling evidence that microbial activity is able to influence subglacial DOM  
572 character in specific micro-environments (e.g. saturated porewaters), which only impact  
573 the bulk runoff signature in the early (low discharge) season. This supposition is further  
574 supported by our molecular-level composition analysis of runoff DOM, which revealed a  
575 discernable microbial signature in the May runoff that was swamped by an overwhelming  
576 terrestrial signature in July runoff (Bhatia et al., 2010).

577

578 5.1.6. Decoupling of radiocarbon and lability in glacial systems?



579 An alternative hypothesis for the low C:N ratios, and proteinaceous material  
580 typical of glacial rivers is that labile DOM fractions remain from the soils and vegetation  
581 initially overrun during past periods of glacial advance. This hypothesis explains both the  
582 depleted  $\text{DO}\Delta^{14}\text{C}$ , typical of glacial systems (Hood et al., 2009), and the observed C:N  
583 ratios. In oxygenated systems, radiocarbon signature and lability are coupled concepts,  
584 since material depleted in radiocarbon is considered to be old, or relict, organic carbon  
585 whose labile components have long-since been consumed (Raymond and Bauer, 2001a).  
586 However, in glacial systems, we propose that these concepts may be decoupled. Although  
587 the organic matter may be depleted in radiocarbon, owing to its ultimate derivation from  
588 previously overridden soils and vegetation, it may still possess labile components since  
589 the ice cover could inhibit the full range of metabolic reactions present in oxygenated soil  
590 environments. In effect, the glacier or ice sheet acts as a freezer, preserving the labile  
591 components of the organic matter, which are then exported in the runoff.

592

## 593 5.2 Proglacial processing of glacially-derived organic carbon

594 Though we possess limited proglacial samples, they are intriguing as they hint  
595 that glacially derived DOC undergoes significant transformation in land-terminating GrIS  
596 systems prior to export to the surrounding marine environments. Our field site is typical  
597 of many land-terminating glacier systems along the western margin of the ice sheet where  
598 several glacial rivers transmit through a floodplain/proglacial region, into a large  
599 proglacial lake, before eventually emptying into a fjord. The general increase in the  
600 dissolved C:N ratios from the ice surface to the proglacial lake outflow (Figure 8) may  
601 broadly indicate that glacially-derived DOM becomes less labile as it traverses through  
602 the proglacial environment. However, the range of DOC:DON ratios observed within  
603 each sample type indicates that variability can be large, and thus more frequent sampling  
604 would be needed to confirm this trend. In this study the 'O' glacier floodplain sample  
605 represents our best analogue for the processing that occurs in glacial runoff prior to entry  
606 into the proglacial lake. From this sample, it appears that floodplain processing adds  
607 newly produced DOC, evidenced by a significantly more enriched radiocarbon content

608 ( $\Delta^{14}\text{C-DOC} > 0$ ). The DOC undergoes further transformation in the proglacial lake. Our  
609 analysis of the proglacial lake dynamics was limited to two samples (Proglacial Lake and  
610 the Lake Outflow), but from these, it seems that the most labile fractions of DOC was  
611 consumed in the lake, as the concentrations decreased and the  $\text{DO}\Delta^{14}\text{C}$  became more  
612 depleted down the lake length. Interestingly, the  $\text{PO}\Delta^{14}\text{C}$  signature between the  
613 Proglacial Lake and Lake Outflow becomes more enriched, perhaps suggesting that as  
614 the labile DOC fractions are consumed, new production adds enriched POC. This  
615 contention is also supported by the low POC:PON ratios, where the nitrogen could be  
616 derived from new production.

617

### 618 5.3 Delivery of glacially-derived organic carbon to the oceans

619 The surface runoff from the Greenland ice sheet is estimated to be on the order of  
620  $\sim 500 \text{ km}^3/\text{y}$  (Mernild et al., 2009) which is comparable to the combined annual discharge  
621 from the four major pan-Arctic North American rivers (Mackenzie, Yukon, Peel, Beck)  
622 as averaged over 1970-2008 (Shiklomanov, 2009). Using this discharge estimate and the  
623 average discharge-weighted DOC (0.32 mg/L) and POC (3.7 mg/L) concentrations  
624 measured at 'N' glacier, we can estimate an annual export of 0.16 Tg of DOC and 1.9 Tg  
625 of POC from the Greenland ice sheet. This DOC flux is equivalent to a recent estimate  
626 from the Gulf of Alaska glaciers (0.13 Tg/year) and smaller Arctic rivers (e.g. Olenek:  
627 0.32 Tg/y, Yana: 0.09 Tg/y), but lower than that from the four major rivers draining into  
628 the Arctic Ocean (Yenisey: 4.1-4.9 Tg/y, Lena: 3.4-4.7 Tg/y, Ob: 3.1-3.2 Tg/y,  
629 Mackenzie: 1.3 Tg/y) (Dittmar and Kattner, 2003). Conversely, our estimated Greenland  
630 ice sheet POC flux is equivalent to that from the Mackenzie (1.8-2.1 Tg/y), the principal  
631 river POC contributor to the Arctic ocean (Dittmar and Kattner, 2003). Thus, DOC flux  
632 from the Greenland ice sheet is similar to that of a minor Arctic river, whereas the POC  
633 flux is comparable to that from the major river contributor.

634 Similar to Arctic river systems, the majority of the annual organic carbon exported  
635 by glacial systems occurs during a short time period, when discharge is at its peak.  
636 However, in contrast to river systems (Benner et al., 2004), the base flow exports

637 comparatively younger, but still  $^{14}\text{C}$ -depleted DOC (-245.9‰), whereas the peak flow  
638 exports older, more  $^{14}\text{C}$ -depleted DOC (-395.3 to -400.9‰). The average surface  
639  $\text{DO}\Delta^{14}\text{C}$  signature in surface ocean waters is between -150‰ and -400‰; in deep ocean  
640 waters  $\text{DO}\Delta^{14}\text{C}$  becomes more depleted, down to -540‰ in North Pacific Deep Water  
641 (McNichol and Aluwihare, 2007). Glacial systems also export a  $^{14}\text{C}$  depleted POC pool (-  
642 257‰ to -263‰) compared to the surface ocean  $\text{PO}\Delta^{14}\text{C}$  signature, which is generally  
643 enriched in  $\Delta^{14}\text{C}$  (Druffel and Bauer, 2000; McNichol and Aluwihare, 2007), and the  
644 deep ocean  $\text{PO}\Delta^{14}\text{C}$  (e.g. -111‰ in the Southern Ocean) (Druffel and Bauer, 2000). Thus,  
645 peak flow glacial runoff may contribute a pre-aged end-member to the oceanic DOC and  
646 POC pools. On a global scale, any glacial contribution is likely orders of magnitude too  
647 small in comparison to the standing surface organic carbon inventory to influence the  
648 oceanic  $\text{DO}\Delta^{14}\text{C}$  /  $\text{PO}\Delta^{14}\text{C}$  signatures. However, export of glacially-derived organic  
649 carbon from land-terminating Greenland ice sheet glaciers may still have localized  
650 impact in the coastal North Atlantic and Arctic Oceans. The likelihood and broader  
651 implications of this export depend on whether the labile fractions of glacial organic  
652 carbon survive biogeochemical processing in the proglacial and estuarine regions. Our  
653 results hint that a significant proglacial transition zone is present and that the most labile  
654 components are likely consumed; but further study is required to confirm this  
655 interpretation. However, we should note, that the majority of surface meltwater runoff  
656 from the Greenland ice sheet is evacuated by large marine-terminating glaciers, as  
657 opposed to land-terminating systems (Rignot and Kanagaratnam, 2006). Such systems  
658 would export subglacially-routed meltwater and associated organic carbon directly to the  
659 coastal ocean, thus circumventing any proglacial processing.

660

## 661 **6. Conclusions**

662

663 Glacial runoff draining the Greenland ice sheet exports a unique brand of organic  
664 carbon, distinct from riverine organic carbon. Glacial organic carbon has low DOC  
665 concentrations, higher POC concentrations, relatively low DOC/DON ratios (~4-25) a

666 terrestrial  $\delta^{13}\text{C}$  signature, is depleted in  $\text{DO}\Delta^{14}\text{C}$ , and is nitrogen-rich. Conversely,  
667 riverine organic carbon though possessing a terrestrial  $\delta^{13}\text{C}$  signature, has high DOC  
668 concentrations, a larger DOC/POC ratio, high DOC/DON ratios ( $>30$ ), is enriched in  
669  $\text{DO}\Delta^{14}\text{C}$ , and is nitrogen-rich (Hedges et al., 1997). Current organic carbon export from  
670 the Greenland ice sheet is not insignificant, estimated to be equivalent to the DOC flux  
671 from a small Arctic river and the POC flux from a major Arctic river. These fluxes will  
672 only increase as surface melt on the ice sheet surface increases. Furthermore, the DOC  
673 flux may disproportionately increase as the subglacial drainage system extends and  
674 develops, perhaps resulting in a constant winter flux of more concentrated, basally-  
675 derived DOC. Further study is needed in order to fully determine the mechanisms which  
676 cause glacial organic carbon to be paradoxically radiocarbon depleted, yet also still retain  
677 some labile components. Here we propose two potential mechanisms: (1) *in situ*  
678 microbial activity utilizing radiocarbon depleted organic carbon stores, and thereby  
679 producing  $^{14}\text{C}$ -depleted proteinaceous material, or (2) labile components of the original  
680 overridden organic matter remain that have been preserved under the ice sheet.  
681 Conceivably, both of these processes could be occurring simultaneously, with regions  
682 populated by subglacial microbial communities accessed by the distributed drainage  
683 system during low flow periods, and isolated organic carbon stores tapped by headward  
684 progression of the subglacial drainage system at the peak summer meltseason.

685

686 *Acknowledgements.* This research was supported by: the WHOI Clark Arctic Research  
687 Initiative (EBK, SBD, MAC), the National Science and Engineering Research Council of  
688 Canada (MPB), the WHOI Climate Change Institute (MPB), and a Horton Hydrology  
689 Grant from the American Geophysical Union (MPB). I am grateful to P. Henderson for  
690 conducting the POC/PON and nutrient analyses, to M. Lafreniere and Steve Koziar for  
691 assistance with the ion chromatography analyses, to M. Nieto-Cid and J. Becker for  
692 assistance with the dissolved organic carbon analyses, to Ann McNichol and the  
693 NOSAMS prep lab staff for assistance with the radiocarbon analyses, to D. Griffith and J.  
694 Saenz for helpful conversations, to K. Longnecker for comments that improved the  
695 manuscript, to M. Behn, I. Joughin, and K. Ponair for assistance in sampling the inland  
696 ice, and to B. Gready, P. Henderson, A. Criscitiello, and M. Evans for their valuable  
697 assistance in the field.  
698

699 **References**

- 700 Barker, J.D., Sharp, M.J., Fitzsimons, S.J., Turner, R.J., 2006. Abundance and dynamics  
701 of dissolved organic carbon in glacier systems. *Arct. Antarct. Alp. Res.* 38, 163-  
702 172.  
703
- 704 Bartholomew, I., Nienow, P., Mair, D., Hubbard, A., King, M.A., Sole, A., 2010.  
705 Seasonal evolution of subglacial drainage and acceleration in a Greenland outlet  
706 glacier. *Nat. Geosci.* 3, 408-411.  
707
- 708 Benner, R., Benitez-Nelson, B., Kaiser, K., Amon, R.M.W., 2004. Export of young  
709 terrigenous dissolved organic carbon from rivers to the Arctic Ocean. *Geophys.*  
710 *Res. Lett.* 31.  
711
- 712 Bhatia, M., Das, S.B., Kujawinski, E.B., Henderson, P., Burke, A., Charette, M.A., 2011.  
713 Seasonal evolution of water contributions to discharge from a Greenland outlet  
714 glacier: Insight from a new isotope-mixing model *J. Glaciol.* 57, 929-941.  
715
- 716 Bhatia, M., S.B. Das, K. Longnecker, M.A. Charette, Kujawinski, E.B., 2010. Molecular  
717 characterization of dissolved organic matter associated with the Greenland ice  
718 sheet. *Geochim. Cosmochim. Acta* 74, 3768-3784.  
719
- 720 Bhatia, M., Sharp, M., Foght, J., 2006. Distinct bacterial communities exist beneath a  
721 high arctic polythermal glacier. *Appl. Environ. Microbiol.* 72, 5838-5845.  
722
- 723 Carpenter, E.J., Lin, S.J., Capone, D.G., 2000. Bacterial activity in South Pole snow.  
724 *Appl. Environ. Microbiol.* 66, 4514-4517.  
725
- 726 Cheng, S.M., Foght, J.M., 2007. Cultivation-independent and -dependent characterization  
727 of Bacteria resident beneath John Evans Glacier. *FEMS Microbiol. Ecol.* 59, 318-  
728 330.  
729
- 730 Das, S.B., Joughin, I., Behn, M.D., Howat, I.M., King, M.A., Lizarralde, D., Bhatia,  
731 M.P., 2008. Fracture propagation to the base of the Greenland Ice Sheet during  
732 supraglacial lake drainage. *Science* 320, 778-781.  
733
- 734 Dittmar, T., Kattner, G., 2003. The biogeochemistry of the river and shelf ecosystem of  
735 the Arctic Ocean: a review. *Mar. Chem.* 83, 103-120.  
736
- 737 Druffel, E.R.M., Bauer, J.E., 2000. Radiocarbon distributions in Southern Ocean  
738 dissolved and particulate organic matter. *Geophys. Res. Lett.* 27, 1495-1498.  
739
- 740 Dubnick, A., Barker, J., Sharp, M., Wadham, J., Lis, G., Telling, J., Fitzsimons, S.,  
741 Jackson, M., 2010. Characterization of dissolved organic matter (DOM) from

742 glacial environments using total fluorescence spectroscopy and parallel factor  
743 analysis. *Ann. Glaciol.* 51, 111-122.  
744

745 Escher, A., 1971. Map Sheet no. 3 Sondre Stromfjord - Nugssu aq Geological Maps of  
746 Greenland 1:500,000. Geological Survey of Denmark and Greenland (GEUS),  
747 Copenhagen.  
748

749 Hansell, D., 2002. in: Hansell, D., Carlson, C. (Eds.), *Biogeochemistry of Marine*  
750 *Dissolved Organic Matter*. Academic Press, New York.  
751

752 Hedges, J.I., Clark, W.A., Quay, P.D., Richey, J.E., Devol, A.H., Santos, U.D., 1986.  
753 Compositions and fluxes of particulate organic material in the amazon river  
754 *Limnol. Oceanogr.* 31, 717-738.  
755

756 Hedges, J.I., Keil, R.G., Benner, R., 1997. What happens to terrestrial organic matter in  
757 the ocean? *Org. Geochem.* 27, 195-212.  
758

759 Hodson, A., Anesio, A.M., Tranter, M., Fountain, A., Osborn, M., Priscu, J., Laybourn-  
760 Parry, J., Sattler, B., 2008. Glacial ecosystems. *Ecological Monographs* 78, 41-67.  
761

762 Hood, E., Berner, L., 2009. Effects of changing glacial coverage on the physical and  
763 biogeochemical properties of coastal streams in southeastern Alaska. *J. Geophys.*  
764 *Res.-Biogeosci.* 114.  
765

766 Hood, E., Fellman, J., Spencer, R.G.M., Hernes, P.J., Edwards, R., D'Amore, D., Scott,  
767 D., 2009. Glaciers as a source of ancient and labile organic matter to the marine  
768 environment. *Nature* 462, 1044-U1100.  
769

770 Hood, E., Scott, D., 2008. Riverine organic matter and nutrients in southeast Alaska  
771 affected by glacial coverage. *Nat. Geosci.* 1, 583-587.  
772

773 Hunt, A.P., Parry, J.D., Hamilton-Taylor, J., 2000. Further evidence of elemental  
774 composition as an indicator of the bioavailability of humic substances to bacteria.  
775 *Limnol. Oceanogr.* 45, 237-241.  
776

777 Kujawinski, E.B., Longnecker, K., Blough, N.V., Vecchio, R.D., Finlay, L., Kitner, J.B.,  
778 Giovannoni, S.J., 2009. Identification of possible source markers in marine  
779 dissolved organic matter using ultrahigh resolution mass spectrometry. *Geochim.*  
780 *Cosmochim. Acta* 73, 4384-4399.  
781

782 Lafreniere, M.J., Sharp, M.J., 2004. The concentration and fluorescence of dissolved  
783 organic carbon (DOC) in glacial and nonglacial catchments: Interpreting  
784 hydrological flow routing and DOC sources. *Arct. Antarct. Alp. Res.* 36, 156-165.

785 McNichol, A.P., Aluwihare, L.I., 2007. The power of radiocarbon in biogeochemical  
786 studies of the marine carbon cycle: Insights from studies of dissolved and  
787 particulate organic carbon (DOC and POC). *Chem. Rev.* 107, 443-466.  
788

789 Mernild, S.H., Liston, G.E., Hiemstra, C.A., Steffen, K., Hanna, E., Christensen, J.H.,  
790 2009. Greenland Ice Sheet surface mass-balance modelling and freshwater flux  
791 for 2007, and in a 1995-2007 perspective. *Hydrol. Processes* 23, 2470-2484.  
792

793 Millot, R., Gaillardet, J., Dupre, B., Allegre, C.J., 2003. Northern latitude chemical  
794 weathering rates: clues from the Mackenzie River Basin, Canada. *Geochim.*  
795 *Cosmochim. Acta* 67, 1305-1329.  
796

797 Pautler, B.G., Simpson, A.J., Simpson, M.J., Tseng, L.-H., Spraul, M., Dubnick, A.,  
798 Sharp, M.J., Fitzsimons, S.J., 2011. Detection and Structural Identification of  
799 Dissolved Organic Matter in Antarctic Glacial Ice at Natural Abundance by SPR-  
800 W5-WATERGATE (1)H NMR Spectroscopy. *Environ. Sci. Technol.* 45, 4710-  
801 4717.  
802

803 Petsch, S.T., Eglinton, T.I., Edwards, K.J., 2001. C-14-dead living biomass: Evidence for  
804 microbial assimilation of ancient organic carbon during shore weathering. *Science*  
805 292, 1127-1131.  
806

807 Raymond, P.A., Bauer, J.E., 2001a. Riverine export of aged terrestrial organic matter to  
808 the North Atlantic Ocean. *Nature* 409, 497-500.  
809

810 Raymond, P.A., Bauer, J.E., 2001b. Use of <sup>14</sup>C and <sup>13</sup>C natural abundances for  
811 evaluating riverine, estuarine, and coastal DOC and POC sources and cycling: a  
812 review and synthesis. *Org. Geochem.* 32, 469-485.  
813

814 Rignot, E., Kanagaratnam, P., 2006. Changes in the Velocity Structure of the Greenland  
815 Ice Sheet. *Science* 311, 986-990.  
816

817 Sharp, M., Parkes, J., Cragg, B., Fairchild, I.J., Lamb, H., Tranter, M., 1999. Widespread  
818 bacterial populations at glacier beds and their relationship to rock weathering and  
819 carbon cycling. *Geology* 27, 107-110.  
820

821 Shiklomanov, A., 2009. River Discharge, in: Richter-Menge, J., Peterson, T.C., Baringer,  
822 M.O. (Eds.), *Arctic Report Card 2009*. NOAA, pp. 28-29.  
823

824 Skidmore, M., Anderson, S.P., Sharp, M., Foght, J., Lanoil, B.D., 2005. Comparison of  
825 microbial community compositions of two subglacial environments reveals a  
826 possible role for microbes in chemical weathering processes. *Appl. Environ.*  
827 *Microbiol.* 71, 6986-6997.

- 828 Skidmore, M., Tranter, M., Tulaczyk, S., Lanoil, B., 2010. Hydrochemistry of ice stream  
829 beds - evaporitic or microbial effects? *Hydrol. Processes* 24, 517-523.  
830
- 831 Skidmore, M.L., Foght, J.M., Sharp, M.J., 2000. Microbial life beneath a high Arctic  
832 glacier. *Appl. Environ. Microbiol.* 66, 3214-3220.  
833
- 834 Tranter, M., 2003. *Geochemical Weathering in Glacial and Proglacial Environments*, in:  
835 Drever, J.I. (Ed.). Elsevier, pp. p.189-205.  
836
- 837 Tranter, M., Sharp, M.J., Lamb, H.R., Brown, G.H., Hubbard, B.P., Willis, I.C., 2002.  
838 Geochemical weathering at the bed of Haut Glacier d'Arolla, Switzerland - a new  
839 model. *Hydrol. Processes* 16, 959-993.  
840
- 841 Wadham, J.L., Tranter, M., Hodson, A.J., Hodgkins, R., Bottrell, S., Cooper, R.,  
842 Raiswell, R., 2010a. Hydro-biogeochemical coupling beneath a large polythermal  
843 Arctic glacier: Implications for subice sheet biogeochemistry. *Journal of*  
844 *Geophysical Research-Earth Surface* 115.  
845
- 846 Wadham, J.L., Tranter, M., Skidmore, M., Hodson, A.J., Priscu, J., Lyons, W.B., Sharp,  
847 M., Wynn, P., Jackson, M., 2010b. Biogeochemical weathering under ice: Size  
848 matters. *Global Biogeochem. Cycles* 24.  
849
- 850 Wadham, J.L., Tranter, M., Tulaczyk, S., Sharp, M., 2008. Subglacial methanogenesis: A  
851 potential climatic amplifier? *Global Biogeochem. Cycles* 22.  
852  
853



854 **Tables**

855

856 **Table 1.** Average percent ionic contributions (rounded to whole percent) from major  
 857 dissolved anions and cations in the ‘N’ glacier outflow waters in Early May (May 18 to  
 858 24), Late May (May 25 to 31) and July (July 10 to 16). Errors represent standard  
 859 deviation from the mean value. Mean values exclude the May 21 outlier sample, whose  
 860 percent ionic contributions and absolute concentrations in  $\mu\text{M}$  (in parentheses) are shown  
 861 in the last row.  
 862

Time	*Ca <sup>2+</sup>	*Mg <sup>2+</sup>	*Na <sup>+</sup>	*K <sup>+</sup>	*SO <sub>4</sub> <sup>2-</sup>	NO <sub>3</sub> <sup>-</sup>	Cl <sup>-</sup>	HCO <sub>3</sub> <sup>-</sup>
<b>Early May</b>	21±1	14±0	8±1	6±1	21±4	1±0	2±0	28±4
<b>Late May</b>	16±2	13±0	10±2	10±1	10±3	0±0	2±0	39±3
<b>July</b>	17±1	13±1	8±1	11±1	5±1	0±0	2±1	45±1
<b>May 21 outlier</b>	28 (666)	15 (357)	3 (60.4)	3 (77.4)	39 (929)	2 (38.7)	1 (29.4)	8 (196)

863

864 **Table 2.** Mean DOC and POC concentrations (mg/L) in supraglacial, subglacial, and  
 865 proglacial samples collected in ‘Early May’ (May 18-24), ‘Late May’ (May 25-June 1),  
 866 and ‘July’ (July 10-16). The ‘Early May’ average does not include the concentrated May  
 867 21 outlier sample ([DOC] = 4.1 mg/L, [POC] = 13.2 mg/L). The notation ‘--’ indicates no  
 868 measurement was taken.  
 869

Sample Type	‘Early May’			‘Late May’			‘July’		
	n	DOC	POC	n	DOC	POC	n	DOC	POC
<b>Supraglacial</b>	1	0.2	0.30	1	0.2	0.57	0	--	--
<b>‘N’ Glacier Outflow</b>	7	0.6±0.1	3.4±1.0	10	0.4±0.1	3.6±1.3	12	0.3±0.2	3.5±1.1
<b>‘M’ Glacier Outflow</b>	1	0.8	2.8	1	1.2	3.9	1	0.2	2.2
<b>‘O’ Glacier Floodplain</b>	1	1.7	0.76	0	--	--	0	--	--
<b>Proglacial Lake</b>	1	7.4	1.0	1	0.7	1.7	1	0.4	--
<b>Lake Outflow</b>	1	2.7	0.5	0	--	--	0	--	--
<b>May 21 outlier</b>	1	4.1	13.23	--	--	--	--	--	--

870

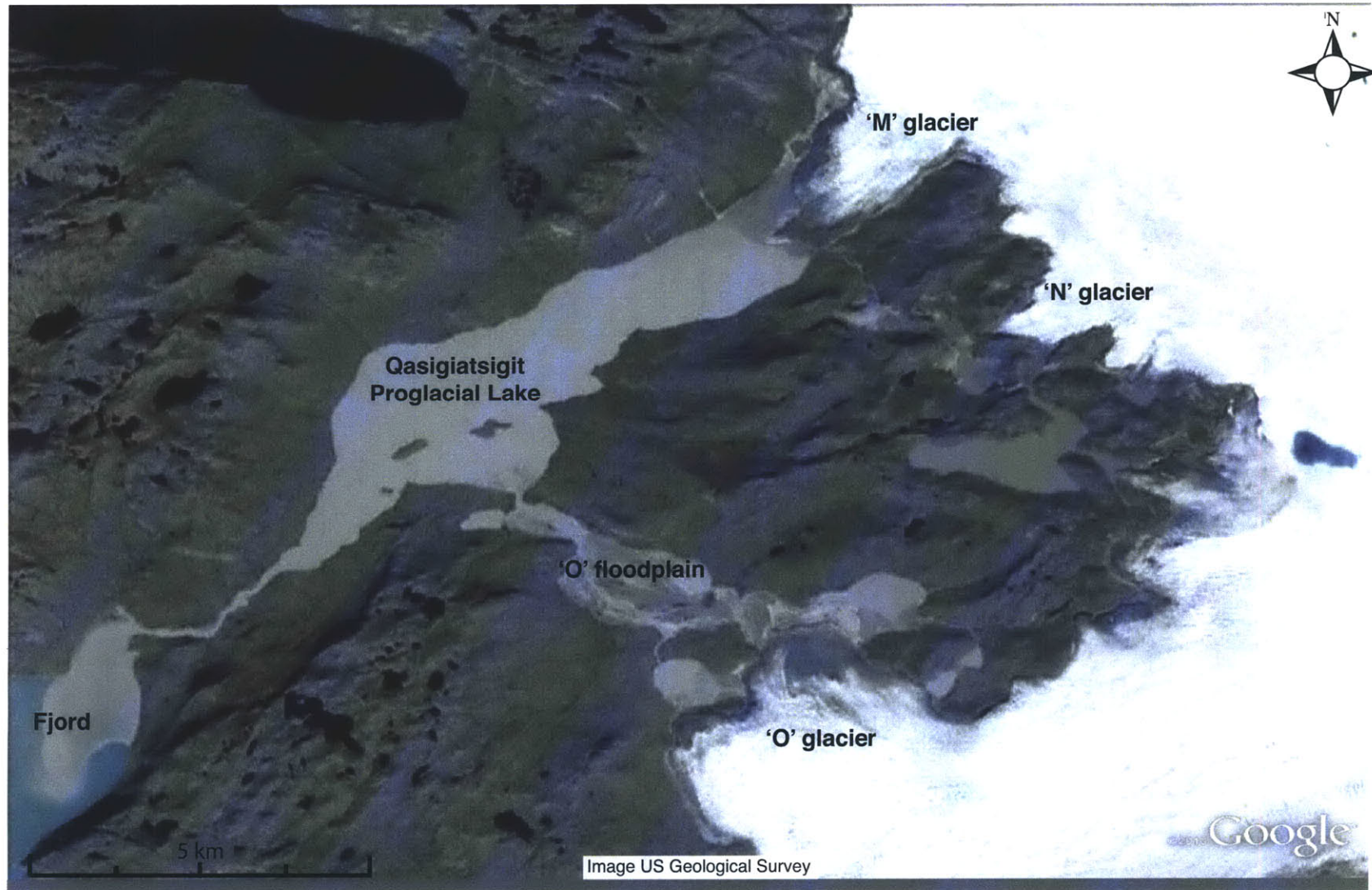


**Figure 1.** Map of field site on the southwestern margin of the Greenland ice sheet.

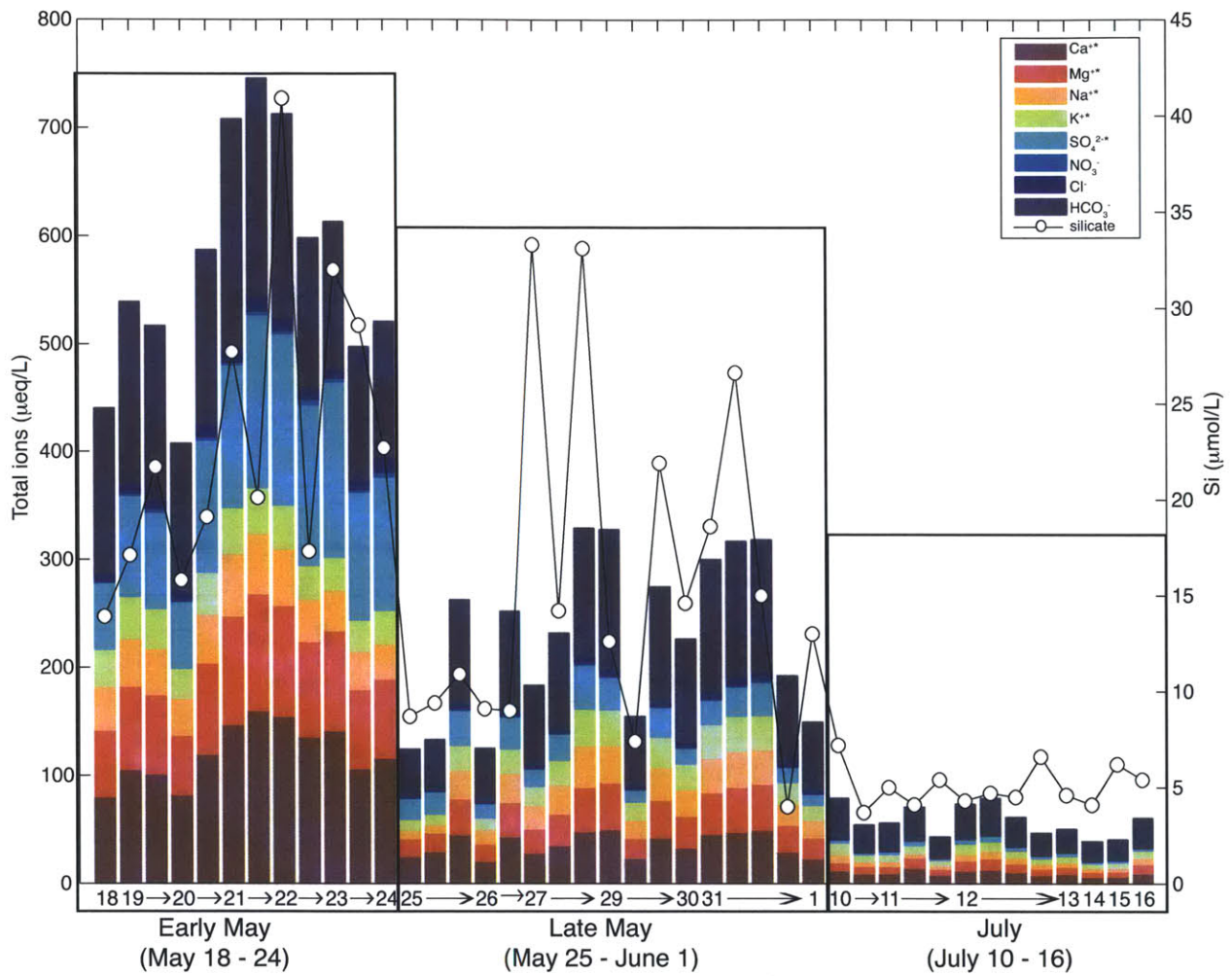


**Figure 2.** Total ionic concentrations of major dissolved anions and cations (left y-axis) and dissolved silicate (right y-axis) in the N glacier outflow waters from May 18 to July 16, 2008. The (\*) indicates crustal contributions (see text for details).

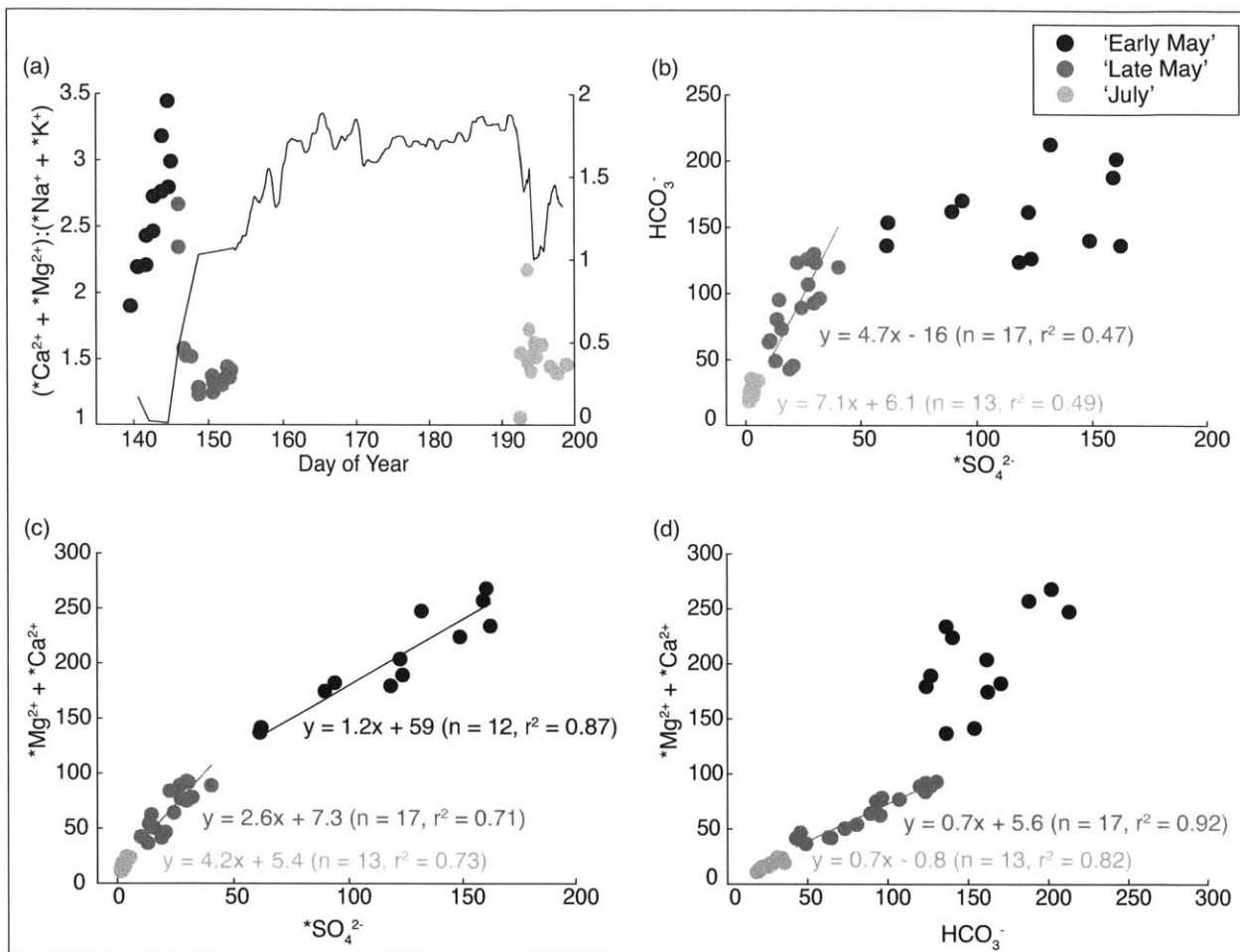


**Figure 3.** (a) Ratio of monovalent to divalent crustal cations, (b) linear regressions (Model II, geometric mean) between  $HCO_3^-$  and  $^*SO_4^{2-}$ , (c) linear regressions (Model II, geometric mean) between  $(^*Mg^{2+} + ^*Ca^{2+})$  and  $^*SO_4^{2-}$  and (d)  $HCO_3^-$  for the 'N' glacier runoff in the 'Early May' (May 18-24), 'Late May' (May 25-June 1) and 'July' (July 10-16) time periods. In (a) measured discharge at 'N' glacier is shown on the right y-axis. All regressions presented are significant to the 99% confidence levels. Associations not shown did not meet this criterion. The Early May (May 21) outlier sample was excluded.

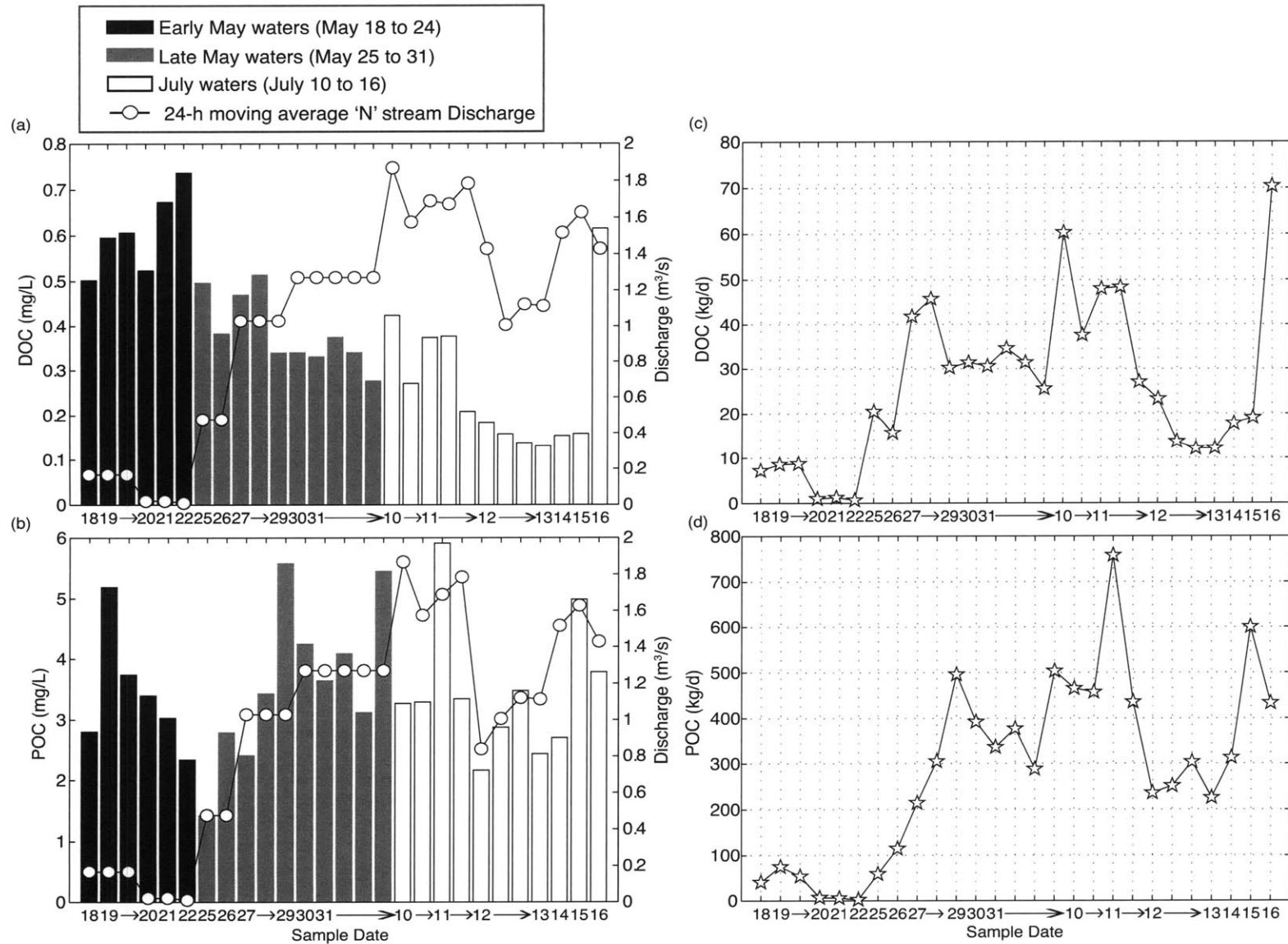


**Figure 4.** (a) DOC and (b) POC concentrations in point samples collected from the 'N' glacier outflow in May and July 2008, with the discharge measured at the time closest to that of the sample collection time shown on the right y-axis. In May the discharge data is limited to point measurements. The daily DOC and POC flux are shown in (c) and (d).



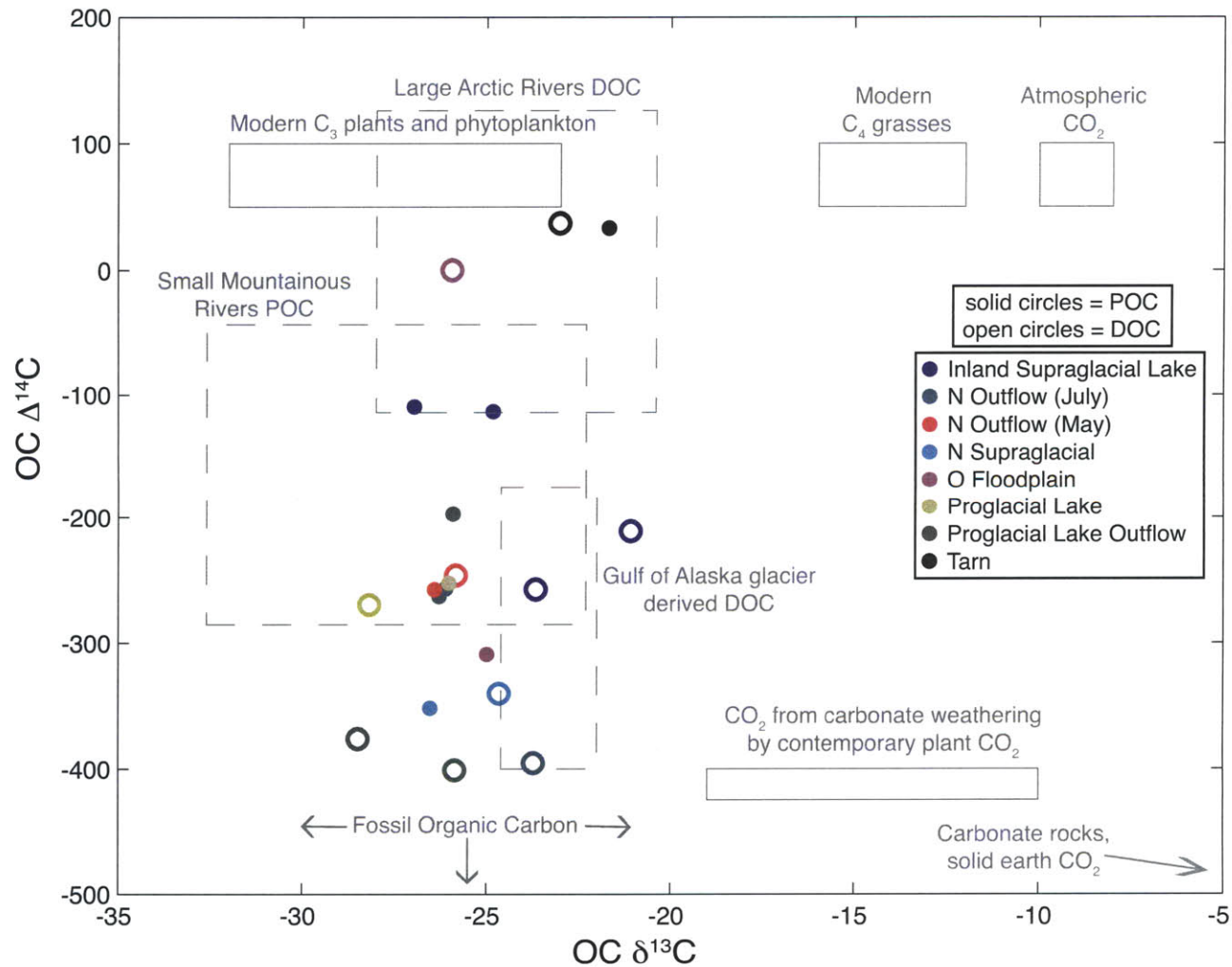


**Figure 5.** Dissolved and particulate organic  $\Delta^{14}\text{C}$  and  $\delta^{13}\text{C}$  in glacial and proglacial samples collected on the western margin of the Greenland ice sheet. Solid grey boxes illustrate isotopic ranges of end-member carbon sources (Mayorga et al., 2005), whereas dashed grey boxes illustrate literature values for large Arctic rivers DOC (Raymond et al., 2007), small mountainous rivers POC (Raymond and Bauer, 2001), and Gulf of Alaska (GOA) glacially-derived DOC (Hood et al., 2009). The fossil organic carbon source is radiocarbon dead ( $\Delta^{14}\text{C} \leq -1000\text{‰}$ ), and can have  $\delta^{13}\text{C}$  values ranging from  $-15\text{‰}$  to  $-35\text{‰}$ .

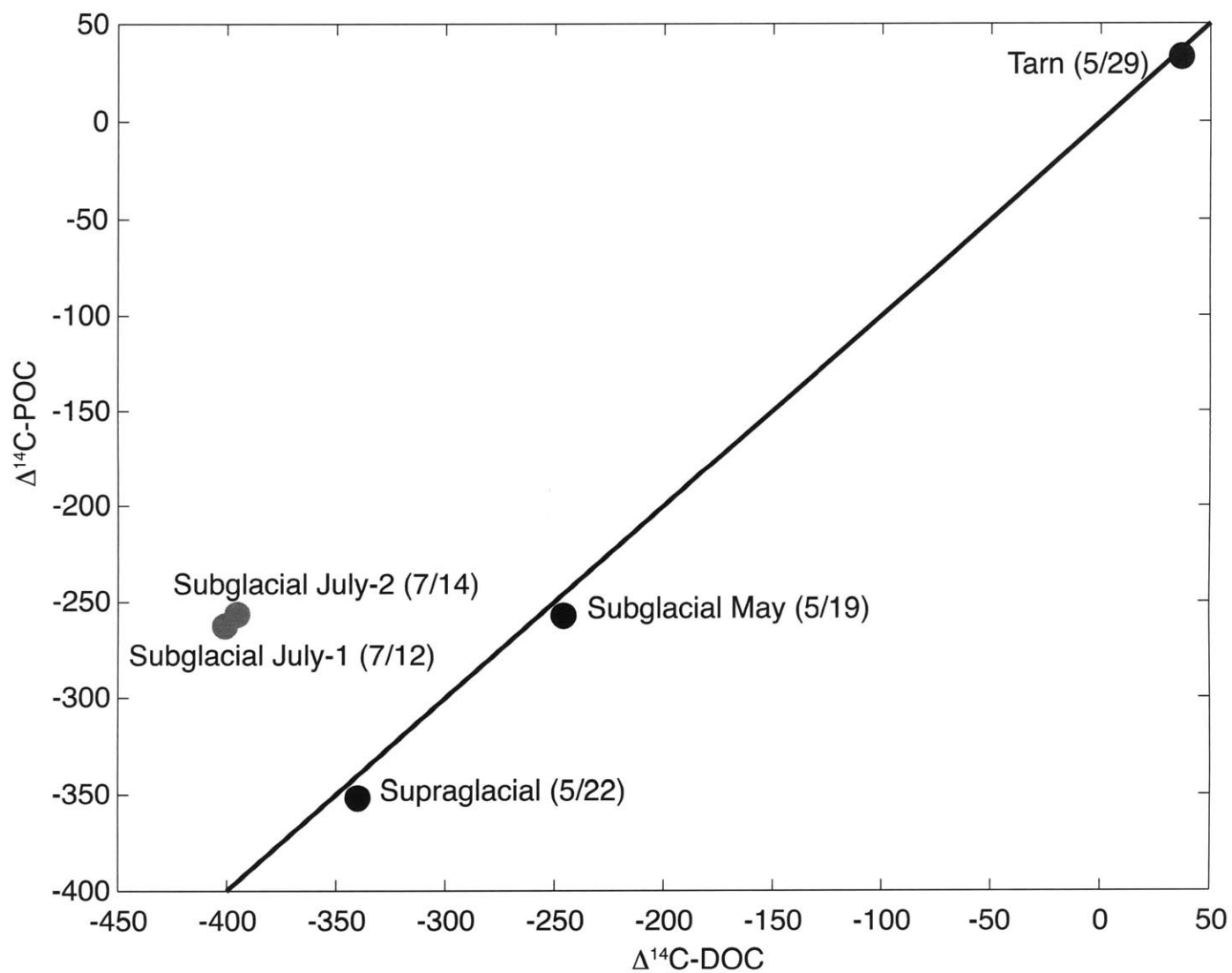


**Figure 6.** Dissolved and particulate organic radiocarbon in the ‘N’ glacier outflow samples collected in May and July as well as end-member samples from ‘N’ supraglacial water and a proglacial tarn. For clarity, dates of collection (in 2008) and a 1:1 line (black) are also shown.

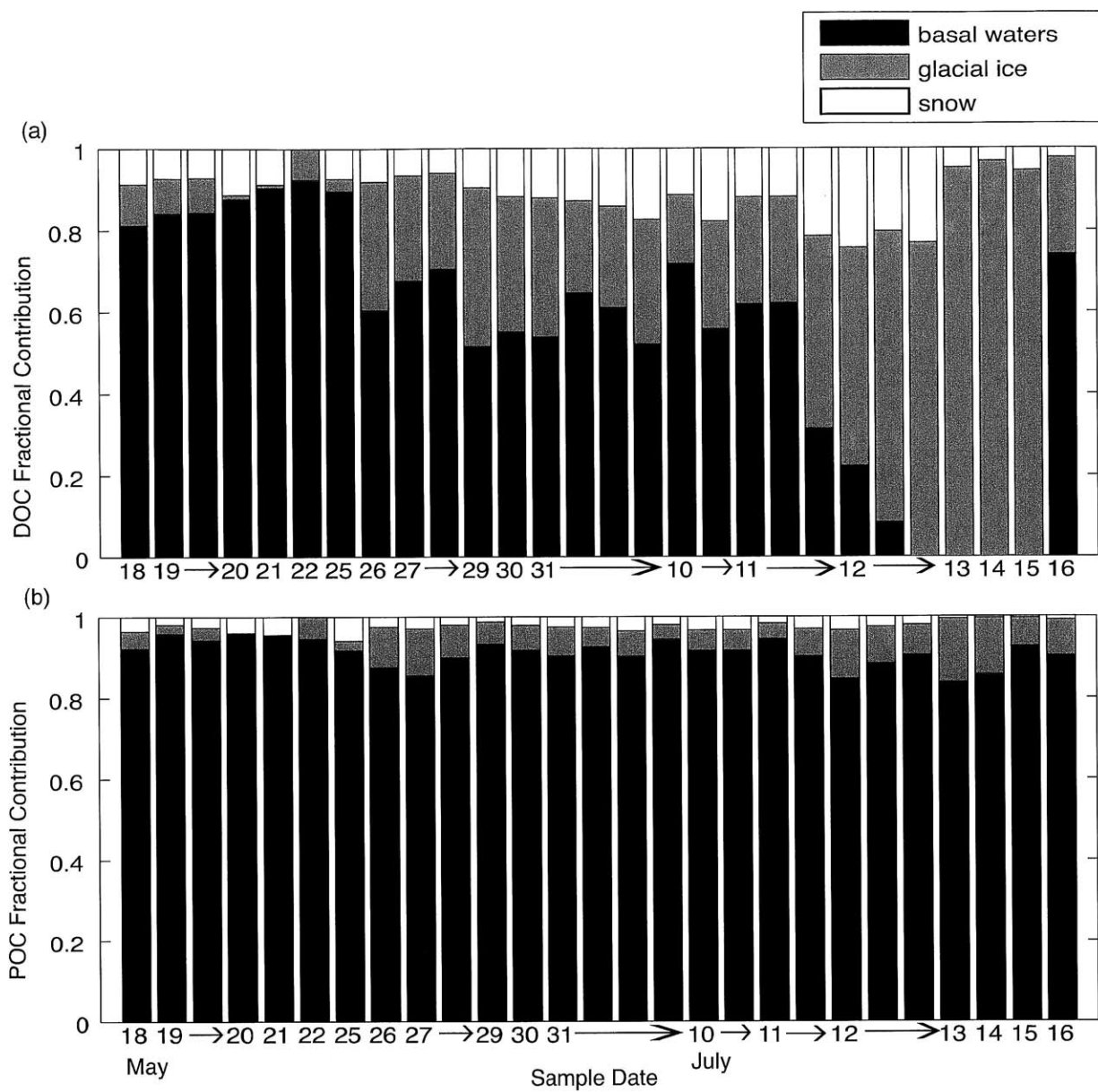


**Figure 7.** Estimates of proportional contributions from the basal waters, glacial ice, and snow end-member pools to the total runoff DOC and POC.



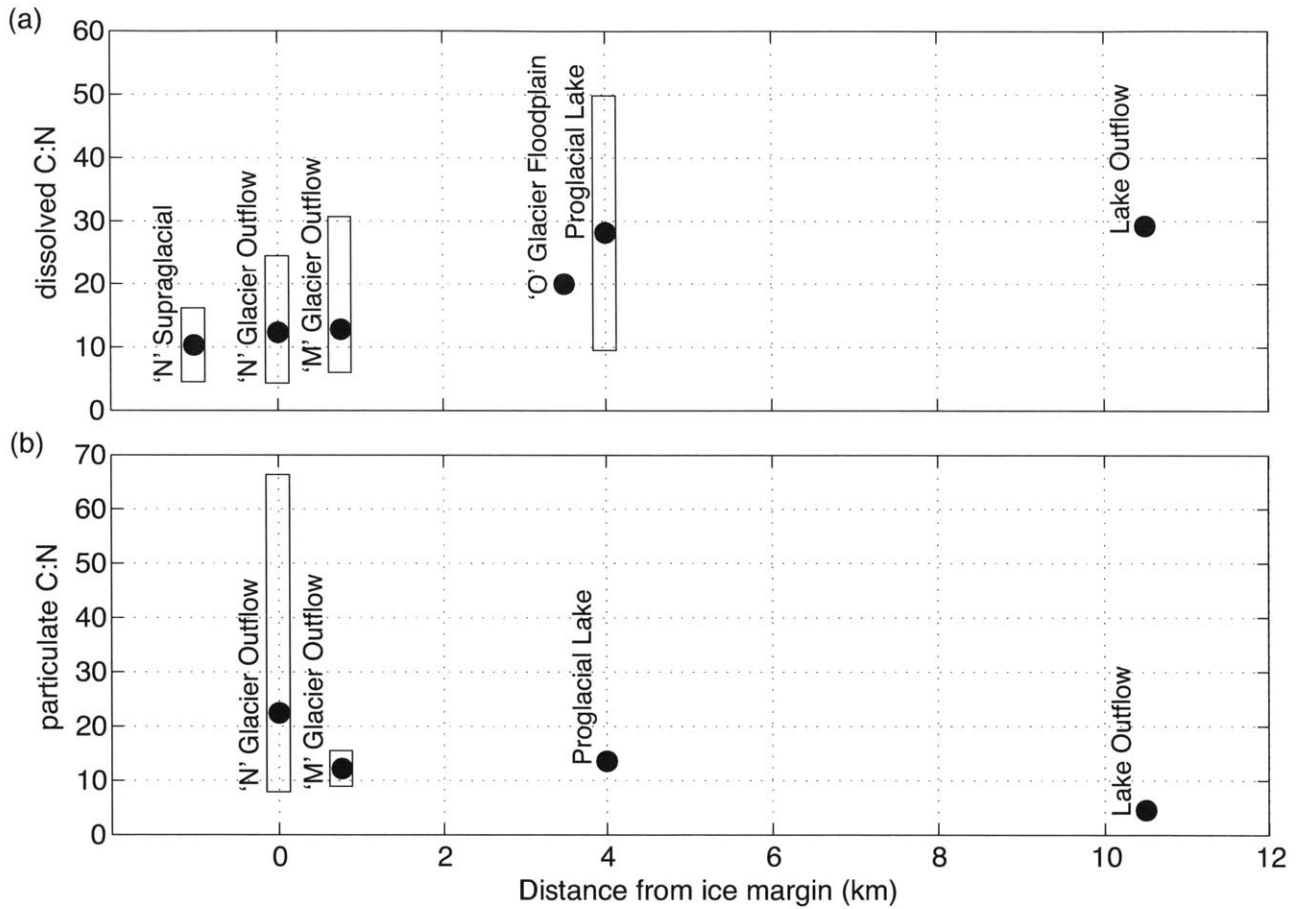


**Figure 8.** (a) Mean dissolved C:N ratios of 'N' supraglacial ice (n=2), 'N' glacier outflow (n=26), 'M' glacier floodplain (n=4), 'O' glacier floodplain (n=1), proglacial lake (n=3), and lake outflow (n=1). (b) Mean particulate C:N ratios of the 'N' glacier outflow (n=18), 'M' glacier floodplain (n=2), proglacial lake (n=1), and lake outflow (n=1) samples. Particulate C:N ratios for the 'N' supraglacial and 'O' glacier floodplain were below detection. Observed ranges for both the dissolved and particulate C:N ratios are shown by the rectangles.

## Chapter 5

### Iron export from the Greenland ice sheet

#### **Abstract**

Here we report dissolved ( $<0.2 \mu\text{m}$ ) and suspended sediment particulate ( $>0.7 \mu\text{m}$ ) Fe concentrations in glacial meltwater runoff from the southwest margin of the Greenland ice sheet and across the surrounding proglacial region. Seasonal variability was evident in both the dissolved and particulate Fe fractions, and is likely tied to the seasonal evolution of the subglacial drainage system. Two sequential leaches were used to dissolve the particulate (oxyhydr)oxide Fe, and on average, a large fraction (50%) of the particulate Fe in glacial runoff was labile. We report average discharge-weighted dissolved (dFe) and labile particulate (pFe<sub>l</sub>) Fe concentrations of  $3.7 \mu\text{M}$  and  $94.6 \mu\text{M}$ , respectively. Using these concentrations, we estimate an annual dFe flux from the Greenland ice sheet of  $\sim 1.5 \times 10^9$  moles/year (0.01 Tg/y), and annual pFe<sub>l</sub> of  $3.6 \times 10^{10}$  moles/year (0.20 Tg/y). Correcting for estuarine removal (90%), this yields a combined dissolved and labile particulate flux of  $\sim 3.8 \times 10^9$  moles/year (0.21 Tg/y). This flux estimate is of the same order of magnitude of the annual soluble Fe dust flux to the North Atlantic Ocean; thus, glacial meltwater runoff from the Greenland ice sheet may provide labile Fe capable of fueling primary productivity to downstream high latitude marine ecosystems during the summer meltseason.

## 1        **1. Introduction**

2  
3            Glacial runoff from the Greenland and Antarctic ice sheets provides a significant  
4 annual freshwater input to high latitude oceans, capable of delivering associated  
5 sediment, carbon and trace metals to coastal ecosystems (Bhatia et al., in prep; Raiswell  
6 et al., 2006; Statham et al., 2008). Primary productivity in large regions of the oceans is  
7 believed to be limited by a deficiency of biologically obligate micronutrients, such as iron  
8 (Fe) (e.g. Moore et al., 2001). The Southern Ocean is one of the most prominent  
9 examples of Fe limitation on phytoplankton primary production (Martin, 1990; Martin et  
10 al., 1990). Although Fe is not considered to be principally limiting in the North Atlantic  
11 or Arctic Ocean waters surrounding the Greenland ice sheet (GrIS) (Martin et al., 1993),  
12 previous work suggests that it may be a co-limiting nutrient in the northeast Atlantic  
13 (Blain et al., 2004; Mills et al., 2004). Other work suggests that aeolian Fe supply may  
14 limit the maximum potential of primary productivity in the North Atlantic at particular  
15 times of the year, such as during or after the spring phytoplankton bloom period (Moore  
16 et al., 2006; Nielsdottir et al., 2009). Recently, studies have illustrated that sediment at  
17 the base of calved ice-bergs (Raiswell et al., 2008; Raiswell et al., 2006) or associated  
18 with glacial runoff (Statham et al., 2008), and glacially-derived dust (Crusius et al., 2011)  
19 can supply bioavailable Fe to the coastal and open ocean, potentially fueling primary  
20 productivity at high latitudes. In Greenland, peak glacial runoff occurs at the height of the  
21 summer melt-season when primary production is limited by a depletion of upwelled  
22 nutrients in the preceding months during the spring bloom. Thus, glacial discharge from  
23 the Greenland ice sheet may annually supply critical Fe at a time when solar radiation is  
24 at its maximum, sustaining primary production during the summer (Statham et al., 2008).  
25 The supply of such glacially-sourced Fe may also be expected to increase as climatic  
26 warming intensifies melting of the GrIS.

27            The majority of meltwater discharged from the Greenland ice sheet first drains  
28 from the surface (supraglacial) to the ice sheet bed (subglacial), where it can interact with  
29 the basal sediment and bedrock material on various timescales before exiting at the base

30 of land- and marine-terminating outlet glaciers (Bartholomew et al., 2010; Das et al.,  
31 2008). Mechanical and chemical weathering beneath glaciers may produce  
32 nanoparticulate iron (oxyhydr)oxides from reactive iron-bearing phases (e.g. sulfides,  
33 carbonates, olivines, and pyroxenes) (Raiswell et al., 2006). Furthermore, subglacial  
34 microbial activity may yield secondary Fe minerals that are more labile than the original  
35 silicate rock matrix, and thus supply dissolved Fe to the runoff waters (Statham et al.,  
36 2008). Finally, the presence of organic carbon and anoxic regions at the bed may serve to  
37 maintain a portion of the comminuted Fe in solution. In this study we present dissolved  
38 (<0.2  $\mu\text{m}$ ) and particulate (>0.7  $\mu\text{m}$ ) Fe concentrations in glacial runoff draining the  
39 GrIS, as well as from the surrounding proglacial region. Our study site is typical of many  
40 land-terminating regions along the western margin of the ice sheet, in that there are  
41 several outlet glaciers whose runoff collects in a single large proglacial lake that then  
42 empties into a fjord. Thus, the effects of proglacial processing on the ultimate magnitude  
43 and type of glacial Fe exported is likely typical of other land-terminating Greenland  
44 glacial systems.

45

## 46 **2. Methods**

47

### 48 **2.1. Field Site Description**

49 The primary sampling region for this study was a three land-terminating outlet  
50 glaciers on the southwestern margin of the Greenland ice sheet ( $\sim 68^{\circ}02'34''\text{N}$ ,  
51  $50^{\circ}16'08''\text{W}$ ), approximately 125-km south of Jakobshavn Isbrae (Figure 1). This region  
52 is underlain by quartz diorite rocks of the Nagssugtdidian Orogenic Complex (K/Ar age:  
53 1790-1650 m.y.) (Escher, 1971). Runoff from the three outlet glaciers (named here, 'M',  
54 'N', and 'O') drained into a large ( $\sim 24 \text{ km}^2$ ) proglacial lake (Qasigiatsigit lake) before  
55 emptying into a fjord. The proglacial lake was ice-covered at the beginning of our  
56 sampling period in May and was ice-free in July. Sampling was conducted during a 2-  
57 week period in May (18 to 31) and  $\sim 1$ -week period in July (10 to 16) 2008. A higher  
58 resolution time-series of daily and sub-daily samples was taken at the 'N' glacier outflow,

59 and point samples were collected from the ‘M’ glacier outflow, ‘O’ glacier floodplain  
60 (~4.5 km downstream of stream outflow mouth), a stream (named ‘Waterfall stream’)  
61 draining the marginal ice area between ‘N’ and ‘O’ glaciers, the proglacial lake, and the  
62 lake outflow to the fjord. The outflow streams draining the ‘N’, ‘M’, and ‘O’ glaciers  
63 were all subglacially routed, exiting at the base of the glaciers. However, our field  
64 inspection of the ‘Waterfall stream’ did not reveal a subglacial water source, indicating  
65 that this stream may primarily consist of supraglacial marginal melt; this hypothesis is  
66 bolstered by the low electrical conductivity ( $4.6 \mu\text{S}/\text{cm}^3$ ) of this sample (Table 1). End-  
67 member samples were also collected from a meltwater pond on the surface of ‘N’ glacier  
68 (‘Supraglacial’), and from groundwater at the ‘M’ glacier floodplain and the bank of ‘N’  
69 glacier. Groundwater samples were taken using a stainless steel piezometer. Additional  
70 end-member samples from a fjord were collected from a secondary sampling region  
71 ( $\sim 68^\circ 55' 70''\text{N}$ ,  $50^\circ 17' 84''\text{W}$ ) along the western margin of the ice sheet, approximately  
72 100-km north of our primary sampling region. At this site, one sample was taken near the  
73 shore at the confluence of a glacial marginal runoff stream and the fjord water (named  
74 “glacial runoff in fjord”, and a second sample was taken offshore, with no visible glacial  
75 meltwater inputs (named “fjord water”). Both samples were taken at the surface.

76 Discharge measurements from ‘N’ glacier are reported in a previous study where  
77 we described the hydrology and subglacial drainage system evolution (Bhatia et al.,  
78 2011). Briefly, the subglacial drainage system beneath ‘N’ glacier seasonally evolves  
79 from a distributed system in early May where a large proportion ( $\geq 49\%$ ) of the runoff is  
80 from delayed flow waters stored at the bed, to a channelized drainage system in late May  
81 (12-36% delayed flow contribution) and July (5-17% delayed flow contribution), in  
82 which the runoff is comprised of increasing amounts of dilute ice-melt with limited basal  
83 contact (Bhatia et al., 2011). In the present study, discharge was also measured at the  
84 ‘Waterfall Stream’. The size of the catchment of the ‘Waterfall stream’ was estimated  
85 using the total measured discharge ( $\text{m}^3/46$  days) and the range of estimated melt-rates  
86 over this period at ‘N’ glacier (2.09 – 0.9  $\text{m}/46$  days), where discharge ( $\text{m}^3/46$  days) is  
87 equal to area ( $\text{m}^2$ ) x melt-rate ( $\text{m}/\text{y}$ ) (Bhatia et al., 2011). The range of estimated melt-

88 rates at 'N' glacier was determined as the product of the discharge at 'N' glacier and  
89 range of potential catchment areas using the catchment delineation method described in  
90 Bhatia et al. (2011). Using this same method we were able to determine a reasonable  
91 range of catchment areas for 'M' glacier, which we combined with the melt-rate from 'N'  
92 glacier (1.28 m/46 days) associated with our best catchment area estimate for 'N' glacier  
93 (5 km<sup>2</sup>) to determine potential discharge from 'M' glacier.

94

## 95 2.2. Sample Collection

96 All LDPE plastic-ware used in trace Fe sample collection and analysis was  
97 cleaned using the following procedure: MilliQ rinse followed by a 5-day soak in 0.1%  
98 citronox, 7x rinse with MilliQ, 5-day soak in 10% trace metal grade HCL, and a final 3x  
99 MilliQ rinse.

100 Samples were collected for both dissolved and particulate Fe analyses. For the  
101 dissolved samples, glacial meltwater was collected directly from the streams/ponds using  
102 new 60-mL plastic syringes. Sample water was filtered through 0.2 µm Sterivex filters  
103 (Millipore). Filters were rinsed with a full syringe volume prior to sample collection.  
104 Filtered samples were stored in trace metal clean 20-mL LDPE bottles spiked with ~40  
105 µL of 8N Optima trace metal grade nitric acid at room temperature until analysis.  
106 Particulate samples were collected on a pre-weighed, combusted 0.7 µm glass fiber filters  
107 (GFF) using a combusted glass filtration apparatus. The volume of runoff filtered through  
108 each GFF filter, and the after-filtration weight (filter + suspended sediment) was also  
109 recorded. A GFF filter was used because these samples were originally collected for  
110 particulate organic carbon analyses. However, the observed particulate Fe concentrations  
111 were substantially higher than a filter process blank (see below) such that we were able to  
112 utilize these samples for Fe analyses.

113

## 114 2.3. Leachable particulate Fe

115 The concentrations of the Fe (oxyhydr)oxides in the suspended sediments on a  
116 weighed fraction of the 0.7 µm GFF filter (particulate Fe) were determined using the

117 selective dissolution protocol described Charette et al. (2005), which was adopted from  
118 Hall et al. (1996). The only modification made to the protocol described in Charette et al.  
119 (2005) was that the leach and sediments were centrifuged post-leach in HDPE centrifuge  
120 tubes to ensure no sediment contamination during liquid sampling. Following Charette et  
121 al. (2005), we used the L3 leach (0.25M hydroxylamine hydrochloride 0.05M HCl acid)  
122 to extract “amorphous (oxy)hydroxides of iron”, followed by the L4 leach (1M  
123 hydroxylamine in 25% acetic acid) on the same filter fraction to extract “crystalline Fe  
124 (hydr)oxides”. In this study, we define the Fe released from the L3 leach as “labile Fe”,  
125 the Fe from the L4 leach as “crystalline Fe”, and the Fe released from the sum of the L3  
126 and L4 leaches as “total (oxyhydr)oxides”. The caveats cited by Charette et al. (2005)  
127 regarding the difficulty in quantifying the specific Fe fractions dissolved by each leach  
128 are applicable here. Thus, the type of Fe extracted in different dissolution leaches is likely  
129 quite broad and the results are method-dependent. To constrain our results, we also  
130 extracted the Fe from a marine sediment reference standard (MESS-3, National Research  
131 Council of Canada) using the L3 and L4 leaches. Among four replicates, our total %  
132 recovery for the MESS-3 standard ranged between 62-69% after the L4 leach. Aliquots of  
133 the L3 and L4 samples were diluted with 5% optima grade nitric acid (~1:20 to 1:600)  
134 prior to Fe concentration analyses.

135

136           2.4.   Dissolved and leachate particulate Fe ICP-MS analysis and blank  
137 corrections

138           Samples were measured for dissolved and particulate Fe using a Thermo-Electron  
139 Element 2 high-resolution single collector inductively coupled plasma mass spectrometry  
140 (ICP-MS) (Woods Hole Oceanographic Institution Plasma Mass Spectrometry facility),  
141 run in medium-resolution mode for <sup>56</sup>Fe. All solution preparations and  
142 standard/sample/blank dilutions for ICP-MS analysis were performed in a class 100  
143 trace-metal clean laboratory. Aliquots of the dissolved and particulate samples were  
144 diluted and spiked with an internal standard solution (5% optima grade nitric acid, 3 ppb  
145 <sup>115</sup>In). The same standard solution was used for all samples, blanks and standards. To

146 correct for instrument drift, the  $^{56}\text{Fe}$  count rate was normalized to  $\text{In}^{115}$  and the instrument  
147 response was quantified using a standard curve that matched the sample concentration  
148 range. Fe standards were prepared from a stock solution created from a certified 1000-  
149 ppm reference standard (Specpure, AlfaAeser). The Fe signal was corrected for the mean  
150 blank count rate. Final Fe concentrations for the dissolved samples were a product of the  
151 measured concentration from the ICP-MS analysis (g/g) and the dilution factor, and are  
152 reported in  $\mu\text{M}$ . Final Fe concentrations for the labile and crystalline Fe fractions were a  
153 product of the ICP-MS concentration (g/g), the dilution factor, and the weight of the  
154 L3/L4 solution divided by the proportion each analyzed filter fraction represented of the  
155 whole filter. The volume of water filtered through each GFF was then used to report the  
156 final particulate concentrations in  $\mu\text{M}$ . It should be noted that this approach of scaling the  
157 filter fraction ICP-MS concentration up to the whole filter assumes an even distribution  
158 of sediment across the filter.

159         Sample concentrations were corrected for possible blank contributions from  
160 materials and filters by measuring process blanks. For the dissolved samples, the average  
161 Fe concentration of two MilliQ-water samples ( $0.0155 \mu\text{M}$ ) processed in the laboratory  
162 analogously to the field samples was subtracted from the final measured sample Fe  
163 concentrations. Three additional process blanks were processed in the laboratory by  
164 filtering MilliQ-water with syringes and Sterivex filters similar to those used in the field.  
165 However, the Fe concentrations in these laboratory process blanks were extremely low,  
166 less than the mean  $\text{HNO}_3\text{-In}^{115}$  blank run on the ICP-MS. For the particulate samples,  
167 fractions of six pre-weighed, combusted GFF's prepared identically to those utilized for  
168 the samples were processed using the sequential L3 and L4 leaches. The average total  
169 GFF L3/L4 leach blank (L3:  $5.06 \times 10^{-6}$  g; L4:  $1.31 \times 10^{-5}$  g) was then multiplied by the  
170 sample filter fraction and subtracted from the measured Fe concentration of the filter  
171 fraction for each leach. Generally, the GFF leach blanks were low relative to the amount  
172 of Fe from the sample, approximately 1.7% on average of the total (oxyhydr)oxide Fe for  
173 both the L3 and L4 leach procedures.

174



### 3. Results

The dissolved and particulate Fe concentrations for the end-member samples (supraglacial ice, groundwater), glacial runoff samples ('N', 'M', and 'O' glacier streams, Waterfall stream), proglacial samples (Proglacial lake, Lake outflow), and fjord samples are shown in Figure 1. The corresponding ranges of dissolved and particulate Fe concentrations are shown in Table 1. The highest dissolved Fe (dFe) concentrations were observed in groundwater collected along the bank of 'N' glacier outflow stream (1.65 – 431  $\mu\text{M}$ ). However, the range of concentrations within the groundwater collected was variable, as a sample collected from the 'M' glacier floodplain was quite low in dFe (0.3  $\mu\text{M}$ ). The dFe concentrations from the mouth of 'N' (mean = 3.7  $\mu\text{M}$ ) and 'M' (3.8  $\mu\text{M}$ ) glaciers were similar, and much larger than the dFe concentration in the supraglacial ice (0.11  $\mu\text{M}$ ) and in the Waterfall Stream (0.19  $\mu\text{M}$ ). The range of dFe concentrations observed in the 'N' glacier runoff, where we had a greater seasonal coverage, encapsulated the range found in the 'M' glacier runoff. In the proglacial area the dFe concentrations steadily increased along a transect from the ice margin 'M' glacier to the proglacial lake outflow in May (Figure 2). However, it is important to emphasize that this trend was limited to our observations along a single transect from 'M' glacier to the lake outflow. Indeed, the highest dFe concentration measured in the 'N' glacier runoff (9.32  $\mu\text{M}$ ) is equivalent to the concentrations in the 'O' glacier floodplain. The fjord samples collected at our second field site showed that the glacial runoff in the fjord had dFe concentrations (2.3 – 2.9  $\mu\text{M}$ ) within the range of that observed in the 'N' glacier runoff, but the fjord water itself had a substantially lower dFe concentration (0.04  $\mu\text{M}$ ).

The particulate Fe (pFe) concentrations were higher for each sample type compared to the dFe concentrations (Figure 1 and Table 1). The highest total (oxyhydr)oxide pFe concentrations were observed in the 'N' glacier runoff and the proglacial lake. Interestingly, both the 'M' and 'O' glacier runoff pFe concentrations were lower than the observed range for the 'N' glacier runoff. The fjord water had the lowest total (oxyhydr)oxide Fe concentration. The percent contribution from the 'labile

204 Fe' and 'crystalline Fe' fractions to the total (oxyhydr)oxides extracted is also shown in  
205 Table 1. The %labile and %crystalline contributions in the 'N', 'M', and 'O' glacier  
206 runoff is generally split evenly between the two fractions, with some exceptions among  
207 the 'N' glacier samples. The proglacial lake and lake outflow total (oxyhydr)oxide Fe  
208 also has approximately equal contributions from the labile and crystalline fractions.  
209 However, the supraglacial sample had a much greater contribution from the crystalline  
210 fraction (84.6%) compared to the labile fraction (15.4%). Conversely, in the fjord sample,  
211 all of the leachable pFe was extracted in the labile fraction. The Fe concentration and %  
212 Fe (g/g) extracted in each particulate fraction is presented in Table 2. Generally, the  
213 average % Fe is higher in the crystalline fraction compared to the labile fraction for all  
214 the sample types (excluding the fjord sample). The highest % Fe values were observed in  
215 the proglacial lake and lake outflow, and the lowest values were observed in the fjord  
216 sample.

217 A higher resolution time-series at 'N' glacier revealed seasonal variability in both  
218 the dFe and pFe concentrations (Figure 3). Generally, the four May runoff samples had  
219 higher dFe concentrations (3.21 – 9.32  $\mu\text{M}$ ) compared to the July runoff (2.20 – 4.27  
220  $\mu\text{M}$ ) (Figure 3c). The dFe concentrations generally corresponded with previously  
221 reported dissolved organic carbon (DOC) concentrations, except for the late May runoff  
222 waters, which had lower DOC concentrations but high dFe concentrations. The pFe  
223 concentrations were more variable; the lowest discharge (day 142) coincided with one of  
224 the lowest pFe concentrations, but the later May samples (days 146 – 153) generally had  
225 higher pFe concentrations than the July samples (Figure 3e). The total suspended  
226 sediment (TSS) in the N glacier runoff waters sampled is shown in Figure 3d. Generally,  
227 the pFe concentrations correlated with the TSS; however, the highest pFe concentrations  
228 were observed in late May, whereas the highest TSS concentrations occurred in the July  
229 runoff waters. The dissolved and particulate Fe concentrations generally varied in tandem  
230 (i.e. higher dFe correlated with higher pFe), with the exception of a sample taken on the  
231 lowest discharge day, when the dFe (7.06  $\mu\text{M}$ ) was among the highest recorded for the  
232 'N' outflow waters, and the pFe was the lowest. The flux of both dissolved (Figure 4) and

233 particulate (Figure 4) Fe was calculated on days with complementary discharge and  
234 concentration data. Generally, both the dFe and pFe fluxes were driven by the discharge  
235 rather than by the Fe concentration. Finally, estimates for the dissolved and labile  
236 particulate Fe fluxes for subglacially-derived runoff streams exiting ‘M’ and ‘N’ glacier,  
237 and the supraglacially-sourced Waterfall stream are presented in Table 3. Total annual  
238 dissolved and labile particulate (pFe<sub>l</sub>) Fe fluxes were calculated for the Greenland ice  
239 sheet using the discharge-weighted average dFe and pFe<sub>l</sub> concentrations in the ‘N’ glacier  
240 runoff (Table 3).

241

#### 242 **4. Discussion**

243

##### 244 4.1. Seasonal dissolved Fe variability in glacial meltwater runoff

245 The seasonal discharge-weighted average dFe concentration for ‘N’ glacier runoff was  
246 3.7  $\mu\text{M}$ , similar to the average dFe concentration from the adjacent, larger ‘M’ glacier  
247 (3.8  $\mu\text{M}$ ). This value is higher than that previously reported for Greenland glacial  
248 discharge (dFe ( $<0.4 \mu\text{m}$ ) = 54 nM) (Statham et al., 2008), Antarctic basal ice (dFe ( $<0.2$   
249  $\mu\text{m}$ ) = 0.09 – 2.0 nM) (Raiswell et al., 2008), and average Arctic river dFe concentrations  
250 (Ob, Yenisey rivers (dFe $<0.4 \mu\text{m}$ ): 251 – 654 nM) (Dai, 1995). The subglacially-routed  
251 ‘N’ and ‘M’ glacial runoff dFe concentrations were much higher than the dFe in the  
252 supraglacial ice and Waterfall stream (comprised primarily of supraglacially-routed  
253 meltwater), thus indicating that passage through the subglacial environment dramatically  
254 alters the dFe signature of glacial runoff relative to its origin as dilute ice-melt. There are  
255 several potential controls on the dFe concentrations observed in the ‘N’ glacier runoff.  
256 First, the high May dFe concentrations may be a result of the higher dissolved organic  
257 carbon (DOC) concentrations observed in these waters (Figure 3b), which can complex  
258 both ferrous (Fe<sup>2+</sup>) and ferric (Fe<sup>3+</sup>) iron to keep it in solution (Kuma and Nishioka, 1996;  
259 Rue, 1995; Rue and Bruland, 1997). Indeed, the highest ‘N’ glacier runoff dFe  
260 concentration was on the lowest discharge day when DOC was extremely high ( $\sim 342$   
261  $\mu\text{M}$ ). Alternatively, in our previous work at ‘N’ glacier, we show that the subglacial

262 drainage system likely accesses hypoxic or anoxic regions of the bed in the early season,  
263 particularly on the lowest discharge day (Bhatia et al., in prep); under such conditions  
264  $\text{Fe}^{2+}$  is thermodynamically stable and would be transported passively into the glacier  
265 runoff (Achterberg et al., 2001). Either process or a combination of the two could result  
266 in the comparatively higher dFe concentrations in May. Finally, it is important to note  
267 that our dissolved fraction may include colloidal nanoparticles, and thus, may not be truly  
268 “dissolved”(Raiswell et al., 2006). Previous examination of fine-grained sediment  
269 fractions from alpine, Arctic, and Antarctic glaciers revealed the universal presence of  
270 iron (oxyhydr)oxide nanoparticles . These nanoparticles were generally less than 10 nm  
271 in diameter, and could be present as isolated grains or aggregates and be separated from  
272 or attached to (alumino)silicate grains (Raiswell et al., 2006). The inclusion of these  
273 nanoparticles in the dissolved load may explain the comparatively high ( $\mu\text{M}$  range) July  
274 dFe concentrations. It is conceivable that this colloidal fraction is also bioavailable  
275 (Chen, 2001; Raiswell et al., 2006; Wu, 2001), but such a discussion is beyond the scope  
276 of this paper.

277

#### 278 4.2. Particulate Fe export in glacial meltwater runoff

279 The leachable pFe fraction lends insight into the Fe content of the underlying bedrock  
280 and sediment from which the dFe load in the ‘N’ glacial runoff is ultimately derived. The  
281 pFe concentrations in the ‘N’ glacier runoff were well correlated with the TSS  
282 concentrations, indicating that the high pFe and dFe concentrations observed may entirely  
283 be a function of TSS. However, the fact that the highest pFe concentrations were  
284 observed in late May when TSS was not as high as in July, hints that other hydrological  
285 or chemical controls on the observed Fe concentrations may also be present. Within the  
286 pFe fraction, the labile Fe component has the most implications for downstream Fe  
287 fertilization as, in this study, it best approximates the abundance and export of  
288 bioavailable Fe. The % labile Fe (g/g) in the ‘N’ glacial runoff (on average  $\sim 1.5\%$ ) is  
289 below the average Fe abundance in continental crust ( $\sim 5.6\%$ ) (Taylor, 1964), but larger  
290 than the percent of highly reactive Fe (0.25%) measured by Raiswell et al., (2006) in

291 subglacial sediments (<2  $\mu\text{m}$ ) beneath Glacier d'Argentiere (French Alps), which has a  
292 similar granite/gneiss bedrock lithology to that beneath the GrIS. In this study Raiswell et  
293 al., (2006) used a buffered sodium dithionite solution to extract their highly reactive Fe  
294 ( $\text{Fe}_{\text{HR}}$ ) fraction, equivalent to the leach used in this study to dissolve the labile particulate  
295 fraction. However, using a subsequent HF-HClO<sub>4</sub>-HNO<sub>3</sub> leach Raiswell et al., (2006)  
296 was able to measure a total %Fe of 2.82% from the Glacier d'Argentiere subglacial  
297 sediments, indicating that most of the Fe was likely comprised of non-labile aluminosilicate  
298 Fe. Conversely, suspended sediments from meltwater runoff at  
299 Finsterwalderbreen glacier (Svalbard) revealed that the majority (70%) of the Fe was  
300 bioavailable (5.51%  $\text{Fe}_{\text{HR}}$ ). However, Finsterwalderbreen is unique in that its bedrock  
301 lithology is comprised of schists, siltstones, sandstones, and shales. The results from the  
302 'N' glacier runoff are distinct in that they lie between the values measured at Glacier  
303 d'Argentiere and Finsterwalderbreen, with on average 50% of the total Fe being labile.  
304 The fact that the pFe in the supraglacial ice was primarily comprised of crystalline Fe  
305 (85% (hydr)oxide contribution), indicates that the labile pFe fraction in the 'N' glacier  
306 runoff likely originates from the subglacial environment, instead of from wind-deposited  
307 sediment on the glacier surface. Potential subglacial sources of labile pFe could be a by-  
308 product of mechanical and/or chemical weathering, or subglacial microbial activities  
309 (Raiswell et al., 2006; Sharp et al., 1999; Tranter et al., 2002).

310

#### 311 4.3. Proglacial processing of glacially-derived Fe and export to the coastal 312 ocean

313 Based on results from the point samples collected in May, we propose that proglacial  
314 processing adds dissolved Fe to runoff originally exported at the glacier snout. In  
315 particular, processes in the proglacial lake increase dFe, while pFe decreases along the  
316 lake length, implying the dissolved and particulate Fe pools are decoupled in this lake  
317 and likely controlled by separate mechanisms. The lake dFe concentration may be  
318 elevated in May because regions of the lake may be driven to anoxia beneath the seasonal  
319 ice cover, serving to keep  $\text{Fe}^{2+}$  in solution. Additionally, organic carbon concentrations

320 were very high ( $\sim 614 \mu\text{M}$ ) in the lake in May (Figure 2), and thus, Fe stabilization with  
321 organic ligands may also contribute to the high dFe concentrations (Rue and Bruland,  
322 1997). Alternatively, the lower suspended sediment (oxyhydr)oxide concentrations in the  
323 lake outflow may also be due to larger particles setting out along the length of the  
324 proglacial lake. Since we do not have a sample from the fjord at this site it is difficult to  
325 speculate what portion of the Fe load ultimately is exported to the coastal ocean. The  
326 fjord samples from our secondary site hint that a significant fraction of both the dissolved  
327 and particulate pools may be removed in the near coastal ocean (Boyle et al., 1977). In  
328 this way, glacial systems may be akin to river systems, where river Fe is generally  
329 depleted in estuaries prior to their entry into the marine environment via removal of the  
330 colloidal fraction by aggregation and deposition (Boyle et al., 1977; Raiswell et al., 2006;  
331 Wen et al., 1999). Additional transects from the ice sheet terminus to the coastal ocean  
332 are needed to confirm this hypothesis, and discover the mechanisms by which glacial-  
333 derived Fe is removed. However, the dissolved (40 nM) Fe concentration in the fjord  
334 water is similar to Arctic river (e.g. Ob, Yenisey) estuary systems (Dai, 1995), is orders  
335 of magnitude higher than the average dissolved Fe concentration in the ocean (0.7 nM)  
336 (Sarmiento and Gruber, 2006), and the particulate Fe exported is comprised entirely of  
337 labile Fe. These observations hint that there is potential for the labile Fe flux to be  
338 enhanced in the proglacial region prior to coastal ocean export, and that though a large  
339 proportion of the dissolved and particulate Fe load is removed, a comparatively  
340 significant fraction may still be exported to the coastal ocean.

341

#### 342 4.4. Fe export from the Greenland ice sheet and impact on primary 343 productivity

344 Using the discharge-weighted dissolved and labile particulate Fe ( $\text{pFe}_l$ ) concentrations  
345 from 'N' glacier and the mean (1995-2007) GrIS estimated annual meltwater runoff of  
346  $397 \text{ km}^3/\text{y}$  (Mernild et al., 2009) we estimate annual dFe and  $\text{pFe}_l$  fluxes for the entire  
347 GrIS to be  $1.5 \times 10^9$  moles/year and  $3.6 \times 10^{10}$  moles/y, respectively. Previously,  
348 Raiswell et al., (2006) hypothesized that the labile Fe in glacial meltwaters would likely

349 be removed during estuarine transport, similar to riverine Fe. Thus, if we assume an  
350 estuarine removal factor of 90% (Boyle et al., 1977), our dFe flux equates to 0.01 Tg/y of  
351 dissolved Fe, an order of magnitude lower than the minimum estimated range for the  
352 annual global riverine dFe flux (dFe (<0.45  $\mu\text{m}$ ) 0.2 – 2.0 Tg/y) (de Baar and de Jong,  
353 2001; Haese, 2000; Raiswell et al., 2006). Comparatively, this estuarine-corrected GrIS  
354 annual dFe flux ( $1.5 \times 10^8$  moles/year) is higher than that estimated by Statham et al.,  
355 (2008) using the same annual discharge (dFe (<0.4  $\mu\text{m}$ )  $\sim 2.1 \times 10^7$  moles/y), due to the  
356 higher dFe concentrations measured in this study. The combined, estuarine-corrected dFe  
357 and pFe<sub>i</sub> is  $\sim 3.8 \times 10^9$  moles/year (0.21 Tg/y). The global Fe flux from atmospheric dust  
358 to the oceans is  $\sim 16$  Tg/y, and the North Atlantic receives  $\sim 43\%$  of this annual flux,  
359 which represents the primary bioavailable Fe input this ocean (Jickells et al., 2005).  
360 Assuming a range of solubility proportions from 1 to 10% (Fan et al., 2006; Sarmiento  
361 and Gruber, 2006), this equates to an annual soluble Fe dust flux to the North Atlantic  
362 between 0.07-0.7 Tg/y. Thus, our dissolved and particulate labile Fe flux from the GrIS is  
363 of the same order of magnitude as the soluble Fe dust estimate, indicating that glacially-  
364 sourced Fe is capable of providing a quantitatively significant portion of labile dissolved  
365 and particulate Fe to surrounding coastal oceans. Indeed, a recent study analyzing spring  
366 phytoplankton bloom dynamics from 1998-2008 using SeaWiFS satellite ocean  
367 chlorophyll data noted a strong correlation between peak bloom magnitude in the north  
368 Labrador Sea, off the coast of west Greenland, and GrIS runoff ( $r^2 = 0.81$ ) (Frajka-  
369 Williams and Rhines, 2010). This observation highlights the potential for labile Fe in  
370 GrIS runoff to stimulate primary productivity in the North Atlantic.

371

## 372 **5. Conclusions**

373 In this study, we examined dissolved (<0.2  $\mu\text{m}$ ) and particulate (>0.7  $\mu\text{m}$ ) Fe in glacial  
374 runoff from the GrIS. We find high (micro-molar) Fe concentrations in the dissolved  
375 fraction that may be caused by: (1) complexing of Fe with DOC, allowing Fe to remain in  
376 solution, (2) colloidal nanoparticles present in the defined dissolved fraction, and (3)  
377 anoxic regions at the glacier bed, allowing Fe<sup>2+</sup> to be thermodynamically stable.

378 Furthermore, results from this study hint that reactions in the proglacial region may  
379 enhance dissolved Fe concentrations prior to export to the marine environment. We  
380 estimate annual dissolved and labile particulate fluxes from the GrIS to be equivalent to  
381 that of the annual soluble Fe dust flux to the North Atlantic Ocean, indicating that  
382 glacially-sourced Fe may provide a quantitatively significant flux of Fe to surrounding  
383 coastal oceans.

384

385 *Acknowledgments.* This research was supported the: the WHOI Clark Arctic Research  
386 Initiative (EBK, SBD, MAC), the National Science Foundation (MAC), the WHOI  
387 Climate Change Institute (MPB), and a Horton Hydrology Grant (MPB). I am grateful to  
388 Scot Birdwhistell for assistance with the ICP-MS analyses, to Phoebe Lam, Dan  
389 Ohnemus, and Ben Gready for helpful conversations, and to Ben Gready, Alison  
390 Criscitiello, and Matt Evans for their valuable assistance in the field.

391



392 **References**

393

394

395 Achterberg, E.P., Holland, T.W., Bowie, A.R., Mantoura, R.F.C., Worsfold, P.J., 2001.  
396 Determination of iron in seawater. *Analytica Chimica Acta* 442, 1-14.

397

398 Bartholomew, I., Nienow, P., Mair, D., Hubbard, A., King, M.A., Sole, A., 2010.

399 Seasonal evolution of subglacial drainage and acceleration in a Greenland outlet  
400 glacier. *Nat. Geosci.* 3, 408-411.

401

402 Bhatia, M., Das, S.B., Kujawinski, E.B., Henderson, P., Burke, A., Charette, M.A., 2011.

403 Seasonal evolution of water contributions to discharge from a Greenland outlet  
404 glacier: Insight from a new isotope-mixing model *J. Glaciol.* 57, 929-941.

405

406 Bhatia, M., Das, S.B., Xu, X.L., Charette, M., Kujawinski, E.B., in prep. Organic carbon  
407 export from the Greenland ice sheet

408

409 Blain, S., Guieu, C., Claustre, H., Leblanc, K., 2004. Availability of iron and major  
410 nutrients for phytoplankton in the northeast Atlantic Ocean. *Limnol. Oceanogr.*

411

412 Boyle, E.A., Edmond, J.M., Sholkovitz, E.R., 1977. The mechanism of iron removal in  
413 estuaries. *Geochim. Cosmochim. Acta* 41, 1313-1324.

414

415 Charette, M.A., Sholkovitz, E.R., Hansel, C.M., 2005. Trace element cycling in a  
416 subterranean estuary: Part 1. Geochemistry of the permeable sediments. *Geochim.*  
417 *Cosmochim. Acta* 69, 2095-2109.

418

419 Chen, M., 2001. Bioavailability of natural colloid-bound iron to marine plankton:  
420 Influences of colloidal size and aging. *Limnol. Oceanogr.*

421

422 Crusius, J., Schroth, A.W., Gasso, S., Moy, C.M., Levy, R.C., Gatica, M., 2011. Glacial  
423 flour dust storms in the Gulf of Alaska: Hydrologic and meteorological controls  
424 and their importance as a source of bioavailable iron. *Geophys. Res. Lett.* 38,  
425 L06602.

426

427 Dai, M.H., 1995. First data on trace metal level and behaviour in two major Arctic river-  
428 estuarine systems (Ob and Yenisey) and in the adjacent Kara Sea, Russia. *Earth*  
429 *Planet. Sci. Lett.*

430

431 Das, S.B., Joughin, I., Behn, M.D., Howat, I.M., King, M.A., Lizarralde, D., Bhatia,  
432 M.P., 2008. Fracture propagation to the base of the Greenland Ice Sheet during  
433 supraglacial lake drainage. *Science* 320, 778-781.

- 434 de Baar, H.J.W., de Jong, J.T.M., 2001. Distribution, sources and sinks of iron in  
435 seawater, in: Turner, D.R., Hunter, K.A. (Eds.), *The Biogeochemistry of Iron in*  
436 *Seawater*. Wiley, New York, pp. 122-153.  
437
- 438 Escher, A., 1971. Map Sheet no. 3 Sondre Stromfjord - Nugssu aq Geological Maps of  
439 Greenland 1:500,000. Geological Survey of Denmark and Greenland (GEUS),  
440 Copenhagen.  
441
- 442 Fan, S.M., Moxim, W.J., Levy, H., 2006. Aeolian input of bioavailable iron to the ocean.  
443 *Geophys. Res. Lett.* 33.  
444
- 445 Frajka-Williams, E., Rhines, P.B., 2010. Physical controls and interannual variability of  
446 the Labrador Sea spring phytoplankton bloom in distinct regions. *Deep-Sea*  
447 *Research Part I-Oceanographic Research Papers* 57, 541-552.  
448
- 449 Haese, R.R., 2000. The reactivity of iron, in: Zabel, M. (Ed.), *Marine Geochemistry*.  
450 Springer-Verlag, Berlin, pp. 233-261.  
451
- 452 Hall, G.E.M., Vaive, J.E., Beer, R., Hoashi, M., 1996. Selective leaches revisited, with  
453 emphasis on the amorphous Fe oxyhydroxide phase extraction. *Journal of*  
454 *Geochemical Exploration* 56, 59-78.  
455
- 456 Jickells, T.D., An, Z.S., Andersen, K.K., Baker, A.R., Bergametti, G., Brooks, N., Cao,  
457 J.J., Boyd, P.W., Duce, R.A., Hunter, K.A., Kawahata, H., Kubilay, N., laRoche,  
458 J., Liss, P.S., Mahowald, N., Prospero, J.M., Ridgwell, A.J., Tegen, I., Torres, R.,  
459 2005. Global iron connections between desert dust, ocean biogeochemistry, and  
460 climate. *Science* 308, 67-71.  
461
- 462 Kuma, K., Nishioka, J., 1996. Controls on iron (III) hydroxide solubility in seawater: The  
463 influence of pH and natural organic chelators. *Limnol. Oceanogr.*  
464
- 465 Martin, J.H., 1990. Glacial-interglacial CO<sub>2</sub> change: The iron hypothesis.  
466 *Paleoceanography*.  
467
- 468 Martin, J.H., Fitzwater, S.E., Michael Gordon, R., Hunter, C.N., Tanner, S.J., 1993. Iron,  
469 primary production and carbon-nitrogen flux studies during the JGOFS North  
470 Atlantic bloom experiment. *Deep Sea Research Part II: Topical Studies in*  
471 *Oceanography* 40, 115-134.  
472
- 473 Martin, J.H., Gordon, R.M., Fitzwater, S.E., 1990. Iron in Antarctic waters. *Nature* 345,  
474 156-158.  
475

476 Mernild, S.H., Liston, G.E., Hiemstra, C.A., Steffen, K., Hanna, E., Christensen, J.H.,  
477 2009. Greenland Ice Sheet surface mass-balance modelling and freshwater flux  
478 for 2007, and in a 1995-2007 perspective. *Hydrol. Processes* 23, 2470-2484.  
479

480 Mills, M.M., Ridame, C., Davey, M., La Roche, J., Geider, R.J., 2004. Iron and  
481 phosphorus co-limit nitrogen fixation in the eastern tropical North Atlantic.  
482 *Nature* 429, 292-294.  
483

484 Moore, C.M., Mills, M.M., Milne, A., Langlois, R., Achterberg, E.P., Lochte, K., Geider,  
485 R.J., La Roche, J., 2006. Iron limits primary productivity during spring bloom  
486 development in the central North Atlantic. *Global Change Biol.* 12, 626-634.  
487

488 Moore, J.K., Doney, S.C., Glover, D.M., Fung, I.Y., 2001. Iron cycling and nutrient-  
489 limitation patterns in surface waters of the World Ocean. *Deep Sea Research Part*  
490 *II: Topical Studies in Oceanography* 49, 463-507.  
491

492 Nielsdottir, M.C., Moore, C.M., Sanders, R., Hinz, D.J., Achterberg, E.P., 2009. Iron  
493 limitation of the postbloom phytoplankton communities in the Iceland Basin.  
494 *Global Biogeochem. Cycles* 23, GB3001.  
495

496 Raiswell, R., Benning, L.G., Tranter, M., Tulaczyk, S., 2008. Bioavailable iron in the  
497 Southern Ocean: the significance of the iceberg conveyor belt. *Geochem. Trans.*  
498 9.  
499

500 Raiswell, R., Tranter, M., Benning, L.G., Siegert, M., De'ath, R., Huybrechts, P., Payne,  
501 T., 2006. Contributions from glacially derived sediment to the global iron  
502 (oxyhydr)oxide cycle: Implications for iron delivery to the oceans. *Geochim.*  
503 *Cosmochim. Acta* 70, 2765-2780.  
504

505 Rue, E.L., 1995. Complexation of iron (III) by natural organic ligands in the Central  
506 North Pacific as determined by a new competitive ligand equilibration/adsorptive  
507 cathodic stripping method. *Mar. Chem.*, 117-138.  
508

509 Rue, E.L., Bruland, K.W., 1997. The role of organic complexation on ambient iron  
510 chemistry in the equatorial Pacific Ocean and the response of a mesoscale iron  
511 addition experiment. *Limnol. Oceanogr.* 42, 901-910.  
512

513 Sarmiento, J., Gruber, N., 2006. *Ocean Biogeochemical Dynamics*. Princeton University  
514 Press, Princeton, NJ.  
515

516 Sharp, M., Parkes, J., Cragg, B., Fairchild, I.J., Lamb, H., Tranter, M., 1999. Widespread  
517 bacterial populations at glacier beds and their relationship to rock weathering and  
518 carbon cycling. *Geology* 27, 107-110.

519 Statham, P.J., Skidmore, M., Tranter, M., 2008. Inputs of glacially derived dissolved and  
520 colloidal iron to the coastal ocean and implications for primary productivity.  
521 *Global Biogeochem. Cycles* 22.  
522

523 Taylor, S.R., 1964. Abundance of chemical elements in the continental crust: a new table.  
524 *Geochim. Cosmochim. Acta*.  
525

526 Tranter, M., Sharp, M.J., Lamb, H.R., Brown, G.H., Hubbard, B.P., Willis, I.C., 2002.  
527 Geochemical weathering at the bed of Haut Glacier d'Arolla, Switzerland - a new  
528 model. *Hydrol. Processes* 16, 959-993.  
529

530 Wen, L.-S., Santschi, P., Gill, G., Paternostro, C., 1999. Estuarine trace metal  
531 distributions in Galveston Bay: importance of colloidal forms in the speciation of  
532 the dissolved phase. *Mar. Chem.* 63, 185-212.  
533

534 Wu, J., 2001. Soluble and Colloidal Iron in the Oligotrophic North Atlantic and North  
535 Pacific. *Science* 293, 847-849.  
536  
537

538 **Tables**

539

540

541 **Table 1.** Ranges of dissolved (<0.2 µm) and particulate (>0.70 µm) concentrations  
 542 measured in different samples from the Greenland ice sheet margin. The range of %  
 543 contributions from labile and crystalline fractions to the total (oxyhydr)oxide Fe is shown  
 544 for all the samples, and the average % labile and crystalline contribution is also shown for  
 545 the 'N' glacier runoff. The fjord samples (\*) are from the secondary (northern) field site.  
 546 The number of samples for each sample type (dissolved (d) and particulate (p)) is shown  
 547 in the "n" column.  
 548

Sample Type	n <sub>d</sub>	Dissolved Fe range (µM)	n <sub>p</sub>	Particulate Fe range (µM)		
				Total (oxyhydr)oxide Fe	% labile	% crystalline
<b>End-member samples</b>						
Supraglacial Ice	1	0.11	1	27.61	15.4	84.6
Groundwater	6	0.30 – 431.2	0	--	--	--
<b>Runoff samples</b>						
'N' glacier runoff	13	2.2 – 9.3	17	50.39 – 321.58	35.9 – 75.3 mean = 49.9	20.7 – 64.1 mean = 50.1
'M' glacier runoff	2	3.5 – 4.1	1	25.53	49.1	50.1
'O' glacier runoff	1	10.0	1	29.98	46.1	53.1
Waterfall stream	1	0.19	0	--	--	--
<b>Proglacial samples</b>						
Proglacial Lake	2	4.8 – 5.2	1	278.11	44.5	55.5
Lake Outflow	1	17.4	1	45.37	48.7	51.3
<b>Fjord samples</b>						
Glacial runoff in fjord	2	2.3 – 2.9	0	--	--	--
Fjord water	1	0.04	1	0.129	100	0

549

550

551 **Table 2.** Concentrations ( $\mu\text{M}$ ) and % Fe (g/g) in different particulate ( $>0.70 \mu\text{m}$ ) samples  
 552 from the Greenland ice sheet margin for the labile and crystalline fractions. For the  
 553 supraglacial and 'O' glacier runoff samples, it was not possible to accurately determine a  
 554 weight for the total sediment on the filter. The crystalline Fe concentration of the Fjord  
 555 sample was below the detection limit (BDL) of the mean process blank.  
 556

Sample Type	Mean labile concentration ( $\mu\text{M}$ )	Mean crystalline concentration ( $\mu\text{M}$ )	Mean labile % Fe (g/g)	Mean crystalline % Fe (g/g)
<b>End-member samples</b>				
Supraglacial Ice	4.2429	23.3667	--	--
<b>Runoff samples</b>				
'N' glacier runoff	90.5155 $\pm$ 31.2864	100.4787 $\pm$ 48.9178	1.44 $\pm$ 0.55	1.55 $\pm$ 0.80
'M' glacier runoff	12.5226	13.0074	0.30	0.35
'O' glacier runoff	13.8272	16.1523	--	--
<b>Proglacial samples</b>				
Proglacial Lake	122.0833	156.0292	2.09	2.71
Lake Outflow	22.0821	23.2849	2.66	2.80
<b>Fjord samples</b>				
Fjord water	0.1290	BDL	0.03	BDL

557  
 558  
 559  
 560  
 561  
 562  
 563  
 564  
 565  
 566  
 567  
 568

**Table 3.** Dissolved (dFe) and particulate (pFe) Fe fluxes from Greenland glacial runoff streams sampled in this study from May 31 to July 16, 2008 (season), and estimated annual fluxes for the entire Greenland ice sheet. The Fe flux was calculated using the discharge-weighted average dissolved ( $3.7 \mu\text{M}$ ) and particulate labile fraction ( $91.8 \mu\text{M}$ ) Fe concentrations for 'N' Glacier, and the average dissolved and particulate Fe concentrations for 'M' Glacier (dissolved:  $3.8 \mu\text{M}$ ; particulate labile fraction:  $12.5 \mu\text{M}$ ) and the Waterfall Stream (dissolved:  $0.2 \mu\text{M}$ ). Values denoted by \* were estimated, see methods for details. The annual Greenland ice sheet dFe and pFe fluxes were estimated using the 'N' glacier Fe values.

Runoff Stream	~ Catchment Area ( $\text{km}^2$ )	Total Discharge ( $\text{m}^3/\text{season}$ )	dFe flux (moles/season)	pFe labile flux (moles/season)
'N' Glacier	5	$6.4 \times 10^6$	$2.4 \times 10^4$	$5.9 \times 10^5$
'M' Glacier	20 – 24*	$2.3 - 2.8 \times 10^7$ *	$8.7 - 10 \times 10^4$	$2.9 - 3.5 \times 10^5$
Waterfall Stream	14 – 32*	$3.2 \times 10^7$	$6.2 \times 10^3$	--
		<b>(<math>\text{m}^3/\text{year}</math>)</b>	<b>(moles/y)</b>	<b>(moles/y)</b>
Greenland Ice Sheet	$1.7 \times 10^6$	$523 \times 10^9$	$1.9 \times 10^9$	$4.8 \times 10^{10}$

569  
 570

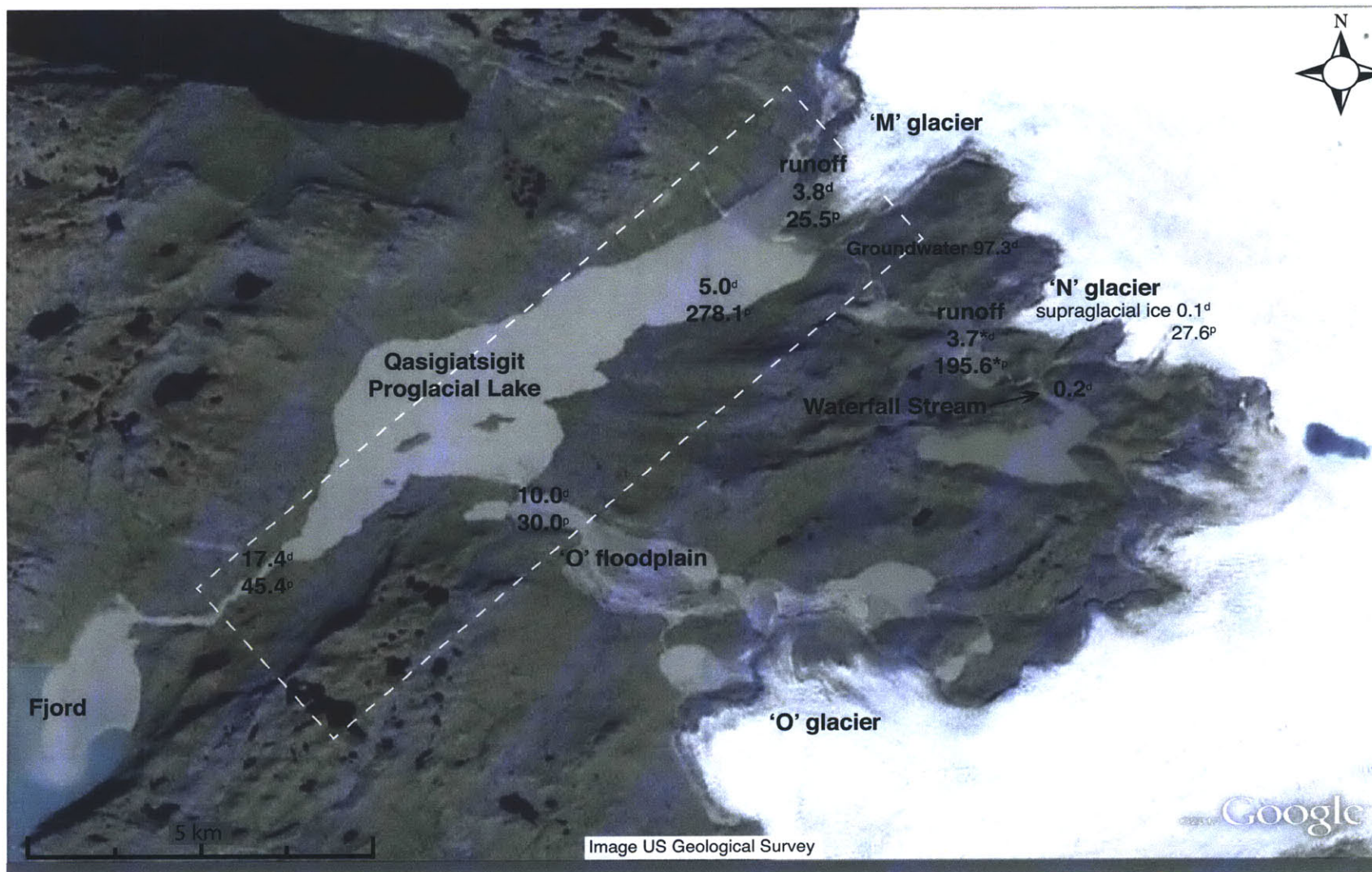


**Figure 1.** Map of sample locations and average dissolved (denoted by d superscript) (<0.2 μm) and particulate (oxyhydr)oxide (denoted by p superscript) (>0.70 μm) Fe concentrations in μM. The 'N' glacier runoff values (denoted by \*) are discharge-weighted average concentrations. The region demarked by the white rectangular box is shown in figure 2.

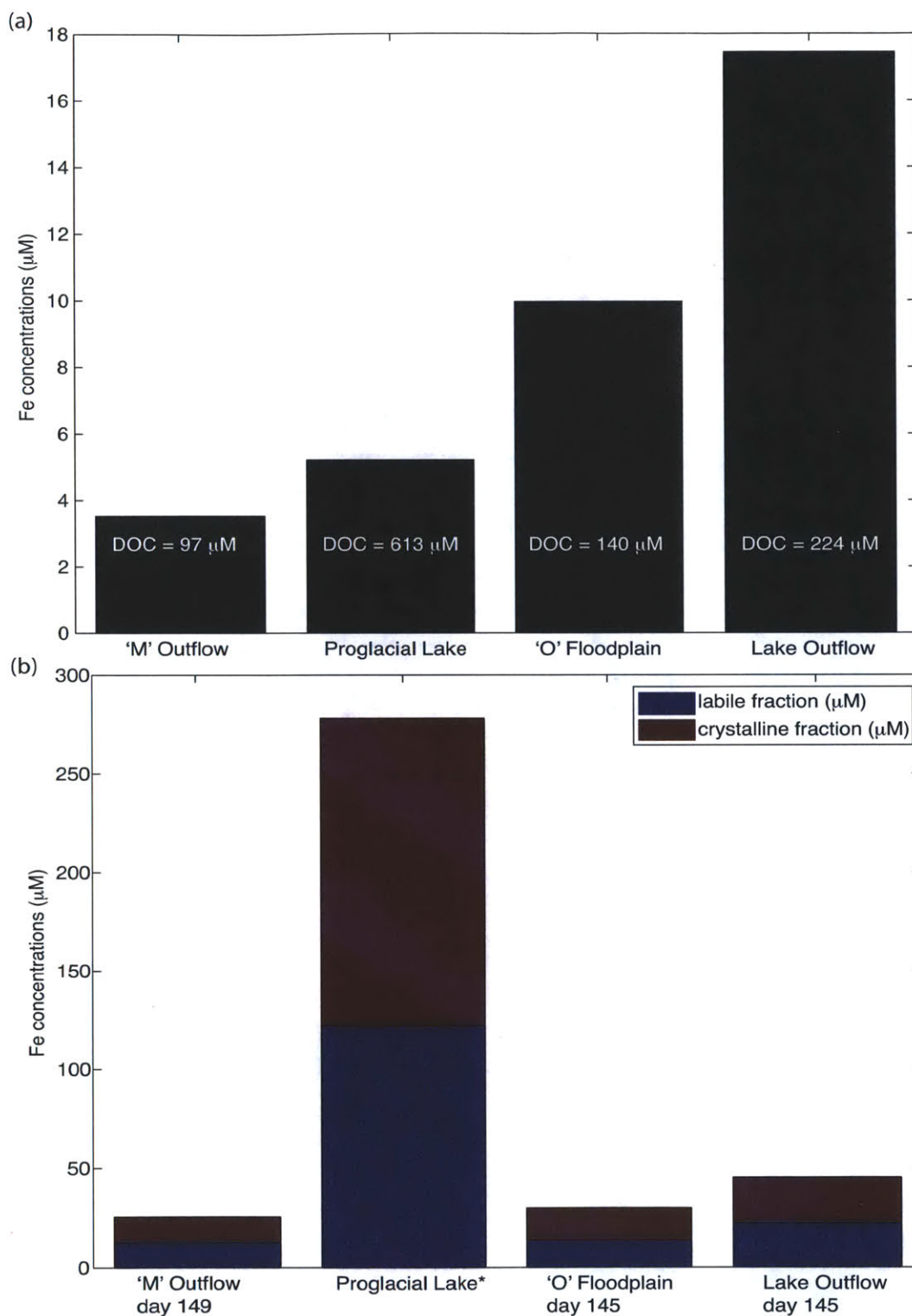


**Figure 2.** (a) Dissolved ( $<0.2 \mu\text{m}$ ) and (b) particulate labile and crystalline fraction ( $>0.7 \mu\text{m}$ ) Fe concentrations along a transect from the 'M' glacier outflow to the Lake Outflow in May 2008. The dissolved and particulate samples were all taken on the same day, except for the proglacial lake, where the dissolved sample was taken on the day 141 and the particulate on day 153. The DOC concentration measured in each dissolved sample is shown in the white text.



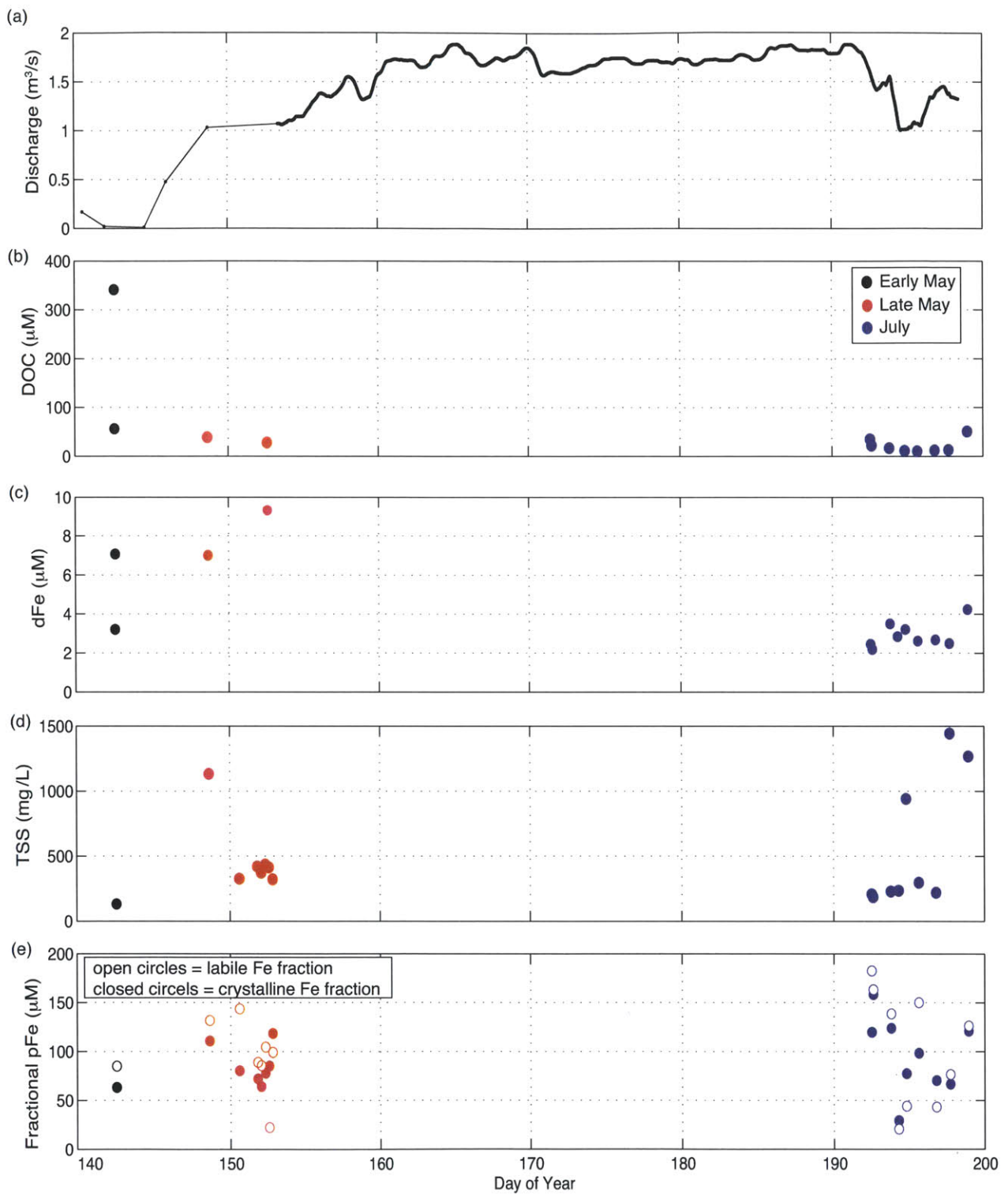


**Figure 3.** (a) 24-h moving average discharge (thick black line) measured at ‘N’ glacier (previously reported in Bhatia et al., 2011) from May 18 to July 16, 2008; the thin black line (days 140-150) indicates discontinuous discharge. (b) Dissolved organic carbon (DOC) concentrations measured in the ‘N’ glacier runoff (previously reported in Bhatia et al., in prep) corresponding to the dissolved (<0.2 mm) Fe concentrations shown in (c). (d) Total suspended sediment (TSS) concentrations measured in the ‘N’ glacier runoff corresponding to the particulate (oxyhydr)oxide Fe (<0.7 mm) concentrations shown in (e).

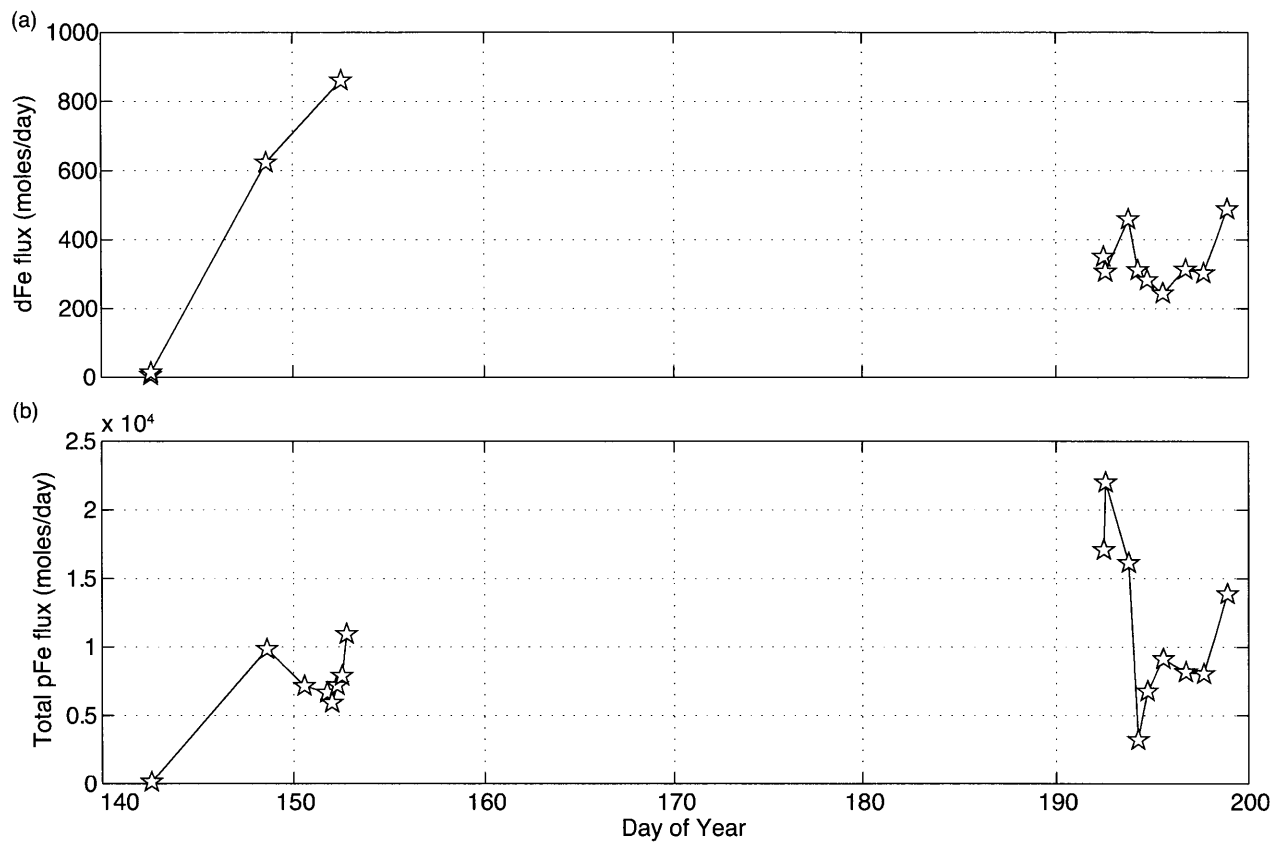


**Figure 4.** (a) Dissolved (<0.2 mm) and (b) total particulate (oxyhydr)oxide Fe (<0.7 mm) flux from 'N' glacier for days with complementary concentration and discharge measurements from May 18 to July 16, 2008.

## Appendix A1

### Data Tables

Table A1. List of samples collected from the Greenland ice sheet margin in 2008. The notation 'NM' indicates that the sample was 'not measured', 'NR' indicates that the data was 'not recorded', and 'N/A' indicates the measurement is not applicable to the sample.

Table A2. Hydrochemical parameters (pH, electrical conductivity (EC), and temperature) measured on-site during the Greenland ice sheet margin 2008 field campaign. The sample descriptions from Table A1 are abbreviated (in the sample type column) as follows: MO is 'M' glacier outflow, PW is proglacial waters, NO is 'N' glacier outflow, PL is proglacial lake, MF is 'M' glacier floodplain, MM is marginal melt, MI is marginal ice, LO is lake outflow, OO is 'O' glacier outflow, SN is snow, B is field blank, GW is groundwater, T is the proglacial tarn, F is fjord water from the second margin site, SWF is subglacial water in the fjord at the second margin site, and IB is ice from an iceberg at the second margin site.

Table A3. Alkalinity measured in Greenland ice sheet margin 2008 samples, using a Hach Alkalinity kit. The samples are described using the abbreviations above.

Table A4. <sup>222</sup>Radon (Rn), <sup>7</sup>Beryllium (Be), and oxygen isotope ( $\delta^{18}\text{O}$ ,  $\delta\text{D}$ ) measurements from Greenland ice sheet inland (2007, 2008) and margin (2008) samples. Electrical conductivity (EC) is also shown for comparison. The samples are described using the abbreviations above for the margin site, and the following abbreviations for the inland site: NLS is the north lake stream, NLI is north lake ice, NCY is north lake cryoconite,>NNLW is north north lake-water, SLLI is south lake lake-ice, SLI is south lake ice, SCY is south lake cryoconite, SLSNF is south lake fractionated snow, and NLSNF is north lake fractionated snow. Additional samples from the vicinity of Russell Glacier (Russell glacier marginal ice (RMI) and Russell glacier proglacial waters (RPW)) were also collected. Rain-water from a pond in Plymouth, MA (USA) was collected as a comparative sample for the <sup>7</sup>Be measurements.

Table A5. Dissolved (<0.2  $\mu\text{m}$ ) nutrients measured in Greenland ice sheet margin 2008 samples. Samples are described as in above.

Table A6. Dissolved (<0.2  $\mu\text{m}$ ) Organic Carbon (DOC) and Total Nitrogen (TN) concentrations measured in Greenland ice sheet margin 2008 samples. Samples are described as in above.

Table A7. Particulate (>0.7  $\mu\text{m}$ ) Organic Carbon (POC) and Particulate Organic Nitrogen (PON) concentrations in Greenland ice sheet margin 2008 samples.

Table A8. Dissolved (<0.2  $\mu\text{m}$ ) and particulate (>0.7  $\mu\text{m}$ ) radiocarbon for inland lake (2010) and margin (2008) samples.

Table A9. Dissolved (>0.45  $\mu\text{m}$ ) anions in Greenland ice sheet margin 2008 samples.

Table A10. Dissolved (>0.45  $\mu\text{m}$ ) cations in Greenland ice sheet margin 2008 samples.

Table A11. Dissolved (>0.2  $\mu\text{m}$ ) iron in Greenland ice sheet margin 2008 samples.

Table A12. Particulate (>0.2  $\mu\text{m}$ ) iron in Greenland ice sheet margin 2008 samples.

Table A1: Greenland Ice Sheet Margins 2008 Samples				
Sample ID	Description	Latitude	Longitude	Collection Date
1	GM2	68 deg 06.431'	50 deg 34.026'	5/17/08 12:30
2	G1	68 deg 04.525'	50 deg 19.640'	5/17/08 13:55
3	G2	68 deg 04.921'	50 deg 20.207'	5/17/08 16:04
4	G3	68 deg 02.623'	50 deg 16.139'	5/18/08 14:20
5	G4	68 deg 04.369'	50 deg 26.921'	5/18/08 14:20
6	G5	68 deg 02.623'	50 deg 16.139'	5/19/08 12:41
7	G6	68 deg 02.601'	50 deg 16.614'	5/19/08 13:55
8	G7	68 deg 03.096'	50 deg 20.165'	5/20/08 14:05
9	G8	68 deg 02.623'	50 deg 16.139'	5/20/08 16:00
10	G9	68 deg 02.601'	50 deg 16.614'	5/20/08 16:30
11	G10	68 deg 03.362'	50 deg 20.054'	5/20/08 16:30
12	G11	68 deg 02.623'	50 deg 16.139'	5/21/08 14:23
13	G12	68 deg 02.623'	50 deg 16.139'	5/21/08 14:10
14	G13	68 deg 02.601'	50 deg 16.614'	5/21/08 16:25
15	G14	68 deg 02.606'	50 deg 17.055'	5/21/2008
16	G15	68 deg 02.739'	50 deg 15.487'	5/22/08 17:00
	G15B	68 deg 02.739'	50 deg 15.487'	5/22/08 17:00
17	G16	68 deg 02.623'	50 deg 16.139'	5/22/08 18:00
18	G17	68 deg 02.601'	50 deg 16.614'	5/22/08 18:10
19	G18	68 deg 02.601'	50 deg 16.614'	5/23/08 13:45
20	G19	68 deg 02.623'	50 deg 16.139'	5/23/08 17:00
21	G20	68 deg 00.139'	50 deg 31.032'	5/24/08 19:00
22	G21	68 deg 00.959'	50 deg 25.785'	5/24/08 21:00
23	G22	68 deg 02.601'	50 deg 16.614'	5/25/2008
24	G23	68 deg 02.623'	50 deg 16.139'	5/25/2008
25	G24	close to N mouth coordinates	close to N mouth coordinates	5/25/2008
26	G25	68 deg 02.606'	50 deg 17.055'	5/25/2008
27	G26	68 deg 02.739'	50 deg 15.487'	5/22/2008
	G26B	68 deg 02.739'	50 deg 15.487'	5/22/2008
28	G27	68 deg 02.601'	50 deg 16.614'	5/24/2008
29	G28	68 deg 02.601'	50 deg 16.614'	5/26/2008
30	G29	68 deg 02.623'	50 deg 16.139'	5/27/08 14:48
	G29B	68 deg 02.623'	50 deg 16.139'	5/27/08 14:53
	G29C	68 deg 02.623'	50 deg 16.139'	5/27/08 14:55
31	G30	68 deg 02.601'	50 deg 16.614'	5/27/08 15:50
32	G31	68 deg 02.606'	50 deg 17.055'	5/27/08 16:00
33	G32	68 deg 02.601'	50 deg 16.614'	5/25/08 16:00
34	G33	68 deg 02.601'	50 deg 16.614'	5/26/08 16:00
35	G34	68 deg 02.601'	50 deg 16.614'	5/27/08 16:00
36	G35	68 deg 04.524'	50 deg 19.754'	5/28/08 16:30
37	G36	68 deg 02.623'	50 deg 16.139'	5/28/08 10:30
38	G37	68 deg 04.219'	50 deg 20.443'	5/28/2008
39	G38	68 deg 03.655'	50 deg 20.191'	5/28/2008
40	G39	M floodplain	M floodplain	5/28/08 19:00
41	G40	68 deg 02.831'	50 deg 17.675'	5/29/08 12:40
42	G41	68 deg 02.601'	50 deg 16.614'	5/29/08 16:00
43	G42	68 deg 02.623'	50 deg 16.139'	5/29/08 13:41
44	G43	68 deg 02.290'	50 deg 15.236'	5/29/08 16:30
45	G44	68 deg 02.601'	50 deg 16.614'	5/29/08 11:45
46	G45	68 deg 02.623'	50 deg 16.139'	5/30/08 18:00
47	G46	68 deg 04.369'	50 deg 26.921'	5/30/08 18:00
48	G47	68 deg 02.623'	50 deg 16.139'	5/31/08 0:00
49	G48	68 deg 02.623'	50 deg 16.139'	5/31/08 6:45
50	G49	68 deg 02.623'	50 deg 16.139'	5/31/08 12:40
51	G50	68 deg 02.739'	50 deg 15.487'	5/31/08 16:05
52	G51	68 deg 02.623'	50 deg 16.139'	5/31/08 18:25
53	G52	68 deg 02.623'	50 deg 16.139'	6/1/2008
54	G53	68 deg 03.096'	50 deg 20.165'	6/1/2008
55	ICE	on surface of N?	on surface of N?	NR

Sample ID	Description	Latitude	Longitude	Collection Date
56	MilliQ Blank 1 (May)	at camp	at camp	6/1/2008
57	MilliQ Blank 2 (May)	at camp	at camp	6/1/2008
58	G55	68 deg 02.623'	50 deg 16.139'	5/25/08 19:36
<b>Groundwater Samples</b>				
59	GM50	68 deg 02.601'	50 deg 16.614'	5/25/08 15:00
60	GM51	68 deg 02.601'	50 deg 16.614'	5/25/08 18:40
61	GM52	68 deg 02.601'	50 deg 16.614'	5/25/08 19:00
62	GM53	68 deg 02.601'	50 deg 16.614'	5/25/08 19:20
63	GM54	68 deg 02.601'	50 deg 16.614'	5/25/08 19:30
<b>July Samples</b>				
64	G56	68 deg 02.601'	50 deg 16.614'	7/10/08 11:23
65	G57	68 deg 02.623'	50 deg 16.139'	7/10/08 13:46
66	G58	68 deg 02.606'	50 deg 17.055'	7/10/08 14:40
67	G59	68 deg 02.623'	50 deg 16.139'	7/11/08 12:30
68	G60	68 deg 02.623'	50 deg 16.139'	7/11/08 12:30
69	Be/Ra-July	68 deg 02.601'	50 deg 16.614'	7/11/08 16:15
70	G61	68 deg 02.623'	50 deg 16.139'	7/11/08 18:00
71	G62	68 deg 02.623'	50 deg 16.139'	7/12/08 0:00
72	G63	68 deg 02.623'	50 deg 16.139'	7/12/08 6:00
73	G64	68 deg 02.623'	50 deg 16.139'	7/12/08 12:50
74	G65	68 deg 02.623'	50 deg 16.139'	7/12/08 18:00
75	G66	68 deg 02.623'	50 deg 16.139'	7/13/08 13:50
76	G67	68 deg 03.096'	50 deg 20.165'	7/13/08 18:45
77	G68	68 deg 02.623'	50 deg 16.139'	7/14/08 18:00
78	G69	68 deg 02.623'	50 deg 16.139'	7/15/08 16:30
79	G70	68 deg 04.525'	50 deg 19.640'	7/15/08 15:24
80	G71	68 deg 02.623'	50 deg 16.139'	7/16/08 22:00
81	G72	NM	NM	7/19/08 20:00
82	G73	68 deg 55.433'	50 deg 17.339'	7/22/08 0:00
83	G74	NM	NM (b/c GPS in boat for 10 AU transacts)	7/24/08 14:15
84	G75	NM	NM (b/c GPS in boat for 10 AU transacts)	7/24/08 15:00
85	G76	NM	NM (b/c GPS in boat for 10 AU transacts)	7/24/08 15:00
86	G77	NM	NM (b/c GPS in boat for 10 AU transacts)	7/24/08 15:00
87	G78	NM	NM (b/c GPS in boat for 10 AU transacts)	7/26/08 11:30
88	G79	NM	NM (b/c GPS in boat for 10 AU transacts)	7/26/08 11:40
89	G80	NM	NM (b/c GPS in boat for 10 AU transacts)	7/26/08 12:00
<b>June Autosampler Samples</b>				
90	A1	68 deg 02.601'	50 deg 16.614'	6/1/08 16:00
91	A2	69 deg 02.601'	51 deg 16.614'	6/3/08 4:00
Sample ID	Description	Latitude	Longitude	Collection Date
92	A3	70 deg 02.601'	52 deg 16.614'	6/4/08 16:00
93	A4	71 deg 02.601'	53 deg 16.614'	6/6/08 4:00
94	A5	72 deg 02.601'	54 deg 16.614'	6/7/08 16:00
95	A6	73 deg 02.601'	55 deg 16.614'	6/9/08 4:00
96	A9	76 deg 02.601'	58 deg 16.614'	6/13/08 16:00
97	A11	77 deg 02.601'	59 deg 16.614'	6/16/08 16:00
98	A12	78 deg 02.601'	60 deg 16.614'	6/18/08 4:00
99	A13	79 deg 02.601'	61 deg 16.614'	6/19/08 16:00
100	A15	80 deg 02.601'	62 deg 16.614'	6/22/08 16:00
101	A17	81 deg 02.601'	63 deg 16.614'	6/25/08 16:00
102	A19	82 deg 02.601'	64 deg 16.614'	6/28/08 16:00
103	A21	83 deg 02.601'	65 deg 16.614'	7/1/08 16:00
104	A23	84 deg 02.601'	66 deg 16.614'	7/4/08 16:00

Table A2: Greenland Ice Sheet Margins 2008 pH, EC, Temperature				
May Samples				
Sample ID	Sample Type	pH	EC ( $\mu\text{S/cm}$ , measured on-site)	Temperature (degrees C, measured on-site)
GM2	MO	NM	NM	NM
G1	MO	8.99	70.5	assume just above freezing
G2	PW	7.80	10.4	assume just above freezing
G3	NO	6.75	30	0.3
G4	MI	6.07	6	0.6
G5	NO	6.95	30.1	0.5
G6	NO	6.68	31.2	1
G7	PL	6.64	18.6	3.9
G8	NO	7.03	38.5	0.4
G9	NO	7.02	38.9	0.9
G10	MF	6.49	NM	assume just above freezing
G11	NO	7.68	41.8	0.3
G12	NO	6.86	144.3	0.3
G13	NO	6.63	45	0.8
G14	MM	6.83	11.5	2.5
G15	MI	9.25	0.4	1.1
G15B	MI	N/A	N/A	N/A
G16	NO	7.23	NM	assume just above freezing
G17	NO	6.90	NM	assume just above freezing
G18	NO	7.96	NM	assume just above freezing
G19	NO	7.17	NM	assume just above freezing
G20	LO	7.83	64.9	3.9
G21	OO	7.36	322	8.4
G22	NO	6.97	9.1	1.4
G23	NO	6.60	6.5	0.3
G24	MM	5.85	33	5
G25	MM	6.18	10.7	5.8
G26	SN	5.10	NM	assume freezing
G26B	SN	N/A	N/A	N/A
G27	NO	6.03	NM	assume just above freezing
G28	NO	6.72	12.9	0.9
G29	NO	7.21	15	0.7
G29B	NO	NM	15	0.7
G29C	NO	NM	15	0.7
G30	NO	6.61	17.1	1.5
G31	MM	6.20	NM	assume just above freezing
G32	NO	6.3	NM	assume just above freezing
G33	NO	6.21	NM	assume just above freezing
G34	NO	6.31	NM	assume just above freezing
G35	MO	7.03	22	assume just above freezing
G36	NO	no	23	1
G37	MO	7.33	22.2	3.4
G38	MO	6.15	5.7	2.6
G39	GW	6.08	NM	
G40	T	6.21	NM	NM
G41	NO	6.4	NM	NM
G42	NO	5.68	7.24	0.6
G43	MM	5.87	5.2	2.6
G44	NO	7.04	18.4	0.9
G45	NO	5.97	11.4	0.5
G46	MI	5.29	1.2	0.3
G47	NO	6.37	16.9	0.4
G48	NO	6.04	17.9	0.5
G49	NO	6.17	18.1	0.5
G50	MI	5.43	0.2	1.3
G51	NO	6.73	11	10.5 (measured at camp)
G52	NO	6.27	NM	NM
G53	PL	6.13	NM	NM
ICE	MI		NM	NM
MilliQ Blank 1 (May)	B		NM	NM
MilliQ Blank 2 (May)	B		NM	NM
G55	NO		NM	NM
<b>Groundwater Samples</b>				
GM50	GW		NM	NM
GM51	GW		NM	NM
GM52	GW		NM	NM
GM53	GW		NM	NM
GM54	GW		NM	NM
<b>July Samples</b>				
G56	NO	6.21	1.5	1.2
G57	NO	6.01	1.2	0.2
G58	MM	6.08	4.6	1
G59	NO	7.4	1.6	0.5
G60	NO	6.84	3.1	0.4
Be/Ra-July	NO	NM	NM	NM
G61	NO	6.45	1.1	0.4
G62	NO	5.94	2.1	0.3

Sample ID	Sample Type	pH	EC (μS/cm, measured on-site)	T (degrees C, measured on-site)
G63	NO	8	3.2	0.5
G64	NO	7.44	0.2	0.4
G65	NO	7.04	1.5	0.7
G66	NO	7.74	2.3	0.3
G67	PL	6.75	47.7	8.9
G68	NO	8.17	1.1	0.4
G69	NO	7.59	4.4 (measured at camp)	NM
G70	MO	7.01	2.4	0.9
G71	NO	6.44	2.3	0.3
G72	F	8.34	27.7	8.88
G73	F	8.28	NM	NM
G74	SWF	8.29	4.9	1.2
G75	F	7.63	30.6	4.7
G76	SWF	NM	NM	NM
G77	IB	NM	NM	NM
G78	F	8.22	NM	NM
G79	SWF	8.72	165.7	5.6
G80	IB	5.65	NM	NM
<b>June Autosampler Samples</b>				
A1	NO	NM	NM	NM
A2	NO	NM	NM	NM
A3	NO	NM	NM	NM
A4	NO	NM	NM	NM
A5	NO	NM	NM	NM
A6	NO	NM	NM	NM
A9	NO	NM	NM	NM
A11	NO	NM	NM	NM
A12	NO	NM	NM	NM
A13	NO	NM	NM	NM
A15	NO	NM	NM	NM
A17	NO	NM	NM	NM
A19	NO	NM	NM	NM
A21	NO	NM	NM	NM
A23	NO	NM	NM	NM



Table A3: Greenland Ice Sheet Margins 2008 Alkalinity						
May Samples						
Sample ID	Sample Type	Alkalinity turns (0.1 H2SO4)	Titration pH	CaCO3 Total Alkalinity (mg/L)	HCO3 Total Alkalinity (mg/L)	
GM2	MO	NM	NM	NM	NM	
G1	MO	NM	NM	NM	NM	
G2	PW	NM	NM	NM	NM	
G3	NO		96	NR	9.6	11.712
G4	MI		25	NR	2.5	3.05
G5	NO		276	NR	27.6	33.672
G6	NO		149	NR	14.9	18.178
G7	PL		150	4.5	15	18.3
G8	NO		160	4.5	16	19.52
G9	NO		194	4.5	19.4	23.668
G10	MF		50	4.45	5	6.1
G11	NO		109	NR	10.9	13.298
G12	NO		38	NR	3.8	4.636
G13	NO		67	NR	6.7	8.174
G14	MM		30	NR	3	3.66
G15	MI		11	4.5	1.1	1.342
G15B	MI	NM	NM	NM	NM	
G16	NO		44	4.47	4.4	5.368
G17	NO		47	4.5	4.7	5.734
G18	NO		44	4.51	4.4	5.368
G19	NO		48	4.49	4.8	5.856
G20	LO		83	4.5	8.3	10.126
G21	OO		150	4.5	15	18.3
G22	NO		25	4.51	2.5	3.05
G23	NO		15	4.49	1.5	1.83
G24	MM		21	4.48	2.1	2.562
G25	MM		39	4.49	3.9	4.758
G26	SN		5	4.48	0.5	0.61
G26B	SN					
G27	NO		42	4.49	4.2	5.124
G28	NO		53	4.5	5.3	6.466
G29	NO		42	4.48	4.2	5.124
G29B	NO	NM	NM	NM	NM	
G29C	NO	NM	NM	NM	NM	
G30	NO		64	4.5	6.4	7.808
G31	MM		30	4.49	3	3.66
G32	NO		40	4.49	4	4.88
G33	NO		38	4.5	3.8	4.636
G34	NO		51	4.49	5.1	6.222
G35	MO		90	4.48	9	10.98
G36	NO	NM	NM	NM	NM	
G37	MO		88	4.5	8.8	10.736
G38	MO		39	4.5	3.9	4.758
G39	GW		51	4.5	5.1	6.222
G40	T		80	4.5	8	9.76
G41	NO		50	4.5	5	6.1
G42	NO		40	4.5	4	4.88
G43	MM		28	4.51	2.8	3.416
G44	NO		115	4.51	11.5	14.03
G45	NO		50	4.5	5	6.1
G46	MI		16	4.51	1.6	1.952
G47	NO		68	4.47	6.8	8.296
G48	NO		70	4.51	7	8.54
G49	NO		68	4.51	6.8	8.296
G50	MI		8	4.5	0.8	0.976
G51	NO		45	4.33	4.5	5.49
G52	NO		48	4.5	4.8	5.856
G53	PL		81	4.5	8.1	9.882
ICE	MI	NM	NM	NM	NM	
MQ Blank 1 (May)	B	NM	NM	NM	NM	
MQ Blank 2 (May)	B	NM	NM	NM	NM	
G55	NO	NM	NM	NM	NM	
Groundwater Samples						
GM50	GW	NM	NM	NM	NM	
GM51	GW	NM	NM	NM	NM	
GM52	GW	NM	NM	NM	NM	
GM53	GW	NM	NM	NM	NM	
GM54	GW	NM	NM	NM	NM	
G56	NO		37	4.5	3.7	4.514
G57	NO		18	4.5	1.8	2.196
G58	MM		29	4.5	2.9	3.538
G59	NO		52	4.5	5.2	6.344
G60	NO		47	4.5	4.7	5.734
Be/Ra-July	NO	NM	NM	NM	NM	
G61	NO		28	4.45	2.8	3.416
G62	NO		34	4.53	3.4	4.148
G63	NO		30	4.46	3	3.66
G64	NO		30	4.5	3	3.66
G65	NO		25	4.5	2.5	3.05
G66	NO		27	4.5	2.7	3.294
G67	PL		80	4.51	8	9.76
G68	NO		35	4.47	3.5	4.27
G69	NO		25	4.5	2.5	3.05
G70	MO		32	4.45	3.2	3.904

Sample ID	Sample Type	Alkalinity turns (0.1 H2SO4)	Titration pH	CaCO3 Total Alkalinity (mg/L)	HCO3 Total Alkalinity (mg/L)
<b>July Samples</b>					
G71	NO	25	4.5	2.5	3.05
G72	F	690	4.48	69	84.18
G73	F	695	4.45	69.5	84.79
G74	SWF	48	4.51	4.8	5.856
G75	F	580	4.51	58	70.76
G76	SWF	NM	NM	NM	NM
G77	IB	NM	NM	NM	NM
G78	F	301	4.3	30.1	36.722
G79	SWF	54	4.53	5.4	6.588
G80	IB	13	4.47	1.3	1.586
<b>June Autosampler Samples</b>					
A1	NO	NM	NM	NM	NM
A2	NO	NM	NM	NM	NM
A3	NO	NM	NM	NM	NM
A4	NO	NM	NM	NM	NM
A5	NO	NM	NM	NM	NM
A6	NO	NM	NM	NM	NM
A9	NO	NM	NM	NM	NM
A11	NO	NM	NM	NM	NM
A12	NO	NM	NM	NM	NM
A13	NO	NM	NM	NM	NM
A15	NO	NM	NM	NM	NM
A17	NO	NM	NM	NM	NM
A19	NO	NM	NM	NM	NM
A21	NO	NM	NM	NM	NM
A23	NO	NM	NM	NM	NM

Table A4: Greenland Ice Sheet Inland and Margins Electrical Conductivity (EC), Radon (Rn)-222, Beryllium (Be)-7, Oxygen Isotopes							
Sample ID	Sample Type	Collection Date	EC (µS/cm, measured on-site)	Rn (dpm/L)	Be (dpm/L)	δ18O VSMOW	δD VSMOW
GM2	MO	5/17/08 12:30		4.282851021			
G1	MO	5/17/08 13:55	70.5	57.47262441		-27.28	-201.13
G2	PW	5/17/08 16:04	10.4	4.124877306		-17.16	-132.63
G3	NO	5/18/08 14:20	30	103.3624792		-25.25	-191.33
G4	MI	5/18/08 14:20	6	0		-29.54	-227.22
G5	NO	5/19/08 12:41	30.1			-25	-189.93
G6	NO	5/19/08 13:55	31.2	4.054964086		-24.97	-189.62
G7	PL	5/20/08 14:05	18.6	25.17975174	0.03	-21.12	-162.6
G8	NO	5/20/08 16:00	38.5			-24.21	-180.3
G9	NO	5/20/08 16:30	38.9	0		-24.04	-178.99
G10	MF	5/20/08 16:30				-26.01	-195.65
G11	NO	5/21/08 14:23	41.8	143.24		-23.82	-178.96
G12	NO	5/21/08 14:10	144.3	8.063867255		-21.49	-164.63
G13	NO	5/21/08 16:25	45		1.05	-23.3	-177.23
G14	MM	5/21/08	11.5			-26.29	-204.99
G15	MI	5/22/08 17:00	0.4	0	7.68	-28.23	-216.05
G15B	MI	5/22/08 17:00					
G16	NO	5/22/08 18:00		209.5031227		-25.02	-187.81
G17	NO	5/22/08 18:10		12.14304544		-25.94	-196.46
G18	NO	5/23/08 13:45		7.856164195		-26.31	-198.7
G19	NO	5/23/08 17:00		151.3936591		-26.18	-198.51
G20	LO	5/24/08 19:00	64.9	3.473167231		-25.52	-194.54
G21	OO	5/24/08 21:00	322	6.6491856		-26.25	-195.73
G22	NO	5/25/08	9.1			-26.35	-198.85
G23	NO	5/25/08	6.5			-26.93	-206.27
G24	MM	5/25/08	33				
G25	MM	5/25/08	10.7			-26.93	-205.94
G26	SN	5/22/08				-12.33	-89.9
G26B	SN	5/22/08					
G27	NO	5/24/08				-25.51	-193.54
G28	NO	5/26/08	12.9			-26.24	-199.83
G29	NO	5/27/08 14:48	15	29.63092664		-26.04	-195.86
G29B	NO	5/27/08 14:55	15	39.36607883		-26.04	-195.86
G29C	NO	5/27/08 14:55	15	39.6198509			
G30	NO	5/27/08 15:50	17.1			-26.38	-198.92
G31	MM	5/27/08 16:00				-26.18	-199.15
G32	NO	5/25/08 16:00				-25.96	-195.44
G33	NO	5/26/08 16:00				-25.41	-194.32
G34	NO	5/27/08 16:00				-26.18	-198.09
G35	MO	5/28/08 16:30	22	36.81513609	0.25	-25.11	-188.27
G36	NO	5/28/08 10:30	23	59.20957369			
G37	MO	5/28/08	22.2			-24.47	-185.77
G38	MO	5/28/08	5.7			-30.95	-236.28
G39	GW	5/28/08 19:00		1625.770623		-27.86	-209.2
G40	T	5/29/08 12:40				-13.34	-116.26
G41	NO	5/29/08 16:00				-26.07	-195.13
G42	NO	5/29/08 13:41	7.24	25.0166977		-25.7	-194.95
G43	MM	5/29/08 16:30	5.2			-26.15	-198.11
G44	NO	5/29/08 11:45	18.4			-25.04	-186.88
G45	NO	5/30/08 18:00	11.4	38.29948513		-25.2	-189.97
G46	MI	5/30/08 18:00	1.2			-29.58	-223.16
G47	NO	5/31/08 0:00	16.9	60.75008104		-24.4	-187.52
G48	NO	5/31/08 6:45	17.9	75.4874663		-25.05	-184.47
G49	NO	5/31/08 12:40	18.1	49.352666		-24.82	-187.87
G50	MI	5/31/08 16:05	0.2	0		-27.48	-212.05
G51	NO	5/31/08 18:25	11	47.53239899		-25.77	-197.04
G52	NO	6/1/08				-25.81	-197.78
G53	PL	6/1/08		4.977991376		-26.3	-201.24
ICE	MI	6/1/08				-28.77	-220.34
MilliQ Blank 1 (May)	B	6/1/08					
MilliQ Blank 2 (May)	B	6/1/08					
G55	NO	5/25/08 19:36		16.85986518			
GM50	GW	5/25/08 15:00		2746.000888			
GM51	GW	5/25/08 18:40					
GM52	GW	5/25/08 19:00					
GM53	GW	5/25/08 19:20					
GM54	GW	5/25/08 19:30					
A1	NO	6/1/08 16:00				-27.55	-205.2
A2	NO	6/3/08 4:00				-25.89	-192.13
A3	NO	6/4/08 16:00				-27.46	-206.29
A4	NO	6/6/08 4:00				-26.28	-196.34
A5	NO	6/7/08 16:00				-27.57	-205.52
A6	NO	6/9/08 4:00				-26.38	-197.75
A9	NO	6/13/08 16:00				-27.16	-202.94
A11	NO	6/16/08 16:00				-27.34	-206.52
A12	NO	6/18/08 4:00				-25.64	-191.88
A13	NO	6/19/08 16:00				-26.9	-202.17
A15	NO	6/22/08 16:00				-27.65	-209.8
A17	NO	6/25/08 16:00				-27.92	-211.11
A19	NO	6/28/08 16:00				-28.02	-212.26
A21	NO	7/1/08 16:00				-28.18	-212.3
A23	NO	7/4/08 16:00				-27.65	-211.74
G56	NO	7/10/08 11:23	1.5	4.598422349		-27.73	-209.19
G57	NO	7/10/08 13:46	1.2	16.73899485		-28.06	-211

Sample ID	Sample Type	Collection Date	EC (µS/cm, measured on-site)	Rn (dpm/L)	Be (dpm/L)	δ18O VSMOW	δD VSMOW
G58	MM	7/10/08 14:40	4.6	6.094806167		-28.28	-216.82
G59	NO	7/11/08 12:30	1.6	20.33389511		-27.91	-213.87
G60	NO	7/11/08 12:30	3.1	10.22925312		-30.03	-230.26
Be/Ra-July	NO	7/11/08 16:15			0.03		
G61	NO	7/11/08 18:00	1.1	29.64785695		-27.66	-211.86
G62	NO	7/12/08 0:00	2.1	30.13613837		-27.16	-207.85
G63	NO	7/12/08 6:00	3.2	30.09828272		-27	-207.24
G64	NO	7/12/08 12:50	0.2	31.78619897		-26.78	-206.82
G65	NO	7/12/08 18:00	1.5	27.26997413		-27.37	-209.7
G66	NO	7/13/08 13:50	2.3	35.6503304		-27.06	-206.45
G67	PL	7/13/08 18:45	47.7	8.879711842		-27.01	-201.02
G68	NO	7/14/08 18:00	1.1	10.37656762		-28.36	-209.75
G69	NO	7/15/08 16:30	4.4	23.68743661		-28.11	-211.83
G70	MO	7/15/08 15:24	2.4	13.52256843		-28.52	-213.43
G71	NO	7/16/08 22:00	2.3	23.39667411		-28.17	-208.27
G72	F	7/19/08 20:00	27.7	0		-10.34	-80.83
G73	F	7/22/08 0:00		0		-10.49	-80.09
G74	SWF	7/24/08 14:15	4.9	0		-35.36	-264.31
G75	F	7/24/08 15:00	30.6	5.896462404		-13.71	-109.45
G76	SWF	7/24/08 15:00					
G77	IB	7/24/08 15:00				-33.16	-252.3
G78	F	7/26/08 11:30		5.994280542		-24.68	-189.14
G79	SWF	7/26/08 11:40	165.7	6.098600106		-33.64	-252.92
G80	IB	7/26/08 12:00				-30.81	-228.58
<b>Inland Supraglacial Samples</b>							
North Lake stream	NLS	7/20/08			0.04		
L15	NLI	7/20/07				-24.6	-186.3
L16	NLI	7/20/07				-26.5	-202.6
L17	NLI	7/20/07				-24.4	-186.3
L18	NCY	7/20/07				-26.1	-199.5
L19	NCY	7/20/07				-25.4	-193.1
L20	NCY	7/20/07				-25.6	-195.5
L21	NCY	7/20/07				-25.2	-192.8
L22	NCY	7/20/07				-25.3	-194.7
L23	NLS	7/20/07				-24.4	-186.2
L24	NNLW	7/20/07				-25.1	-191.6
L5	SLLI	7/13/07				-23.3	-176.8
L6	SLLI	7/13/07				-23.4	-176.9
L7	SLLI	7/13/07				-26.3	-198.7
L8	SLI	7/17/07				-24.8	-187.9
L9	SLI	7/17/07				-25.1	-189.5
L10	SLI	7/17/07				-24.1	-183.5
L11	SCY	7/17/07				-22.6	-171.1
L12	SCY	7/17/07				-22.7	-171.5
L13	SLW	7/13/07				-24.1	-183.8
L14	SLW	7/13/07				-24.1	-184
L1	SLSNF	7/16/07				-21.5	-162.1
L2	SLSNF	7/16/07				-21.9	-164.4
L3	SLSNF	7/17/07				-20.3	-154.9
L4	NLSNF	7/20/07				-21.4	-161.2
L25	RMI	7/26/07				-27.4	-211.9
L27	RMI	7/26/07				-27.4	-212.5
L26	RMI	7/26/07				-27.4	-213.2
L28	RPW	7/26/07				-25.8	-201.3
L29	RPW	7/26/07				-26.9	-206.5
<b>Other Samples</b>							
Plymouth pond rain water	PPR	4/28/08			4.6		

Sample ID	Collection Date	Sample Type	$\mu\text{M NH}_4$	$\mu\text{M Silicate}$	$\mu\text{M PO}_4$	$\mu\text{M NO}_2+\text{NO}_3$	$\mu\text{M DIN}$	$\mu\text{M DON}$	$\mu\text{M TDN}$
1 GM2	5/17/08 12:30	MO							
2 G1	5/17/08 13:55	MO	1.47404	51.28873	0.07608	1.74656	3.22060	11.30538	14.52598
3 G2	5/17/08 16:04	PW	0.42202	8.41504	0.08676	0.06852	0.49054	10.86533	11.35587
4 G3	5/18/08 14:20	NO	1.16106	13.92269	0.08491	0.82057	1.98163	8.42320	10.40483
5 G4	5/18/08 14:20	MI	1.36298	7.89294	NaN	0.57047	1.93345	9.42241	11.35587
6 G5	5/19/08 12:41	NO	1.43365	17.09624	NaN	3.05907	4.49272	NaN	NaN
7 G6	5/19/08 13:55	NO	0.96519	21.70302	0.09231	1.77757	2.74276	11.14920	13.89196
8 G7	5/20/08 14:05	PL	0.19687	8.28195	0.08933	0.22013	0.41700	21.71725	22.13426
9 G8	5/20/08 16:00	NO	1.18125	15.76540	NaN	1.34351	2.52476	17.39042	19.91518
10 G9	5/20/08 16:30	NO	0.53610	19.14370	NaN	4.35090	4.88701	6.15184	11.03885
11 G10	5/20/08 16:30	MF	0.20394	11.67049	NaN	2.44932	2.65326	19.79801	22.45127
12 G11	5/21/08 14:23	NO	1.10048	27.74301	NaN	3.29677	4.39724	10.44575	14.84299
13 G12	5/21/08 14:10	NO	4.17980	45.35112	0.07875	20.87607	25.05587	22.43931	47.49518
14 G13	5/21/08 16:25	NO	1.84759	20.06505	0.08081	5.41538	7.26297	12.65221	19.91518
15 G14	5/21/08	MM	0.05563	16.17489	0.10781	0.36171	0.41734	14.74266	15.16000
16 G15	5/22/08 17:00	MI	1.21154	5.86596	0.11089	0.36688	1.57842	9.46044	11.03885
17 G16	5/22/08 17:00	MI							
18 G17	5/22/08 18:00	NO	0.75721	40.94909	NaN	2.99706	3.75427	7.28458	11.03885
19 G18	5/22/08 18:10	NO	0.84202	17.30099	0.43843	4.78496	5.62698	15.55624	21.18322
20 G19	5/23/08 13:45	NO	1.33269	32.04266	NaN	4.87797	6.21066	9.26635	15.47702
21 G20	5/23/08 17:00	NO	2.21105	29.07385	NaN	2.61468	4.82573	9.70025	14.52598
22 G21	5/24/08 19:00	LO	0.43817	49.85552	0.05551	3.05907	3.49724	14.83288	18.33012
23 G22	5/25/08	NO	5.79518	25.28606	0.07557	2.44932	8.24450	9.45159	17.69610
24 G23	5/25/08	NO	1.86778	8.71192	0.05421	1.55020	3.41799	22.52041	25.93840
25 G24	5/25/08	MM	2.12019	9.42853	NaN	1.22983	3.35002	9.90792	13.25793
26 G25	5/25/08	MM	2.03942	14.02506	0.06469	2.34597	4.38539	NaN	NaN
27 G26	5/25/08	MM	0.79759	13.20608	0.11192	2.74903	3.54662	6.54120	10.08782
28 G27	5/22/08	SN	3.08942	7.26846	NaN	3.12108	6.21049	13.70468	19.91518
29 G28	5/22/08	SN	3.25096	6.59280	0.10093	3.74116	6.99211	NaN	NaN
30 G29	5/24/08	NO	1.14086	22.72674	NaN	2.82137	3.96223	13.41685	17.37908
31 G30	5/26/08	NO	2.38269	9.11117	0.05438	1.22983	3.61252	5.52427	9.13678
32 G31	5/27/08 14:48	NO	1.24182	33.27113	NaN	1.31251	2.55433	10.70360	13.25793
33 G32	5/27/08 14:55	NO							
34 G33	5/27/08 14:55	NO							
35 G34	5/27/08 15:50	NO	11.00479	14.22981	NaN	0.61285	11.61763	1.64030	13.25793
36 G35	5/27/08 16:00	MM	<0.05	5.93762	0.06600	0.38962	0.38962	18.57452	18.96414
37 G36	5/25/08 16:00	NO	<0.05	10.85151	0.06550	0.67382	0.67382	12.26710	12.94092
38 G37	5/26/08 16:00	NO	1.03990	9.01904	NaN	1.48820	2.52810	16.75306	19.28115
39 G38	5/27/08 16:00	NO	1.33269	33.06639	0.05514	1.36418	2.69687	8.97601	11.67288
40 G39	5/28/08 16:30	MO	0.64413	39.61824	0.05750	1.99460	2.63873	12.20426	14.84299
41 G40	5/28/08 10:30	NO							
42 G41	5/28/08	MO	0.82384	31.01894	0.05000	1.44686	2.27070	19.54654	21.81725
43 G42	5/28/08	MO	0.21202	3.42949	0.08522	0.17156	0.38357	8.75321	9.13678
44 G43	5/29/08 19:00	GW	0.20798	77.90564	NaN	0.57151	0.77949	4.87017	5.64966
45 G44	5/29/08 12:40	T	0.58558	3.49091	NaN	0.12298	0.70856	29.35099	30.05954
46 G45	5/29/08 16:00	NO	1.35288	21.90776	0.05432	1.31251	2.66539	13.20681	15.87220
47 G46	5/29/08 13:41	NO	0.99649	7.37084	0.06284	0.88878	1.88527	18.66393	20.54920
48 G47	5/29/08 16:30	MM	0.27966	6.58257	NaN	0.72239	1.00206	6.23266	7.23472
49 G48	5/29/08 11:45	NO	1.25192	12.59184	0.06356	1.82924	3.08116	7.64068	10.72184
50 G49	5/30/08 18:00	NO	1.09038	14.63930	NaN	1.32284	2.41322	7.04057	9.45380
51 G50	5/30/08 18:00	MI	0.35740	0.88348	0.06253	0.26870	0.62611	6.92562	7.55173
52 G51	5/31/08 0:00	NO	1.23173	18.63184	NaN	1.94292	3.17465	NaN	NaN
53 G52	5/31/08 6:45	NO	1.25192	26.61691	0.05421	2.10828	3.36020	12.75084	16.11104
54 G53	5/31/08 12:40	NO	0.94096	15.04879	NaN	2.10828	3.04924	9.89169	12.94092
55 G54	5/31/08 16:05	MI	0.49976	3.14284	0.16018	0.28627	0.78603	8.98478	9.77081
56 G55	5/31/08 18:25	NO	1.15096	4.01301	0.05904	1.35384	2.50480	8.21704	10.72184
57 G56	6/1/08	NO	1.24182	13.00134	0.23000	0.90635	2.14818	16.18194	18.33012
58 G57	6/1/08	PL	0.51490	35.42096	0.23513	2.69735	3.21226	14.80085	18.01311
59 G58	6/1/08	MI							
60 G59	6/1/08	B							
61 MQ nutrient blank 1 (May)	6/1/08	B	0.05490	1.61376	NaN	NaN	0.05490	NaN	NaN
62 MQ nutrient blank 2 (May)	6/1/08	B							
63 MQ1 MayDOC	6/1/08								
64 MQ2 MayDOC	6/1/08								
65 MQ1 MayTOC	6/2/08								
66 MQ2 MayTOC	6/2/08								
67 G55	5/25/08 19:36	NO							
68 GM50	5/25/08 15:00	GW	0.33923	18.73421	0.05457	21.39281	21.73204	NaN	NaN
69 GM51	5/25/08 18:40	GW	16.15382	72.88938	0.16428	26.87019	43.02401	55.19301	98.21702
70 GM52	5/25/08 19:00	GW	6.49181	57.84059	0.06653	62.83491	69.32673	42.83880	112.16553
71 GM53	5/25/08 19:20	GW	1.02981	5.95809	0.06058	77.61352	78.64332	1.82105	80.46438
72 GM54	5/25/08 19:30	GW	1.32259	14.84404	0.06606	75.64993	76.97252	6.66197	83.63449
73 G56	7/10/08 11:23	NO	1.16106	7.24799	0.78035	0.48366	1.64472	6.85804	8.50276
74 G57	7/10/08 13:46	NO	0.18274	3.66494	0.53597	0.28007	0.46281	18.81834	19.28115
75 G58	7/10/08 14:40	MM	<0.05	10.06324	0.57396	1.21949	1.21949	4.43016	5.64966
76 G59	7/11/08 12:30	NO	0.37356	4.97531	0.64789	0.27904	0.65259	29.08994	29.74253
77 G60	7/11/08 12:30	NO	<0.05	4.07443	0.06715	0.21083	0.21083	23.19148	23.40230
78 Be/Ra-July	7/11/08 16:15	NO							
79 G61	7/11/08 18:00	NO	0.05997	5.36433	0.07629	0.21600	0.27597	4.42266	4.69862
80 G62	7/12/08 0:00	NO	<0.05	4.28942	0.07608	NaN	0.00000	3.11357	3.11357
81 G63	7/12/08 6:00	NO	0.12418	4.73986	0.06610	0.37412	0.49830	7.05343	7.55173
82 G64	7/12/08 12:50	NO	<0.05	4.54535	NaN	0.51467	0.51467	6.08603	6.60069
83 G65	7/12/08 18:00	NO	<0.05	6.62352	0.05249	0.31934	0.31934	4.69629	5.01564

Sample ID	Collection Date	Sample Type	µM NH4	µM Silicate	µM PO4	µM NO2+NO3	µM DIN	µM DON	µM TDN
79 G66	7/13/08 13:50	NO	<0.05	4.62725	NaN	0.46713	0.46713	5.81655	6.28368
80 G67	7/13/08 18:45	PL	<0.05	38.69689	NaN	2.28397	2.28397	2.73167	5.01564
81 G68	7/14/08 18:00	NO	0.38163	4.14610	0.06308	0.25113	0.63277	6.28494	6.91770
82 G69	7/15/08 16:30	NO	0.43817	6.19355	NaN	0.23666	0.67484	6.24287	6.91770
83 G70	7/15/08 15:24	MO	<0.05	3.95159	0.05277	0.05002	0.05002	17.01205	17.06207
84 G71	7/16/08 22:00	NO	<0.05	5.35409	NaN	NaN	0.00000	4.06460	4.06460
85 G72	7/19/08 20:00	F	7.57210	3.66494	0.05559	NaN	7.57210	6.31986	13.89196
86 G73	7/22/08 0:00	F	1.42355	4.71938	0.06588	NaN	1.42355	23.56381	24.98736
87 G74	7/24/08 14:15	SWF	<0.05	4.65796	0.05270	NaN	0.00000	15.47702	15.47702
88 G75	7/24/08 15:00	F	<0.05	10.01205	0.15402	2.22196	2.22196	23.08241	25.30437
89 G76	7/24/08 15:00	SWF							
90 G77	7/24/08 15:00	IB							
91 G78	7/26/08 11:30	F	0.08390	6.82826	0.05175	NaN	0.08390	12.54001	12.62391
92 G79	7/26/08 11:40	SWF	<0.05	7.72914	0.10473	0.07823	0.07823	10.64361	10.72184
93 G80	7/26/08 12:00	IB	0.22211	2.53884	0.06293	0.17569	0.39780	19.51737	19.91518
94 A1	6/1/08 16:00	NO	1.58509	17.81285	0.09272	3.26576	4.85085	NaN	NaN
95 A2	6/3/08 4:00	NO	2.24134	17.19862	NaN	1.48820	3.72954	17.45369	21.18322
96 A3	6/4/08 16:00	NO	1.84759	8.95761	0.06643	0.88775	2.73534	22.56903	25.30437
97 A4	6/6/08 4:00	NO	2.03942	19.75794	NaN	1.35384	3.39326	20.64306	24.03633
98 A5	6/7/08 16:00	NO	2.01923	7.68819	0.16018	0.71619	2.73542	18.13079	20.86621
99 A6	6/9/08 4:00	NO	1.61538	11.46574	NaN	0.99936	2.61475	19.20250	21.81725
100 A9	6/13/08 16:00	NO	1.74663	13.71794	0.09446	0.75960	2.50623	16.14090	18.64713
101 A11	6/16/08 16:00	NO	3.33172	10.19632	0.07328	0.49400	3.82572	18.94256	22.76828
102 A12	6/18/08 4:00	NO	0.16558	16.89150	NaN	0.66865	0.83423	24.15313	24.98736
103 A13	6/19/08 16:00	NO	1.54471	6.67470	0.05382	0.67796	2.22266	11.98630	14.20897
104 A15	6/22/08 16:00	NO	2.12019	26.00267	0.06356	0.54671	2.66689	19.15035	21.81725
105 A17	6/25/08 16:00	NO	1.95865	27.53826	0.08409	0.43922	2.39787	18.78535	21.18322
106 A19	6/28/08 16:00	NO	1.41346	20.78166	0.05483	0.43406	1.84752	16.79961	18.64713
107 A21	7/1/08 16:00	NO	1.89807	12.79659	0.06896	0.48160	2.37967	16.58447	18.96414
108 A23	7/4/08 16:00	NO	1.18125	28.45962	0.06345	2.40798	3.58923	14.74089	18.33012

Table A6: Greenland Ice Sheet Margins 2008 Dissolved Organic Carbon (DOC) and Total Nitrogen (TN)														
Sample ID	Collection Date	Sample Type	DOC (µM)	14DOC (µM) aliquot	DOC aliquot (µM)	TN (µM)	DOC aliquot (µM)	TN (µM)	DOC (µM)	TN (µM)	DOC run 11.27.10	TN run 11.27.10	DOC run 11.28.10	TN run 11.28.10
			run 11.25/26.08	run 03.25.10	run 11.01.10	run 11.01.10	run 11.27.10	run 11.27.10	run 11.28.10	run 11.28.10	same day rep	same day rep	same day rep	same day rep
Mean MilliQ Blank		Instrument Blank	1.86000											
Low Carbon Water		Instrument Std	1.46900											
Deep Sea Reference Water		Instrument Std	47.60300											
Mean MilliQ Blank		Instrument Blank	1.52400											
Low Carbon Water		Instrument Std	0.64200											
Deep Sea Reference Water		Instrument Std	46.52000											
Mean MilliQ Blank		Instrument Blank		3.79369										
Low Carbon Water		Instrument Std		0.99										
Deep Sea Reference Water		Instrument Std		47.34										
Mean MilliQ Blank		Instrument Blank			1.30000	0.00000								
Low Carbon Water		Instrument Std			0.11000	0.00000								
Deep Sea Reference Water		Instrument Std			47.13000	38.04000								
Mean MilliQ Blank		Instrument Blank					0.35	0.02000						
Low Carbon Water		Instrument Std					2.98000	0.13000						
Deep Sea Reference Water		Instrument Std					48.97000	36.09000						
Mean MilliQ Blank		Instrument Blank							0.12000	0.00462				
Low Carbon Water		Instrument Std							0.80000	0.00000				
Deep Sea Reference Water		Instrument Std							47.54000	33.03000				
GM2	5/17/08 12:30	MO	NaN											
G1	5/17/08 13:55	MO	62.47900		83.51279	10.53710							264.46511	8.25417
G2	5/17/08 16:04	PW	254.56300						266.48346	8.55553				
G3	5/18/08 14:20	NO	41.87600		41.71098	6.55931								
G4	5/18/08 14:20	MI	22.04600											
G4-TOC-DOC (0.3 um)	5/18/08 14:20	MI							21.29080	1.38045				
G5	5/19/08 12:41	NO	49.62800	44.18451										
G5-TOC-DOC (0.3 um)	5/19/08 12:41	NO							73.39478	11.16017				
G6	5/19/08 13:55	NO	80.52600											
G6-TOC-DOC (0.3 um)	5/19/08 13:55	NO							77.30915	10.22738				
G7	5/20/08 14:05	PL	613.51200						652.47734	12.74591				
G8	5/20/08 16:00	NO	43.63200		46.97482	10.59690								
G9	5/20/08 16:30	NO												
G10	5/20/08 16:30	MF	193.48800						188.31832	5.66172				
G11	5/21/08 14:23	NO	56.09600		56.78820	9.81956			59.65166	9.78968				
G12	5/21/08 14:10	NO	341.71800											
G12-TOC-DOC (0.3 um)	5/21/08 14:10	NO							347.52322	60.05756				
G13	5/21/08 16:25	NO												
G14	5/21/08	MM												
G15	5/22/08 17:00	MI	15.02800	7.75	14.24638	2.42577			16.20211	1.50530				
G15B	5/22/08 17:00	MI												
G16	5/22/08 18:00	NO	61.42400		73.98898	8.23927								
G17	5/22/08 18:10	NO												
G18	5/23/08 13:45	NO												
G19	5/23/08 17:00	NO												
G20	5/24/08 19:00	LO		146.94962										6.29
G21	5/24/08 21:00	OO		140.50760										8.80
G22	5/25/08	NO												
G23	5/25/08	NO	41.39100		41.01600	5.22674			44.91159	4.93199				
G24	5/25/08	MM												
G25	5/25/08	MM												
G26	5/22/08	SN												
G26B	5/22/08	SN												
G27	5/24/08	NO												
G28	5/24/08	NO	31.93500											
G28-TOC-DOC (0.3 um)	5/26/08								68.50181	10.64594				
G29	5/27/08 14:48	NO	39.16900		38.96967	5.72788								
G29B	5/27/08 14:55	NO												
G29C	5/27/08 14:55	NO												
G30	5/27/08 15:50	NO	42.87800		39.02115	6.28596								
G31	5/27/08 16:00	MM												
G32	5/25/08 16:00	NO												
G33	5/26/08 16:00	NO												
G34	5/27/08 16:00	NO												
G35	5/28/08 16:30	MO	96.50200						97.43147	5.20226				
G36	5/28/08 10:30	NO												
G37	5/28/08	MO												
G38	5/28/08	MO	33.27200		35.26311	5.75350								
G39	5/28/08 19:00	GW												
G40	5/29/08 12:40	T	406.43800	375.44621					467.76786	28.82819				
G41	5/29/08 16:00	NO												
G42	5/29/08 13:41	NO	28.35000		30.19232	3.36740								
G43	5/29/08 16:30	MM	46.99400		43.15886	9.99325								

Sample ID	Collection Date	Sample Type	DOC (µM)	14DOC (µM) aliquot	DOC aliquot (µM)	TN (µM)	DOC aliquot (µM)	TN (µM)	DOC (µM)	TN (µM)	DOC run 11.27.10	TN run 11.27.10	DOC run 11.28.10	TN run 11.28.10
			run 11.25/26.08	run 03.25.10	run 11.01.10	run 11.01.10	run 11.27.10	run 11.27.10	run 11.28.10	run 11.28.10	same day rep	same day rep	same day rep	same day rep
G44	5/29/08 11:45	NO												
G45	5/30/08 18:00	NO	28.39600		31.88473	8.17093								
G46	5/30/08 18:00	MI												
G47	5/31/08 0:00	NO	27.62300		24.53595	6.07241								
G48	5/31/08 6:45	NO	31.26784				39.56971	5.47377	39.20517	5.44862	38.18809	6.39218		
G49	5/31/08 12:40	NO	28.39883				33.28243	6.31961						
G50	5/31/08 16:05	MI	16.13685				23.08766	4.22252						
G51	5/31/08 18:25	NO	23.06976				28.85151	5.36115						
G52	6/1/08	NO												
G53	6/1/08	PL		60.78510										
ICE	6/1/08	MI												
MQ nutrient blank 1 (May)	6/1/08	B	5.08892											
MQ nutrient blank 2 (May)	6/1/08	B	7.97710											
MQ1_MayDOC	6/1/08		5.08892				11.57823	1.62141	10.19600	1.33716				
MQ2_MayDOC	6/1/08		7.97710				7.09862	2.17497	7.10120	1.97457				
MQ1_MayTOC	6/2/08		5.88765						12.33667	-0.00462				
MQ2_MayTOC	6/2/08		5.28062						7.38254	0.39050			12.40395	0.11489
G55	5/25/08 19:36	NO												
GM50	5/25/08 15:00	GW												
GM51	5/25/08 18:40	GW												
GM52	5/25/08 19:00	GW												
GM53	5/25/08 19:20	GW												
GM54	5/25/08 19:30	GW												
G56	7/10/08 11:23	NO	35.35091				30.05662	5.38868						
G57	7/10/08 13:46	NO	22.57774				31.43824	3.38167						
G58	7/10/08 14:40	MM												
G59	7/11/08 12:30	NO	31.20394				33.31895	3.03383						
G60	7/11/08 12:30	NO	31.43397				32.06514	3.85715						
Be/Ra-July	7/11/08 16:15	NO												
G61	7/11/08 18:00	NO	17.34452				27.81682	2.56836	28.42841	3.03293	27.34207	2.69349		
G62	7/12/08 0:00	NO	15.29979				27.88377	3.73703						
G63	7/12/08 6:00	NO		14.10522										
G64	7/12/08 12:50	NO	13.14004				22.60075	3.08137						
G65	7/12/08 18:00	NO	11.57455				19.02193	1.26205						
G66	7/13/08 13:50	NO	10.98030				19.86794	0.25755	18.06144	0.70980	17.69509	1.27181		
G67	7/13/08 18:45	PL	30.35410				37.98724	4.55034						
G68	7/14/08 18:00	NO	12.81416				16.89776	1.48127	16.97887	1.53065	16.27695	1.23628		
G69	7/15/08 16:30	NO	13.20384	22.13297			18.37068	2.36891						
G70	7/15/08 15:24	MO	12.44995				21.73647	1.77156						
G71	7/16/08 22:00	NO	51.29340				58.06636	2.48328						
G72	7/19/08 20:00	F	60.08573	46.30542			59.84360	3.78708						
G73	7/22/08 0:00	F	85.44036						101.16236	4.78370				
G74	7/24/08 14:15	SWF												
G75	7/24/08 15:00	F												
G76	7/24/08 15:00	SWF												
G77	7/24/08 15:00	IB												
G78	7/26/08 11:30	F												
G79	7/26/08 11:40	SWF												
G80	7/26/08 12:00	IB												



Table A7: Greenland Ice Sheet Margins 2008 Particulate Organic Carbon (POC) and Nitrogen (PON)												
Sample ID	GFF #	Dry Filter Mass (mg)	Vol Fil (mL)	Date Collected	Sample Type	mmol N	mmol C	Total Filter + Spl (mg)	Sub-sample run (mg)	mg of sample run	% OC	%N
G1#35	35	127.1	120	5/17/08 13:55	MO	0.277542	4.296135	273.79	42.74	22.89904891	0.225321962	0.016980459
G2#25	25	115.7	200	5/17/08 16:04	PW	NaN	3.082921	126.5	23.13	1.974735178	1.87497976	NaN
G3#2	2	127.9	200	5/18/08 14:20	NO	0.123126	8.175528	278.66	48.8	26.40166511	0.371901122	0.006533653
G4#50	50	127.2	200	5/18/08 14:20	MI	0	3.768187	153.49	19.83	3.396512476	1.332423228	0
G5#77	77	130.6	120	5/19/08 12:41	NO	0.270584	7.414562	173.62	24.83	6.152439811	1.447375295	0.061615936
G6#87	87	132.5	150	5/19/08 13:55	NO	NaN	6.496627	171.55	23.86	5.431262023	1.436581169	NaN
G7#54	54	130.5	220	5/20/08 14:05	PL	0.045862	3.134611	133.71	24.02	0.576652457	6.528486469	0.111424122
G8#49	49	127.4	125	5/20/08 16:00	NO	NaN	7.154256	159.48	32.27	6.491231502	1.323672001	NaN
G10#1	1	127.7	150	5/20/08 16:30	MF	0.101247	3.856474	150.37	18.95	2.856929574	1.621189933	0.049650042
G11#40	40	124.9	150	5/21/08 14:23	NO	NaN	5.162527	155.09	21.15	4.117083629	1.505967698	NaN
G12#90	90	133.2	150	5/21/08 14:10	NO	1.022957	24.12706	153.24	22.37	2.925442443	9.905031333	0.489896128
G15#85	85	132.4	250	5/22/08 17:00	MI	0	2.788566	130.15	58.85	NaN	NaN	NaN
G16#84	84	131.6	175	5/22/08 18:00	NO	0.024484	6.972121	157.07	32.18	5.218212262	1.604671638	0.006573537
G20#98	98	133.2	1025	5/24/08 19:00	LO	1.36338	6.204377	191.25	28.95	8.787176471	0.847992112	0.217372982
G21#23	23	124.4	300	5/24/08 21:00	OO	0	7.384476	116.4	45.46	NaN	NaN	NaN
G23#20	20	72.4	450	5/25/08	NO	1.102413	8.669142	444.59	72.14	60.39224139	0.172400285	0.02557416
G28#21	21	128.2	150	5/26/08	NO	0	4.08573	301.28	35.33	20.29645645	0.241764442	0
G29#39	39	128.1	150	5/27/08 14:48	NO	0.325543	4.559665	298.13	45.13	25.73861705	0.212760349	0.017719897
G30#46	46	125.7	100	5/27/08 15:50	NO	0	4.4584	165.6	25.82	6.221123188	0.860702883	0
G35#28	28	126.5	150	5/28/08 16:30	MO	0.025649	7.296061	158.12	23.94	4.787394384	1.830342121	0.007505964
G38#82	82	132.9	150	5/28/08	MO	0.141854	4.533516	199.84	30.95	10.36725881	0.525187285	0.019169678
G40#10	10	105.8	850	5/29/08 12:40	T	0.065672	11.271672	130.04	28.66	5.342343894	2.533958677	0.01722231
G40#42	42	124	400	5/29/08 12:40	T	NaN	1.408601	129.06	19.38	0.759823338	2.226477289	NaN
G40#51	51	134.2	150	5/29/08 12:40	T	NaN	2.171532	132.18	21.13	NaN	NaN	NaN
G42#80	80	130.9	150	5/29/08 13:41	NO	0.041543	7.204174	180.05	18.62	5.082882533	1.702225724	0.011450492
G43#88	88	131.3	150	5/29/08 16:30	MM	0.343741	11.982439	208.3	35.13	12.98612578	1.108175728	0.037084287
G45#27	27	128	150	5/30/08 18:00	NO	NaN	6.784466	191.18	24.44	8.07678209	1.008835406	NaN
G47#24	24	126	150	5/31/08 0:00	NO	0.356797	7.808198	182.01	31.2	9.601186748	0.976717337	0.052063638
G48#4	4	128.7	150	5/31/08 6:45	NO	0.051144	7.752725	194.42	29.49	9.968536159	0.934041101	0.00718792
G49#22	22	107.5	150	5/31/08 12:40	NO	NaN	6.664277	170.02	29.04	10.67863075	0.749515296	NaN
G50#13	13	114.2	150	5/31/08 16:05	MI	NaN	1.230902	126.54	22	2.145408566	0.689059116	NaN
G51#43	43	125.7	150	5/31/08 18:25	NO	0.275453	11.391775	174.15	29.12	8.101429802	1.68877871	0.047634718
G53#16	16	106.3	250	6/1/08	PL	NaN	4.597002	201.71	29.35	13.88272024	0.397688626	NaN
G53#30	30	127.7	250	6/1/08	PL	0.362953	5.260505	201.28	26.65	9.742185016	0.648506093	0.052195342
G56#75	75	131.3	150	7/10/08 11:23	NO	0.288378	5.479742	162.647	21.804	4.202290777	1.5666090953	0.096142315
G57#61	61	129.1	150	7/10/08 13:46	NO	0.281382	5.471271	157.098	20.904	3.72551014	1.763784377	0.105815405
G60#73	73	131	160	7/11/08 12:30	NO	0.378035	7.982309	198.546	20.132	6.848972389	1.39973594	0.077329337
G61#72	72	130.1	180	7/11/08 18:00	NO	0.377347	7.707486	171.506	26.348	6.361091087	1.455204918	0.083108905
G63 #32	32	124	250	7/12/08 6:00	NO	0.547705	4.82467	142.935	22.273	2.950566726	1.963835917	0.26063431
G63 #33	33	127.8	250	7/12/08 6:00	NO	0.604943	11.272938	348.731	45.934	29.10049452	0.465242892	0.021291401
G63#29	29	127.6	250	7/12/08 6:00	NO	0.352117	11.522167	228.73	33.034	14.60555423	0.947456194	0.033775902
G63#31	31	128.4	250	7/12/08 6:00	NO	0.227422	4.292362	149.089	19.661	2.72834635	1.889469439	0.116780926
G63#36	36	128.7	250	7/12/08 6:00	NO	0.190678	3.791131	148.229	18.064	2.379911191	1.91315883	0.112248104

Sample ID	GFF #	Dry Filter Mass (mg)	Vol Fil (mL)	Date Collected	Sample Type	mmol N	mmol C	Total Filter + Spl (mg)	Sub-sample run (mg)	mg of sample run	% OC	%N
G63#37	37	128.3	250	7/12/08 6:00	NO	0.443648	8.061312	174.189	33.759	8.893596903	1.088607432	0.069887394
G63#38	38	126.7	250	7/12/08 6:00	NO	0.16677	3.499376	147.445	16.913	2.379600427	1.766158014	0.098186317
G63#41	41	128.2	250	7/12/08 6:00	NO	0.268091	4.697603	158.682	20.14	3.868790915	1.458290536	0.097083282
G63#53	53	127.5	250	7/12/08 6:00	NO	0.247867	4.436359	154.772	20	3.524151655	1.511872155	0.098537783
G63#58	58	131.4	250	7/12/08 6:00	NO	0.260259	4.863794	149.752	21.591	2.645961536	2.207672726	0.137803658
G63#8	8	122.8	250	7/12/08 6:00	NO	0.40107	7.064618	186.877	30.758	10.54640414	0.804502236	0.053278785
G63#9	9	102.1	500	7/12/08 6:00	NO	0.659649	10.83842	194.52	31.93	15.1705254	0.858041601	0.060918702
G63#93	93	131.6	250	7/12/08 6:00	NO	0.280912	5.58679	151.324	21.26	2.77108879	2.421335271	0.142022684
G63#94	94	130.6	250	7/12/08 6:00	NO	0.557181	10.803018	323.73	42.291	25.2298546	0.514248879	0.030939983
G63#95	95	130.9	250	7/12/08 6:00	NO	0.431809	7.603239	172.705	31.796	7.69654486	1.186440183	0.078602025
G64#70	70	128.7	170	7/12/08 12:50	NO	0.274106	5.637766	219.152	30.317	12.5129284	0.541116923	0.030690023
G65#69	69	129.7	175	7/12/08 18:00	NO	0.316257	5.866677	294.569	34.095	19.08282458	0.369226194	0.023218563
G66#6	6	105.9	175	7/13/08 13:50	NO	0.209195	4.000165	158.111	17.829	5.887445649	0.816007128	0.049780952
G68#14	14	123.9	175	7/14/08 18:00	NO	0.527302	4.417633	162.606	18.218	4.336530682	1.223461206	0.170354982
G69#1	1-Jul	129.7	180	7/15/08 16:30	NO	0.325954	6.733187	389.806	35.102	23.42252508	0.34524707	0.019496664
G70#2	2-Jul	130.6	200	7/15/08 15:24	MO	0.557213	4.951474	223.819	30.036	12.50977747	0.475365837	0.062403601
G71 #12	12-Jul	130.8	600	7/16/08 22:00	NO	0.935084	14.768116	224.296	36.376	15.16304569	1.169719311	0.086397745
G71#10	10-Jul	130.2	200	7/16/08 22:00	NO	1.106692	16.515882	238.229	32.036	14.52727016	1.365402692	0.106728657
G71#11	11-Jul	132.1	600	7/16/08 22:00	NO	0.851009	13.619846	465.699	42.165	30.20449225	0.541556366	0.039473067
G71#13	13-Jul	130.5	500	7/16/08 22:00	NO	0.514759	7.886768	207.341	20.788	7.704075451	1.229480259	0.093609793
G71#17	17-Jul	133	550	7/16/08 22:00	NO	0.944958	18.119363	1650.47	108.862	100.0895618	0.21741883	0.013227016
G71#18	18-Jul	132.9	600	7/16/08 22:00	NO	0.701155	11.208638	269.046	35.681	18.05574298	0.745556354	0.054404719
G71#19	19-Jul	132.8	500	7/16/08 22:00	NO	1.417413	22.457277	2378.427	272.616	257.3944251	0.104785448	0.00771499
G72#15	15-Jul	130.2	2200	7/19/08 20:00	F	2.791187	4.232608	155.6	29.79	4.862892031	1.04533736	0.804141475
G73#16	16-Jul	133.4	4700	7/22/08 0:00	F	0.788436	5.016597	172.505	28.701	6.506203327	0.92602894	0.169776148

<b>Table A8. Dissolved and Particulate Radiocarbon for Inland Lake and Margin Samples</b>										
<b>2008 MARGIN &amp; 2010 LAKE DOC SAMPLES</b>										
Receipt #	Sample	Type	F Modern	Fm Err	Age	Age Err	δ13C	Δ14C	[DOC] (µm/kg) on line	
82413	SL DOC (South Lake - Das July 6 2010 21:00 GRT)	DOC	0.7484	0.004	2330	45	-23.66	-257	43	
82414	NNL DOC (North Lake - Das July 3 2010 14:15 GRT)	DOC	0.795	0.0041	1840	40	-21.08	-210.74	22.1	
78141	Greenland15 (G15) (N Supraglacial May 22)	DOC	0.6647	0.0015	3280	20	-24.66	-340.1	9.85	
79623	MC 2FjordWater (Fjord seawater July 19)	DOC	0.5863	0.0027	4290	35	-21.61	-417.8	42.4	
79622	Greenland53 TOCfiltered (Clark Lake June 1)	DOC	0.698	0.0026	2890	30	-26.91	-306.8	75.2	
78142	Greenland20 (G20-TOC) (Clark Lake Outflow May 24)	DOC	0.6281	0.0025	3730	30	-28.49	-376.2	224.4	
78143	Greenland21 (G21) (O glacier floodplain May 24)	DOC	1.0074	0.0033	>Mod		-25.94	0.4	139.4	
78140	Greenladn 5 (G5) (N outflow May 19 12:41 GRT)	DOC	0.7594	0.0028	2210	30	-25.83	-245.9	42.2	
78144	Greenland40 (G40) (Tarn May 29)	DOC	1.0442	0.004	>Mod		-23.02	36.9	369.9	
78145	Greenland53 (G53) (Clark Lake June 1)	DOC	0.7362	0.0029	2460	30	-28.18	-269	67.5	
78146	Greenland63 (G63) (N outflow July 12 6:00 GRT)	DOC	0.6033	0.0039	4060	50	-25.86	-400.9	12.9	
78147	Greenland68 (G68) (N outflow July 14 18:00 GRT)	DOC	0.609	0.0047	3980	60	-23.73	-395.3	13	
78148	Greenland72 (G72) (Fjord Water in Plume July 19)	DOC	0.7914	0.0029	1880	30	-21.2	-214.1	47.5	
<b>2008 MARGIN &amp; 2010 LAKE POC SAMPLES</b>										
Receipt #	Sample	Type	F Modern	Fm Err	Age	Age Err	δ13C	Δ14C	POC Conc (mg/L)	
83674	SL-2010-POC (South Lake July 6 2010 21:00 GRT)	Sediment OC	0.8932	0.006	905	55	-24.82	-113.3	Not Measured	
83673	NNL-2010-POC (North Lake July 3 2010 14:15 GRT)	Sediment OC	0.8972	0.0066	870	60	-26.96	-109.41	Not Measured	
79866	G15 TOC-POC	Sediment OC	0.653	0.0046	3420	55	-26.53	-351.7	below detection limit	
79873	G72 TOC-POC	Sediment OC	0.8995	0.0025	850	20	-23.87	-107	12.07	
79874	MF2 TOC-POC	Sediment OC	0.8935	0.0024	905	20	-22.18	-113	Not Measured	
79865	G5 TOC-POC	Sediment OC	0.7481	0.0028	2330	30	-26.41	-257.1	518.9	
79867	G20 TOC-POC	Sediment OC	0.8085	0.0032	1710	30	-25.91	-197.2	48.03	
79868	G21 TOC-POC	Sediment OC	0.696	0.0037	2910	40	-24.99	-308.8	below detection limit	
79869	G40 TOC-POC	Sediment OC	1.0404	0.0032	>Mod		-21.69	33.1	50.21	
79870	G53 TOC-POC	Sediment OC	0.7534	0.0034	2270	35	-26.02	-251.9	171.3	
79871	G63 TOC-POC	Sediment OC	0.7426	0.0029	2390	30	-26.29	-262.6	223.6	
79872	G68 TOC-POC	Sediment OC	0.7487	0.0032	2320	35	-26.11	-256.5	270.6	
<b>2010 LAKE DIC SAMPLES - Taken in plastic bottles, seems like plastic is leaching some 14C dead material; NOT USABLE</b>										
Receipt #	Sample	Type	F Modern	Fm Err	Age	Age Err	δ13C	Δ14C		
82409	NNL DIC1,	DIC	0.9103	0.002	755	20	-13.91	-96.24		
82410	NNL DIC2,	DIC	0.9134	0.0025	725	20	-14.67	-93.16		
82411	SL DIC1,	DIC	0.8912	0.0022	925	20	-14.42	-115.21		

Table A9: Greenland Ice Sheet Margins 2008 Anions													
Sample	Sample Type	Dil.Fac.	Amount ppm F	Amount ppm Acetate	Amount ppm Formate	Amount ppm Pyruvate	Amount ppm Cl	Amount ppm NO2	Amount ppm Br	Amount ppm SO4	Amount ppm NO3	Amount ppm Oxalate	Amount ppm PO4
Cation #1 090113	standard	1	0.001	NaN	NaN	NaN	0.2259	NaN	NaN	NaN	NaN	NaN	NaN
Cation #1 090113	standard	1	NaN	NaN	NaN	NaN	0.2249	NaN	NaN	NaN	0.1884	NaN	NaN
Cation #2 090113	standard	1	NaN	NaN	NaN	NaN	0.4389	NaN	NaN	NaN	0.4291	NaN	NaN
Cation #3 090113	standard	1	0.0004	NaN	NaN	NaN	2.8471	NaN	NaN	NaN	3.267	NaN	NaN
Cation #3 090113	standard	1	NaN	NaN	NaN	NaN	2.8149	NaN	NaN	NaN	3.0617	NaN	NaN
Cation #4 090113	standard	1	0.0005	NaN	NaN	NaN	7.7319	NaN	NaN	NaN	8.0562	NaN	NaN
Cation #4 090113	standard	1	0.0007	NaN	NaN	NaN	7.7159	NaN	NaN	NaN	8.0303	NaN	NaN
Cation #5 090113	standard	1	NaN	NaN	NaN	NaN	20.4035	NaN	NaN	NaN	19.1072	NaN	NaN
Cation #5 090113	standard	1	NaN	NaN	NaN	NaN	20.4067	NaN	NaN	NaN	18.9096	NaN	NaN
Cation #6 090113	standard	1	NaN	NaN	NaN	NaN	216.5163	0.0006	NaN	116.2791	NaN	NaN	NaN
Cation #6 090113	standard	1	NaN	NaN	NaN	NaN	217.5363	NaN	NaN	116.5833	NaN	NaN	NaN
A#1 090113	standard	1	0.0008	NaN	NaN	NaN	0.0141	NaN	NaN	NaN	NaN	NaN	NaN
A#1 090113	standard	1	0.0004	NaN	NaN	NaN	0.0136	NaN	NaN	NaN	NaN	NaN	NaN
A#2 090113	standard	1	0.003	NaN	NaN	NaN	0.0195	NaN	NaN	NaN	0.0005	NaN	NaN
A#2 090113	standard	1	0.001	NaN	NaN	NaN	0.0201	0.0041	NaN	NaN	NaN	NaN	NaN
A#2 090113	standard	1	0.0012	NaN	NaN	NaN	0.02	0.0037	NaN	NaN	NaN	NaN	NaN
A#3 090113	standard	1	0.0086	NaN	NaN	NaN	0.0243	0.0336	0.0319	0.0123	0.0367	NaN	0.0647
A#3 090113	standard	1	0.0061	NaN	NaN	NaN	0.0228	0.0331	NaN	0.0141	0.0375	NaN	0.0029
A#4 090113	standard	1	0.0157	NaN	NaN	NaN	0.0477	0.0722	0.0779	0.037	0.0788	NaN	0.1403
A#4 090113	standard	1	0.017	NaN	NaN	NaN	0.0475	0.0747	0.0818	0.0371	0.0802	NaN	0.0032
A#5 090113	standard	1	0.0339	NaN	NaN	NaN	0.1033	0.1643	0.1616	0.0761	0.1693	NaN	0.2967
A#5 090113	standard	1	0.0323	NaN	NaN	NaN	0.1042	0.1668	0.0084	0.0815	0.1761	NaN	0.3076
A#6 090113	standard	1	0.1961	NaN	NaN	NaN	2.5106	0.9273	1.0384	0.5644	0.0437	NaN	1.896
A#6 090113	standard	1	0.1984	NaN	NaN	NaN	2.4491	0.932	1.0349	0.5658	1.0589	NaN	1.8621
A#7 090113	standard	1	0.4106	NaN	NaN	NaN	17.8859	2.0683	NaN	21.9796	2.2846	NaN	4.1451
A#7 090113	standard	1	0.418	NaN	NaN	NaN	17.873	2.0711	NaN	21.9705	2.2939	NaN	4.1491
Blank - NEW 125uL sample loops	blank	1	NaN	NaN	NaN	NaN	NaN	NaN	NaN	NaN	NaN	NaN	NaN
Blank - DI's are filled with Elix	blank	1	NaN	NaN	NaN	NaN	0.0135	NaN	NaN	NaN	NaN	NaN	NaN
Blank	blank	1	NaN	NaN	NaN	NaN	0.0115	NaN	NaN	NaN	NaN	NaN	NaN
DI - CD2 stabilized before CD1;	unknown	1	NaN	NaN	NaN	NaN	0.0016	NaN	NaN	NaN	NaN	NaN	NaN
DI	unknown	1	NaN	NaN	NaN	NaN	NaN	NaN	NaN	NaN	NaN	NaN	NaN
MC Cation 090113	unknown	1	NaN	NaN	NaN	NaN	0.3691	NaN	NaN	NaN	0.4157	NaN	NaN
MC Anion 090113	unknown	1	0.0067	NaN	NaN	NaN	0.0298	0.0369	0.0312	0.0156	0.0404	NaN	0.0688
DI	unknown	1	NaN	NaN	NaN	NaN	NaN	NaN	NaN	NaN	NaN	NaN	NaN
A17	unknown	1	0.0167	NaN	NaN	NaN	0.0378	NaN	NaN	2.9732	NaN	NaN	NaN
A2	unknown	1	0.0105	NaN	NaN	NaN	0.1757	NaN	NaN	0.9225	0.0531	NaN	NaN
G69	unknown	1	0.0015	NaN	NaN	NaN	0.024	NaN	NaN	0.0945	0.0051	NaN	NaN
G59	unknown	1	0.0021	NaN	NaN	NaN	0.0428	NaN	NaN	0.1414	0.0058	NaN	NaN
G48	unknown	1	0.0199	NaN	NaN	NaN	0.2787	NaN	NaN	1.4238	0.0891	NaN	NaN
DI	unknown	1	NaN	NaN	NaN	NaN	NaN	NaN	NaN	NaN	NaN	NaN	NaN
MC Cation 090113	unknown	1	NaN	NaN	NaN	NaN	0.3552	NaN	NaN	NaN	0.3953	NaN	NaN
MC Anion 090113	unknown	1	0.0114	NaN	NaN	NaN	0.0269	0.0339	0.0361	0.0189	0.0346	NaN	0.0628
DI	unknown	1	NaN	NaN	NaN	NaN	NaN	NaN	NaN	NaN	NaN	NaN	NaN
G49	unknown	1	0.0221	NaN	NaN	NaN	0.2664	NaN	NaN	1.5915	0.0937	NaN	NaN
G39 - peak at 20.8 mins in CD2	unknown	1	0.0379	NaN	NaN	NaN	0.5251	NaN	73.7608	NaN	NaN	NaN	NaN
G28	unknown	1	0.0084	NaN	NaN	NaN	0.0812	NaN	NaN	0.66	0.0226	NaN	NaN
G19	unknown	1	0.0096	NaN	NaN	NaN	0.3387	NaN	NaN	5.8429	0.1242	NaN	NaN
G58	unknown	1	0.0058	NaN	NaN	NaN	0.0501	NaN	NaN	0.2204	0.0498	NaN	NaN
DI	unknown	1	NaN	NaN	NaN	NaN	NaN	NaN	NaN	NaN	NaN	NaN	NaN
MC Anion 090113	unknown	1	0.012	NaN	NaN	NaN	0.0253	0.0353	0.0212	0.0115	0.03	NaN	0.0622
MC Cation 090113	unknown	1	NaN	NaN	NaN	NaN	0.336	NaN	NaN	NaN	0.3599	NaN	NaN
DI	unknown	1	NaN	NaN	NaN	NaN	0.0065	NaN	NaN	NaN	NaN	NaN	NaN
G10	unknown	1	0.0203	NaN	NaN	NaN	0.3042	NaN	NaN	1.2552	0.1127	NaN	NaN
A15	unknown	1	0.0207	NaN	NaN	NaN	0.0298	NaN	NaN	2.3965	NaN	NaN	NaN
A1	unknown	1	0.0176	NaN	NaN	NaN	0.1296	0.003	NaN	1.1288	0.0578	NaN	NaN
G68	unknown	1	0.001	NaN	NaN	NaN	0.0305	NaN	NaN	0.0882	NaN	NaN	NaN
G9	unknown	1	0.0171	NaN	NaN	NaN	0.4543	NaN	NaN	6.0907	0.1723	NaN	NaN
DI	unknown	1	NaN	NaN	NaN	NaN	NaN	NaN	NaN	NaN	NaN	NaN	NaN
MC Anion 090113	unknown	1	0.0085	NaN	NaN	NaN	0.025	0.0341	0.0227	0.0136	0.0387	NaN	0.0699
MC Cation 090113	unknown	1	NaN	NaN	NaN	NaN	0.3276	NaN	NaN	NaN	0.3551	NaN	NaN
DI	unknown	1	NaN	NaN	NaN	NaN	NaN	NaN	NaN	NaN	NaN	NaN	NaN
A2-2	unknown	1	0.0107	NaN	NaN	NaN	0.159	0.0019	NaN	0.8527	0.0567	NaN	NaN
G49-2	unknown	1	0.0207	NaN	NaN	NaN	0.2501	NaN	NaN	1.525	0.0858	NaN	NaN
G10-2	unknown	1	0.0222	NaN	NaN	NaN	0.2984	NaN	NaN	1.2354	0.1086	NaN	NaN
DI	unknown	1	NaN	NaN	NaN	NaN	NaN	NaN	NaN	NaN	NaN	NaN	NaN
Shutdown	unknown	1	NaN	NaN	NaN	NaN	NaN	NaN	NaN	NaN	NaN	NaN	NaN
Cation #1 090113	standard	1	0.001	NaN	NaN	NaN	0.2259	NaN	NaN	NaN	NaN	NaN	NaN
Cation #1 090113	standard	1	NaN	NaN	NaN	NaN	0.2249	NaN	NaN	NaN	0.1884	NaN	NaN
Cation #2 090113	standard	1	NaN	NaN	NaN	NaN	0.4389	NaN	NaN	NaN	0.4291	NaN	NaN
Cation #3 090113	standard	1	0.0004	NaN	NaN	NaN	2.8471	NaN	NaN	NaN	3.267	NaN	NaN
Cation #3 090113	standard	1	NaN	NaN	NaN	NaN	2.8149	NaN	NaN	NaN	3.0617	NaN	NaN
Cation #4 090113	standard	1	0.0005	NaN	NaN	NaN	7.7319	NaN	NaN	NaN	8.0562	NaN	NaN
Cation #4 090113	standard	1	0.0007	NaN	NaN	NaN	7.7159	NaN	NaN	NaN	8.0303	NaN	NaN
Cation #5 090113	standard	1	NaN	NaN	NaN	NaN	20.4035	NaN	NaN	NaN	19.1072	NaN	NaN
Cation #5 090113	standard	1	NaN	NaN	NaN	NaN	20.4067	NaN	NaN	NaN	18.9096	NaN	NaN
Cation #6 090113	standard	1	NaN	NaN	NaN	NaN	216.5163	0.0006	NaN	116.2791	NaN	NaN	NaN
Cation #6 090113	standard	1	NaN	NaN	NaN	NaN	217.5363	NaN	NaN	116.5833	NaN	NaN	NaN
A#1 090113	standard	1	0.0008	NaN	NaN	NaN	0.0141	NaN	NaN	NaN	NaN	NaN	NaN
A#1 090113	standard	1	0.0004	NaN	NaN	NaN	0.0136	NaN	NaN	NaN	NaN	NaN	NaN
A#2 090113	standard	1	0.003	NaN	NaN	NaN	0.0195	NaN	NaN	NaN	0.0005	NaN	NaN
A#2 090113	standard	1	0.001	NaN	NaN	NaN	0.0201	0.0041	NaN	NaN	NaN	NaN	NaN
A#2 090113	standard	1	0.0012	NaN	NaN	NaN	0.02	0.0037	NaN	NaN	NaN	NaN	NaN
A#3 090113	standard	1	0.0086	NaN	NaN	NaN	0.0243	0.0336	0.0319	0.0123	0.0367	NaN	0.0647
A#3 090113	standard	1	0.0061	NaN	NaN	NaN	0.0228	0.0331	NaN	0.0141	0.0375	NaN	0.0029
A#4 090113	standard	1	0.0157	NaN	NaN	NaN	0.0477	0.0722	0.0779	0.037	0.0788	NaN	0.1403
A#4 090113	standard	1	0.017	NaN	NaN	NaN	0.0475	0.0747	0.0818	0.0371	0.0802	NaN	0.0032
A#5 090113	standard	1	0.0339	NaN	NaN	NaN	0.1033	0.1643	0.1616	0.0761	0.1693	NaN	0.2967
A#5 090113	standard	1	0.0323	NaN	NaN	NaN	0.1042	0.1668	0.0084	0.0815	0.1761	NaN	0.3076
A#6 090113	standard	1	0.1961	NaN	NaN	NaN	2.5106	0.9273	1.0384	0.5644	0.0437	NaN	1.896
A#6 090113	standard	1	0.1984	NaN	NaN	NaN	2.4491	0.932	1.0349	0.5658	1.0589	NaN	1.8621
A#7 090113	standard	1	0.4106	NaN	NaN	NaN	17.8859	2.0683	NaN	21.9796	2.2846	NaN	4.1451

Sample	Sample Type	Dil.Fac.	Amount ppm	Amount ppm	Amount ppm	Amount ppm	Amount ppm	Amount ppm	Amount ppm	Amount ppm	Amount ppm	Amount ppm	Amount ppm	Amount ppm
			F	Acetate	Formate	Pyruvate	Cl	NO2	Br	SO4	NO3	Oxalate	PO4	
A#7 090113	standard	1	0.418	NaN	NaN	NaN	17.873	2.0711	NaN	21.9705	2.2939	NaN	4.1491	
Blank - NEW 125uL sample loops	blank	1	NaN	NaN	NaN	NaN	NaN	NaN	NaN	NaN	NaN	NaN	NaN	
Blank - DI's are filled with Elix	blank	1	NaN	NaN	NaN	NaN	NaN	NaN	NaN	NaN	NaN	NaN	NaN	
Blank	blank	1	NaN	NaN	NaN	NaN	NaN	NaN	NaN	NaN	NaN	NaN	NaN	
DI - CD2 stabilized before CD1;	unknown	1	NaN	NaN	NaN	NaN	0.0013	NaN	NaN	NaN	NaN	NaN	NaN	
DI	unknown	1	NaN	NaN	NaN	NaN	NaN	NaN	NaN	NaN	NaN	NaN	NaN	
MC Cation 090113	unknown	1	NaN	NaN	NaN	NaN	0.3413	NaN	NaN	NaN	0.3691	NaN	NaN	
MC Anion 090113	unknown	1	0.0126	NaN	NaN	NaN	0.024	0.0314	0.0277	0.0148	0.0325	NaN	0.0695	
DI	unknown	1	NaN	NaN	NaN	NaN	NaN	NaN	NaN	NaN	NaN	NaN	NaN	
G38	unknown	1	0.021	NaN	NaN	NaN	0.0689	NaN	NaN	0.5241	NaN	NaN	NaN	
G27	unknown	1	0.0096	NaN	NaN	NaN	0.5038	NaN	NaN	6.1673	0.2528	NaN	NaN	
G18	unknown	1	0.0175	NaN	NaN	NaN	0.3331	NaN	NaN	7.9476	0.215	NaN	NaN	
A13	unknown	1	0.0163	NaN	NaN	NaN	0.0359	NaN	NaN	0.8931	0.018	NaN	NaN	
G67	unknown	1	0.0209	NaN	NaN	NaN	5.766	NaN	NaN	1.3399	0.0833	NaN	NaN	
G65	unknown	1	0.0054	NaN	NaN	NaN	0.022	NaN	NaN	0.1256	0.0028	NaN	NaN	
DI	unknown	1	NaN	NaN	NaN	NaN	NaN	NaN	NaN	NaN	NaN	NaN	NaN	
MC Cation 090113	unknown	1	NaN	NaN	NaN	NaN	0.342	NaN	NaN	NaN	0.3579	NaN	NaN	
MC Anion 090113	unknown	1	0.0103	NaN	NaN	NaN	0.0248	0.0328	0.0234	0.0098	0.0343	NaN	0.0639	
DI	unknown	1	NaN	NaN	NaN	NaN	0.0029	NaN	NaN	NaN	NaN	NaN	NaN	
G57	unknown	1	0.002	NaN	NaN	NaN	0.03	NaN	NaN	0.1034	NaN	NaN	NaN	
G47	unknown	1	0.0155	NaN	NaN	NaN	0.2206	NaN	NaN	1.1802	0.0747	NaN	NaN	
G37	unknown	1	0.0438	NaN	NaN	NaN	0.3814	NaN	NaN	1.3633	0.0512	NaN	NaN	
G26B	unknown	1	NaN	NaN	NaN	NaN	0.4577	NaN	NaN	0.2045	0.1306	NaN	NaN	
G17	unknown	1	0.018	NaN	NaN	NaN	0.3554	NaN	NaN	7.3072	0.3076	NaN	NaN	
MQ	unknown	1	NaN	NaN	NaN	NaN	0.0698	NaN	NaN	NaN	NaN	NaN	NaN	
DI	unknown	1	NaN	NaN	NaN	NaN	NaN	NaN	NaN	NaN	NaN	NaN	NaN	
MC Anion 090113	unknown	1	0.0116	NaN	NaN	NaN	0.025	0.0313	0.0208	0.0091	0.0276	NaN	0.065	
MC Cation 090113	unknown	1	NaN	NaN	NaN	NaN	0.3362	NaN	NaN	NaN	0.3514	NaN	NaN	
DI	unknown	1	NaN	NaN	NaN	NaN	NaN	NaN	NaN	NaN	NaN	NaN	NaN	
G8	unknown	1	0.0228	NaN	NaN	NaN	0.3416	NaN	NaN	3.0978	0.0816	NaN	NaN	
A12	unknown	1	0.0224	NaN	NaN	NaN	0.0313	NaN	NaN	2.5606	0.0744	NaN	NaN	
G66	unknown	1	0.0059	NaN	NaN	NaN	0.0197	NaN	NaN	0.1623	0.0033	NaN	NaN	
G56	unknown	1	0.0064	NaN	NaN	NaN	0.1195	NaN	NaN	0.1766	NaN	NaN	NaN	
G46	unknown	1	0.0025	NaN	NaN	NaN	0.0506	NaN	NaN	0.2326	NaN	NaN	NaN	
G45	unknown	1	0.0108	NaN	NaN	NaN	0.1891	NaN	NaN	0.7838	0.0538	NaN	NaN	
DI	unknown	1	NaN	NaN	NaN	NaN	NaN	NaN	NaN	NaN	NaN	NaN	NaN	
MC Anion 090113	unknown	1	0.012	NaN	NaN	NaN	0.0254	0.0313	0.0335	0.0177	0.0347	NaN	0.0671	
MC Cation 090113	unknown	1	NaN	NaN	NaN	NaN	0.3439	NaN	NaN	NaN	0.3609	NaN	NaN	
DI	unknown	1	NaN	NaN	NaN	NaN	0.0028	NaN	NaN	NaN	NaN	NaN	NaN	
G35	unknown	1	0.0421	NaN	NaN	NaN	0.3323	NaN	NaN	1.5095	0.0769	NaN	NaN	
G26	unknown	1	NaN	NaN	NaN	NaN	0.4315	NaN	NaN	0.1993	0.13	NaN	NaN	
G16	unknown	1	0.0178	NaN	NaN	NaN	0.4728	NaN	NaN	7.8546	0.1315	NaN	NaN	
G7	unknown	1	0.0519	NaN	NaN	NaN	1.3142	NaN	NaN	0.3208	NaN	NaN	NaN	
A11	unknown	1	0.0229	NaN	NaN	NaN	0.0311	NaN	NaN	1.7981	0.0009	NaN	NaN	
G18-2	unknown	1	0.0129	NaN	NaN	NaN	0.3257	NaN	NaN	7.9297	0.2064	NaN	NaN	
G8-2	unknown	1	0.0228	NaN	NaN	NaN	0.344	NaN	NaN	3.2097	0.085	NaN	NaN	
G7-2	unknown	1	0.0583	NaN	NaN	NaN	1.3088	NaN	NaN	0.3181	NaN	NaN	NaN	
MQ-2	unknown	1	NaN	NaN	NaN	NaN	0.0711	NaN	NaN	NaN	NaN	NaN	NaN	
DI	unknown	1	NaN	NaN	NaN	NaN	NaN	NaN	NaN	NaN	0.0002	NaN	NaN	
Shutdown	unknown	1	NaN	NaN	NaN	NaN	NaN	NaN	NaN	NaN	NaN	NaN	NaN	
Cation #1 090113	standard	1	0.001	NaN	NaN	NaN	0.2259	NaN	NaN	NaN	NaN	NaN	NaN	
Cation #1 090113	standard	1	NaN	NaN	NaN	NaN	0.2249	NaN	NaN	NaN	0.1884	NaN	NaN	
Cation #2 090113	standard	1	NaN	NaN	NaN	NaN	0.4389	NaN	NaN	NaN	0.4291	NaN	NaN	
Cation #3 090113	standard	1	0.0004	NaN	NaN	NaN	2.8471	NaN	NaN	NaN	3.267	NaN	NaN	
Cation #3 090113	standard	1	NaN	NaN	NaN	NaN	2.8149	NaN	NaN	NaN	3.0617	NaN	NaN	
Cation #4 090113	standard	1	0.0005	NaN	NaN	NaN	7.7319	NaN	NaN	NaN	8.0562	NaN	NaN	
Cation #4 090113	standard	1	0.0007	NaN	NaN	NaN	7.7159	NaN	NaN	NaN	8.0303	NaN	NaN	
Cation #5 090113	standard	1	NaN	NaN	NaN	NaN	20.4035	NaN	NaN	NaN	19.1072	NaN	NaN	
Cation #5 090113	standard	1	NaN	NaN	NaN	NaN	20.4067	NaN	NaN	NaN	18.9096	NaN	NaN	
Cation #6 090113	standard	1	NaN	NaN	NaN	NaN	216.5163	0.0006	NaN	116.2791	NaN	NaN	NaN	
Cation #6 090113	standard	1	NaN	NaN	NaN	NaN	217.5363	NaN	NaN	116.5833	NaN	NaN	NaN	
A#1 090113	standard	1	0.0008	NaN	NaN	NaN	0.0141	NaN	NaN	NaN	NaN	NaN	NaN	
A#1 090113	standard	1	0.0004	NaN	NaN	NaN	0.0136	NaN	NaN	NaN	NaN	NaN	NaN	
A#2 090113	standard	1	0.003	NaN	NaN	NaN	0.0195	NaN	NaN	NaN	0.0005	NaN	NaN	
A#2 090113	standard	1	0.001	NaN	NaN	NaN	0.0201	0.0041	NaN	NaN	NaN	NaN	NaN	
A#2 090113	standard	1	0.0012	NaN	NaN	NaN	0.02	0.0037	NaN	NaN	NaN	NaN	NaN	
A#3 090113	standard	1	0.0086	NaN	NaN	NaN	0.0243	0.0336	0.0319	0.0123	0.0367	NaN	0.0647	
A#3 090113	standard	1	0.0061	NaN	NaN	NaN	0.0228	0.0331	NaN	0.0141	0.0375	NaN	0.0029	
A#4 090113	standard	1	0.0157	NaN	NaN	NaN	0.0477	0.0722	0.0779	0.037	0.0788	NaN	0.1403	
A#4 090113	standard	1	0.017	NaN	NaN	NaN	0.0475	0.0747	0.0818	0.0371	0.0802	NaN	0.0032	
A#5 090113	standard	1	0.0339	NaN	NaN	NaN	0.1033	0.1643	0.1616	0.0761	0.1693	NaN	0.2967	
A#5 090113	standard	1	0.0323	NaN	NaN	NaN	0.1042	0.1668	0.0084	0.0815	0.1761	NaN	0.3076	
A#6 090113	standard	1	0.1961	NaN	NaN	NaN	2.5106	0.9273	1.0384	0.5644	0.0437	NaN	1.896	
A#6 090113	standard	1	0.1984	NaN	NaN	NaN	2.4491	0.932	1.0349	0.5658	1.0589	NaN	1.8621	
A#7 090113	standard	1	0.4106	NaN	NaN	NaN	17.8859	2.0683	NaN	21.9796	2.2846	NaN	4.1451	
A#7 090113	standard	1	0.418	NaN	NaN	NaN	17.873	2.0711	NaN	21.9705	2.2939	NaN	4.1491	
Blank - NEW 125uL sample loops	blank	1	NaN	NaN	NaN	NaN	NaN	NaN	NaN	NaN	NaN	NaN	NaN	
Blank - DI's are filled with Elix	blank	1	NaN	NaN	NaN	NaN	NaN	NaN	NaN	NaN	NaN	NaN	NaN	
Blank	blank	1	NaN	NaN	NaN	NaN	0.0023	NaN	NaN	NaN	NaN	NaN	NaN	
DI - CD2 stabilized before CD1;	unknown	1	NaN	NaN	NaN	NaN	0.0028	NaN	NaN	NaN	NaN	NaN	NaN	
DI	unknown	1	NaN	NaN	NaN	NaN	NaN	NaN	NaN	NaN	NaN	NaN	NaN	
MC Cation 090113	unknown	1	NaN	NaN	NaN	NaN	0.3147	NaN	NaN	NaN	0.3399	NaN	NaN	
MC Anion 090113	unknown	1	0.0076	NaN	NaN	NaN	0.0215	0.0348	0.0201	0.0115	0.033	NaN	0.0671	
DI	unknown	1	NaN	NaN	NaN	NaN	NaN	NaN	NaN	NaN	NaN	NaN	NaN	
G34	unknown	1	0.018	NaN	NaN	NaN	0.2055	NaN	NaN	2.0359	0.1075	NaN	NaN	
G25	unknown	1	0.0058	NaN	NaN	NaN	0.2253	NaN	NaN	0.708	0.1055	NaN	NaN	
G15B	unknown	1	NaN	NaN	NaN	NaN	0.1259	NaN	NaN	0.023	0.0179	NaN	NaN	
G6	unknown	1	0.0147	NaN	NaN	NaN	0.2987	NaN	NaN	4.4245	0.192	NaN	NaN	
A9	unknown	1	0.0181	NaN	NaN	NaN	0.1263	NaN	NaN	1.5029	0.0164	NaN	0.3232	
G64	unknown	1	0.0064	NaN	NaN	NaN	0.0384	NaN	NaN	0.1891	0.0127	NaN	NaN	
MQ	unknown	1	NaN	NaN	NaN	NaN	0.0759	NaN	NaN	NaN	NaN	NaN	NaN	
MC Cation 090113	unknown	1	NaN	NaN	NaN	NaN	0.3114	NaN	NaN	NaN	0.34	NaN	NaN	

Sample	Sample Type	Dil.Fac.	Amount	Amount	Amount	Amount	Amount	Amount	Amount	Amount	Amount	Amount	Amount	Amount
			ppm	ppm	ppm	ppm	ppm	ppm	ppm	ppm	ppm	ppm	ppm	ppm
			F	Acetate	Formate	Pyruvate	Cl	NO2	Br	SO4	NO3	Oxalate	PO4	
MC Anion 090113	unknown	1	0.0092	NaN	NaN	NaN	0.021	0.0325	0.0223	0.0094	0.035	NaN	0.0653	
DI	unknown	1	NaN	NaN	NaN	NaN	NaN	NaN	NaN	NaN	NaN	NaN	NaN	
G44	unknown	1	0.0202	NaN	NaN	NaN	0.228	NaN	NaN	1.5386	0.0653	NaN	NaN	
G33	unknown	1	0.0139	NaN	NaN	NaN	0.1573	NaN	NaN	1.4964	0.0534	NaN	0.0475	
G24	unknown	1	0.0207	NaN	NaN	NaN	0.1537	NaN	NaN	3.5922	0.1719	NaN	NaN	
G15	unknown	1	NaN	NaN	NaN	NaN	0.0555	NaN	NaN	0.016	0.0137	NaN	NaN	
G5	unknown	1	0.0144	NaN	NaN	NaN	0.2924	NaN	NaN	4.6341	0.1087	NaN	NaN	
A6	unknown	1	0.0153	NaN	NaN	NaN	0.0756	NaN	NaN	0.4988	0.0314	NaN	NaN	
DI	unknown	1	NaN	NaN	NaN	NaN	NaN	NaN	NaN	NaN	NaN	NaN	NaN	
MC Anion 090113	unknown	1	0.016	NaN	NaN	NaN	0.0199	0.0322	0.0284	0.0146	0.0307	NaN	0.0632	
MC Cation 090113	unknown	1	NaN	NaN	NaN	NaN	0.3062	NaN	NaN	NaN	0.3342	NaN	NaN	
DI	unknown	1	NaN	NaN	NaN	NaN	NaN	NaN	NaN	NaN	NaN	NaN	NaN	
G63	unknown	1	0.005	NaN	NaN	NaN	0.0238	NaN	NaN	0.2712	NaN	NaN	NaN	
G53	unknown	1	0.0221	NaN	NaN	NaN	7.933	NaN	NaN	2.1856	0.2069	NaN	NaN	
G43	unknown	1	0.011	NaN	NaN	NaN	0.1737	NaN	NaN	0.3908	0.034	NaN	NaN	
G32	unknown	1	0.0128	NaN	NaN	NaN	0.1925	0.001	NaN	1.638	0.0591	NaN	NaN	
G23	unknown	1	0.008	NaN	NaN	NaN	0.0987	NaN	NaN	0.9616	0.0348	NaN	NaN	
G14	unknown	1	0.0178	NaN	NaN	NaN	0.1823	NaN	NaN	0.6032	0.1131	NaN	NaN	
G4	unknown	1	0.0009	NaN	NaN	NaN	0.0756	NaN	NaN	0.3232	0.0132	NaN	NaN	
DI	unknown	1	NaN	NaN	NaN	NaN	NaN	NaN	NaN	NaN	NaN	NaN	NaN	
MC Anion 090113	unknown	1	0.0146	NaN	NaN	NaN	0.0213	0.0353	0.0223	0.0115	0.0349	NaN	0.065	
MC Cation 090113	unknown	1	NaN	NaN	NaN	NaN	0.3087	NaN	NaN	NaN	0.3388	NaN	NaN	
DI	unknown	1	NaN	NaN	NaN	NaN	NaN	NaN	NaN	NaN	NaN	NaN	NaN	
A23	unknown	1	0.0231	NaN	NaN	NaN	0.0225	NaN	NaN	0.5742	0.0006	NaN	NaN	
A5	unknown	1	0.0124	NaN	NaN	NaN	0.0574	0.0013	NaN	0.4575	0.0219	NaN	NaN	
G62	unknown	1	0.0055	NaN	NaN	NaN	0.0302	NaN	NaN	0.2085	0.0083	NaN	NaN	
G8-REP0225	unknown	1	0.0176	NaN	NaN	NaN	0.3371	NaN	NaN	3.1746	0.0857	NaN	NaN	
G10-REP0225	unknown	1	0.0144	NaN	NaN	NaN	0.3061	NaN	NaN	1.2655	0.1078	NaN	NaN	
G15B-2	unknown	1	0.0017	NaN	NaN	NaN	0.1267	NaN	NaN	0.0245	0.0215	NaN	NaN	
G5-2	unknown	1	0.0153	NaN	NaN	NaN	0.3075	NaN	NaN	4.7541	0.1115	NaN	NaN	
G4-2	unknown	1	0.0038	NaN	NaN	NaN	0.0721	NaN	NaN	0.3001	0.0118	NaN	NaN	
DI	unknown	1	NaN	NaN	NaN	NaN	NaN	NaN	NaN	NaN	NaN	NaN	NaN	
Shutdown	unknown	1	NaN	NaN	NaN	NaN	NaN	NaN	NaN	NaN	NaN	NaN	NaN	
Cation #1 090113	standard	1	0.001	NaN	NaN	NaN	0.2259	NaN	NaN	NaN	NaN	NaN	NaN	
Cation #1 090113	standard	1	NaN	NaN	NaN	NaN	0.2249	NaN	NaN	NaN	0.1884	NaN	NaN	
Cation #2 090113	standard	1	NaN	NaN	NaN	NaN	0.4389	NaN	NaN	NaN	0.4291	NaN	NaN	
Cation #3 090113	standard	1	0.0004	NaN	NaN	NaN	2.8471	NaN	NaN	NaN	3.267	NaN	NaN	
Cation #3 090113	standard	1	NaN	NaN	NaN	NaN	2.8149	NaN	NaN	NaN	3.0617	NaN	NaN	
Cation #4 090113	standard	1	0.0005	NaN	NaN	NaN	7.7319	NaN	NaN	NaN	8.0562	NaN	NaN	
Cation #4 090113	standard	1	0.0007	NaN	NaN	NaN	7.7159	NaN	NaN	NaN	8.0303	NaN	NaN	
Cation #5 090113	standard	1	NaN	NaN	NaN	NaN	20.4035	NaN	NaN	NaN	19.1072	NaN	NaN	
Cation #5 090113	standard	1	NaN	NaN	NaN	NaN	20.4067	NaN	NaN	NaN	18.9096	NaN	NaN	
Cation #6 090113	standard	1	NaN	NaN	NaN	NaN	216.5163	0.0006	NaN	116.2791	NaN	NaN	NaN	
Cation #6 090113	standard	1	NaN	NaN	NaN	NaN	217.5363	NaN	NaN	116.5833	NaN	NaN	NaN	
A#1 090113	standard	1	0.0008	NaN	NaN	NaN	0.0141	NaN	NaN	NaN	NaN	NaN	NaN	
A#1 090113	standard	1	0.0004	NaN	NaN	NaN	0.0136	NaN	NaN	NaN	NaN	NaN	NaN	
A#2 090113	standard	1	0.003	NaN	NaN	NaN	0.0195	NaN	NaN	NaN	0.0005	NaN	NaN	
A#2 090113	standard	1	0.001	NaN	NaN	NaN	0.0201	0.0041	NaN	NaN	NaN	NaN	NaN	
A#2 090113	standard	1	0.0012	NaN	NaN	NaN	0.02	0.0037	NaN	NaN	NaN	NaN	NaN	
A#3 090113	standard	1	0.0086	NaN	NaN	NaN	0.0243	0.0336	0.0319	0.0123	0.0367	NaN	0.0647	
A#3 090113	standard	1	0.0061	NaN	NaN	NaN	0.0228	0.0331	NaN	0.0141	0.0375	NaN	0.0029	
A#4 090113	standard	1	0.0157	NaN	NaN	NaN	0.0477	0.0722	0.0779	0.037	0.0788	NaN	0.1403	
A#4 090113	standard	1	0.017	NaN	NaN	NaN	0.0475	0.0747	0.0818	0.0371	0.0802	NaN	0.0032	
A#5 090113	standard	1	0.0339	NaN	NaN	NaN	0.1033	0.1643	0.1616	0.0761	0.1693	NaN	0.2967	
A#5 090113	standard	1	0.0323	NaN	NaN	NaN	0.1042	0.1668	0.0084	0.0815	0.1761	NaN	0.3076	
A#6 090113	standard	1	0.1961	NaN	NaN	NaN	2.5106	0.9273	1.0384	0.5644	0.0437	NaN	1.896	
A#6 090113	standard	1	0.1984	NaN	NaN	NaN	2.4491	0.932	1.0349	0.5658	1.0589	NaN	1.8621	
A#7 090113	standard	1	0.4106	NaN	NaN	NaN	17.8859	2.0683	NaN	21.9796	2.2846	NaN	4.1451	
A#7 090113	standard	1	0.418	NaN	NaN	NaN	17.873	2.0711	NaN	21.9705	2.2939	NaN	4.1491	
Blank - NEW 125uL sample loops	blank	1	0.0013	NaN	NaN	NaN	NaN	NaN	NaN	NaN	NaN	NaN	NaN	
Blank - DI's are filled with Elix	blank	1	NaN	NaN	NaN	NaN	NaN	NaN	NaN	NaN	NaN	NaN	NaN	
Blank	blank	1	NaN	NaN	NaN	NaN	NaN	NaN	NaN	NaN	NaN	NaN	NaN	
DI - CD2 stabilized before CD1;	unknown	1	NaN	NaN	NaN	NaN	NaN	NaN	NaN	NaN	NaN	NaN	NaN	
DI	unknown	1	NaN	NaN	NaN	NaN	NaN	NaN	NaN	NaN	NaN	NaN	NaN	
MC Cation 090113	unknown	1	NaN	NaN	NaN	NaN	0.3064	NaN	NaN	NaN	0.3293	NaN	NaN	
MC Anion 090113	unknown	1	0.0132	NaN	NaN	NaN	0.0211	0.0329	0.0126	0.0115	0.0352	NaN	0.0646	
DI	unknown	1	NaN	NaN	NaN	NaN	NaN	NaN	NaN	NaN	NaN	NaN	NaN	
G52	unknown	1	0.0081	NaN	NaN	NaN	0.1307	NaN	NaN	0.5435	0.0284	NaN	NaN	
G42	unknown	1	0.0087	NaN	NaN	NaN	0.118	0.0023	NaN	0.5685	0.0301	NaN	NaN	
G31	unknown	1	0.01	NaN	NaN	NaN	0.1942	NaN	NaN	0.8598	0.0886	NaN	NaN	
G22	unknown	1	0.0086	NaN	NaN	NaN	0.0888	NaN	NaN	1.0316	0.0409	NaN	NaN	
G13	unknown	1	0.0329	NaN	NaN	NaN	0.5095	NaN	NaN	7.9378	0.1889	NaN	NaN	
G3	unknown	1	0.0233	NaN	NaN	NaN	0.263	NaN	NaN	3.0835	0.0672	NaN	NaN	
A21	unknown	1	0.0259	NaN	NaN	NaN	0.0254	0.001	NaN	0.9432	0.0089	NaN	NaN	
DI	unknown	1	NaN	NaN	NaN	NaN	NaN	NaN	NaN	NaN	NaN	NaN	NaN	
MC Cation 090113	unknown	1	NaN	NaN	NaN	NaN	0.3039	NaN	NaN	NaN	0.3275	NaN	NaN	
MC Anion 090113	unknown	1	0.0129	NaN	NaN	NaN	0.0267	0.0325	0.0145	0.012	0.0327	NaN	0.0654	
DI	unknown	1	NaN	NaN	NaN	NaN	0.0014	NaN	NaN	NaN	NaN	NaN	NaN	
A4	unknown	1	0.0278	NaN	NaN	NaN	0.1253	0.0026	NaN	0.7888	0.0428	NaN	NaN	
G71	unknown	1	0.0138	NaN	NaN	NaN	0.0273	NaN	NaN	0.1172	NaN	NaN	0.0033	
G61	unknown	1	0.0064	NaN	NaN	NaN	0.0126	NaN	NaN	0.0828	NaN	NaN	NaN	
G51	unknown	1	0.0178	NaN	NaN	NaN	0.1385	NaN	NaN	0.7169	0.0518	NaN	NaN	
G41	unknown	1	0.0319	NaN	NaN	NaN	0.1542	0.0012	NaN	1.3821	0.0497	NaN	NaN	
G30	unknown	1	0.0313	NaN	NaN	NaN	0.1365	NaN	NaN	1.2295	0.0326	NaN	NaN	
G21	unknown	1	0.0241	NaN	NaN	NaN	48.7834	NaN	NaN	5.2044	0.1094	NaN	0.0031	
DI	unknown	1	NaN	NaN	NaN	NaN	NaN	NaN	NaN	NaN	NaN	NaN	NaN	
MC Anion 090113	unknown	1	0.0122	NaN	NaN	NaN	0.0251	0.0307	0.0248	0.0148	0.0341	NaN	0.0655	
MC Cation 090113	unknown	1	NaN	NaN	NaN	NaN	0.2983	NaN	NaN	NaN	0.3214	NaN	NaN	
DI	unknown	1	NaN	NaN	NaN	NaN	NaN	NaN	NaN	NaN	NaN	NaN	NaN	
G12	unknown	1	0.0606	NaN	NaN	NaN	1.0413	NaN	NaN	45.0898	2.4026	NaN	NaN	
G2	unknown	1	0.0385	NaN	NaN	NaN	0.9676	NaN	NaN	0.185	NaN	NaN	NaN	
A19	unknown	1	0.0357	NaN	NaN	NaN	0.0226	NaN	NaN	2.2716	NaN	NaN	NaN	

Sample	Sample Type	Dil.Fac.	Amount ppm	Amount ppm	Amount ppm	Amount ppm	Amount ppm	Amount ppm	Amount ppm	Amount ppm	Amount ppm	Amount ppm	Amount ppm	Amount ppm
			F	Acetate	Formate	Pyruvate	Cl	NO2	Br	SO4	NO3	Oxalate	PO4	
A3	unknown	1	0.0122	NaN	NaN	NaN	0.0771	0.0024	NaN	0.5924	0.0283	NaN	NaN	
G70	unknown	1	0.0089	NaN	NaN	NaN	0.0413	NaN	NaN	0.1661	0.0074	NaN	NaN	
G60	unknown	1	0.0219	NaN	NaN	NaN	0.0135	NaN	NaN	0.199	0.0036	NaN	NaN	
G50	unknown	1	NaN	NaN	NaN	NaN	0.0633	NaN	NaN	0.0037	NaN	NaN	NaN	
DI	unknown	1	NaN	NaN	NaN	NaN	NaN	NaN	NaN	NaN	NaN	NaN	NaN	
MC Anion 090113	unknown	1	0.0122	NaN	NaN	NaN	0.0254	0.0336	0.027	0.0168	0.0346	NaN	NaN	0.0644
MC Cation 090113	unknown	1	NaN	NaN	NaN	NaN	0.2941	NaN	NaN	NaN	0.3208	NaN	NaN	
DI	unknown	1	NaN	NaN	NaN	NaN	NaN	NaN	NaN	NaN	NaN	NaN	NaN	
G40	unknown	1	0.0672	NaN	NaN	NaN	1.8468	NaN	NaN	1.7347	NaN	NaN	NaN	
G29	unknown	1	0.0336	NaN	NaN	NaN	0.1556	NaN	NaN	0.8247	0.0238	NaN	NaN	
G20	unknown	1	0.0368	NaN	NaN	NaN	6.7709	NaN	NaN	1.3245	0.078	NaN	NaN	
G7-REP0226	unknown	1	0.0695	NaN	NaN	NaN	1.2357	NaN	NaN	0.2895	NaN	NaN	NaN	
G8-REP0226	unknown	1	0.0295	NaN	NaN	NaN	0.3221	NaN	NaN	3.0926	0.0816	NaN	NaN	
G3-2	unknown	1	0.025	NaN	NaN	NaN	0.2512	NaN	NaN	3.0443	0.0654	NaN	NaN	
G21-2	unknown	1	0.0231	NaN	NaN	NaN	48.6592	NaN	NaN	5.1521	0.1084	NaN	NaN	0.0026
G29-2	unknown	1	0.0357	NaN	NaN	NaN	6.6958	NaN	NaN	1.2792	0.0751	NaN	NaN	
G79	unknown	1	0.0262	NaN	NaN	NaN	45.6981	NaN	NaN	4.4572	NaN	NaN	NaN	
DI	unknown	1	NaN	NaN	NaN	NaN	NaN	NaN	NaN	NaN	NaN	NaN	NaN	
Shutdown	unknown	1	NaN	NaN	NaN	NaN	NaN	NaN	NaN	NaN	NaN	NaN	NaN	
Cation #1 090113	standard	1	0.001	NaN	NaN	NaN	0.2259	NaN	NaN	NaN	NaN	NaN	NaN	
Cation #1 090113	standard	1	NaN	NaN	NaN	NaN	0.2249	NaN	NaN	NaN	0.1884	NaN	NaN	
Cation #2 090113	standard	1	NaN	NaN	NaN	NaN	0.4389	NaN	NaN	NaN	0.4291	NaN	NaN	
Cation #3 090113	standard	1	0.0004	NaN	NaN	NaN	2.8471	NaN	NaN	NaN	3.267	NaN	NaN	
Cation #3 090113	standard	1	NaN	NaN	NaN	NaN	2.8149	NaN	NaN	NaN	3.0617	NaN	NaN	
Cation #4 090113	standard	1	0.0005	NaN	NaN	NaN	7.7319	NaN	NaN	NaN	8.0562	NaN	NaN	
Cation #4 090113	standard	1	0.0007	NaN	NaN	NaN	7.7159	NaN	NaN	NaN	8.0303	NaN	NaN	
Cation #5 090113	standard	1	NaN	NaN	NaN	NaN	20.4035	NaN	NaN	NaN	19.1072	NaN	NaN	
Cation #5 090113	standard	1	NaN	NaN	NaN	NaN	20.4067	NaN	NaN	NaN	18.9096	NaN	NaN	
Cation #6 090113	standard	1	NaN	NaN	NaN	NaN	216.5163	0.0006	NaN	116.2791	NaN	NaN	NaN	
Cation #6 090113	standard	1	NaN	NaN	NaN	NaN	217.5363	NaN	NaN	116.5833	NaN	NaN	NaN	
A#1 090113	standard	1	0.0008	NaN	NaN	NaN	0.0141	NaN	NaN	NaN	NaN	NaN	NaN	
A#1 090113	standard	1	0.0004	NaN	NaN	NaN	0.0136	NaN	NaN	NaN	NaN	NaN	NaN	
A#2 090113	standard	1	0.003	NaN	NaN	NaN	0.0195	NaN	NaN	NaN	0.0005	NaN	NaN	
A#2 090113	standard	1	0.001	NaN	NaN	NaN	0.0201	0.0041	NaN	NaN	NaN	NaN	NaN	
A#2 090113	standard	1	0.0012	NaN	NaN	NaN	0.02	0.0037	NaN	NaN	NaN	NaN	NaN	
A#3 090113	standard	1	0.0086	NaN	NaN	NaN	0.0243	0.0336	0.0319	0.0123	0.0367	NaN	NaN	0.0647
A#3 090113	standard	1	0.0061	NaN	NaN	NaN	0.0228	0.0331	NaN	0.0141	0.0375	NaN	NaN	0.0029
A#4 090113	standard	1	0.0157	NaN	NaN	NaN	0.0477	0.0722	0.0779	0.037	0.0788	NaN	NaN	0.1403
A#4 090113	standard	1	0.017	NaN	NaN	NaN	0.0475	0.0747	0.0818	0.0371	0.0802	NaN	NaN	0.0032
A#5 090113	standard	1	0.0339	NaN	NaN	NaN	0.1033	0.1643	0.1616	0.0761	0.1693	NaN	NaN	0.2967
A#5 090113	standard	1	0.0323	NaN	NaN	NaN	0.1042	0.1668	0.0084	0.0815	0.1761	NaN	NaN	0.3076
A#6 090113	standard	1	0.1961	NaN	NaN	NaN	2.5106	0.9273	1.0384	0.5644	0.0437	NaN	NaN	1.896
A#6 090113	standard	1	0.1984	NaN	NaN	NaN	2.4491	0.932	1.0349	0.5658	1.0589	NaN	NaN	1.8621
A#7 090113	standard	1	0.4106	NaN	NaN	NaN	17.8859	2.0683	NaN	21.9796	2.2846	NaN	NaN	4.1451
A#7 090113	standard	1	0.418	NaN	NaN	NaN	17.873	2.0711	NaN	21.9705	2.2939	NaN	NaN	4.1491
Blank - NEW 125uL sample loops	blank	1	NaN	NaN	NaN	NaN	NaN	NaN	NaN	NaN	NaN	NaN	NaN	
Blank - DI's are filled with Elix	blank	1	NaN	NaN	NaN	NaN	NaN	NaN	NaN	NaN	NaN	NaN	NaN	
Blank	blank	1	NaN	NaN	NaN	NaN	NaN	NaN	NaN	NaN	NaN	NaN	NaN	
DI - CD2 stabilized before CD1;	unknown	1	NaN	NaN	NaN	NaN	NaN	NaN	NaN	NaN	NaN	NaN	NaN	
DI	unknown	1	NaN	NaN	NaN	NaN	NaN	NaN	NaN	NaN	NaN	NaN	NaN	
MC Cation 090113	unknown	1	NaN	NaN	NaN	NaN	0.297	NaN	NaN	NaN	0.3302	NaN	NaN	
MC Anion 090113	unknown	1	0.0126	NaN	NaN	NaN	0.0191	0.031	0.0264	0.0137	0.0325	NaN	NaN	0.0624
DI	unknown	1	NaN	NaN	NaN	NaN	NaN	NaN	NaN	NaN	NaN	NaN	NaN	
G11	unknown	1	0.0156	NaN	NaN	NaN	0.4809	NaN	NaN	6.5608	0.1336	NaN	NaN	
G1	unknown	1	0.0586	NaN	NaN	NaN	0.8436	NaN	NaN	2.6313	0.0814	NaN	NaN	
G12-REP0227	unknown	1	0.0671	NaN	NaN	NaN	1.2244	NaN	NaN	48.0354	2.8606	NaN	NaN	
G21-REP0227	unknown	1	0.0246	NaN	NaN	NaN	62.8053	NaN	NaN	6.9525	0.0555	NaN	NaN	
DI	unknown	1	NaN	NaN	NaN	NaN	NaN	NaN	NaN	NaN	NaN	NaN	NaN	
MC Cation 090113	unknown	1	NaN	NaN	NaN	NaN	0.2917	NaN	NaN	NaN	0.3147	NaN	NaN	
MC Anion 090113	unknown	1	0.0106	NaN	NaN	NaN	0.0197	0.0321	0.0178	0.0076	0.0346	NaN	NaN	0.064
DI	unknown	1	NaN	NaN	NaN	NaN	NaN	NaN	NaN	NaN	NaN	NaN	NaN	
G79-REP0227	unknown	1	0.0105	NaN	NaN	NaN	56.5144	NaN	NaN	5.8007	NaN	NaN	NaN	
G78	unknown	1	NaN	NaN	NaN	NaN	NaN	NaN	NaN	NaN	NaN	NaN	NaN	
G75	unknown	1	0.3878	NaN	NaN	NaN	NaN	NaN	NaN	NaN	NaN	NaN	NaN	
G74	unknown	1	0.0147	NaN	NaN	NaN	27.4739	NaN	NaN	2.3891	NaN	NaN	NaN	
G73	unknown	1	NaN	NaN	NaN	NaN	NaN	NaN	NaN	NaN	NaN	NaN	NaN	
G72 - "NO2" peak inserted by SK	unknown	1	NaN	NaN	NaN	NaN	NaN	17194.46	NaN	NaN	NaN	NaN	NaN	
DI	unknown	1	NaN	NaN	NaN	NaN	0.2088	NaN	0.1499	NaN	NaN	NaN	NaN	
G11-2	unknown	1	0.0205	NaN	NaN	NaN	0.5528	NaN	NaN	6.1409	0.2846	NaN	NaN	
G75-2	unknown	1	0.3408	NaN	NaN	NaN	NaN	NaN	NaN	NaN	NaN	NaN	NaN	
G72-2	unknown	1	NaN	NaN	NaN	NaN	NaN	NaN	NaN	NaN	NaN	NaN	NaN	
DI	unknown	1	0.0564	NaN	NaN	NaN	0.2319	NaN	0.1531	NaN	NaN	NaN	NaN	
MC Anion 090113	unknown	1	0.0136	NaN	NaN	NaN	0.1676	0.0357	0.0327	0.0383	0.0359	NaN	NaN	
MC Cation 090113	unknown	1	NaN	NaN	NaN	NaN	0.3337	NaN	NaN	NaN	0.3447	NaN	NaN	
DI	unknown	1	NaN	NaN	NaN	NaN	0.0028	NaN	NaN	NaN	NaN	NaN	NaN	
Shutdown	unknown	1	NaN	NaN	NaN	NaN	NaN	NaN	NaN	NaN	NaN	NaN	NaN	
Shutdown	unknown	1	NaN	NaN	NaN	NaN	NaN	NaN	NaN	NaN	NaN	NaN	NaN	

Table A10: Greenland Ice Sheet Margins 2008 Cations									
Sample	Sample Type	Dil.Fac.	Amount ppm Li	Amount ppm Na	Amount ppm NH4	Amount ppm K	Amount ppm Mg	Amount ppm Ca	Amount ppm Sr
Cation #1 090113	standard	1	0.0017	0.0078	0.025	0.0051	0.0398	0.0355	NaN
Cation #1 090113	standard	1	0.0017	0.0078	0.0255	0.005	0.04	0.0348	0.0023
Cation #2 090113	standard	1	0.0034	0.0148	0.0474	0.0103	0.082	0.0702	0.0053
Cation #3 090113	standard	1	0.0197	0.0803	0.2218	0.0671	0.5522	0.3968	0.0176
Cation #3 090113	standard	1	0.0197	0.0804	0.2224	0.0692	0.5527	0.4007	0.0185
Cation #4 090113	standard	1	0.0496	0.1963	0.4675	0.1787	1.3259	0.9965	0.095
Cation #4 090113	standard	1	0.0497	0.197	0.471	0.1851	1.3264	1.0004	0.0947
Cation #5 090113	standard	1	0.1254	0.4979	0.9743	0.5082	2.9991	2.4927	0.2405
Cation #5 090113	standard	1	0.1257	0.4976	0.9743	0.5101	3.0039	2.5034	0.2406
Cation #6 090113	standard	1	1.3017	5.1457	NaN	5.3029	31.3221	25.815	1.305
Cation #6 090113	standard	1	1.2884	5.0585	10.7963	5.0055	28.5307	25.989	1.3162
A#1 090113	standard	1	NaN	0.0177	0.0066	0.0025	NaN	0.0116	NaN
A#1 090113	standard	1	NaN	0.0181	0.0069	0.0027	NaN	0.0035	NaN
A#2 090113	standard	1	NaN	0.031	0.002	0.0051	NaN	0.0028	NaN
A#2 090113	standard	1	NaN	0.031	0.0022	0.0053	NaN	0.0026	NaN
A#2 090113	standard	1	NaN	0.0308	0.0026	0.0054	NaN	0.0026	NaN
A#3 090113	standard	1	NaN	0.1531	0.0028	0.0283	NaN	0.0018	NaN
A#3 090113	standard	1	NaN	0.1542	0.003	0.0286	NaN	0.0023	NaN
A#4 090113	standard	1	NaN	0.3094	0.0008	0.0592	NaN	0.0028	NaN
A#4 090113	standard	1	NaN	0.3109	0.0009	0.0591	NaN	0.0033	NaN
A#5 090113	standard	1	NaN	0.6358	0.0096	0.1183	NaN	0.0027	NaN
A#5 090113	standard	1	NaN	0.6378	0.0102	0.1191	NaN	NaN	NaN
A#6 090113	standard	1	NaN	3.2256	NaN	0.6301	NaN	0.0058	NaN
A#6 090113	standard	1	NaN	3.2259	NaN	0.6307	NaN	0.0051	NaN
A#7 090113	standard	1	NaN	17.2763	NaN	14.1764	NaN	0.0026	NaN
A#7 090113	standard	1	NaN	17.323	NaN	14.197	NaN	0.0032	NaN
Blank - NEW 125ul sample loops	blank	1	NaN	NaN	NaN	NaN	NaN	NaN	NaN
Blank - DI's are filled with Elix	blank	1	NaN	NaN	NaN	NaN	NaN	NaN	NaN
Blank	blank	1	NaN	NaN	NaN	NaN	NaN	NaN	NaN
DI - CD2 stabilized before CD1;	unknown	1	NaN	NaN	0.0012	NaN	NaN	0.002	NaN
DI	unknown	1	NaN	NaN	NaN	NaN	NaN	0.0024	NaN
MC Cation 090113	unknown	1	0.0039	0.0154	0.0515	0.0114	0.1071	0.077	0.0113
MC Anion 090113	unknown	1	NaN	0.1683	0.0009	0.0328	NaN	0.0098	NaN
DI	unknown	1	NaN	NaN	0.0008	NaN	NaN	0.0052	NaN
A17	unknown	1	0.0016	0.3597	0.069	1.1289	0.3573	0.7997	0.0028
A2	unknown	1	0.0009	0.5085	0.102	0.7277	0.3261	0.6211	NaN
G69	unknown	1	0.0003	0.0888	0.0255	0.1923	0.0612	0.1307	NaN
G59	unknown	1	0.0004	0.1306	0.0301	0.2437	0.0866	0.1846	NaN
G48	unknown	1	0.0013	0.9197	0.0441	1.2753	0.5239	0.9571	0.0021
DI	unknown	1	NaN	NaN	NaN	NaN	0.0004	0.0048	NaN
MC Cation 090113	unknown	1	0.0039	0.0156	0.052	0.012	0.1077	0.08	0.0116
MC Anion 090113	unknown	1	NaN	0.1711	0.0009	0.0333	0.001	0.0085	NaN
DI	unknown	1	NaN	NaN	0.0012	NaN	NaN	0.003	NaN
G49	unknown	1	0.0012	0.8904	0.0479	1.2342	0.5348	0.9938	0.0039
G39 - peak at 20.8 mins in CD2	unknown	1	0.0025	1.0511	0.0664	2.14	1.4097	7.6809	0.0204
G28	unknown	1	0.0004	0.3462	0.0459	0.4305	0.2025	0.4117	NaN
G19	unknown	1	0.0012	1.0032	0.0535	1.1336	0.9138	2.1357	0.0076
G58	unknown	1	0.0005	0.2008	0.006	0.3812	0.1834	0.4239	NaN
DI	unknown	1	NaN	NaN	0.0009	NaN	NaN	0.0052	NaN
MC Anion 090113	unknown	1	NaN	0.1709	0.001	0.0332	NaN	0.0092	NaN
MC Cation 090113	unknown	1	0.0039	0.0156	0.0525	0.0118	0.1073	0.0807	0.011
DI	unknown	1	NaN	0.009	0.0024	0.0012	0.0009	0.0059	NaN
G10	unknown	1	0.0009	0.7012	0.0024	0.7509	0.5402	1.1783	0.0049
A15	unknown	1	0.0015	0.2917	0.0865	0.9966	0.3071	0.7071	0.0022
A1	unknown	1	0.0009	0.4612	0.1201	0.7491	0.3148	0.6209	NaN
G68	unknown	1	0.0002	0.096	0.0192	0.1672	0.0614	0.1253	NaN
G9	unknown	1	0.0014	1.2973	0.049	1.5134	1.0591	2.398	0.0093
DI	unknown	1	NaN	NaN	0.0008	NaN	0.0008	0.007	NaN
MC Anion 090113	unknown	1	NaN	0.1725	0.001	0.0336	0.0006	0.0095	NaN
MC Cation 090113	unknown	1	0.0039	0.0157	0.0524	0.012	0.1082	0.082	0.0117
DI	unknown	1	NaN	NaN	0.0009	NaN	0.0005	0.0037	NaN
A2-2	unknown	1	0.0009	0.5156	0.1034	0.737	0.3252	0.632	0.0042
G49-2	unknown	1	0.0012	0.8934	0.0483	1.2364	0.5337	1.0038	0.0037
G10-2	unknown	1	0.0009	0.7052	0.0025	0.7544	0.5433	1.1863	0.0043
DI	unknown	1	NaN	NaN	0.001	NaN	0.001	0.008	NaN
Shutdown	unknown	1	NaN	NaN	NaN	NaN	NaN	NaN	NaN
Cation #1 090113	standard	1	0.0017	0.0078	0.025	0.0051	0.0398	0.0355	NaN
Cation #1 090113	standard	1	0.0017	0.0078	0.0255	0.005	0.04	0.0348	0.0023
Cation #2 090113	standard	1	0.0034	0.0148	0.0474	0.0103	0.082	0.0702	0.0053
Cation #3 090113	standard	1	0.0197	0.0803	0.2218	0.0671	0.5522	0.3968	0.0176
Cation #3 090113	standard	1	0.0197	0.0804	0.2224	0.0692	0.5527	0.4007	0.0185
Cation #4 090113	standard	1	0.0496	0.1963	0.4675	0.1787	1.3259	0.9965	0.095
Cation #4 090113	standard	1	0.0497	0.197	0.471	0.1851	1.3264	1.0004	0.0947
Cation #5 090113	standard	1	0.1254	0.4979	0.9743	0.5082	2.9991	2.4927	0.2405
Cation #5 090113	standard	1	0.1257	0.4976	0.9743	0.5101	3.0039	2.5034	0.2406
Cation #6 090113	standard	1	1.3017	5.1457	NaN	5.3029	31.3221	25.815	1.305
Cation #6 090113	standard	1	1.2884	5.0585	10.7963	5.0055	28.5307	25.989	1.3162
A#1 090113	standard	1	NaN	0.0177	0.0066	0.0025	NaN	0.0116	NaN
A#1 090113	standard	1	NaN	0.0181	0.0069	0.0027	NaN	0.0035	NaN
A#2 090113	standard	1	NaN	0.031	0.002	0.0051	NaN	0.0028	NaN
A#2 090113	standard	1	NaN	0.031	0.0022	0.0053	NaN	0.0026	NaN
A#2 090113	standard	1	NaN	0.0308	0.0026	0.0054	NaN	0.0026	NaN
A#3 090113	standard	1	NaN	0.1531	0.0028	0.0283	NaN	0.0018	NaN
A#3 090113	standard	1	NaN	0.1542	0.003	0.0286	NaN	0.0023	NaN
A#4 090113	standard	1	NaN	0.3094	0.0008	0.0592	NaN	0.0028	NaN
A#4 090113	standard	1	NaN	0.3109	0.0009	0.0591	NaN	0.0033	NaN
A#5 090113	standard	1	NaN	0.6358	0.0096	0.1183	NaN	0.0027	NaN
A#5 090113	standard	1	NaN	0.6378	0.0102	0.1191	NaN	NaN	NaN
A#6 090113	standard	1	NaN	3.2256	NaN	0.6301	NaN	0.0058	NaN
A#6 090113	standard	1	NaN	3.2259	NaN	0.6307	NaN	0.0051	NaN
A#7 090113	standard	1	NaN	17.2763	NaN	14.1764	NaN	0.0026	NaN



Sample	Sample Type	Dil.Fac.	Amount	Amount	Amount	Amount	Amount	Amount	Amount	Amount
			ppm	ppm	ppm	ppm	ppm	ppm	ppm	ppm
			Li	Na	NH4	K	Mg	Ca	Sr	
A#7 090113	standard	1	NaN	17.323	NaN	NaN	14.197	NaN	0.0032	NaN
Blank - NEW 125uL sample loops	blank	1	NaN	NaN	NaN	NaN	NaN	NaN	NaN	NaN
Blank - DI's are filled with Elix	blank	1	NaN	NaN	NaN	NaN	NaN	NaN	NaN	NaN
Blank	blank	1	NaN	NaN	NaN	NaN	NaN	NaN	NaN	NaN
DI - CD2 stabilized before CD1;	unknown	1	NaN	0.001	NaN	NaN	0.0006	NaN	0.0506	NaN
DI	unknown	1	NaN	NaN	NaN	NaN	NaN	NaN	0.0038	NaN
MC Cation 090113	unknown	1	0.004	0.0191	0.0528	0.0127	0.1102	0.1374	0.011	
MC Anion 090113	unknown	1	NaN	0.1759	0.0005	0.033	0.0008	0.0272	NaN	
DI	unknown	1	NaN	NaN	NaN	NaN	NaN	0.005	NaN	
G38	unknown	1	0.0008	0.3203	0.004	0.6874	0.267	0.5979	0	
G27	unknown	1	0.0013	1.0178	0.0914	1.233	0.9261	2.3334	0.0082	
G18	unknown	1	0.0013	1.0385	0.0522	1.2124	1.1481	2.8404	0.0106	
A13	unknown	1	0.0008	0.1526	0.0653	0.4515	0.1742	0.41	NaN	
G67	unknown	1	0.0015	5.1842	NaN	0.8596	0.8344	0.7251	NaN	
G65	unknown	1	0.0003	0.1061	0.0056	0.2022	0.0778	0.1556	NaN	
DI	unknown	1	NaN	NaN	NaN	NaN	0.0006	0.0045	NaN	
MC Cation 090113	unknown	1	0.004	0.0282	0.0535	0.0137	0.1128	0.1737	0.0116	
MC Anion 090113	unknown	1	NaN	0.1796	0.0008	0.0339	0.0012	0.0289	NaN	
DI	unknown	1	NaN	0.0039	0.0011	NaN	0.0012	0.0515	NaN	
G57	unknown	1	0.0004	0.1178	0.0141	0.2392	0.0924	0.1748	NaN	
G47	unknown	1	0.0012	0.8593	0.0376	1.2134	0.4869	0.9097	0.0034	
G37	unknown	1	0.0017	1.2442	0.0135	1.458	0.6065	1.6647	0.0059	
G26B	unknown	1	NaN	0.5317	0.112	0.0298	0.081	0.0661	NaN	
G17	unknown	1	0.0013	1.0952	0.0476	1.2345	1.0981	2.7229	0.01	
MQ	unknown	1	NaN	0.0101	0.0115	0.0048	0.0046	0.0196	NaN	
DI	unknown	1	NaN	NaN	0.0007	NaN	NaN	0.0045	NaN	
MC Anion 090113	unknown	1	NaN	0.1795	0.0009	0.0338	0.001	0.0314	NaN	
MC Cation 090113	unknown	1	0.004	0.0272	0.0538	0.0136	0.1124	0.1659	0.0115	
DI	unknown	1	NaN	NaN	0.0008	NaN	NaN	0.0045	NaN	
G8	unknown	1	0.001	0.9805	0.055	1.0876	0.6934	1.6468	0.0107	
A12	unknown	1	0.0015	0.2756	0.0748	0.9869	0.3165	0.7649	0.0033	
G66	unknown	1	0.0003	0.1085	0.0006	0.214	0.0855	0.1744	NaN	
G56	unknown	1	0.0004	0.241	0.0252	0.4239	0.1013	0.2361	NaN	
G46	unknown	1	NaN	0.0917	0.0063	0.0778	0.0716	0.2007	NaN	
G45	unknown	1	0.0009	0.6701	0.036	0.922	0.3745	0.657	NaN	
DI	unknown	1	NaN	NaN	0.0007	NaN	0.0009	0.006	NaN	
MC Anion 090113	unknown	1	NaN	0.1785	0.0009	0.0337	0.0011	0.0319	0.0003	
MC Cation 090113	unknown	1	0.004	0.0271	0.0537	0.0133	0.1125	0.1647	0.0118	
DI	unknown	1	NaN	0.0038	0.0009	NaN	0.0013	0.0517	NaN	
G35	unknown	1	0.0021	1.2923	0.0148	1.7192	0.6395	1.7413	0.006	
G26	unknown	1	NaN	0.5014	0.1051	0.0267	0.0795	0.0617	NaN	
G16	unknown	1	0.0014	1.4784	0.0457	1.5851	1.2772	3.1097	0.0111	
G7	unknown	1	0.0011	1.5736	0.0078	0.5944	0.7284	0.8833	0.0061	
A11	unknown	1	0.0013	0.2397	0.0983	0.8765	0.2661	0.6389	0.0027	
G18-2	unknown	1	0.0014	1.0461	0.0501	1.2214	1.1555	2.8622	0.0101	
G8-2	unknown	1	0.001	0.9834	0.0554	1.0908	0.6968	1.6595	0.0063	
G7-2	unknown	1	0.0011	1.5709	0.008	0.5915	0.7276	0.8842	0.0031	
MQ-2	unknown	1	NaN	0.0104	0.0119	0.0045	0.0066	0.0257	NaN	
DI	unknown	1	NaN	NaN	0.0011	NaN	0.0014	0.0086	NaN	
Shutdown	unknown	1	NaN	NaN	NaN	NaN	NaN	NaN	NaN	
Cation #1 090113	standard	1	0.0017	0.0078	0.025	0.0051	0.0398	0.0355	NaN	
Cation #1 090113	standard	1	0.0017	0.0078	0.0255	0.005	0.04	0.0348	0.0023	
Cation #2 090113	standard	1	0.0034	0.0148	0.0474	0.0103	0.082	0.0702	0.0053	
Cation #3 090113	standard	1	0.0197	0.0803	0.2218	0.0671	0.5522	0.3968	0.0176	
Cation #3 090113	standard	1	0.0197	0.0804	0.2224	0.0692	0.5527	0.4007	0.0185	
Cation #4 090113	standard	1	0.0496	0.1963	0.4675	0.1787	1.3259	0.9965	0.095	
Cation #4 090113	standard	1	0.0497	0.197	0.471	0.1851	1.3264	1.0004	0.0947	
Cation #5 090113	standard	1	0.1254	0.4979	0.9743	0.5082	2.9991	2.4927	0.2405	
Cation #5 090113	standard	1	0.1257	0.4976	0.9743	0.5101	3.0039	2.5034	0.2406	
Cation #6 090113	standard	1	1.3017	5.1457	NaN	5.3029	31.3221	25.815	1.305	
Cation #6 090113	standard	1	1.2884	5.0585	10.7963	5.0055	28.5307	25.989	1.3162	
A#1 090113	standard	1	NaN	0.0177	0.0006	0.0025	NaN	0.0116	NaN	
A#1 090113	standard	1	NaN	0.0181	0.0009	0.0027	NaN	0.0035	NaN	
A#2 090113	standard	1	NaN	0.031	0.002	0.0051	NaN	0.0028	NaN	
A#2 090113	standard	1	NaN	0.031	0.0022	0.0053	NaN	0.0026	NaN	
A#2 090113	standard	1	NaN	0.0308	0.0026	0.0054	NaN	0.0026	NaN	
A#3 090113	standard	1	NaN	0.1531	0.0028	0.0283	NaN	0.0018	NaN	
A#3 090113	standard	1	NaN	0.1542	0.003	0.0286	NaN	0.0023	NaN	
A#4 090113	standard	1	NaN	0.3094	0.0008	0.0592	NaN	0.0028	NaN	
A#4 090113	standard	1	NaN	0.3109	0.0009	0.0591	NaN	0.0033	NaN	
A#5 090113	standard	1	NaN	0.6358	0.0096	0.1183	NaN	0.0027	NaN	
A#5 090113	standard	1	NaN	0.6378	0.0102	0.1191	NaN	NaN	NaN	
A#6 090113	standard	1	NaN	3.2256	NaN	0.6301	NaN	0.0058	NaN	
A#6 090113	standard	1	NaN	3.2259	NaN	0.6307	NaN	0.0051	NaN	
A#7 090113	standard	1	NaN	17.2763	NaN	14.1764	NaN	0.0026	NaN	
A#7 090113	standard	1	NaN	17.323	NaN	14.197	NaN	0.0032	NaN	
Blank - NEW 125uL sample loops	blank	1	NaN	NaN	NaN	NaN	NaN	NaN	NaN	
Blank - DI's are filled with Elix	blank	1	NaN	NaN	NaN	NaN	NaN	0.0021	NaN	
Blank	blank	1	NaN	NaN	NaN	NaN	NaN	0.0019	NaN	
DI - CD2 stabilized before CD1;	unknown	1	NaN	0.0041	0.002	NaN	0.0013	0.056	NaN	
DI	unknown	1	NaN	NaN	0.0017	NaN	NaN	0.0068	NaN	
MC Cation 090113	unknown	1	0.004	0.0161	0.0518	0.0124	0.1118	0.0844	0.0117	
MC Anion 090113	unknown	1	NaN	0.1794	0.0038	0.0337	0.0018	0.1006	0.0004	
DI	unknown	1	NaN	NaN	0.001	NaN	NaN	0.0085	NaN	
G34	unknown	1	0.0013	0.9927	0.0482	1.3459	0.511	0.966	0.0029	
G25	unknown	1	0.0008	0.5031	0.0108	0.6299	0.3798	0.8913	0.0065	
G15B	unknown	1	NaN	0.1769	0.0228	0.0704	0.0242	0.0745	NaN	
G6	unknown	1	0.0013	1.1467	0.052	1.4501	0.9141	2.0291	0.0078	
A9	unknown	1	0.0012	0.2738	0.0774	0.6639	0.268	0.5895	0.0023	
G64	unknown	1	0.0003	0.1464	0.0097	0.2408	0.1022	0.2129	NaN	
MQ	unknown	1	NaN	0.0117	0.0118	0.005	0.006	0.0331	NaN	
MC Cation 090113	unknown	1	0.004	0.0168	0.0538	0.0139	0.1131	0.0854	0.012	

Sample	Sample Type	Dil.Fac.	Amount		Amount	Amount	Amount	Amount	Amount	Amount
			ppm	ppm	ppm	ppm	ppm	ppm	ppm	ppm
			Li	Na	NH4	K	Mg	Ca	Sr	
MC Anion 090113	unknown	1	NaN	0.177	0.0006	0.0334	0.0014	0.0488	0.0071	0.0033
DI	unknown	1	NaN	NaN	0.0012	NaN	NaN	NaN	NaN	NaN
G44	unknown	1	0.0013	0.92	0.0469	1.3047	0.5401	1.0014	0.0035	0.0035
G33	unknown	1	0.0009	0.7065	0.0362	0.8823	0.3985	0.8678	0.0034	0.0034
G24	unknown	1	0.0013	0.376	0.1135	0.6995	0.4781	1.2486	0.0053	0.0053
G15	unknown	1	NaN	0.0667	0.0147	0.0211	0.0153	0.0476	NaN	NaN
G5	unknown	1	0.0014	1.1826	0.0513	1.5177	0.9582	2.1107	0.0079	0.0079
A6	unknown	1	0.0008	0.3454	0.0879	0.6007	0.2454	0.4854	NaN	NaN
DI	unknown	1	NaN	NaN	NaN	NaN	NaN	0.0056	NaN	NaN
MC Anion 090113	unknown	1	NaN	0.177	0.0005	0.033	0.001	0.0483	NaN	NaN
MC Cation 090113	unknown	1	0.004	0.0165	0.0528	0.0123	0.1125	0.0865	0.0121	0.0121
DI	unknown	1	NaN	NaN	0.0024	NaN	0.0013	0.0051	NaN	NaN
G63	unknown	1	0.0005	0.1651	0.0169	0.3451	0.1302	0.2607	NaN	NaN
G53	unknown	1	0.002	7.1742	NaN	1.1745	1.2434	1.1606	0.0063	0.0063
G43	unknown	1	0.0005	0.4343	0.0271	0.5085	0.1912	0.4193	NaN	NaN
G32	unknown	1	0.001	0.7186	0.0629	0.9029	0.4173	0.9066	NaN	NaN
G23	unknown	1	0.0007	0.2276	0.075	0.4016	0.2062	0.5056	NaN	NaN
G14	unknown	1	0.0008	0.4908	0.0043	0.5765	0.3978	0.9242	0.0038	0.0038
G4	unknown	1	0.0002	0.1378	0.0109	0.1052	0.0865	0.2456	NaN	NaN
DI	unknown	1	NaN	NaN	0.001	NaN	NaN	0.0008	0.0078	NaN
MC Anion 090113	unknown	1	NaN	0.1738	NaN	0.0336	0.0011	0.048	NaN	NaN
MC Cation 090113	unknown	1	0.004	0.0166	0.0533	0.0123	0.1133	0.088	0.0125	0.0125
DI	unknown	1	NaN	NaN	0.0018	NaN	0.0013	0.0047	NaN	NaN
A23	unknown	1	0.0006	0.1346	0.0529	0.3482	0.1161	0.2573	NaN	NaN
A5	unknown	1	0.0007	0.1977	0.1186	0.4228	0.1729	0.3643	NaN	NaN
G62	unknown	1	0.0005	0.161	0.001	0.3524	0.1213	0.2347	NaN	NaN
G8-REP0225	unknown	1	0.001	0.998	0.061	1.1098	0.7069	1.6838	0.0066	0.0066
G10-REP0225	unknown	1	0.0009	0.7395	0.0044	0.7746	0.5541	1.2335	0.0046	0.0046
G15B-2	unknown	1	NaN	0.1797	0.0231	0.0714	0.0247	0.0741	NaN	NaN
G5-2	unknown	1	0.0014	1.1931	0.0523	1.5304	0.965	2.1229	0.0084	0.0084
G4-2	unknown	1	0.0002	0.1384	0.0126	0.1053	0.0846	0.2473	NaN	NaN
DI	unknown	1	NaN	NaN	NaN	NaN	NaN	0.0058	NaN	NaN
Shutdown	unknown	1	NaN	NaN	NaN	NaN	NaN	NaN	NaN	NaN
Cation #1 090113	standard	1	0.0017	0.0078	0.025	0.0051	0.0398	0.0355	NaN	NaN
Cation #1 090113	standard	1	0.0017	0.0078	0.0255	0.005	0.04	0.0348	0.0023	0.0023
Cation #2 090113	standard	1	0.0034	0.0148	0.0474	0.0103	0.082	0.0702	0.0053	0.0053
Cation #3 090113	standard	1	0.0197	0.0803	0.2218	0.0671	0.5522	0.3968	0.0176	0.0176
Cation #3 090113	standard	1	0.0197	0.0804	0.2224	0.0692	0.5527	0.4007	0.0185	0.0185
Cation #4 090113	standard	1	0.0496	0.1963	0.4675	0.1787	1.3259	0.9965	0.095	0.095
Cation #4 090113	standard	1	0.0497	0.197	0.471	0.1851	1.3264	1.0004	0.0947	0.0947
Cation #5 090113	standard	1	0.1254	0.4979	0.9743	0.5082	2.9991	2.4927	0.2405	0.2405
Cation #5 090113	standard	1	0.1257	0.4976	0.9743	0.5101	3.0039	2.5034	0.2406	0.2406
Cation #6 090113	standard	1	1.3017	5.1457	NaN	5.3029	31.3221	25.815	1.305	1.305
Cation #6 090113	standard	1	1.2884	5.0585	10.7963	5.0055	28.5307	25.989	1.3162	1.3162
A#1 090113	standard	1	NaN	0.0177	0.0006	0.0025	NaN	0.0116	NaN	NaN
A#1 090113	standard	1	NaN	0.0181	0.0009	0.0027	NaN	0.0035	NaN	NaN
A#2 090113	standard	1	NaN	0.031	0.002	0.0051	NaN	0.0028	NaN	NaN
A#2 090113	standard	1	NaN	0.031	0.0022	0.0053	NaN	0.0026	NaN	NaN
A#2 090113	standard	1	NaN	0.0308	0.0026	0.0054	NaN	0.0026	NaN	NaN
A#3 090113	standard	1	NaN	0.1531	0.0028	0.0283	NaN	0.0018	NaN	NaN
A#3 090113	standard	1	NaN	0.1542	0.003	0.0286	NaN	0.0023	NaN	NaN
A#4 090113	standard	1	NaN	0.3094	0.0008	0.0592	NaN	0.0028	NaN	NaN
A#4 090113	standard	1	NaN	0.3109	0.0009	0.0591	NaN	0.0033	NaN	NaN
A#5 090113	standard	1	NaN	0.6358	0.0096	0.1183	NaN	0.0027	NaN	NaN
A#5 090113	standard	1	NaN	0.6378	0.0102	0.1191	NaN	NaN	NaN	NaN
A#6 090113	standard	1	NaN	3.2256	NaN	0.6301	NaN	0.0058	NaN	NaN
A#6 090113	standard	1	NaN	3.2259	NaN	0.6307	NaN	0.0051	NaN	NaN
A#7 090113	standard	1	NaN	17.2763	NaN	14.1764	NaN	0.0026	NaN	NaN
A#7 090113	standard	1	NaN	17.323	NaN	14.197	NaN	0.0032	NaN	NaN
Blank - NEW 125uL sample loops	blank	1	NaN	NaN	NaN	NaN	NaN	NaN	NaN	NaN
Blank - DI's are filled with Elix	blank	1	NaN	NaN	NaN	NaN	NaN	NaN	NaN	NaN
Blank	blank	1	NaN	NaN	NaN	NaN	NaN	NaN	NaN	NaN
DI - CD2 stabilized before CD1;	unknown	1	NaN	NaN	NaN	NaN	NaN	NaN	NaN	NaN
DI	unknown	1	NaN	NaN	NaN	NaN	NaN	NaN	NaN	NaN
MC Cation 090113	unknown	1	0.0041	0.0162	0.053	0.0125	0.1138	0.0838	0.0117	0.0117
MC Anion 090113	unknown	1	NaN	0.1821	0.0012	0.0342	0.0009	0.0468	0.0002	0.0002
DI	unknown	1	NaN	NaN	0.0011	NaN	NaN	0.0057	NaN	NaN
G52	unknown	1	0.0006	0.4408	0.0488	0.5464	0.2491	0.4562	NaN	NaN
G42	unknown	1	0.0008	0.4494	0.0276	0.6673	0.2359	0.4651	NaN	NaN
G31	unknown	1	0.001	0.5531	0.0052	0.7835	0.437	0.9285	0.0031	0.0031
G22	unknown	1	0.0006	0.2319	0.0654	0.3754	0.2172	0.588	NaN	NaN
G13	unknown	1	0.0017	1.5708	0.0656	1.6669	1.3485	3.2133	0.0118	0.0118
G3	unknown	1	0.0012	1.0795	0.0542	1.3349	0.7669	1.6091	0.0063	0.0063
A21	unknown	1	0.001	0.2117	0.0865	0.6796	0.2013	0.4666	NaN	NaN
DI	unknown	1	NaN	NaN	0.0029	NaN	0.0009	0.0078	NaN	NaN
MC Cation 090113	unknown	1	0.0041	0.0174	0.0547	0.0137	0.1149	0.0872	0.0126	0.0126
MC Anion 090113	unknown	1	NaN	0.1931	0.0021	0.035	0.0018	0.0763	0.0004	0.0004
DI	unknown	1	NaN	NaN	NaN	NaN	NaN	0.0041	NaN	NaN
A4	unknown	1	0.001	0.5496	0.0935	0.8497	0.3466	0.6564	0.0022	0.0022
G71	unknown	1	0.0003	0.1451	NaN	0.2675	0.1082	0.1899	NaN	NaN
G61	unknown	1	0.0003	0.0761	0.0078	0.1929	0.0712	0.1584	NaN	NaN
G51	unknown	1	0.0008	0.5385	0.0599	0.7683	0.3105	0.5869	NaN	NaN
G41	unknown	1	0.0011	0.7806	0.0412	1.1039	0.4328	0.8492	0.0025	0.0025
G30	unknown	1	0.001	0.6926	0.0468	0.9029	0.3614	0.7069	NaN	NaN
G21	unknown	1	0.0022	30.6297	NaN	1.4524	4.2676	2.7357	0.0225	0.0225
DI	unknown	1	NaN	0.0005	NaN	NaN	0.0029	0.0078	NaN	NaN
MC Anion 090113	unknown	1	NaN	0.1942	0.0015	0.0353	0.0018	0.0755	0.0003	0.0003
MC Cation 090113	unknown	1	0.0041	0.0172	0.0541	0.0129	0.1153	0.0901	0.0129	0.0129
DI	unknown	1	NaN	NaN	NaN	NaN	0.0008	0.0032	NaN	NaN
G12	unknown	1	0.0058	1.969	0.1955	3.047	4.4109	13.3702	0.0439	0.0439
G2	unknown	1	0.0003	1.2362	NaN	0.3713	0.4814	0.817	NaN	NaN
A19	unknown	1	0.0017	0.3168	0.0569	1.015	0.3443	0.7894	0.0034	0.0034

Sample	Sample Type	Dil.Fac.	Amount	Amount	Amount	Amount	Amount	Amount	Amount
			ppm Li	ppm Na	ppm NH4	ppm K	ppm Mg	ppm Ca	ppm Sr
A3	unknown	1	0.0008	0.3095	0.1087	0.5445	0.2346	0.4887	0.0012
G70	unknown	1	0.0005	0.2256	NaN	0.345	0.1465	0.3595	NaN
G60	unknown	1	0.0004	0.0934	0.0175	0.2911	0.1211	0.2889	NaN
G50	unknown	1	NaN	0.1108	0.0115	0.058	0.0066	0.0202	NaN
DI	unknown	1	NaN	NaN	NaN	NaN	NaN	0.0046	NaN
MC Anion 090113	unknown	1	NaN	0.1951	0.0015	0.0358	0.0015	0.0755	NaN
MC Cation 090113	unknown	1	0.0041	0.0173	0.0545	0.0127	0.116	0.0905	0.0125
DI	unknown	1	NaN	NaN	NaN	NaN	0.0012	0.0036	NaN
G40	unknown	1	0.0005	1.9547	0.0064	1.7103	1.3465	2.0146	0.0115
G29	unknown	1	0.0007	0.5842	0.0372	0.7004	0.2797	0.5704	NaN
G20	unknown	1	0.0016	6.0721	NaN	0.9057	1.0162	0.9272	0.0067
G7-REP0226	unknown	1	0.0011	1.5991	NaN	0.6061	0.7494	0.9112	NaN
G8-REP0226	unknown	1	0.0011	1.0294	0.0781	1.142	0.7332	1.7504	0.0064
G3-2	unknown	1	0.0012	1.082	0.0522	1.3451	0.7707	1.6182	0.0106
G21-2	unknown	1	0.0022	30.6841	NaN	1.4572	4.2814	2.7464	0.0228
G29-2	unknown	1	0.0016	6.0753	NaN	0.9056	1.0234	0.9387	0.005
G79	unknown	1	0.0007	27.3086	NaN	1.0466	4.2591	2.1144	0.0146
DI	unknown	1	NaN	0.0008	NaN	NaN	0.0039	0.0092	NaN
Shutdown	unknown	1	NaN	NaN	NaN	NaN	NaN	NaN	NaN
Cation #1 090113	standard	1	0.0017	0.0078	0.025	0.0051	0.0398	0.0355	NaN
Cation #1 090113	standard	1	0.0017	0.0078	0.0255	0.005	0.04	0.0348	0.0023
Cation #2 090113	standard	1	0.0034	0.0148	0.0474	0.0103	0.082	0.0702	0.0053
Cation #3 090113	standard	1	0.0197	0.0803	0.2218	0.0671	0.5522	0.3968	0.0176
Cation #3 090113	standard	1	0.0197	0.0804	0.2224	0.0692	0.5527	0.4007	0.0185
Cation #4 090113	standard	1	0.0496	0.1963	0.4675	0.1787	1.3259	0.9965	0.095
Cation #4 090113	standard	1	0.0497	0.197	0.471	0.1851	1.3264	1.0004	0.0947
Cation #5 090113	standard	1	0.1254	0.4979	0.9743	0.5082	2.9991	2.4927	0.2405
Cation #5 090113	standard	1	0.1257	0.4976	0.9743	0.5101	3.0039	2.5034	0.2406
Cation #6 090113	standard	1	1.3017	5.1457	NaN	5.3029	31.3221	25.815	1.305
Cation #6 090113	standard	1	1.2884	5.0585	10.7963	5.0055	28.5307	25.989	1.3162
A#1 090113	standard	1	NaN	0.0177	0.0006	0.0025	NaN	0.0116	NaN
A#1 090113	standard	1	NaN	0.0181	0.0009	0.0027	NaN	0.0035	NaN
A#2 090113	standard	1	NaN	0.031	0.002	0.0051	NaN	0.0028	NaN
A#2 090113	standard	1	NaN	0.031	0.0022	0.0053	NaN	0.0026	NaN
A#2 090113	standard	1	NaN	0.0308	0.0026	0.0054	NaN	0.0026	NaN
A#3 090113	standard	1	NaN	0.1531	0.0028	0.0283	NaN	0.0018	NaN
A#3 090113	standard	1	NaN	0.1542	0.003	0.0286	NaN	0.0023	NaN
A#4 090113	standard	1	NaN	0.3094	0.0008	0.0592	NaN	0.0028	NaN
A#4 090113	standard	1	NaN	0.3109	0.0009	0.0591	NaN	0.0033	NaN
A#5 090113	standard	1	NaN	0.6358	0.0096	0.1183	NaN	0.0027	NaN
A#5 090113	standard	1	NaN	0.6378	0.0102	0.1191	NaN	NaN	NaN
A#6 090113	standard	1	NaN	3.2256	NaN	0.6301	NaN	0.0058	NaN
A#6 090113	standard	1	NaN	3.2259	NaN	0.6307	NaN	0.0051	NaN
A#7 090113	standard	1	NaN	17.2763	NaN	14.1764	NaN	0.0026	NaN
A#7 090113	standard	1	NaN	17.323	NaN	14.197	NaN	0.0032	NaN
Blank - NEW 125uL sample loops	blank	1	NaN	NaN	NaN	NaN	NaN	NaN	NaN
Blank - DI's are filled with Elix	blank	1	NaN	NaN	NaN	NaN	NaN	NaN	NaN
Blank	blank	1	NaN	NaN	NaN	NaN	NaN	NaN	NaN
DI - CD2 stabilized before CD1;	unknown	1	NaN	NaN	NaN	NaN	NaN	NaN	NaN
DI	unknown	1	NaN	NaN	NaN	NaN	NaN	0.0042	NaN
MC Cation 090113	unknown	1	0.0042	0.0166	0.0544	0.0127	0.1182	0.088	0.0129
MC Anion 090113	unknown	1	NaN	0.1801	0.0008	0.0336	0.0008	0.0117	NaN
DI	unknown	1	NaN	NaN	NaN	NaN	NaN	0.0043	NaN
G11	unknown	1	0.0015	1.5946	0.0485	1.6823	1.2541	2.9532	0.0111
G1	unknown	1	0.0028	2.9167	0.0037	2.8536	1.2571	4.1587	0.014
G12-REP0227	unknown	1	0.0067	2.3031	0.2055	3.5714	5.0078	13.8287	0.0457
G21-REP0227	unknown	1	0.0028	NaN	NaN	1.869	5.2719	3.0047	0.0264
DI	unknown	1	NaN	0.0014	NaN	NaN	0.006	0.0127	NaN
MC Cation 090113	unknown	1	0.0041	0.0166	0.0541	0.0125	0.1188	0.0909	0.013
MC Anion 090113	unknown	1	NaN	0.18	0.0009	0.0339	0.0016	0.0129	NaN
DI	unknown	1	NaN	NaN	NaN	NaN	NaN	0.0047	NaN
G79-REP0227	unknown	1	0.0009	33.3984	NaN	1.2131	5.2138	2.3752	0.0192
G78	unknown	1	NaN	NaN	NaN	2380.4388	NaN	NaN	0.8091
G75	unknown	1	NaN	NaN	NaN	1253.8129	0.5525	NaN	0.8054
G74	unknown	1	0.001	16.3925	NaN	0.6642	2.2828	1.2206	NaN
G73	unknown	1	NaN	NaN	NaN	NaN	215.6089	NaN	0.7601
G72 - "NO2" peak inserted by SK	unknown	1	NaN	NaN	NaN	1033.8447	76.8963	NaN	0.7725
DI	unknown	1	NaN	0.1354	NaN	NaN	0.0323	NaN	NaN
G11-2	unknown	1	0.0015	1.5121	0.017	1.582	1.1164	2.8042	NaN
G75-2	unknown	1	NaN	NaN	NaN	1260.2546	0.4831	NaN	0.7334
G72-2	unknown	1	NaN	NaN	NaN	1049.2592	185.7085	NaN	0.6928
DI	unknown	1	0.0004	0.1292	NaN	0.0018	0.0278	0.0004	NaN
MC Anion 090113	unknown	1	NaN	0.1745	NaN	0.0312	0.0043	0.0103	NaN
MC Cation 090113	unknown	1	0.0042	0.0295	0.0303	0.0112	0.1125	0.0888	NaN
DI	unknown	1	NaN	0.026	NaN	NaN	0.0042	0.0022	NaN
Shutdown	unknown	1	NaN	NaN	NaN	NaN	NaN	NaN	NaN
Shutdown	unknown	1	NaN	NaN	NaN	NaN	NaN	NaN	NaN

<b>Table A11: Greenland Ice Sheet Margins 2008 Dissolved Iron (Fe)</b>				
	<b>Sample ID</b>	<b>Sample Type</b>	<b>Nutrient sample?</b>	<b>Fe concentration (µM)</b>
<b>Clean Lab Blanks</b>				
	MQ 10.28.08	clean lab blank	n/a	0.0461
	MQ 10.29.08	clean lab blank	n/a	0.0056
	Milli-Q1	clean lab blank	yes	0.031
	Milli-Q2	clean lab blank	yes	0
<b>Supraglacial</b>				
	G15	MI	yes	0.1256
<b>Proglacial Lake</b>				
	G7	PL	yes	5.2323
	G67	PL	yes	4.8283
<b>Proglacial Lake Outflow</b>				
	G20	LO	yes	17.462
<b>Marginal Melt</b>				
	G58	MM	yes	0.2091
<b>O Glacier</b>				
	G21	OF	yes	9.9741
<b>M Glacier</b>				
	G35	MO	yes	3.54
	G70	MO	yes	4.0887
<b>Groundwater</b>				
	G39	GW	no	0.311
	GM50	GW	no	3.0239
	GM51	GW	no	431.2633
	GM52	GW	no	143.227
	GM53	GW	no	4.6735
	GM54	GW	no	1.6652
<b>N Glacier</b>				
	G11	NO	yes	7.0796
	G12	NO	yes	3.2296
	G29	NO	yes	7.0217
	G49	NO	yes	9.3351
	G56	NO	yes	2.4776
	G57	NO	yes	2.2206
	G61	NO	yes	3.5426
	G63	NO	yes	2.8707
	G65	NO	yes	3.2424
	G66	NO	yes	2.6434
	G68	NO	yes	2.7228
	G69	NO	yes	2.5264
	G71	NO	yes	4.2826
<b>Fjord Samples</b>				
	G72	F	yes	0.0519
	G75	F	yes	-0.0092
	G76	SWF	no	2.8796
	G79	SWF	yes	2.3627

Table A12: Greenland Ice Sheet Margins 2008 Particulate Iron (Fe)															
Sample ID	GFF#	Sample Type	Sample Date	Leach	% Blk Corr	Fe56 µmol/L	% Fe (g/g)	Fe (g/g)	Leach	% Blk Corr	Fe56 µmol/L	% Fe (g/g)	Fe (g/g)	% L3 contribution	% L4 contribution
B1A-rerun	NaN	process blank no plunger sterivex blk	9/12/11	NaN	NaN	0.032411236									
B1B-rerun	NaN	process blank no plunger sterivex blk	9/12/11	NaN	NaN	0.004332543									
B1C-rerun	NaN	process blank no plunger sterivex blk	9/12/11	NaN	NaN	0.201113291									
B2A	NaN	process blank wplunger sterivex blk	9/12/11	NaN	NaN	-0.042611337									
B2B	NaN	process blank wplunger sterivex blk	9/12/11	NaN	NaN	-0.05321401									
B2C	NaN	process blank wplunger sterivex blk	9/12/11	NaN	NaN	-0.046767524									
B3	NaN	process blank water from beaker	9/12/11	NaN	NaN	-0.050399045									
G15	NaN	MI	5/22/08 17:00	dissolved	NaN	0.077780486									
G68	NaN	NO	7/14/08 18:00	dissolved	NaN	4.396469876									
G71	NaN	NO	7/16/08 22:00	dissolved	NaN	6.377897933									
G35	NaN	MO	5/28/08 16:30	dissolved	NaN	3.560152189									
G12	NaN	NO	5/21/08 14:10	dissolved	NaN	3.419827251									
G7	NaN	PL	5/20/08 14:05	dissolved	NaN	6.499304723									
G29	NaN	NO	5/27/08 14:48	dissolved	NaN	9.68743014									
G11	NaN	NO	5/21/08 14:23	dissolved	NaN	8.87163796									
G49	NaN	NO	5/31/08 12:40	dissolved	NaN	8.086910215									
G21	NaN	OO	5/24/08 21:00	dissolved	NaN	14.7109933									
G20	NaN	LO	5/24/08 19:00	dissolved	NaN	20.99694467									
G56	75	NO	7/10/08 11:23	d2 L3	0.94	63.22329376	1.69	0.016922169	d2 L4	1.81	84.8503	2.27	0.0227108	42.7	57.3
G49	22	NO	5/31/08 12:40	d2 L3	0.54	110.6874283	1.49	0.01485437	d2 L4	1.77	131.5928	1.77	0.017659889	45.69	54.31
G51	43	NO	5/31/08 18:25	d2 L3	0.74	80.48811427	1.39	0.013938398	d2 L4	1.08	143.6606	2.49	0.024878195	35.91	64.09
G53	30	PL	6/1/08	d2 L3	0.26	136.7452941	2.6	0.025988203	d2 L4	0.48	194.5304	3.7	0.03697017	41.28	58.72
G53	16	PL	6/1/08	d2 L3	0.34	107.4213602	1.57	0.015744193	d2 L4	0.79	117.5281	1.72	0.017225485	47.75	52.25
G57	61	NO	7/10/08 13:46	d2 L3	0.83	72.17828089	2.16	0.021629896	d2 L4	1.72	89.2962	2.68	0.026759676	44.7	55.3
G61	72	NO	7/11/08 18:00	d2 L3	0.78	64.20307169	1.56	0.015611645	d2 L4	1.49	85.9603	2.09	0.020902144	42.76	57.24
G63	36	NO	7/12/08 6:00	d2 L3	0.62	58.39693443	4.18	0.041815153	d2 L4	1.61	57.1697	4.09	0.0409364	50.53	49.47
G65	69	NO	7/12/08 18:00	d2 L3	0.66	78.03788103	0.46	0.004633276	d2 L4	1.26	104.4974	0.62	0.006204234	42.75	57.25
G63	53	NO	7/12/08 6:00	d2 L3	0.58	61.80342112	3.17	0.031689777	d2 L4	1.29	71.772	3.68	0.036801154	46.27	53.73
G35	28	MO	5/28/08 16:30	d2 L3	4.59	12.52258085	0.33	0.00332282	d2 L4	10.72	13.0074	0.35	0.003451461	49.05	50.95
G42	80	NO	5/29/08 13:41	d2 L3	0.7	85.57280104	1.46	0.014607878	d2 L4	6.55	22.268	0.38	0.0038013	79.35	20.65
G45	27	NO	5/30/08 18:00	d2 L3	0.51	118.469363	1.57	0.01573263	d2 L4	1.54	99.5306	1.32	0.013217579	54.34	45.66
G48	4	NO	5/31/08 6:45	d2 L3	0.5	120.0203351	1.53	0.01532259	d2 L4	0.85	182.8193	2.33	0.023339918	39.63	60.37
G63	41	NO	7/12/08 6:00	d2 L3	0.53	67.88088219	3.11	0.03114065	d2 L4	1.26	73.2015	3.36	0.033581521	48.11	51.89
G63	7	NO	7/12/08 6:00	d2 L3	0.36	99.89631052	0.48	0.004771554	d2 L4	0.7	132.024	0.63	0.006306136	43.07	56.93
G71	85	MI	7/16/08 22:00	d2 L3	0.09	183.3146803	0.37	0.003716409	d2 L4	0.26	164.3214	0.33	0.00333135	52.73	47.27
G15	85	MI	5/22/08 17:00	d2 L3	7.85	4.242896374	NaN	NaN	d2 L4	3.85	23.36670607	NaN	NaN	15.37	84.63
G29	39	NO	5/27/08 14:48	d2 L3	0.38	158.3463651	0.78	0.007813713	d2 L4	0.95	163.2326	0.81	0.008054827	49.24	50.76
G47	24	NO	5/31/08 0:00	d2 L3	0.48	123.835762	1.86	0.018550491	d2 L4	1.11	138.9204	2.08	0.020810151	47.13	52.87
G12	90	NO	5/21/08 14:10	d2 L3	1.99	29.6413796	1.24	0.012410109	d2 L4	7	20.7501	0.87	0.008687557	58.82	41.18
G66	6	NO	7/13/08 13:50	d2 L3	0.66	77.32689669	1.45	0.014497405	d2 L4	2.94	44.1201	0.83	0.008271732	63.67	36.33
G69	1	NO	7/15/08 16:30	d2 L3	0.51	98.29064959	0.38	0.003804679	d2 L4	0.86	150.2732294	0.58	0.005816844	39.54	60.46
G71	19	NO	7/16/08 22:00	d2 L3	0.06	308.7435632	0.38	0.003845156	d2 L4	0.11	421.5065732	0.52	0.005249529	42.28	57.72
G63	94	NO	7/12/08 6:00	d2 L3	0.34	107.4378	0.78	0.00779132	d2 L4	0.79	117.1215706	0.85	0.008480292	47.84	52.16
G63	92	NO	7/12/08 6:00	d2 L3	0.59	60.4758	4.69	0.046942982	d2 L4	2	45.9895819	3.57	0.0356987	56.8	43.2
G63	37	NO	7/12/08 6:00	d2 L3	0.51	70.783	2.16	0.02156971	d2 L4	0.94	98.37711954	3	0.029978449	41.84	58.16
G63	8	NO	7/12/08 6:00	d2 L3	0.43	82.8012	1.81	0.018069996	d2 L4	1.33	69.25911387	1.51	0.015114661	54.45	45.55
G72	15	F	7/19/08 20:00	d2 L3	41.2	0.129	0.03	0.000284088	d2 L4	111.74	-0.02460666	-0.01	-5.42E-05	NaN	NaN
G71	13	NO	7/16/08 22:00	d2 L3	0.29	62.4569	2.27	0.022732162	d2 L4	0.8	58.04808551	2.11	0.021127521	51.83	48.17
G71	10	NO	7/16/08 22:00	d2 L3	0.65	68.5898	0.71	0.007102851	d2 L4	1.18	98.45851343	1.02	0.010195923	41.06	58.94
G63	32	NO	7/12/08 6:00	d2 L3	0.83	43.1861	3.19	0.031893531	d2 L4	1.85	49.7322539	3.67	0.036727933	46.48	53.52
G63	93	NO	7/12/08 6:00	d2 L3	0.8	45.0338	3.19	0.031927666	d2 L4	1.96	46.77188871	3.32	0.033159927	49.05	50.95
G63	58	NO	7/12/08 6:00	d2 L3	0.66	54.6566	4.16	0.041646939	d2 L4	1.84	49.94295816	3.81	0.038051842	52.25	47.75
G63	33	NO	7/12/08 6:00	d2 L3	0.37	98.2586	0.62	0.006219242	d2 L4	0.87	106.520519	0.67	0.006741576	47.98	52.02
G63	38	NO	7/12/08 6:00	d2 L3	0.72	49.9194	3.36	0.033649542	d2 L4	1.44	64.11242233	4.32	0.043212916	43.78	56.22
G63	29	NO	7/12/08 6:00	d2 L3	0.48	75.3327	1.04	0.01041663	d2 L4	0.77	120.0181699	1.66	0.016594028	38.56	61.44
G63	9	NO	7/12/08 6:00	d2 L3	0.43	41.4857	1.26	0.012554108	d2 L4	0.71	65.24714686	1.97	0.019742875	38.87	61.13
G63	31	NO	7/12/08 6:00	d2 L3	0.71	50.7112	3.43	0.034275814	d2 L4	1.64	56.31191202	3.81	0.038057968	47.38	52.62
Mess 5	NaN	pStd	9/12/11	d2 L3	NaN	214.6604	1.2	1.20E-02	d2 L4	NaN	322.512406	1.8	0.018038119	39.96	60.04
Mess 6	NaN	pStd	9/12/11	d2 L3	NaN	214.7825	1.2	1.20E-02	d2 L4	NaN	282.2722454	1.58	0.015787487	43.21	56.79
Mess 7	NaN	pStd	9/12/11	d2 L3	NaN	190.7954	1.07	1.07E-02	d2 L4	NaN	292.9540645	1.64	0.016384921	39.44	60.56
G21	23	OO	5/24/08 21:00	d2 L3	0.74	13.8272	NaN	NaN	d2 L4	1.63	16.15230678	NaN	NaN	46.12	53.88
G20	98	LO	5/24/08 19:00	d2 L3	0.33	22.0821	2.66	0.026596941	d2 L4	0.8	23.2848505	2.8	0.038057968	48.67	51.33
Leach blank 1	NaN	LB	9/12/11	d1 L3	NaN	0.7639	0	4.27E-08	d1 L4	NaN	2.854072414	0	1.60E-07	21.11	78.89
Leach blank 2	NaN	LB	9/12/11	d1 L3	NaN	0.5474	0	3.06E-08	d1 L4	NaN	1.972964062	0	1.10E-07	21.72	78.28
Leach blank 3	NaN	LB	9/12/11	d1 L3	NaN	0.553	0	3.09E-08	d1 L4	NaN	1.969332279	0	1.10E-07	21.92	78.08
Filter blank 4	4	FB	9/12/11	d1 L3	NaN	0.2916	0	3.23E-05	d1 L4	NaN	0.616428343	0.01	6.82E-05	32.11	67.89

Sample ID	GFF#	Sample Type	Sample Date	Leach	% Blk Corr	Fe56 umol/L	% Fe (g/g)	Fe (g/g)	Leach	% Blk Corr	Fe56 umol/L	% Fe (g/g)	Fe (g/g)	% L3 contribution	% L4 contribution
Filter blank 5	5	FB	9/12/11	d1 L3	NaN	0.2321	0	2.55E-05	d1 L4	NaN	0.649576826	0.01	7.13E-05	26.32	73.68
Filter blank 6	6	FB	9/12/11	d1 L3	NaN	0.2942	0	3.25E-05	d1 L4	NaN	0.623278379	0.01	6.89E-05	32.07	67.93
Filter blank 7	7	FB	9/12/11	d1 L3	NaN	0.4261	0	4.70E-05	d1 L4	NaN	1.082191996	0.01	0.000119336	28.25	71.75
Filter blank 8	8	FB	9/12/11	d1 L3	NaN	0.3567	0	3.93E-05	d1 L4	NaN	1.172696086	0.01	0.000129112	23.32	76.68
Filter blank 9	9	FB	9/12/11	d1 L3	NaN	0.4109	0	4.57E-05	d1 L4	NaN	1.373968685	0.02	0.000152836	23.02	76.98
Filter blank 10	10	FB	9/12/11	d1 L3	NaN	0.52	0.01	5.76E-05	d1 L4	NaN	1.039301566	0.01	0.00011506	33.35	66.65
G71	11	NO	7/16/08 22:00	d2 L3	0.13	119.702	1.2	0.038057968	d2 L4	0.23	21.52543407	1.7	0.016963235	84.76	15.24
G71	18	NO	7/16/08 22:00	d2 L3	0.29	51.4724	1.27	0.038057968	d2 L4	0.76	50.97844999	1.26	0.012566566	50.24	49.76
G71	12	NO	7/16/08 22:00	d2 L3	0.28	53.4193	1.92	0.038057968	d2 L4	0.54	71.51627198	2.57	0.025671233	42.76	57.24
G68	14	NO	7/14/08 18:00	d2 L3	0.73	70.588	1.78	0.038057968	d2 L4	3	43.27381957	1.09	0.010943812	61.99	38.01
Mess 8	NaN	pSid	9/12/11	d2 L3	NaN	196.4095	1.87	1.10E-02	d2 L4	NaN	334.210082	1.87	0.01869237	37.02	62.98
G7	54	PL	5/20/08 14:05	d2 L3	4.96	7.88	-0.46	0	d1 L4	8.58	11.34	NaN	NaN	40.99	59.01
G11	40	NO	5/21/08 14:23	d2 L3	0.73	82.08	7.61	0.08	d2 L4	0.49	121.61	11.28	0.11	40.3	59.7
G50	13	MI	5/31/08 16:05	d1 L3	479.22	NaN	NaN	0	d1 L4	164.36	NaN	0.11	0	28.53	71.47

## **Appendix A2**

### **Supplemental Material for Chapter 3: Molecular-level characterization of dissolved organic matter associated with the Greenland ice sheet**

Table EA1. List of  $m/z$  values used for internal calibration of positive and negative ion mode data.

Figure EA1. Negative ion mode van Krevelen diagrams illustrating potential contamination present within the Supraglacial Inland, Subglacial May, and Subglacial July-1 samples.

**Table A1.** List of  $m/z$  values used for internal calibration of (A) positive ion mode data and (B) negative ion mode data. Exact mass refers to the mass calculated from the elemental formula, and charged mass is the exact mass value corrected for positive mode (by adding a Na atom and subtracting an electron) or negative mode (by subtracting a H atom and adding an electron). For the positive ion mode data, we utilized Na adducts. These compounds were chosen because of their frequent occurrence among the different samples analyzed in each mode, and their low error of observed  $m/z$  values (e.g. the error in mass accuracy ranged from 0.5 to 1.4 for the positive mode calibrants, and 0.3 to 0.8 ppm for the negative ion mode calibrants). In positive mode, calibrants were present in at least six of the seven samples, and in negative mode, calibrants were present in at least half the samples. On occasion, calibrants were added for specific spectra when the original list of calibrants was insufficient to calibrate the desired mass range. In positive mode the internal calibrants span the full range of observed  $m/z$  values; whereas, in negative mode it was not possible to find calibrants above  $\sim 600$   $m/z$  that fit our criteria. However, it is unlikely that the mass error of peaks outside our calibrated range fall outside the 1 ppm error set by the external calibrants because all of the negative mode samples were run within one week.

**A. Positive Mode Calibrants (Na Adducts)**

	<b>Elemental Formula</b>	<b>Exact Mass</b>	<b>Charged Mass</b>
1	C <sub>8</sub> H <sub>18</sub> O <sub>5</sub>	194.115423	217.104642
2	C <sub>10</sub> H <sub>22</sub> O <sub>6</sub>	238.141638	261.130856
3	C <sub>12</sub> H <sub>26</sub> O <sub>7</sub>	282.167853	305.157071
4	C <sub>17</sub> H <sub>36</sub> O <sub>6</sub>	336.251188	359.240407
5	C <sub>24</sub> H <sub>38</sub> O <sub>4</sub>	390.277009	413.266228
6	C <sub>18</sub> H <sub>38</sub> O <sub>10</sub>	414.246497	437.235715
7	C <sub>20</sub> H <sub>42</sub> O <sub>11</sub>	458.272712	481.261930
8	C <sub>22</sub> H <sub>46</sub> O <sub>12</sub>	502.298926	525.288145
9	C <sub>24</sub> H <sub>50</sub> O <sub>13</sub>	546.325141	569.314360
10	C <sub>26</sub> H <sub>54</sub> O <sub>14</sub>	590.351356	613.340574
11	C <sub>28</sub> H <sub>58</sub> O <sub>15</sub>	634.377571	657.366789
12	C <sub>30</sub> H <sub>62</sub> O <sub>16</sub>	678.403785	701.393004
13	C <sub>37</sub> H <sub>68</sub> O <sub>12</sub>	704.471077	727.460296
14	C <sub>35</sub> H <sub>62</sub> O <sub>16</sub>	738.403785	761.393004
15	C <sub>42</sub> H <sub>86</sub> O <sub>15</sub>	830.596672	853.585890
16	C <sub>45</sub> H <sub>92</sub> O <sub>16</sub>	888.638536	911.627755



## B. Negative Mode Calibrants

	<b>Elemental Formula</b>	<b>Exact Mass</b>	<b>Charged Mass</b>
1	C <sub>10</sub> H <sub>16</sub> O <sub>6</sub>	232.094688	231.087411
2	C <sub>10</sub> H <sub>21</sub> O <sub>5</sub> N <sub>3</sub>	263.148120	262.140844
3	C <sub>13</sub> H <sub>20</sub> O <sub>6</sub>	272.125988	271.118711
4	C <sub>13</sub> H <sub>10</sub> O <sub>9</sub>	310.032481	309.025205
5	C <sub>16</sub> H <sub>24</sub> O <sub>8</sub>	344.147117	343.139841
6	C <sub>24</sub> H <sub>18</sub> O <sub>3</sub> N <sub>2</sub>	382.131742	381.124466
7	C <sub>19</sub> H <sub>24</sub> O <sub>9</sub>	396.142032	395.134755
8	C <sub>21</sub> H <sub>26</sub> O <sub>10</sub>	438.152597	437.145320
9	C <sub>25</sub> H <sub>32</sub> O <sub>8</sub>	460.209718	459.202441
10	C <sub>21</sub> H <sub>24</sub> O <sub>14</sub>	500.116605	499.109329
11	C <sub>27</sub> H <sub>26</sub> O <sub>12</sub>	542.142426	541.135149
12	C <sub>28</sub> H <sub>24</sub> O <sub>15</sub>	600.111520	599.104243
13	C <sub>26</sub> H <sub>52</sub> O <sub>15</sub>	604.330620	603.323344

**EA Figure 1.** Negative ion mode van Krevelen diagrams illustrating the potential contamination present within the Supraglacial Inland (A), Subglacial May (B), and Subglacial July-1 (C) samples. The contamination was detected in the Yellow Snow mass spectra, likely originating from plasticizers, and consisted of an 18 peak series. Peaks from this potential contamination found in the Supraglacial Inland, Subglacial May, and Subglacial July-1 samples are outlined in red in panels A, B, and C respectively. In Supraglacial Inland the potential contamination represented 6 out of 1865 total sample peaks (0.35%), in Subglacial May the potential contamination represented 9 out of 1737 total sample peaks (0.52%), and in Subglacial July-1 the potential contamination represented 8 out of 3330 total sample peaks (0.24%). The colored boxes represent elemental compositions for some major compound classes, as approximated from Kim et al. (2003) and Hedges (1990). The grey box represents condensed hydrocarbons, the blue box represents lipids, the green box represents lignin, the yellow box represents proteins, and the pink box represents carbohydrates. The black oval represents elemental formula assignments for a sample of Suwannee River Fulvic Acid.

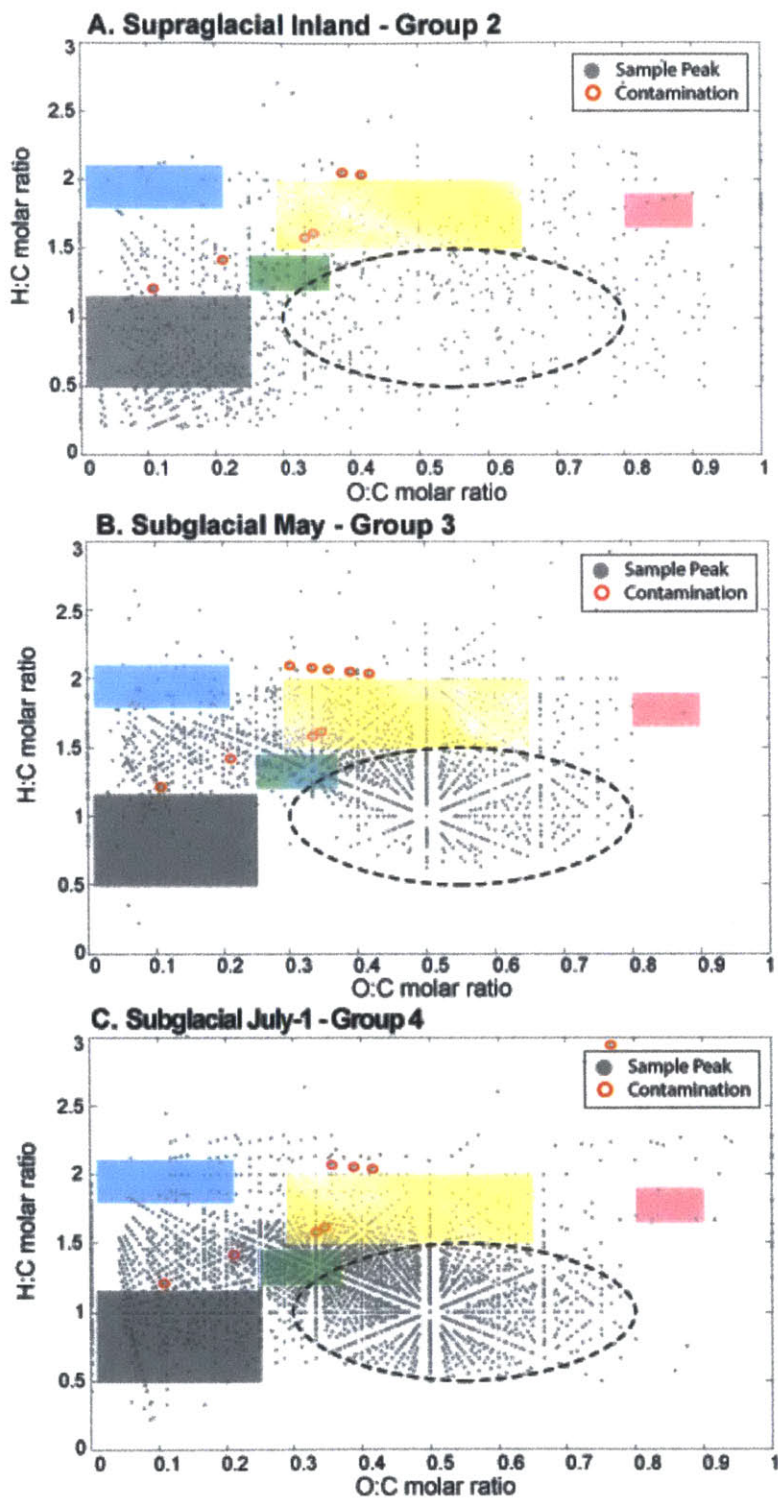


Figure EA1.